THE UNIVERSITY
of EDINBURGH

Ontogeny of Canine Myxomatous Mitral Valve Disease; Cellular and Molecular Events over a Lifetime

Greg Robert Markby

Thesis presented for the degree of

Doctor of Philosophy

Division of Veterinary Clinical Science

Royal (Dick) School of Veterinary Studies

College of Medicine and Veterinary Medicine

University of Edinburgh

Doctor of Philosophy – The University of Edinburgh - 2018

Declaration

I hereby declare that all the work included in this thesis submitted for the degree of Doctorate of Philosophy at the University of Edinburgh is my own original work, with the exception of Chapter 6 section 6.3.2 **Figure 6.2** which was kindly provided by Dr. Karen Tan. Chapter 1 contains published work from reviews that I am first author of and wrote. No part of this has been, or will be, submitted for any other degree or qualification.

Greg Robert Markby

September 2018

(This page has been left intentionally blank)

Abstract

Myxomatous mitral valve disease (MMVD) is the most common cardiac disease in dogs and the second most common cardiac valvular disease in humans. MMVD is particularly prevalent in small breed dogs (such as the Cavalier King Charles Spaniel (CKCS)) but by age 10, almost all dogs will have some form disease developing on the valve. Pathologically, there is a progressive deterioration in the organised structure of the valve extracellular matrix with an accumulation of proteoglycans and glycosaminoglycans, breakdown of collagen fibrils and loss of elastin and basement membrane components. Alongside this, there is an activation of quiescent valvular interstitial cells (VICs) into a myofibrotic phenotype, denuding of endothelial cells and endothelial-to-mesenchymal transition. Despite this knowledge of pathology and the clinical significance of MMVD, there is a lack of understanding of the underlying cellular and molecular mechanisms controlling the disease. This is particularly true of early disease development as the majority of previous studies have focused on comparing normal valves with end-stage disease.

This project aimed to address this problem by examining the transcriptomic changes occurring in MMVD in the dog: across the entire pathogenesis of the disease, in regional development of the disease on the valve and in *in vitro* models of disease.

Utilising the Whitney grading system (Grades 0-4), where Grade 4 represents severe disease, valves were collected (5 grades, n=6 per grade) from the entire spectrum of disease and in a mixture of dog breeds. Transcriptomic profiling (Affymetrix GeneChip™ Canine Gene 1.1 Sense Target (ST) Array) was performed and 1002 differentially expressed genes were identified across all

grades of disease. Network analysis was used to cluster genes with similar expression profiles and establish trends of progressive up- or down-regulation over the course of MMVD. Gene enrichment analysis highlighted GO terms both associated with these trends and in a grade-specific manner. Pathway analysis established the top canonical pathways, upstream regulators and disease function networks associated with each grade of disease. As a whole, these results indicated dysregulation of metalloproteases (both up- and down-regulation) and involvement of immune-related pathways as well as, most importantly, the repeated implication that TGFβ signalling is a controller in disease development. Furthermore, sample-to-sample analysis indicated CKCS, who have an earlier onset of disease than other dogs, had a slightly different transcriptomic profile compared to other valves, with analysis indicating a role for down-regulated calcium signalling and cell contractility in early disease development in this breed.

Transcriptomic analysis comparing distinct diseased and normal areas of the same moderately affected valves (n=7) found 289 differentially expressed genes, including hallmarks of disease *ACTA2* and *5HTR2B* which were up-regulated in the diseased sections of the valves. Comparison of the 'normal' tissue in this dataset with the whole normal valve dataset and dissection of comparable regions of normal valves and assessment by RT-qPCR indicated that the changes being measured were disease-specific and validated the approach used. Gene enrichment analysis of this dataset also implicated TGFβ1 as the top upstream regulator of disease.

To further explore the role of TGFβ1 signalling in MMVD, VICs from normal (n=3) and diseased (n=3) valves were treated with 5ng/mL TGFβ1 and 10 μM SB431542 (TGFβ pathway inhibitor) respectively, with appropriate vehicle controls. Differential gene expression was identified comparing normal VIC to

normal VIC TGF-β1-treated (275 genes), diseased VIC to diseased VIC SB431542-treated (236 genes) and diseased VIC to normal VIC (902 genes). Normal VICs transformed to myofibrotic cells in the presence of TGFβ1, with increased αSMA (*ACTA2*) expression and a 5 fold increase in proteoglycan secretion ($p<0.05$), consistent with the pathology *in vivo*. Diseased VICs showed a significant 2 fold increase in TGFβ1 secretion compared to normal VICs, and in the presence of SB431542 reverted to a normal phenotype with a reduction in αSMA expression and 2.8 fold decrease in proteoglycan secretion ($p<0.05$).

To summarise, this study provides insights into the molecular pathogenesis of MMVD from its early development to its end stage consequences and identifies TGFβ1 signalling as a central pathway in disease development.

(This page has been left intentionally blank)

Lay Summary

Myxomatous Mitral Valve Disease (MMVD) is a common disease that affects both dogs and humans. The disease causes a gradual deterioration in the structure of a major heart valve to the point where the valve is no longer functional, so that blood can flow back towards the lungs. If left untreated MMVD can lead to death. Despite the prevalence of this disease in both species and the dire consequences that can result, there is a poor understanding of the underlying mechanism that causes the disease to develop. By studying the disease in dogs a full understanding of these mechanisms is achievable due to the ready availability of owner donated tissue that will encompass the entire development of the disease. By examining RNA (the intermediate step between DNA and proteins) from normal valves and those at different stages of the disease, a comprehensive assessment of MMVD can be carried out.

In this project, whole valves spanning the entire course of disease, moderately affected valves dissected into diseased and normal tissue sections and cell culture assessment of valvular interstitial cells (the cells inside the valve responsible for their structure) had their RNA investigated.

Analysis of the RNA from the tissue samples (both whole and dissected valves) indicated the involvement of factors that would cause a dysregulation and breakdown of the valve structure. Perhaps most importantly, however, TGFβ1 (a factor responsible for various cellular processes) was implicated consistently as the driving factor in disease development.

Investigating TGFβ1's effect on the valvular interstitial cells grown in culture in the laboratory, we saw that treating normal cells with this factor induced a disease-like state in the cells that shared many similarities with the diseased tissue. Likewise, treatment of diseased cells with a TGFβ pathway inhibitor, to

block the effects of TGFβ, resulted in a reversal towards a more normal-appearing cell.

Collectively this study has shown that TGFβ1 plays a major contributing role in the development of MMVD. It is hoped that new drugs and treatments can be developed by targeting this factor to help slow or prevent disease progression.

Acknowledgements

The work presented in this thesis would not have been possible without the support, guidance, help and friendship of many different people both before and during the PhD. This has both come in the form of help with all things scientific as well as helping me maintain, for the most part, the thin veil of sanity from day to day.

First and foremost, I would like to thank my three supervisors, Prof. Brendan Corcoran, Prof. Kim Summers and Dr. Vicky MacRae, for giving me the opportunity to be a part of this project in the first place. Your vision, guidance and mentorship was the driving force behind this project.

I would like to thank all members, past and present, of Prof. David Argyle lab group for all the help you provided in and out of both the lab as well as the cake! In particular, I would like to thank Rhona Muirhead for providing all the answers that no one else could. I would also like to thank the members of the MacRae and Summer's lab groups for your insights and support, especially Fiona Roberts and Lucy Lin for always being around for a coffee and a laugh. I also have a special thank you to Dr. Karen Tan, the fourth supervisor I never had, your guidance throughout the course of the project was truly invaluable and in particular, Chapter 6 would not have been possible without your help.

A special thank you as well to Conor O'Halloran and all the members of the hospital and anatomy department for help with the collection of tissue. I wish to express my gratitude to all animals that contributed samples for the research performed in this project, the knowledge gathered and presented here would not have been possible without you.

To my family especially my parents Robert and Alison, without your help, support and encouragement I would not be where I am today. And to all my

friends, old and new, I wish to express my sincere gratitude for the help in all respects you have given me, without it I would not be where I am today. To Corey, Tyrannous, Jhonny and Ross, may Bahamut's blessing be upon you and may our quest to bring peace and Bahamut's wisdom to all be successful.

Finally, I would like to thank the Dogs Trust who provided funding for this project and Zoetis that contributed to the microarray costs.

Table of Contents

Table of Figures

Table of tables

(This page has been left intentionally blank)

Chapter 1 Introduction

1.1 Overview of Myxomatous mitral valve disease

Myxomatous mitral valve disease (MMVD) is a progressive disorder which, over the lifetime of the affected individual, causes a deterioration in the left atrioventricular (mitral) valve to the point where it is no longer functional[1-9]. Spontaneously developing non-syndromic MMVD is primarily found in humans and dogs, although there have been indications that it can arise naturally in Fischer 344 rats and be induced by gene interference or surgical intervention in the mouse, pig, sheep and cow[1, 2, 10-18]. Disease typically presents clinically in older individuals and can result in valvular prolapse, regurgitation and backflow of blood into the left atrium, congestive heart failure and eventually death[2, 19-21]. It is the most common acquired cardiac disease of the dog, with almost all dogs developing some form of the disease over the course of their natural lifespan, and is a major cause of morbidity and mortality in this species[1, 2, 22-26]. MMVD occurrence in humans, both spontaneous and syndromic, is estimated at approximately 2%–3% of the global population and approximately 15% of those affected will require valve surgery[27-29]. Although key differences exist, there is a level of shared pathophysiology in spontaneous MMVD development between the dog and human so that research in both species is likely to be applicable to a broader disease understanding[1, 10, 11, 19, 22, 30]. Reference to MMVD has been present in the literature for well over a century and is even alluded to by Sir Arthur Conan Doyle in the adventures of Sherlock Holmes, for example when, in *The Sign of Four*, the neurotic Thaddeus Sholto confides that he has "grave doubts as to my mitral valve" [20, 31, 32]. However, despite the clinical significance and the long standing natural history of the disease, the underlying mechanisms for the development of disease in both species is poorly understood, especially

the events governing early disease development[1, 33]. Without this fundamental understanding, the advancement of new therapeutics that could halt the progress or reverse and cure MMVD has faltered. Currently, surgery is the only form of treatment in humans, whereas dogs almost exclusively only receive palliative treatment for the effects of the disease[20, 34, 35]. Research into the overall development of mitral valve pathology is therefore clearly warranted to allow for new perspectives and hypotheses to be generated that could eventually lead to improved outcomes in both humans and dogs. This study aims to investigate the biology of MMVD development in dogs.

1.2 Features of the normal and pathological canine valve

1.2.1 Normal valve structure

The mitral valve consists of two leaflets the anterior and posterior, which are also commonly referred to as septal and parietal respectively in veterinary science. These are connected to the heart by the annulus fibrosus, a highly fibrous ring encircling the entire mitral valve, which is made of dense collagen and elastin and acts (amongst other functions) to anchor the valve leaflets in place[2, 36, 37]. The leaflets are also connected to papillary muscles in the left ventricle by the chordae tendineae which are thin fibrous chords again composed of elastin and collagen bundles[2, 36]. The chordae attach either to the valve leaflet edge (first order), preventing prolapse during left ventricular contraction, or to the ventricular surface close to the valve edge (second order), helping to maintain valve geometry[2, 38, 39]. The latter's attachment results in a rough and irregular surface to the underside of the leaflets, while the atrial surface is smooth. There can be marked variation in chordae/papillary muscle organization, and such variation is regarded as normal[2]. Overall, the normal leaflet has a partially translucent appearance and is roughly divided into

proximal, mid- and distal zones, the latter also known as the 'free edge'[2]. The features described here are highlighted in **Figure 1-1**.

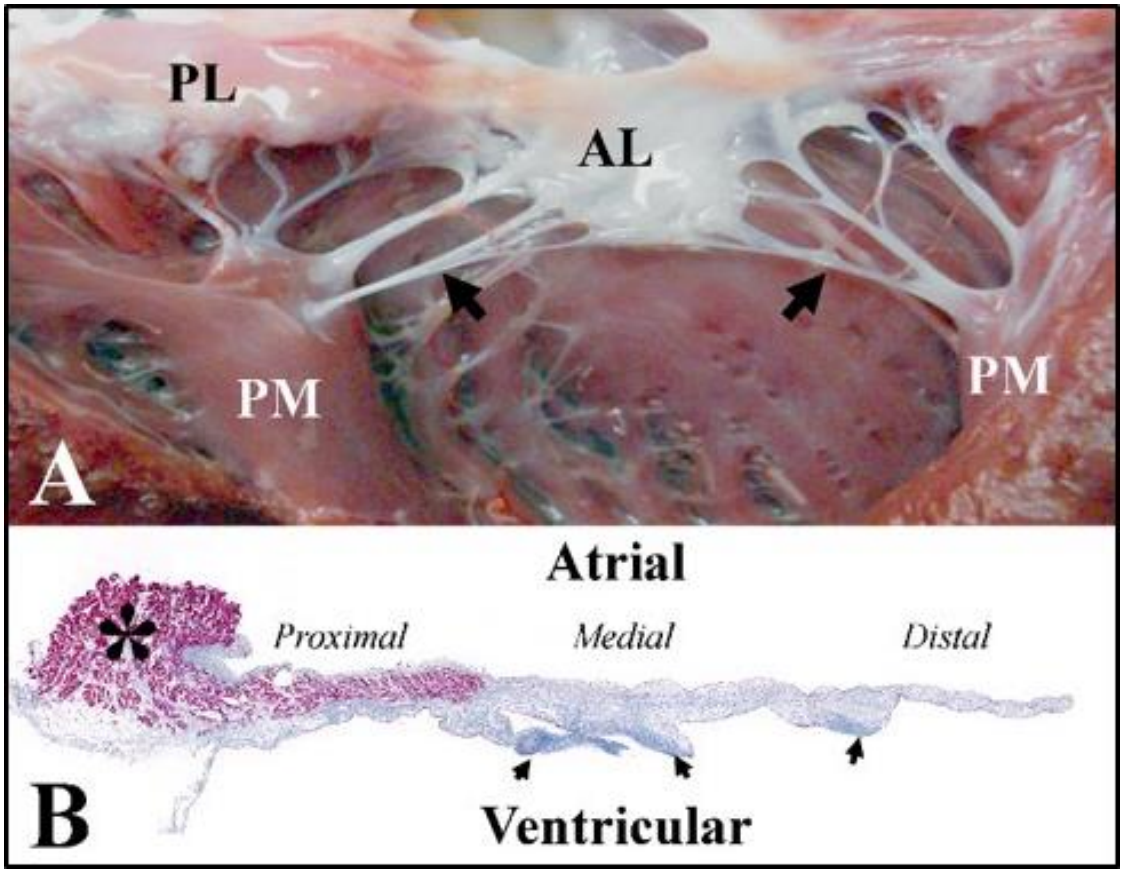

Figure 1-1. Healthy canine mitral valve. (A) Gross view of the valve after dissection. Note the presence of an anterior leaflet (AL), posterior leaflet (PL) and chordae tendineae (arrows) connecting the leaflets to the ventricular papillary muscles (PM). (B) Masson's trichrome stain of the anterior leaflet of the mitral valve, highlighting its two surfaces (atrial and ventricular), the proximal/medial/distal areas, the presence of myocardium extending into the base of the valve (*), and the attachment of the chordae tendineae. Note that all of the chordae included are of second order. Arrowheads indicate chordae. Taken with permission from Markby *et al* (2017)[2].

Each leaflet has an atrial and a ventricular surface and a single layer of valvular endothelial cells (VECs), continuous with that lining the atrium and ventricle,

covers each surface[2, 40]. VECs are attached to a thin basement membrane layer, which consists of a mixture of fibronectin, laminin, a small amount of collagens I, III, IV and VI and the basement membrane-specific proteoglycan, heparan sulphate[1, 36]. In the mid-zone, there are three identifiable layers: the atrialis, the spongiosa and the fibrosa. The thin atrialis contains some valvular interstitial cells (VICs) and is rich in elastin and highly-organised mature collagen fibres (types I, III, IV and VI), which support valve movement through extension and recoil[1, 2, 41]. VICs in normal valves have overwhelmingly a quiescent phenotype and operate in a homeostatic role, discussed later (section 1.3.2)[1, 2, 41-45]. The spongiosa, which contributes to valve structure and compressibility, consists of loose collagen fibres (I and III) and small numbers of thin elastin fibres. These are embedded in a ground substance rich in glycosaminoglycans (GAGs) such as hyaluronan, and proteoglycans, including large proteoglycans like versican and small leucine rich proteoglycans (SLRPs) such as keratocan and decorin [1, 2, 36, 37, 41, 42, 46]. The majority of cells in the spongiosa, and throughout the whole valve, are quiescent VICs, but there is also the presence of a small number of mast cells as well as adipocytes, with extension of atrial myocardial cells into the proximal/ base end of the valve (as seen in **Figure 1-1**)[1, 2, 36, 44, 47-49]. These myocardial cells extend from the atrial myocardium for a variable length along the valve leaflets, and this decreases with age, with likely important functional implications in valve mechanics[2, 47]. Immediately beneath the spongiosa is the dense well-organized fibrosa layer with predominantly well-defined collagen bundles (types I, III and V) and scattered VICs[1, 2, 36]. The fibrosa is continuous with the annulus fibrosus and branches off to form the core of the chordae tendineae[2]. The thin sub-endothelial layer on the ventricular side has collagen fibres and occasional elastin, and is suggested to be an additional fourth layer

(ventricularis) similar to that seen in the aortic valve[2]. The fibrosa and the ventricularis have a tensile role, protecting against prolapse from the strong haemodynamic forces during left ventricular contraction[2, 41]. Towards the distal zone (free edge), the distinction between spongiosa and fibrosa, at least in some dogs, can become indistinct and the valve at this level appears to consist almost entirely of spongiosa covered by endothelium[2]. These features are schematised in **Figure 1-2**.

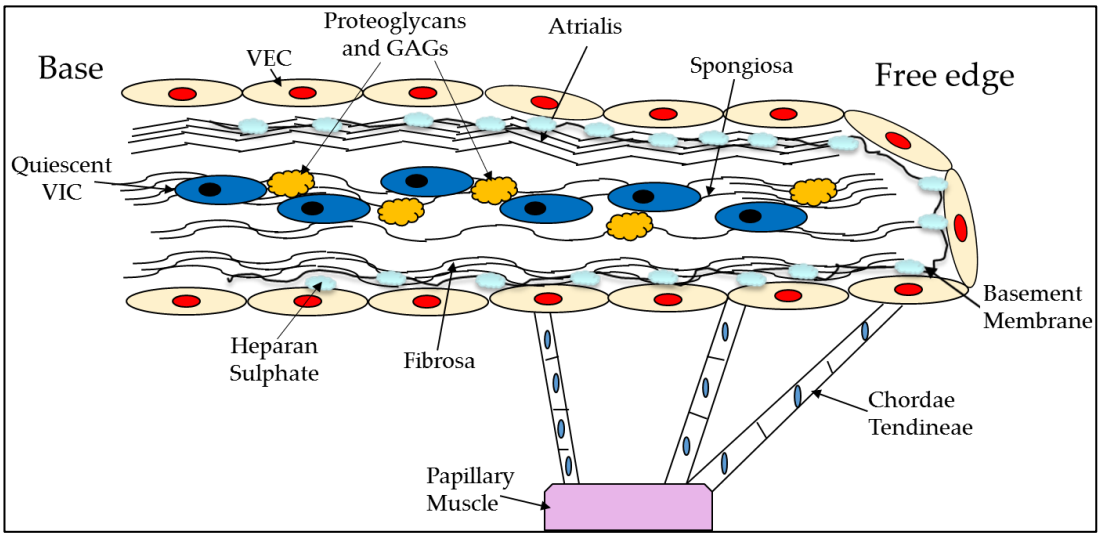

Figure 1-2. Schematic diagram of the normal mitral valve. Taken with permission from Markby *et al* (2017)[1].

1.2.2 Whitney grading and gross pathogenesis of MMVD

In canine MMVD, gross changes to the leaflets, including increasing nodularity, thickening and deformity, are thought to develop relatively slowly over the course of the dog's lifetime[2]. These changes are often classified according to the Whitney grading system, proposed by J.C. Whitney in 1967, and are graded 0 to 4 with 0 being normal and 4 the most advanced form of the disease[2, 4, 9, 11, 19, 50]. This simple system is based on the degree of nodularity, thickening and deformity of the valve and allows quick and straightforward categorisation of the severity of valve pathology. Furthermore, this system is

clinically relevant with a close association of the assigned grade to the degree of cardiac murmur, a cardinal clinical sign of MMVD[2, 49]. Typically, the disease starts with small numbers of discrete nodules developing on the free edge of the leaflet with intervening areas of translucent leaflet (grade 1), progressing to the development of larger nodules (grade 2), coalescence of these nodules (grade 3), involvement of the chordae and, finally, gross distortion and ballooning of the leaflets with marked chordal thickening and eventual chordal rupture (grade 4). An alternative method has been proposed for assessing the disease grade on dogs. This is based on measuring the thickness of the nodules on valves with 1-2.5mm thick nodules being early disease and >2.5mm nodules being late-disease, however given the variability in nodule size across a valve and the time required to make such measurements this method has not been widely adopted[43, 51]. Gross and histological images of each Whitney grade are shown in **Figure 1-3**.

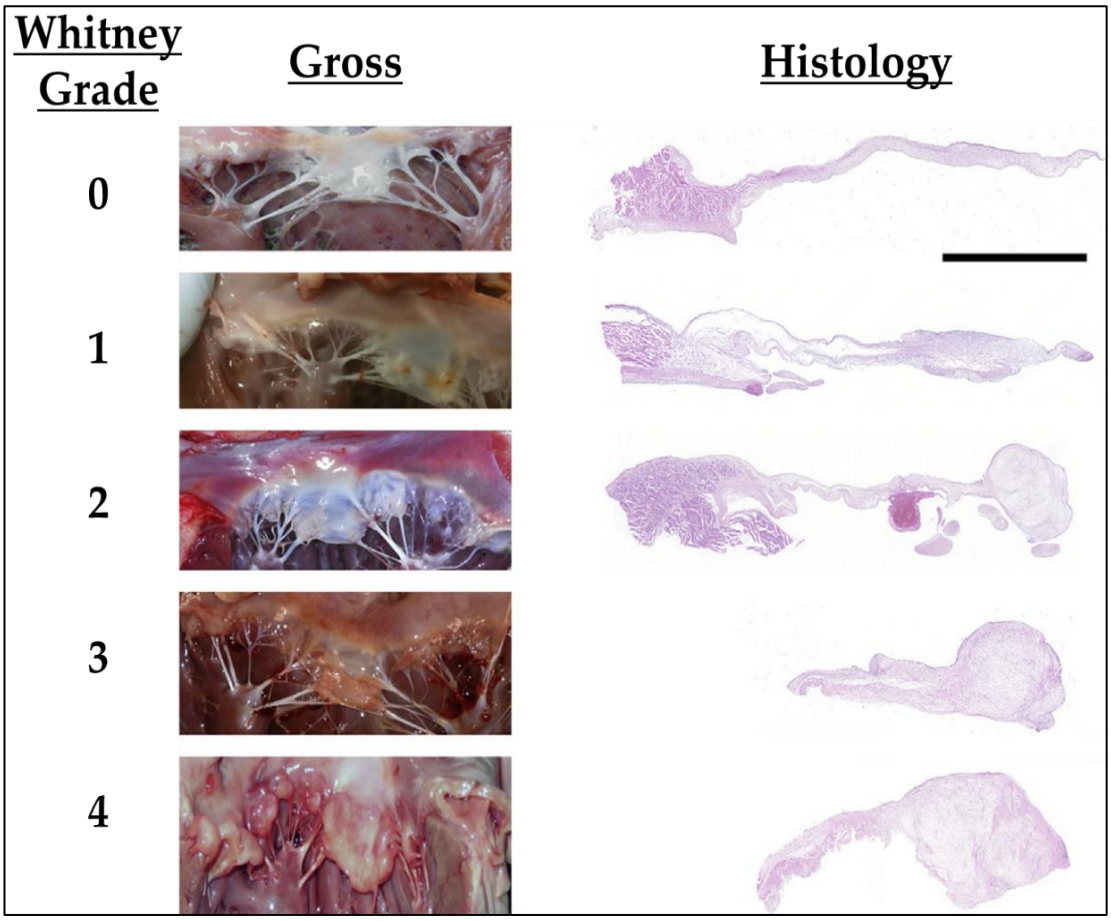

Figure 1-3. Whitney grading scheme for myxomatous valvular degeneration. Both the gross and haematoxylin and eosin stained histological presentations are illustrated. Histological images are all shown with the free edge (distal portion of the leaflet) on the right. Note the location of myxomatous nodules at the tip of the mitral leaflets. There is an increase in nodule size with grade, which results in marked distortion of the leaflet tip at higher grades. In grade 4, there is an evident thickening of chordae tendineae. Scale bar, 2 mm. Taken with permission from Markby *et al* (2017)[2].

Change in the thickness of the edge of the valve, associated with disease progression, has also been confirmed on histological samples, with the posterior leaflet being slightly thicker than the anterior leaflet in disease in the dog[2, 49]. Interestingly, while MMVD regularly affects both leaflets in the dog,

it mainly affects the posterior leaflet in humans[1, 5, 30, 52]. Additionally, in both canine and human disease, there is a lengthening of the valve with advancing disease as evidenced by the alteration in the ratio of the anterior-to-posterior leaflet length, but the anterior leaflet is always longer than the posterior leaflet, irrespective of disease severity[2, 49]. Chordal changes mirror those seen with the valve proper with swelling, thickening and eventual rupture, but chordal changes have not been reported in detail[2, 36].

1.2.3 Pathological valve structure and features

Myxomatous degeneration is typified by a disorganisation and dysregulation of the extracellular matrix. In canine MMVD this is seen with an expansion of the spongiosa and loss of the fibrosa and atrialis. In areas of myxomatous degeneration, the expansion of the spongiosa involves an increased presence of GAGs, proteoglycans, disorganised collagen fibrils as well as increased retention of water and amorphous metachromatically-stained mucoid material[1-3, 11, 19, 36, 42, 49, 53-55]. In depleted areas of atrialis and fibrosa, there is a breakdown of the ordered collagen and elastin layers, contributing to the eventual valvular incompetency due to a loss in tensile strength and ordered structure[1, 49]. Overall, depending on the grade of disease, there are also changes in laminin, elastin and collagens IV and VI in the sub-endothelium, and elastin, fibronectin and collagens I and II deeper in the leaflet[2, 56].

Alongside the breakdown of the valve extracellular structure, there are also cellular changes occurring during disease development. There is dysfunction and loss of basement membrane, which can also result in the loss and denuding of VECs[1, 2, 40]. Furthermore, it has been shown VEC loss can be exacerbated by the activation of endothelial-to-mesenchymal transition (EndoMT), a developmental pathway involved in the formation of valves,

which contributes to the VIC population[2, 57-59]. Perhaps most important of all is the activation of the VICs from a quiescent to a myofibroblast-like phenotype [1, 36, 40, 42, 43, 48, 60, 61]. It is the activation of VICs which is thought to play a pivotal role in the development of MMVD through the release of catabolic enzymes and the dysregulation of proteoglycan and collagen synthesis resulting in aberrant remodelling[1, 42, 43, 49, 60]. Further aspects of cellular changes will be described in more depth in section 1.3 and the pathological features are schematised in **Figure 1-4**.

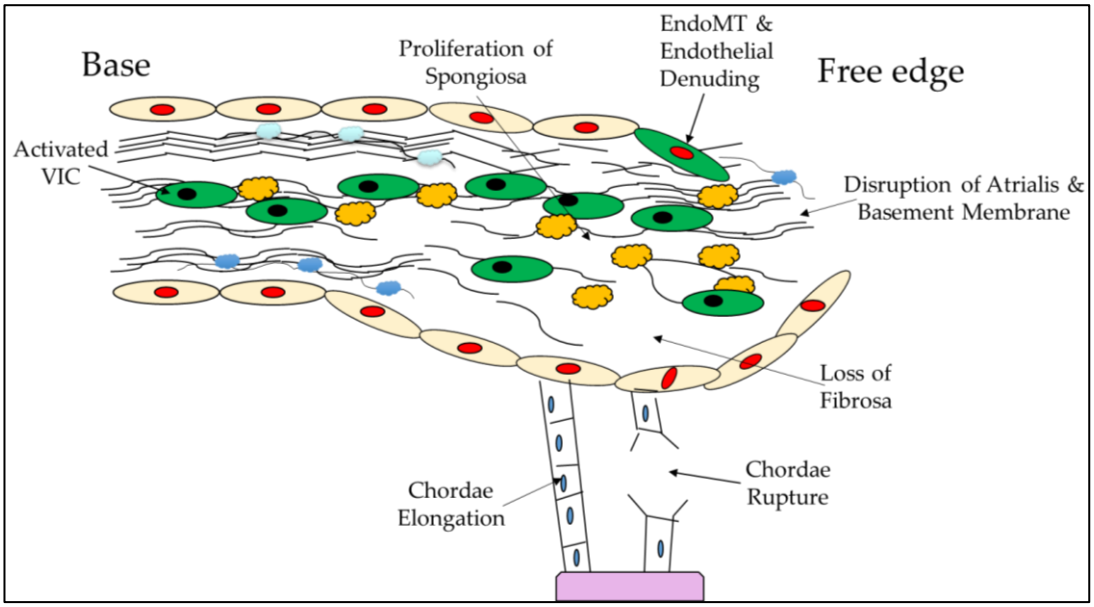

Figure 1-4. Schematic of pathological changes associated with MMVD. Taken with permission from Markby *et al* (2017)[1].

1.2.4 Normal and pathological valve haemodynamics and biomechanics

Despite their small size and relatively basic design, heart valves are critical for proper functioning of the heart. They experience a huge amount of stress over the course of an animal's lifetime, in the form of haemodynamic shear stress (which is caused by the force of blood flow passing over the valve) and biomechanical flexure (the force exerted whilst the valve is opening and closing) and tension (the force during coaptation just prior to ventricular

ejection)[62]. Of all valves, the mitral valve is required to deal with the greatest stress due to the higher pressures involved in left ventricular ejection[15]. Under normal circumstances, the valve should adequately accommodate these forces due to the structure and composition of the valve (described in section 1.2.1)[15]. However, these forces do have an effect on the valvular cells in the long term. VEC phenotype differs not only in general from other vascular endothelial cells, but also on whether they are on the atrial or ventricular side of the valve, where there are marked differences in exposure to shear stress force[63-66]. VIC phenotype can also be mechanically manipulated, both *in vitro* and *in vivo.* Exposure both to forces, such as tension, or to pathological flail (chordae rupture causing prolapse) can transiently induce a more activated VIC phenotype with the production of extracellular matrix components to compensate[67-70]. The fact that valvular cells show a plasticity in response to these forces supports the hypothesis that these forces could, in part, be responsible for MMVD development[71]. However, while the role of these forces in the chronic progression of MMVD is yet to be fully elucidated, it is an important consideration in MMVD pathogenesis, especially for studies *in vitro.*

1.2.5 Comparative pathology of canine and human MMVD

Spontaneously developing non-syndromic MMVD regularly occurs in both the dog and the human, with the dog proposed as a candidate model of disease in humans[1, 10, 11, 22]. Although broadly speaking the previously described (section 1.2.3) pathological features of MMVD are similar in both the dog and human, some key differences do exist. Spontaneous disease in the dog has been characterised as likely to be a single disease with the features described above, but the reason behind disease development unknown. In humans, both spontaneous and syndromic MMVD have been identified and the valvular

disease can also be a consequence of other diseases (such as rheumatic fever and bacterial endocarditis)[1]. Examples of syndromic MMVD include Marfan syndrome (caused by mutation of the *FBN1* gene), Loey-Dietz syndrome (caused by mutation of the *TGFBR1*, *TGFBR2*, *SMAD3*, *TGFB2* or *TGFB3* gene) and Ehlers-Danlos syndrome (caused by mutation of various genes including different collagens and *ADAMTS2* with some of these resulting in valvular pathology)[72-79]. Human spontaneous MMVD can be separated into two diseases; Barlow's disease and fibroelastic deficiency (FED)[1, 5, 21, 80-82]. Both include the development of myxoid lesions but differ in how they progress. FED is known to have relatively fast onset (months) affecting typically older individuals (>60 years old) and is a result of the deficiency in key connective tissue components including collagens, proteoglycans and elastin with chordae rupture being a common occurrence[1, 27, 80-82]. This deficiency results in prolapse typically of a single valve segment and it is at these areas of prolapse that myxoid degeneration can be found[81]. Barlow's disease, in contrast, has a much longer pathogenesis (years-to-decades), typically becoming clinically significant earlier in life (30-50s) but can also affect older individuals[81]. Like MMVD in the dog, Barlow's disease has an unknown aetiology but seems to predominantly involve a myxomatous degeneration affecting all layers of the valve and can be found in multiple segments at once[80-82]. Additionally, differences in microRNA expression between the two human conditions have been shown, indicating potentially different mechanisms controlling non-syndromic MMVD in humans[83]. Parallels can be drawn with MMVD in the dog from certain aspects of both diseases, such as the later age onset in FED or the longer pathogenesis of Barlow's[1]. However, important differences do exist including the preponderance for the development of fibrosis in particular and sometimes calcification in the human disease which is not observed in the

dog[1, 80, 81, 84]. Nonetheless, the level of similarity in the myxoid regions of the valve, such as the presence of activated VICs, between the dog and both human diseases would allow reciprocal and comparative research to be valuable as long as the caveats are taken into account when interpreting data[1, 10, 30, 82].

1.3 Cellular changes

1.3.1 Valvular endothelial cells (VECs)

Under normal circumstances, VECs play a critical role in acting as a barrier between the blood flow and the extracellular structure within the valve[63, 85]. They form a cobblestone-like smooth layer across the valve surface (**Figure 1-2**), easing blood flow across the valve surface, with tight cell-to-cell contact facilitated by the cell-to-cell adhesion protein vascular endothelial cadherin (CDH5) (often used as a marker for VECs)[40, 57-59, 63]. Other adhesion molecules involved include platelet endothelial cell adhesion molecule (PECAM1/CD31) as well as the glycoprotein Von Willebrand factor (vWF)[57-59]. Aside from acting as a barrier VECs also play an important role in interacting with the forces and factors in the blood pool as well as with the VICs internally in the valve[86-89]. Both shear stress to VECs and interaction of VECs with circulating cytokines and platelets have been shown to induce phenotypic changes in VICs[40, 48, 63, 90-92]. VECs have been shown to play a role in maintaining the quiescent phenotype of VICs even when these cells are under stress or undergoing activation[93, 94]. As discussed in section 1.2.3, normal VECs play a critical role in early valve development. EndoMT is the process by which endothelial cells undergo a transformation into a mesenchymal phenotype[95]. This involves the loss of the VEC markers and the expression of the mesenchymal markers such as α-smooth muscle actin (αSMA) and hyaluronic

acid synthase 2 (HAS2) as well as an increase in the expression of matrix metalloproteinases (MMPs)[41, 57, 96-101]. In valvular development, these changes facilitate the migration of VECs undergoing EndoMT into the hyaluronan-rich cardiac jelly, which allows for the elongation and expansion of the valve leaflets and population of the inner valve stroma with VICs[41, 58, 59, 62, 97-100]. This process is under the tight control of several different factors including NOTCH, vascular endothelial growth factor (VEGF) and members of the transforming growth factor β (TGFβ) superfamily including TGFβ1, 2 and 3 and bone morphogenetic proteins (BMPs) 2 and 4[41, 85, 96-98, 102-107].

Changes to the endothelium are clearly seen in MMVD. Scanning electron microscopy demonstrates areas of endothelial loss, cellular pleomorphism and increased numbers of surface micro-appendages[2, 40, 108, 109]. These changes are suggestive of basement membrane abnormalities, endothelial cell death and reactive changes in the endothelium in response to insult. Similar changes can be identified with transmission electron microscopy, with VIC accumulation in the immediate sub-endothelium[2, 48, 61]. Additionally, the denudation of the valvular surface allows for the interaction of circulating cells and cell fragments such as platelets, with the underlying valve structure and VICs[40]. Endothelial damage has also been detected with a clear reduction of expression in CD31 and vWF in canine MMVD, and further reduction as the disease progresses[2, 43, 57, 110]. The transition of VECs as part of EndoMT is also an important change in disease. It has been hypothesised for many years that repeated damage to the leaflet edge is likely to play a role in the aetiopathogenesis of canine MMVD and the localisation of lesions to the valve edge with demonstrable changes to the endothelium would support that assertion. Functional changes in canine valve endothelium have been identified, with increased nitric oxide (NO) synthase activity (i.e. expression

of NADH, NADPH reductase and diaphorase), increased endothelin (ET) receptor expression (associated with severity), sub-endothelial collagen degeneration and deposition of mucopolysaccharides[2, 109, 111, 112]. This suggests that NO and ET might contribute to the development of MMVD, as both have an effect on extracellular matrix production[112]. The migration and localisation of activated VICs towards the endothelium in MMVD may be a part of this process and would fit into the endothelial injury model of disease pathogenesis[2, 43, 44, 61].

1.3.2 Valvular interstitial cells (VICs)

VICs are the prevalent cell type and can be identified in all internal layers of the valve[2]. They can exist as a heterogeneous population in normal valves with five identifiable phenotypes: (1) embryonic progenitor endothelial/mesenchymal cells, (2) quiescent VICs (qVICs), (3) activated VICs (aVICs), (4) progenitor VICs (pVICs) and (5) osteoblastic VICs (obVICs)[45]. The embryonic progenitor cells arise from VECs undergoing EndoMT in the developing heart[2, 107]. Once the valve is formed, qVICs predominate and are thought to maintain valve structure and function (i.e. normal life-long valve remodelling) and inhibit angiogenesis in the leaflets. The qVICs are presumed to become activated to become aVICs in response to disease and injury, and then the latter regulates the pathobiological responses of the valve[113]. These two cell types are distinguished typically by assessment of the expression of *ACTA2*/αSMA, *MYH10*/embryonic smooth muscle myosin (SMemb) and *TAGLN*/Transgelin (SM22α) (*gene*/protein) with aVICs showing increased expression of these markers compared to qVICs[2, 43, 60, 114-116]. However, although expression of a marker indicates the aVIC phenotype, not all aVICs will express all markers at the same time, indicating different levels of differentiation capacity[2, 43, 110, 117]. Interestingly, all three of these proteins play

a positive role in cell contractility and it has been suggested that aVICs increase their expression of these proteins in response to the loss of valvular competence and integrity in disease acting to increase tensile strength[60, 61, 118-120]. In addition, SM22α also contributes to the migratory capacity of myofibroblasts[120]. Morphologically qVICs differ from aVICs *in vitro.* qVICs show an orthogonal, honeycomb-like organisation with an elongated morphology, and aVICs show a far more disorganised structure with varying morphologies including a large rhomboid ("fried egg") and a hyper-elongated morphology[45, 113, 121]. Also, in comparison to qVICs, aVICs show differential expression of metalloproteases, such as the MMPs and members of the ADAMTS family (a disintegrin and metalloprotease with thrombospondin motif) and other extracellular remodelling components, which is thought aid in their response to valve injury[1, 2, 27, 33, 60, 122-125]. Small numbers of desmin-positive VICs with chondroblast morphology (obVICs) can be seen in some diseased valves, but, as discussed in section 1.2.5, calcification is not a clearly identified feature of mitral valve disease in the dog[44, 45].

As stated in section 1.2.3, and importantly, there is a consistent phenotypic alteration of the VICs during MMVD pathogenesis from the quiescent to the activated (myofibroblast-like) phenotype. These αSMA-positive cells increase in number with disease progression and are located primarily in the sub-endothelium, with a preference for the atrialis layer[2, 43, 44, 48]. Throughout the diseased valve stroma many cells express SMemb, while some co-express αSMA and SMemb, with this dual expression suggestive of heightened differentiation capacity[2, 43, 110]. Increased expression of Ki-67 suggests there is cellular proliferation, but what contribution cell migration might make to the increased cell numbers in the sub-endothelium is unknown[110]. The contribution from the endothelium via EndoMT should also be considered[2, 57].

There are also data suggesting that aVICs in MMVD have an altered apoptotic mechanism with cells entering a pro-apoptotic state, but are not undergoing apoptosis[126]. The persistence of aVICs has been hypothesised as a mechanism for disease pathogenesis[45]. Irrespective of their origin or lineage aVICs are found to lie in areas of loose collagen bundles and can be seen to exude fibrillar collagen on electron microscopy, with many localised away from the central myxomatous areas and close to the valve edge[61, 108, 109, 127]. This change in cell phenotype and localisation coincides with disease progression with demonstrable temporal and spatial alteration in valve cellularity[43, 44, 110]. However, the increased numbers of SMemb-positive cells in the spongiosa, and to a lesser extent the fibrosa, suggests a distribution of aVICs throughout the entire depth of the affected valve[43]. The relative contributions of the SMemb and αSMA activated myofibroblast subpopulations to the overall disease process are unknown[2]. The SMemb-positive cells show a much greater expression of 5-hydroxytryptamine (5HT) compared with αSMA-positive cells. This is of interest considering the putative role of 5HT/TGFβ signalling in disease pathogenesis which will be discussed more in-depth in sections 1.5.1 and 1.5.2[43]. In the more advanced stages of the disease, VICs can appear more like smooth muscle cells in that they form syncytia and anchor to collagen bundles, and it has been suggested that this is to compensate for the reduction in valve tensile strength caused by disease[61, 108]. Coupled with this regionalisation of stromal cells, there is a reduction in cell number in overtly myxomatous areas compared with normal spongiosa, but there is no further change in cell numbers as the disease progresses[44, 109]. However, in both human and canine mitral valve disease, there is an increase in total cell number through the entire depth of the valve[44, 60, 114]. A confounding factor in interpreting changes in cell number is the increased thickness of diseased

valves compared with normal, and when cell numbers are indexed to area, there is, in fact, a decrease in cell density[49]. It is clear that there is a congregation of cells towards the periphery, close to the overlying endothelium and in areas of endothelial loss[43, 44, 48]. Experimental ovine valve injury models show the same effect[12, 14, 49, 61].

1.3.3 Other cell types

The exact identity of all cells present in myxomatous areas is not known, as some are both vimentin (VIC marker) and αSMA negative. However, in diseased valves, the majority of the cells throughout the valve are SMemb positive and this, coupled with αSMA expression in some cells and their spindle shape, indicates that they mostly have an interstitial phenotype[43, 44]. In human MMVD, some cells are CD34 and CD117 positive, suggesting a circulating fibrocyte, mast cell and/or stem cell lineage, but further work is needed to determine their precise phenotypes and to see if the same populations occur in dogs[128, 129]. Additionally, in recent studies an increased presence of macrophages and T-cells have been shown in human MMVD[130-132]. Furthermore, an involvement in immune-related pathways has been reported in transcriptomic studies in both humans and dogs[33, 131]. In dogs with advanced disease, there is evidence of a marginal increase in the number of mast cells in affected valves[44]. However, there is no evidence of the involvement of the resident macrophage population in disease pathogenesis, or recruitment of inflammatory cells, as evidenced by the lack of expression of CD68, CD11c, CD45 and MAC387[43, 44, 133]. This again is despite increased expression of gene transcripts encoding for several inflammatory cytokines and adhesion molecules[33, 110]. Electron microscopy has also failed to identify inflammatory cells in the stroma of diseased canine valves[61, 108]. Finally, there are adipocytes and myocardial cells, especially in the proximal third of the

valve. These cells increase in the valve as the dog ages, but this appears to be independent of the development of MMVD[36, 47].

1.3.4 Valvular cells in culture

Both VICs and VECs have been successfully cultured from a variety of different species including pig, sheep, mouse, rat, human and dog[42, 60, 88, 121, 134, 135]. *In vitro* study has provided valuable insight into both normal and pathological functions in these cells. For example; the identification of both the different VIC phenotypes and the sub-phenotypes in the aVIC population (section 1.3.2), the role of TGFβ as a potent activator of VICs in human VICs (section 1.5.1), and the effects of cyclic strain have on valvular cell phenotype (section 1.2.4) were elucidated using cell culture [45, 60, 69, 70, 85, 113, 136]. However, a major drawback of this approach to understanding MMVD pathogenesis has been the spontaneous activation of VICs in culture[45, 113, 137]. This has made deciphering the role of different factors in disease progression difficult and is a caveat that should be taken into account when interpreting the results from these studies. For example, all 'quiescent' porcine VICs will have transformed into activated myofibroblastic aVICs by passage 3-5 making long-term comparisons in culture difficult[138]. More recently, a study on human aortic VICs in 2D culture established a low serum protocol which maintained the quiescent phenotype, so allowing further study of this cell type in culture[138]. Using this low serum approach, simple 2D cultures can be used to test the effect of molecules of interest and allow for more credible studies comparing VICs isolated from normal and diseased valves.

1.4 Molecular and biochemical changes in MMVD

Molecular and biochemical changes that have been associated with MMVD have a focus, unsurprisingly, on the alteration to the extracellular matrix,

which is the key feature of MMVD (sections 1.2.3 and 1.3). Assessment of these changes has been made through the focused study of specific gene and protein changes, performed by RT-qPCR, immunohistochemistry or western blotting, and broader studies through transcriptomic and proteomic analysis. Expectedly, given the pathogenesis of the disease, a great number of these studies have concentrated on the extracellular matrix. Activation of VICs has been shown to be associated with the increased production of extracellular matrix which supports the hypothesis that this cell type is crucial to the development of MMVD (section 1.3.2)[1, 2, 43, 44, 51, 85, 114, 139, 140]. The extracellular matrix derangement may in part be due to altered expression of matrix metalloproteinases (MMPs), tissue inhibitors of MMPs (TIMPs), the ADAMTS family of metalloproteases as well as cathepsins (another form of protease)[27, 30, 33, 46, 114, 141-145]. As measured by immunohistochemistry in the dog with advancing valvular disease there is a decreased expression of the gelatinase MMP2, an increase in the cell surface bound MMP14 and an increase in TIMP2 and TIMP3[56, 124]. MMP14 is important in the degradation of collagens I, II and III and its presence in the valves of dogs with MMVD, but not in human diseased valves, probably reflects a dog-specific alteration in VIC phenotype[56, 124, 141]. Mice with cardiac-specific transgenic expression of active MMP2 developed marked mitral valve thickening and prolapse with a major loss of collagen bundles and a large accumulation of acidic GAGs, somewhat similar to the pathological changes observed in canine MMVD[56, 146]. MMP substrates can also include basement membrane components, and as mentioned previously (sections 1.2.3 and 1.3.1), disruption of the basement membrane is seen on transmission electron microscopy of diseased dog valves[48, 61, 147-149]. Interestingly, changes in gene expression (measured by microarray) for the MMPs and TIMPs in both human and canine MMVD do not always match

those seen on immunohistochemistry, possibly because of the transient nature of their expression. Of note in these microarray studies is an increase in *TIMP1* and *MMP12* (an elastase) gene expression[27, 33, 150]. Nevertheless, any change in the balance of catabolic enzymes and their inhibitors would cause valve remodelling. Gene and protein expression changes implicated in basement membrane disarray have been reported, including alterations in expression of genes encoding nidogen 1 (*NID1*), laminins 1 and 2 (*LAMA1* and *2*), collagens (*COL4* and *COL6*) and fibronectin[33, 46, 56]. Likewise, the cathepsin-encoding genes *CTSK* and *CTSS* are significantly up-regulated in diseased valves and in human MMVD aVICs, with these proteins having the same substrates as those altered in the basement membrane[33, 60]. While tissue protein expression of the ADAMTS peptidases has not been reported, there are interesting gene changes found in both human and canine MMVD[33, 131]. There is significant down-regulation of *ADAMTS2*, *ADAMTS19* and *ADAMTSL4* in diseased canine valves with ADAMTS2 and ADAMTSL4 proteins having roles in procollagen maturation and fibrillin-1 binding respectively, whereas the function of ADAMTS19 is currently unknown[33, 151, 152]. Likewise, down-regulation of *ADAMTS1*, *ADAMTS5* and *ADAMTS9* has been observed in human valves[131]. These dysregulated proteases seen in diseased human valves are involved in the cleavage of the proteoglycans aggrecan and versican, as well as some other extracellular matrix components. The knockout ADAMTS5 and haplo-insufficient ADAMTS9 mouse models, which target and clear the proteoglycans aggrecan and versican from the extracellular matrix, have also shown a MMVD phenotype[17, 18, 151]. Considering their function in pro-collagen maturation, deposition of the proteoglycan versican and regulation of fibrillin-1 and elastin production (Marfan syndrome) these changes in ADAMTS gene expression fit extracellular matrix changes seen in valvular pathology.

Alterations in proteoglycan and GAG deposition are also a prominent feature of mitral valve disease (section 1.2.3), but have been reported only to a limited extent in the dog[49, 109]. Increased proteoglycan content in canine valves has been inferred indirectly by using cell maceration scanning electron microscopy[153]. Reduction in fibrillar connective tissue components in human myxomatous mitral valve disease coincides with increased expression of GAGs[49, 53, 54, 154-157]. However, the relative proportions of the different GAGs also change with age in normal human subjects, and this is a confounding factor when considering disease-associated changes in a disease that is age-dependent[158, 159]. Proteoglycans and GAGs are necessary for the proper assembly of the extracellular matrix as they interact with other important structural proteins such as fibronectin and laminin and have a role in elastin fibrogenesis[160]. Hyaluronic acid is the most abundant GAG in mitral valves, but other proteoglycans particularly the SLRPs, are likely to have an equally important role in maintaining a healthy extracellular matrix[161]. SLRP gene transcripts have the highest signal intensity of all transcripts in normal and diseased canine valves and there is a significantly decreased expression of *CHAD* and *KERA* (encoding keratocan) in the canine valve[33]. Keratocan is of particular interest as it is important in collagen assembly. Decorin and biglycan are increased in the diseased canine valvular proteome and biglycan, decorin and the proteoglycan versican are increased in the extracellular matrix of human MMVD tissue[51, 55, 69, 161]. Decorin plays a critical role in collagen fibrillogenesis, while biglycan is found in both collagen- and elastin-rich regions and also influences elastic fibre formation[69, 162]. Elastin is particularly interesting as it has greater tensile strength than collagen and may contribute a disproportionately larger extent to valve mechanical integrity and strength[157]. An increase in elastic fibres has been reported in human and

canine myxomatous mitral valves, but the fibres are thinner than normal, are arranged into more distinct bundles, and the bundles are more widely separated than in normal leaflets[157]. The signalling pathways that drive all of these structural changes are complex and only partially understood.

Global valve tissue transcriptomic profiling has identified a wide range of gene changes associated with MMVD in man and dogs[27, 125, 131, 150, 163]. In the dog, cluster analysis of all gene changes suggested that the most affected biologically relevant functions are inflammatory/immune response, cellular movement, cardiovascular development, extracellular matrix organization and epithelial-to-mesenchymal transition (EMT), as well as the endothelial function pathways, caveolar-mediated endocytosis signalling, endothelin-1 signalling and epithelial adherens junctions remodelling[33, 150]. Caveolar-mediated endocytosis regulates endothelial cell growth, endocytosis and cell migration and reduces TGFβ-induced fibroblast activation[164, 165]. In canine and human MMVD there is increased expression of genes encoding inflammatory molecules such as vascular cell adhesion molecule (VCAM) 1, intercellular adhesion molecule (ICAM) 1, selectin E (SELE), Toll-like receptor (TLR) 4, TLR8, interleukin (IL) 18 and IL6, which can trigger ECM changes and EndoMT/EMT[33, 91, 125, 150, 163]. There is now evidence of a moderate increase in some immune-related cells in both canine and human MMVD valves (although not localised to the myxoid regions) (section 1.3.3). However what contribution these may have to the expression of these factors or to disease is unknown[44, 132]. Likewise, aVICs themselves have been implicated in the expression of some immune/inflammation-related genes including *IL6* and tumour necrosis factor (*TNF*)[45, 117]. Activation of low-density lipoprotein receptor (LDLR) has been reported in valves affected by MMVD, where this molecule is predicted to upregulate expression of a variety of inflammatory

mediators[33, 166]. An experimental mechanical endothelial shear stress model has been shown to generate reactive oxygen species (ROS) that act as intracellular secondary messengers and result in elevation of inflammatory cytokines, particularly ICAM-1[167]. The increase in expression of genes encoding IL6, IL1 and IL10, as well as the adhesion molecules VCAM1 and ICAM1, may represent a response to the endothelial damage associated with MMVD[40, 48]. Up-regulation of genes associated with oxidative stress has been identified in canine and human MMVD and the increase in inflammation-associated cytokines might be in response to ROS generated by endothelial shear stress[27, 33, 125, 131, 163]. All of these protein functions are not unexpected considering what is known about valve pathology. Groups of gene changes, which on first examination might not appear to have related functions, clearly contribute to valve pathology by affecting VEC function, transition and loss, VIC activation, proliferation and migration, catabolism of the ECM and aberrant remodelling, without inducing a fibrotic response in the dog[1, 2].

1.5 Current Hypotheses for disease development

Despite what is known about the pathological, cellular and molecular features of this disease the exact mechanism by which MMVD develops remains elusive. Many different effectors have been suggested, including ROS (including the metallothionein family), angiotensin II, BMPs, WNT/β catenin, TNF and shear/tensile stress[27, 30, 33, 42, 50, 71, 88, 90-92, 125, 131, 163, 168]. Perhaps most consistently, and convincingly, a role for TGFβ and/or serotonin (5HT) signalling has been shown for MMVD in both the dog and human[30, 60, 70, 71, 85, 103, 126, 130, 133, 136, 168-177].

1.5.1 TGFβ signalling

The TGFβ superfamily consists of thirty three different genes separated into sub-families including the BMPs, activin, nodal, growth and differentiation factors as well as TGFβ1, 2 and 3[178]. This superfamily is vital for many different cellular responses throughout the body[179]. Of particular interest in MMVD is the TGFβ1-3 sub-family[1, 2, 174]. These exogenous ligands exist in a latent form, bound to the latent TGFβ-binding proteins (LTBPs) in the extracellular matrix, where different stimuli, including proteolytic activity, mechano-sensing, integrins, thrombospondin-1 and ROS can release them in the active form[180]. Signalling is through TGFβ receptor 1 and 2 (TGFβRI and TGFβRII) dimerisation, as well as the potential involvement of endoglin (TGFβIII)[178, 179, 181, 182]. Both canonical (SMAD) and non-canonical (MAPK cascades (ERK and JNK/P38), JAK/STAT, PI3K/AKT and Rho-like GTPase) signalling can occur to induce a large variety of cellular processes many of which can be implicated in MMVD (summarised in **Figure 1-5**)[178, 179, 181-183]. With so many potential downstream targets, TGFβ signalling is under tight regulation and is also highly context specific to elicit the correct cellular response[178, 179]. Unsurprisingly, when this regulation is disrupted there are severe consequences, with TGFβ signalling already implicated in various diseases including fibrotic conditions and cancer[179, 184, 185].

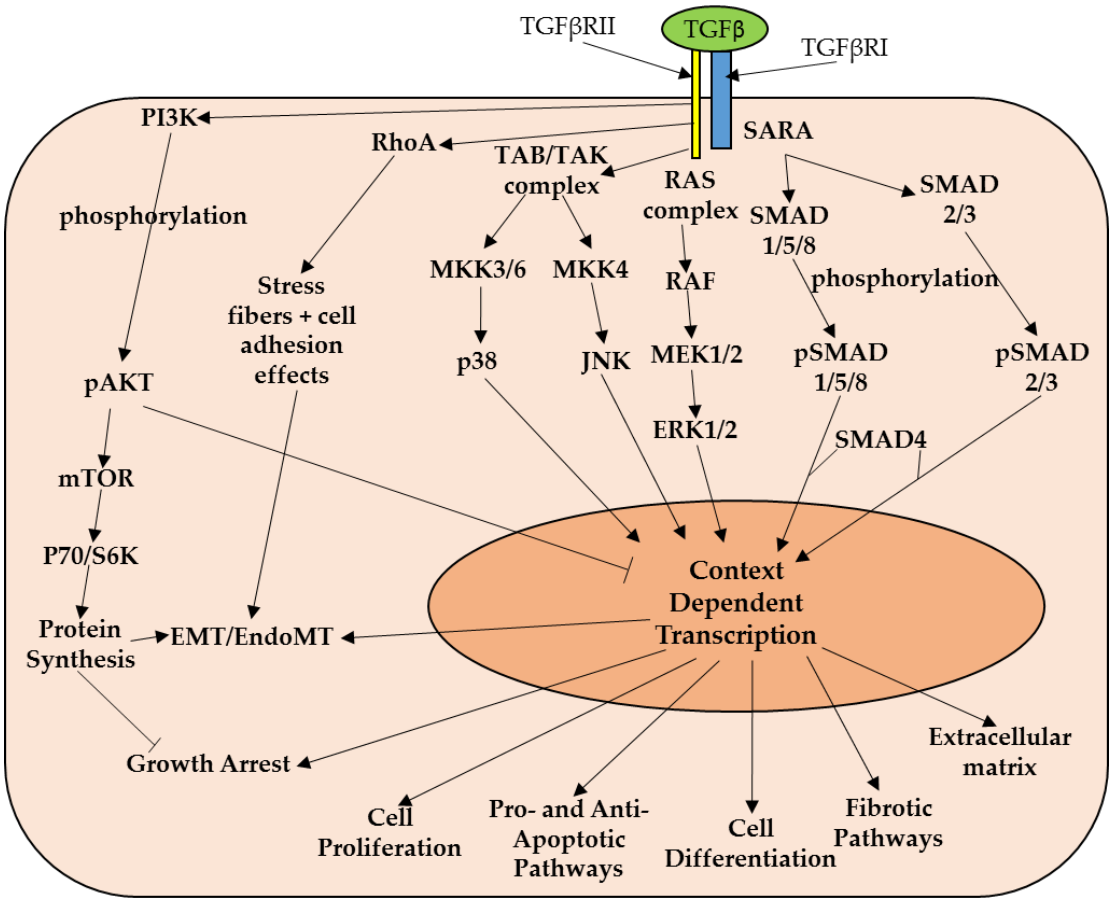

Figure 1-5. Overview of aspects of TGFβ signalling. This schematic diagram highlights just some of the signalling mechanisms induced by TGFβ signalling and their consequences. Adapted and amalgamated from Shi and Massague (2003), Zhang (2009), Poniatowski *et al* (2015) and Meng *et al* (2016)[178, 181, 182, 185].

TGFβ signalling has been repeatedly implicated in MMVD. As mentioned earlier, in syndromic MMVD in humans, TGFβ signalling is directly affected in Loeys-Dietz syndrome as well as indirectly in Marfan syndrome[73-76, 130]. Exogenous TGFβ1 and TGFβ3 are potent activators of VICs *in vitro* and TGFβ1 is regularly used to induce the aVIC phenotype for experimentation[45, 60, 85, 114, 117, 136]. In tissue samples, up-regulation of TGFβ1, TGFβ3, TGFβRI and TGFβRII has been detected at the protein level in canine myxomatous valves with *TGFB1* and *TGFB2* increased at the gene level[122, 124, 126, 133, 174]. Likewise, in

human MMVD, increased TGFβ1 has been detected in spontaneous diseased valves alongside increased phosphorylated SMAD2/3 indicating downstream signalling[130, 176]. Additionally, in human transcriptomic studies, TGFβ2 has repeatedly been implicated as an important component of disease progression[125, 131, 168]. However, in similar studies in the dog a direct involvement is yet to be shown[33, 143, 186].

1.5.2 5HT signalling

Serotonin or 5-hydroxytryptamine (5HT) is primarily considered a neurotransmitter important in the feeling of happiness, but has other important functions across the body including in cardiac development and function[169, 172, 187, 188]. 5HT is synthesised in the body through hydroxylation of tryptophan by the enzyme tryptophan hydroxylase (TPH)[189-191]. There are two isoforms of TPH termed TPH1 and TPH2, with TPH1 expressed in 'peripheral' tissues (gut, pineal gland etc.) and TPH2 expressed solely in the central nervous system[190, 191]. The majority of serotonin (90-95%) is synthesised by enterochromaffin cells in the gut by TPH1 and is released into the blood where it is taken up by platelets through the serotonin transporter (SERT) and circulated around the body[187, 189, 192]. Under normal circumstances in the cardiovascular system, 5HT can facilitate both vasodilation and vasoconstriction, depending on the receptors expressed on the vessel wall, as well as play an important role in platelet aggregation in response to a wound[187]. Signalling can either be through the 7 families of receptor or by direct uptake into the cell by SERT where it can then be metabolised by monoamine oxidase into 5-hydroxyindoleacetic acid[172, 187, 193].

5HT was first implicated in MMVD development after it was found that the appetite suppressing drug fenfluramine, which induces the release of 5HT as

well as binding to the 5HTR2 family of receptors, induced MMVD in a small but significant proportion of patients[194-196]. This effect was also recapitulated in rats treated with 5HT for several months[197]. Additionally, this association was also made in carcinoid tumours (which can affect the enterochromaffin cells) were approximately 50% of patients developed hyper-physiological levels of 5HT in the blood and 50% of these patients showed heart-related lesions[198, 199]. Since these associations were discovered, analysis of spontaneous disease has further connected 5HT signalling with MMVD. VICs have been found to express TPH1, indicating that local synthesis of serotonin and potential autocrine signalling is possible, with an increase in TPH1 expression found in MMVD valves from both dogs and humans as well as in VICs exposed to tensile strain[70, 133]. In conjunction with this, SERT was down-regulated in myxoid valves, which may allow for reduced clearance of 5HT and longer activation of receptor signalling[133]. Following these studies, 5HT was found to be significantly increased in dogs with MMVD, both in platelets and in mitral valve tissue[200]. SERT has further been implicated in disease, through a study of Maltese dogs which indicated that genetic variation in the exons of this gene may be associated with MMVD development[201].

The 5HT receptors that have been most widely associated with MMVD are the G-protein q coupled receptors 5HTR2B and to a lesser extent 5HTR2A[33, 131, 150, 170, 171, 173, 202]. The up-regulation of 5HTR2B in canine MMVD has been a primary driver for the 5HT hypothesis since it was detected in the first transcriptomic study and has been consistently shown in studies following this as well as in humans and rats[33, 71, 133, 150, 170, 171, 202]. Additionally, increased phosphorylation of ERK1 and ERK2, a downstream signalling target of 5HTR2B (as well as other pathways), is detected in MMVD valve tissue and in VICs treated with 5HT, demonstrating activation of 5HT signalling[71, 133, 171, 203]. However, 5HT

treatment of VICs, although capable of inducing cell proliferation and proteoglycan deposition is not capable of inducing a full aVIC phenotype on its own, at least in short-term culture[171, 203, 204]. This seeming lack of ability to fully induce disease phenotype has led to the speculation that 5HT produces disease phenotype by inducing TGFβ signalling[30, 71, 133]. 5HT induced TGFβ3 expression in the embryonic avian heart and TGFβ1 in ovine aortic VICs[169, 205]. 5HTR2B antagonism ablated TGFβ1-mediated porcine aortic VIC activation[206]. Furthermore, 5HT interacts with other pathways implicated in MMVD, such as angiotensin II signalling, and combined treatment with these factors induced MMVD in a mouse model and activated VICs in culture. The angiotensin type 1 receptor interacted with 5HTR2B directly[204, 207]. It may be the case that cross talk between various pathways is important in MMVD development.

1.6 Prevalence and breed association for MMVD

Almost all dogs will show some form of MMVD disease at necropsy if they live to an advanced age, with age being a major contributor to the prevalence of disease[4, 11, 50]. In Whitney's study which classified the grades of disease, it was observed that 9% of one year old dogs had grade 1 disease and 35% of dogs under the age of five years of age had grade one or two disease[4, 9]. However, only 3% of these were thought to be clinically significant, and in the vast majority of cases, the disease will not reach a clinically significant point[4, 9, 50, 208]. For MMVD to reach clinical significance in a dog it likely has to begin to develop earlier in life or the animal has to live for an exceptionally long time. It has been shown that 82% of dogs with Grade 1-3 disease will remain asymptomatic, defined as signs of mitral valve thickening with or without cardiac enlargement and the presence of a murmur without congestive heart failure or other signs of disease (described in section 1.7), for at least one year

before developing any clinical signs[209]. Indeed, it is worth noting that there appears to a large proportion of dogs that will remain asymptomatic and never develop clinically significant disease[210].

Although all dogs can develop disease, it is typically associated with small breed dogs (with a higher incidence of clinical significance in males) with a particular predisposition in toy dog breeds including the Cavalier King Charles Spaniel (CKCS), Dachshund, Miniature Poodle, Miniature Pinscher and Whippet[24, 166, 211]. This predisposition is thought to be related to the earlier development of disease in these breeds of dog, with a study in CKCS indicating that on average, clinical signs develop 6 years earlier in CKCSs than in other breeds[24]. While the high prevalence of a disease in a specific breed is not uncommon, the high prevalence of disease in several breeds with a shared trait suggests that the shared trait, in this case size, may be involved in the development of the disease. This could be through either morphological similarities (including skeletal and chest cavity size) or genetic similarities that may or may not be due to a shared ancestor[212]. There are some indications in both dogs and humans that the physical morphology of smaller individuals and the effect this has on chest cavity size may be responsible for the increased prevalence of MMVD, but this is yet to be fully explained[212-215]. Examples of genes that have been associated with small size include the genes encoding insulin-like growth factor 1 (as well as other genes encoding proteins that are associated with this protein) and SMAD2 (implicating TGFβ signalling)[212, 216-218]. GWAS studies aiming to determine variants that are specifically associated with MMVD have thus far been inconclusive. Three studies have been published; one in a cohort of CKCS associated two loci with MMVD, another in Whippets associated a different two loci and a third small study, again in CKCS, did not associate any variants significantly with MMVD[219-221]. This

indicates that MMVD is most likely polygenic and increased prevalence in these breeds may be multi-factorial.

1.6.1 Cavalier King Charles Spaniels

The breed that has been most associated with MMVD development is the CKCS[23, 24, 222, 223]. This is due to the early development of the disease with 10% of one year old dogs and 100% of dogs over 10 showing clinical signs[24]. This particularly high prevalence is likely to have arisen following inbreeding when, after the second world war, the breed numbers dwindled drastically. As a result, only 6 animals were used to propagate the breed resulting in a high level of homozygosity for alleles of genes involved in disease development. There are now 25 inherited diseases in this breed including (other than MMVD) syringomyelia, chronic fibrosing pancreatitis and cataracts[224]. In addition, CKCS have defects in platelet function (although there are conflicting reports of increased and decreased platelet aggregation in MMVD) and 50% of animals show macro-thrombocytopenia (giant platelet disorder)[225-227]. Dysfunction of platelets could be involved in the development of MMVD, especially considering their role as 5HT transporters and that forms of macro-thrombocytopenia in humans have resulted in early (3 years old) mitral valve surgery[228]. However, in addition to these defects, it has recently been shown that healthy CKCS have amongst 25 breeds, the highest level of circulating 5HT as well as showing greater elevated levels of circulating 5HT in CKCSs with MMVD, as with other breeds[200, 229]. Factors such as these could play a role in early MMVD development. Likewise, fundamental differences in CKCS valve morphology could be partly responsible for the disease. However, histopathological comparison of MMVD valves from CKCS and non-CKCS showed no difference, indicating a shared pathology in disease[110].

It seems likely given the current evidence that multiple factors may be responsible for early disease development in this breed.

1.7 Presentation and Diagnosis

Diagnosis of canine MMVD often occurs late in the disease development as dogs with low-grade disease appear healthy. Late diagnoses can also be due to owners mistaking signs of exercise intolerance as part of the ageing process and hence delaying presentation of dogs for veterinary examination. The first sign that may be noticed by an owner is coughing, which can either be the result of bronchial compression from the enlarged left atrium and ventricle or due to pulmonary oedema from mitral regurgitation[230, 231]. Once these signs are present the dog likely has advanced disease. For a clinician, one of the principal indicators of disease is the presence of a systolic murmur which worsens over time as MMVD develops[231]. Ultimately diagnosis can be made based on a variety of different factors including physical assessment (presence of signs such as heart murmur, exercise intolerance etc.), history (history of murmur or predisposing factors) and thoracic radiographs (for the presence of enlarged heart)[230, 231]. The gold standard, however, for confirmation of MMVD is echocardiography with this also being used to determine prognosis as the disease develops and helps classify the severity of disease in the dog[231, 232]. Classification is based on criteria set out by the American College of Veterinary Internal Medicine (ACVIM) (**Table 1-1**) and is used both to help distinguish whether an animal is asymptomatic (Stage A and B) and what treatment approach should be used[230, 231]. Broadly speaking, the same signs and diagnostic methods are also used in human disease, with particular emphasis given to echocardiographic assessment to distinguish what disease (i.e. FED, Barlow's etc.) is causing MMVD and its severity. These factors influence what the be the best clinical course of action to be taken is[233].

ACVIM Classfication	Description	Associated Grade
Stage A	No evidence of disease but predisposed	0-2
Stage B	Evidence of heart disease but no congestive heart failure	
	B1: No echocardiogrpahic/radiographic evidence of disease	2
	B2: echocardiogrpahic/radiographic evidence of left-sided heart enlargement	2/3
Stage C	Evidince of congestive heart failure	3-4
Stage D	End-stage disease with congesitve heart failure that is refactory to treatment	4

Table 1-1. ACVIM classification summary with associated Whitney Grade of disease. Green colouration indicates asymptomatic stages, orange colouration clinically significant stages. Adapted from Hezzell (2018).

In conjunction with these established diagnostic approaches, in the dog, the use of diagnostic and prognostic biomarkers has begun to be established. Typically this has been with the use of N-terminal pro-brain natriuretic peptide (NT-proBNP) and cardiac troponin I[234-236]. Both of these markers increase significantly in the blood of MMVD dogs. NT-proBNP in particular increases early in the disease (Stage B1) and continues to rise as disease progresses allowing it to be used prognostically[231, 234-237]. However, both markers have shown significant individual biological variability as well as breed variability making both interpretation and the use of reference intervals difficult[231, 234, 238]. Recently, attempts to find circulating microRNA biomarkers associated with MMVD have been made, but thus far results have been inconclusive in the four studies performed[239-242].

1.8 Treatment

Following diagnoses in humans, clinicians decide on the appropriate course of action depending on the individual patient's medical circumstances. This can include: 'watch and wait' (where regular check-ups are scheduled until disease advances to a stage when surgery is required), lifestyle modifications, administration of drugs such as ACE inhibitors, mitral repair (using

technologies such as the MitraClip, which clips the flailing portions of valve together to prevent regurgitation) or mitral valve replacement (where all or part of the valve is removed and replaced with either a mechanical or bioprosthetic alternative)[243, 244]. Surgical approaches have likewise been attempted in the dog to a limited extent. Both mechanical and bioprosthetic valve replacement has been attempted with bioprosthetics showing the best clinical outcome[244-249]. However, given the nature of this open heart surgical procedure, a high level of expertise and an associated high level of cost is required[244]. Currently, there is only one team routinely performing such types of surgery on canines and is unlikely to become a common occurrence in the near future[250-253].

Far more common practice in dogs is the use of palliative treatments to ameliorate the symptoms of MMVD by reducing cardiac load and to treat congestive heart failure. A range of drugs are used mainly to treat dogs in stage C and D of disease. This includes Benazepril and Spironolactone, an ACE inhibitor and aldosterone inhibitor respectively, that are used to reduce renin-angiotensin-aldosterone system (RAAS) activation. Furosemide, an inhibitor of sodium and potassium reabsorption in the kidney, is prescribed to provide diuresis in congestive heart failure to alleviate pulmonary oedema[244, 254-256]. One of the most commonly used drugs is the phosphodiesterase III inhibitor and calcium sensitiser, Pimobendan[257-259]. Alongside its use for treatment for stage C diseased animals, recent studies have shown that this vasodilator may help to prolong the period of time an animal is in stage B2 by up to 15 months[35, 260]. Likewise, a recent pilot study has found similar promising results for spironolactone treatment in extending canine life span[261].

1.9 Study aims and hypothesis

Although drug therapies exist for dogs with MMVD, there are currently no treatments that can completely halt or reverse MMVD. This is due to a lack of understanding of the fundamental processes involved in the cellular and molecular development of the disease. Previous studies have elucidated some of the processes potentially involved but none have been able to fully establish pathways causal in disease development. This is primarily due to a focus on the comparison of late-stage diseased samples with normal samples, omitting the early disease groups. By examining tissue encompassing the entire pathogenesis of disease (Whitney grade 0-4), a better understanding should be achieved. Furthermore, taking this information and testing it *in vitro* could lead to a greater appreciation of the role, different cell types play in disease as well as targeting specific pathways of interest for therapeutic exploitation. As such, this thesis aims to:

1) Investigate the molecular events occurring in each Whitney grade of disease. By studying disease in its entirety important pathways in disease development will be uncovered.
2) Investigate the molecular events within early diseased valves. This will allow for causal pathways in disease development to be identified.
3) Investigate the role of pathways of interest in VICs in culture. The proposition is that manipulation of the identified pathways will cause disease-related changes in VICs and elucidate the processes occurring *in vivo*.

It is hypothesised that clear and discernible changes in gene expression will occur dependent on the Whitney grade of the disease and will be related to MMVD development.

Chapter 2 Materials and Methods

2.1 Introduction

This project as a whole aims to understand the molecular reasons why MMVD develops. The broad central dogma of molecular biology states:

By studying the components of this model a researcher can begin to understand the molecular controls in a biological system. Transcriptomics, the study of the RNA repertoire in a sample, is a commonly used approach by researchers to investigate a biological system. It has the advantage of looking at the transcribed components of the genome giving a level of functionality over genomics (the study of DNA in a sample) but is less technically challenging and costly than proteomics (the study of all proteins in a sample)[262]. Two approaches for studying the transcriptome of a sample are gene expression microarray and RNA-sequencing (RNA-seq).

Expression microarrays were the first approach developed that allowed for transcriptome-wide analysis of a sample to be performed. They work with a simple and elegant approach where specific sequences of nucleic acids, that each represent a transcript of a gene, are repeatedly printed on a glass surface called a chip[263]. Each cluster of nucleic acid representing a transcript is called a probe. Initially the probes were complementary DNA (cDNA) copies of RNA transcripts cloned into plasmid vectors; currently, the probes are synthetic oligonucleotides targeted along the gene of interest. When fluorescently labelled reverse-transcribed cDNA produced from total RNA is hybridised with this chip the level of fluorescence from a probe can be measured and quantified as a raw signal[263]. This raw signal can then be normalised to the

other samples and to normalisation probes included on the chip. Comparisons of the level of signal for all the probes on the chips can be performed. For example, the Affymetrix Canine Gene 1.1ST array contains 590,097 probes, each of 25 base pairs, to cover the 27,681 genes in the CanFam 2.0 database (representing 24 probes/gene) allowing for the vast majority of the dog transcriptome to be analysed at once.

RNA-seq is a newer method that uses deep sequencing technologies to quantify the transcripts in a sample[264]. In this approach, fragmented RNA is converted into a library of cDNA which is then sequenced with the addition of specific linkers attached to the 5′ and 3′ ends of each fragment of cDNA. Sequenced fragments are then mapped back to the genome and the number of reads matching any part of the sequence of a specific gene is used to quantify the expression of that gene (the more reads the higher the expression)[264].

Although both technologies ultimately allow for a comparison of the transcriptomes between samples, both have their advantages and disadvantages. As a sequencing technology, RNA-seq offers far more in-depth analyses as it can detect the presence of sequence mutations, splice variants and transcriptional regulation [265, 266]. In addition, as there is no need for a pre-defined probe set, it is thought this approach is more suited to lesser studied organisms[267]. However, microarrays that do not rely on the original 3′ biased detection are able to be used to detect transcript variants and alternative splicing events and with the continued improvement in organism gene annotation, these discrepancies may be improving. Technically RNA-seq offers a greater dynamic range of detection with typically a lower background noise and no saturation point, unlike microarrays, which allows for the more accurate detection of lowly or highly expressed transcripts[264] (although the majority of transcripts will be unaffected by this). However, RNA-seq does

have its disadvantages particularly in the downstream analysis and bioinformatic interpretation of results which can be difficult and require large data storage capacities which is of particular concern with large or multiple datasets[264]. In contrast, as a longer standing approach the interpretation and analysis of microarray data has been simplified, requires less computing power and is approachable to most researchers. Moreover, at the time of starting this project, the cost of microarrays was substantially lower than RNA-seq allowing for a greater number of biological replicates to be run by this approach. For these reasons, microarray technology was chosen over RNA-seq to allow for analysis of multiple datasets by a relatively simple, validated and robust computational approach.

2.2 Tissue collection and processing

2.2.1 Tissue collection and disease grading

Full owner consent was given for all tissue samples collected during the course of this PhD project and ethical approval given by the Roslin institute. The majority of samples were recruited from animal's euthanised at the Hospital for Small animals (The Royal (Dick) School of Veterinary Studies, The University of Edinburgh, U.K.) for a wide range of medical and behavioural reasons and donated by the owner for research purposes. A small subset of the tissue samples collected were donated by Charles Rivers Laboratories (U.K.).

Collection occurred typically within 1 hour of euthanasia by intravenous phenobarbital overdose. After excision of the heart, the mitral valve was exposed by cutting through the left atrium and down the left posterior wall to the apex. The left atrium, ventricle and mitral valve were then briefly and carefully washed with cold sterile phosphate buffered saline (PBS) to remove any excess blood. The degree of disease on the valve leaflet cusps was assessed

grossly by at least two investigators with a Whitney grade being assigned to score disease severity confirmed by a veterinary cardiologist (MVB DipPharm, PhD MRCVS, Chair of Veterinary Cardiopulmonary Medicine)[4]. When possible, a photograph was taken of the valve *in situ*. The mitral valve complex (posterior and anterior leaflet cusps and chordae tendineae) was removed from the heart by cutting along the annulus to detach the leaflet cusps. The chordae tendineae remained attached to the leaflet cusps and were removed where they attach to the papillary muscles of the left ventricular wall. The mitral valve complex was again washed in a bijou tube containing cold sterile PBS to remove any remaining blood before processing for future work.

2.2.2 Tissue processing for RNA extraction, cell culture and dissection

Tissue samples to be utilised for whole valve analysis of gene expression were immediately stored in cold RNAlater (Invitrogen, U.S.A.). Samples were either proceeded immediately to RNA extraction (detailed in section 2.3.1) or were incubated at 4ºC overnight before long term storage at either -20 or -70ºC. Prior to RNA extraction any excess annulus, the chordae tendineae and any atrial myocardium were removed, leaving only the leaflet cusps and the remnants of the chordal attachments. Tissue samples used for whole valve cell isolation and culture were stored immediately in a 50 mL falcon tube containing cold sterile PBS. The Falcon tube was then placed immediately on ice and transported for cell isolation and culture (detailed in section 2.3.2).

A subset of normal valve samples and samples that were determined to have a Whitney score of grade 2 (areas of normal valve adjacent to visibly diseased areas) were used for regional analysis of gene expression. In this instance, the valve was stored in RNAlater as for whole valve analysis of gene expression. However, prior to RNA extraction valves were dissected into diseased and

normal areas of tissue. Valves were placed in a 10 cm^3 petri-dish and kept in RNAlater for the duration of dissection. Valves were examined under a light microscope (Leica Mx8 stereomicroscope, Leica Biosystems, Germany) with backlighting allowing identification of diseased regions. All areas identified as diseased (typically along the free edge) were dissected from one end of the valve to the other in a methodical manner and stored immediately in RNAlater. The remaining tissue was assessed as normal and both tissue samples were then taken forward for RNA extraction. Four normal valves also underwent this process with areas from the free edge dissected and compared as described in Chapter 5. The method for tissue collection and processing are summarised in **Figure *2-1***.

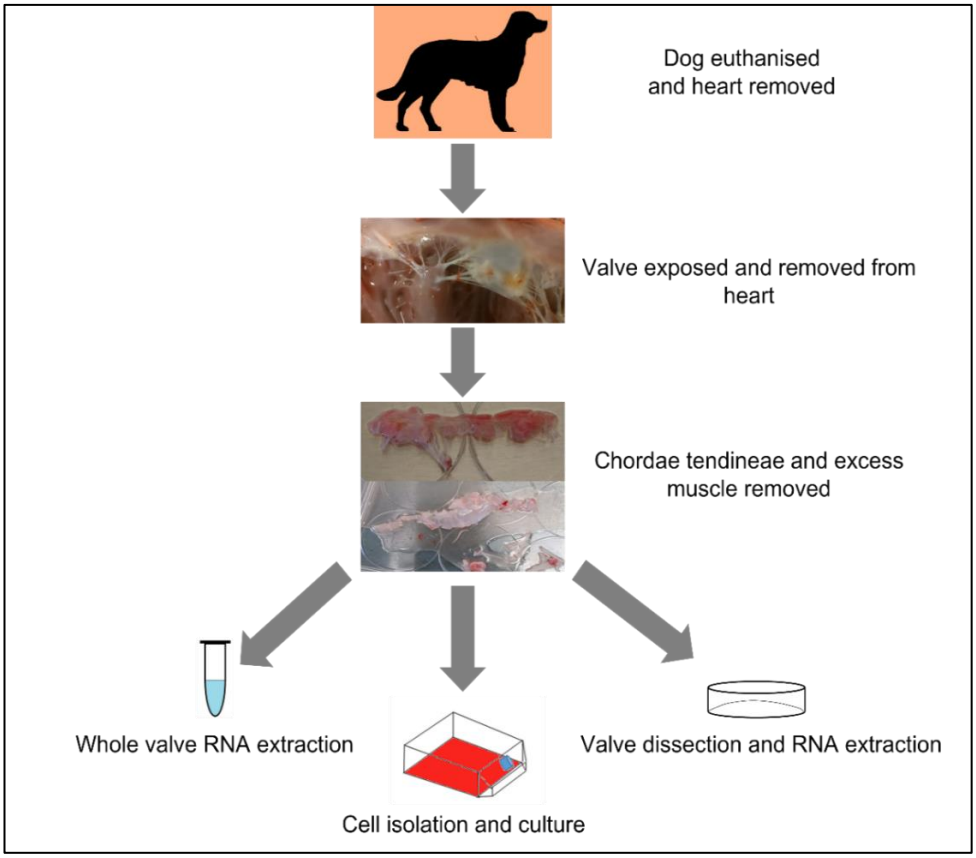

Figure 2-1. Summary of tissue collection process for valve tissue used for RNA extraction, cell culture and valve dissection.

2.3 RNA extraction and assessment

2.3.1 RNA extraction from valve tissue

Post processing, valve tissues (whole and dissected) were dried with tissue paper, separated into approximately 100 mg of tissue, placed in a clean Eppendorf tube and snap-frozen in liquid nitrogen. Tissues were disaggregated using a dismembranator (Braun Mikro Dismembranator, Braun Biotech International, Melsungen, Germany). The dismembranator equipment (steel ball lid and flask) was submerged in liquid nitrogen and allowed to freeze. Following this, 500 μL of Trizol reagent (Life technologies, U.S.A.) was pipetted into the dismembranator flask alongside 100 mg of frozen tissue and the steel ball before being sealed. This then oscillated in the dismembranator at 30 m/s for 120 seconds. Once macerated the combined frozen tissue/Trizol powder was thoroughly mixed with a further 500 μL of Trizol in a nuclease-free screw-topped Eppendorf tube and incubated for 45 minutes at room temperature. Samples were then centrifuged for ten minutes at 13,400*g* and at 4°C in an Eppendorf 5415R tabletop centrifuge (Sigma Aldrich, U.S.A.). The supernatant was carefully pipetted into a nuclease-free screw-topped Eppendorf tube and cell debris discarded. Two hundred microliters of chloroform (Fisher Scientific, U.S.A.) was mixed vigorously with the supernatant and then incubated at room temperature for 3 minutes, followed by centrifugation for 15 minutes as described previously. The aqueous phase was carefully pipetted, avoiding any phenol contamination from the interphase (illustrated in **Figure 2-2**), into a clean nuclease-free Eppendorf tube and mixed with equal parts of nuclease-free 70% ethanol (Fisher Scientific).

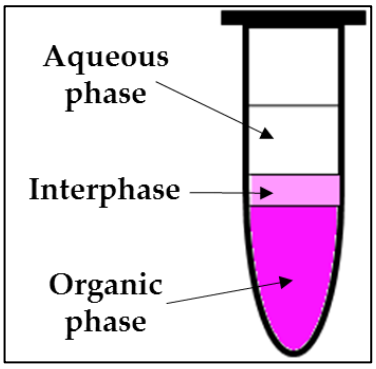

Figure 2-2. Illustration of the three phases in a phenol-chloroform extraction.

RNA extraction and DNA digestion were then performed using the Qiagen RNeasy mini kit as specified in the manufacturer's manual (Qiagen, Germany). The 1:1 ethanol-aqueous phase mix was pipetted, 700 µL aliquots at a time, onto the RNeasy mini column. The columns were then centrifuged at 8,000*g* for 15 seconds allowing the RNA in solution to bind to the column. The remaining solution was discarded. Three hundred and fifty microliters of buffer RW1 was then added to the column and centrifuged through the column, at 8,000*g* for 15 seconds, to wash out contaminants (such as proteins and carbohydrates). Eighty microliters of buffered DNAse I (Qiagen) was incubated on the column for 15 minutes at room temperature to minimise potential genomic DNA contamination. Another wash step with buffer RW1 was then performed as described previously. Two washes with 500 µL per wash of buffer RPE (to remove potential salt contaminants) were then performed with the first using a 15 second centrifugation at 8,000*g* and the second requiring a longer 2 minute centrifugation at 8,000*g*. The column was then spun at 13,400*g* for 1 minute to remove any carryover solvents. Total RNA was eluted in 30 µL nuclease-free water in nuclease-free, labelled 1.5 mL Eppendorf tubes by centrifugation at 8,000*g*. In cases where more than one 100 mg tissue segment was collected from a single valve, the RNA eluted from the separate columns was combined and stored at -70°C for downstream use. A

small number of samples used for transcriptomic analysis had been extracted as part of a previous project following the same protocol and stored at -70°C for no more than 2 years. These samples are indicated in the appropriate sections of Chapters 3 and 4.

2.3.2 RNA extraction from cells

Cells for RNA extraction were harvested by treating with TrypLE™ express (Thermo Fisher Scientific) for 5 minutes at 37ºC to dissociate cells from the flask surface. TrypLE™ express was inactivated with media and the cells were pelleted by centrifugation at 400*g* for 5 minutes in a Heraeus® Labofuge 400 centrifuge (Thermo Scientific, U.S.A.). Cells were re-suspended in 1 ml of sterile chilled PBS and pelleted by centrifugation at 5,000*g* for 5 minutes with the Eppendorf 5415R tabletop centrifuge in a nuclease-free 1.5 ml Eppendorf tubes. These pellets were stored at -70°C pending RNA extraction. Pellets were thawed on ice and re-suspended in 350 μL of buffer RLT (from Qiagen RNeasy mini kit) and then passed through the QIAshredder (Qiagen) homogenisation column, by centrifugation at 5,000*g*, in order to lyse the cells. The flow-through was then mixed thoroughly with 1 volume (350 μL) of 70% ethanol. RNA extraction with the Qiagen RNeasy mini kit was performed as described in section 2.3.1, and the eluted RNA was stored at -70°C until needed.

2.3.3 RNA quantification, quality assessment and quality control for microarray

Quantification of RNA was performed by spectrophotometry in the NanoDrop™ 1000 (Thermo Scientific). Absorbance at 260 nm wavelength was measured in 1 μL of extracted RNA solution. Ratios of absorbance (260/280 and 260/230) were also analysed to check for possible impurities that absorb at either 280 (proteins, carbohydrates etc.) or 230 (phenol for example) of the

sample. Ratios below 1.8 were viewed as contaminated and 2 as the ideal measurement.

To assess degradation of RNA the ratio of ribosomal 28S and 18S RNA was measured in samples. This was performed using the Agilent RNA Screentape system and Agilent 2200 tapestation analyser (Agilent Technologies, U.S.A.), following the manufacturer's instructions. This approach uses gel electrophoresis of the total RNA, quantifies the intensity of the 28S and 18S rRNA bands to calculate the 28S/18S ratio (with a ratio of 2 being regarded as minimally degraded). RNA integrity number (RIN), which scores the level of degradation on an arbitrary 1-10 scale, was then assigned with 10 being minimally degraded and ≥7 being taken as suitable for transcriptomic analysis[268]. In some cases, due to a lack of samples, the stringency of RIN ≥7 was relaxed as described in Chapter 3 section 3.3.2 and Chapter 5 section 5.3.1.

2.4 Cell isolation and culture conditions

Following collection, valves being used for cell isolation were transported immediately, in sterile PBS, to a cell culture hood and put into a sterile 10cm^3 plastic dish. Excess annulus and chordae tendineae were excised. The remaining valve leaflet tissue was incubated for 10 minutes at 37ºC in a 3.5 cm^3 sterile plastic dish with 3-5 mL of pre-warmed collagenase II (Invitrogen) (600 units/mL) dissolved in a low serum (2% v/v Fetal bovine serum (FBS)) Dulbecco's Modified Eagle Medium (DMEM) (Life Technologies) supplemented with 150 units/mL Penicillin/streptomycin, 2 mM L-glutamine, 50 ng/mL insulin and FGF-2 (10 ng/mL) which was added freshly to medium before use. Low serum medium with FGF-2 was used as this has previously been shown to prevent the activation of valvular interstitial cells (VICs) from a quiescent to an activated myofibrotic cell phenotype [138] and will be referred

to as DLF from now onwards. After incubation, the valve endothelial cells (VECs) were gently removed from the valve surface by rotating a sterile swab over the atrial and ventricular surfaces 5-6 times. The swab was dabbed in the collagenase medium to release the VECs; the remaining valve tissue was placed in 10-15 mL of the collagenase medium for VIC isolation. The VEC containing medium was then aspirated from the well and VECs were collected for use in other experiments not described in this thesis. VICs were isolated from the remaining valve tissue after VEC isolation. The leaflets were diced into the 10-15 mL of collagenase medium and incubated at 37ºC and 5% CO_2 for 18 hours. The valve tissue was then disrupted by pipetting and degraded tissue and cells were pelleted by centrifugation at 400*g* for 5 minutes in a Heraeus® Labofuge 400 centrifuge. VICs were re-suspended in DLF media and cultured in T75 flasks (Thermo Scientific) at 37ºC and 5% CO_2. VIC media was changed every 48-72 hours during propagation.

2.5 Affymetrix Canine Gene 1.1ST microarray analysis

2.5.1 RNA processing and Affymetrix chip hybridisation

The Affymetrix GeneChip™ Canine Gene 1.1 Sense Target (ST) Array plate was used for transcriptomic profiling of samples of normal canine mitral valves, each of the four whole valve disease grades, dissected valves comparing normal and adjacent diseased tissue and VICs cultures from both normal and diseased valves and under various treatment conditions. This was performed by Edinburgh Genomics (Edinburgh, U.K.). As informed by Edinburgh Genomics and summarised in **Figure 2-3**, 500 ng of total RNA was used per sample for analysis. Sample preparation was then performed using the WT Expression Kit (Invitrogen P/N4411974) and as described in the Ambion® WT expression kit manual (P/N 4425209 Rev. D) and the GeneChip™ WT Terminal Labeling and Hybridization User Manual (P/N 702808). First

strand cDNA synthesis utilised random primers with T7 promoter sequence to minimise rRNA contamination, which was followed by second strand cDNA synthesis. Following this, *in vitro* transcription was used to produce antisense RNA (aRNA) which was purified with magnetic beads and used in another first strand cDNA synthesis reaction with dUTP/dNTP mix. Sense strand cDNA was purified, again with magnetic beads, and following the Affymetrix terminal labelling kit protocol (Affymetrix P/N 900652), was treated with UTP-recognising endonucleases that fragmented cDNA. This was then labelled with Terminal deoxynucleotidyl Transferase (TdT) linked to biotin. 3 μg of this fragmented and labelled cDNA was hybridised to the Affymetrix GeneChip™ Canine Gene 1.1ST Array plate and scanned in the GeneTitan® multi-channel instrument (Thermo Fisher Scientific, U.S.A) following Affymetrix standard protocols. Results were reported as CEL files.

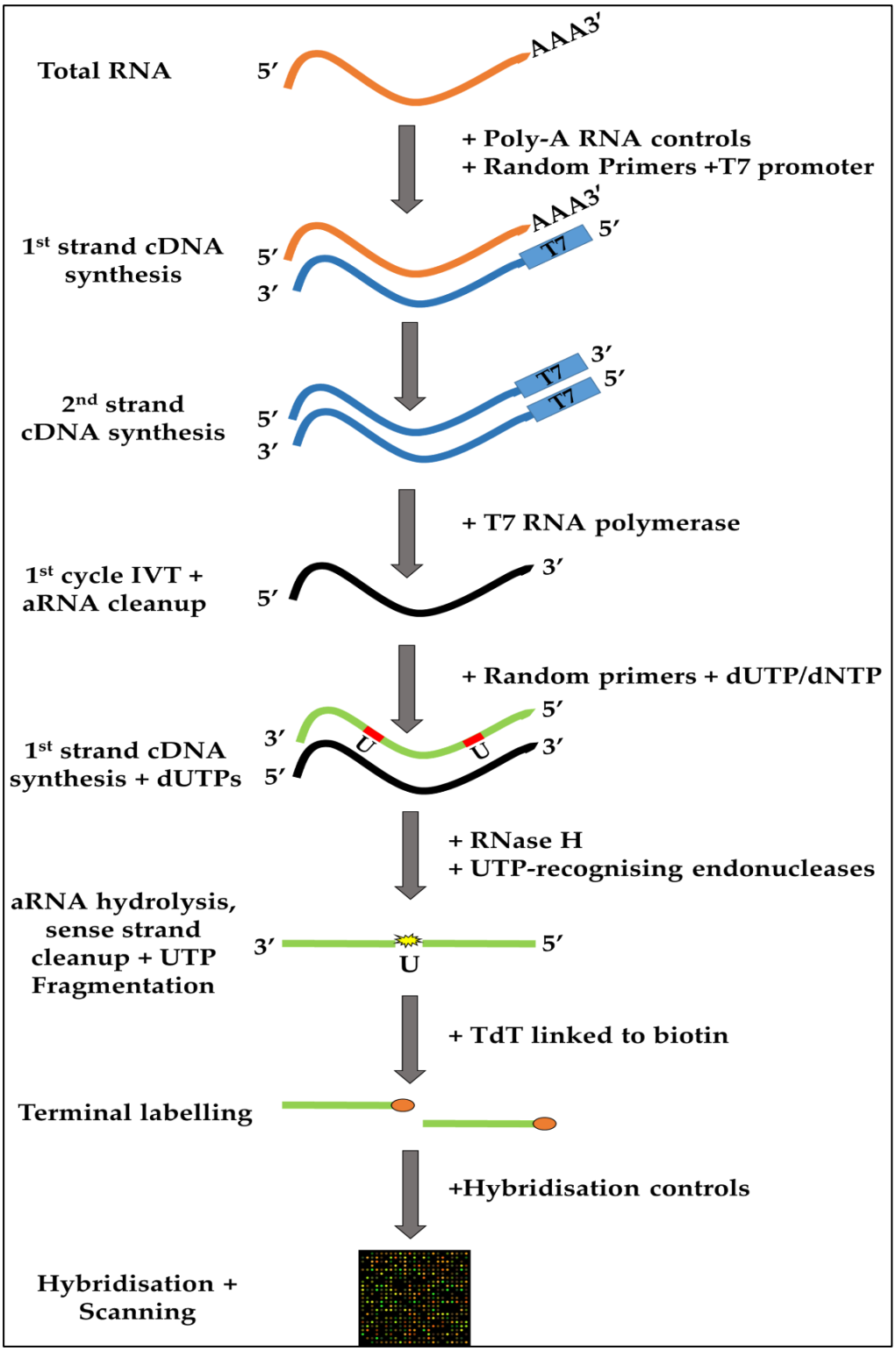

Figure 2-3 Schematic workflow of sample preparation for microarray analysis. Adapted from Ambion® WT expression kit manual (P/N 4425209 Rev. D) and the GeneChip™ WT Terminal Labeling and Hybridization User Manual (P/N 702808).

2.5.2 Post-hybridisation quality control and summarisation file creation

CEL files supplied by Edinburgh Genomics were opened in the Affymetrix expression console (version 1.4.1.46) using the canine 1.1ST library files from Affymetrix. Robust Multi-array Average (RMA) was used to perform gene-level normalisation and signal level summarisation[269]. Following this, quality control assessment was performed on the data set. This included assessment of hybridisation (spike in) controls, labelling (poly-A) controls and area under the curve (AUC) control, probe cell intensity boxplots, a signal histogram graph and, when possible, principle component analysis (PCA) plot. PCA plot creation was not possible in the initial microarray analysis (Chapters 3 and 4) due to a technical error made by Edinburgh genomics. Following this assessment, the datasets were exported with annotation as a text file or as a CHT file.

2.5.3 Transcriptome analysis console

Affymetrix transcriptome analysis console (version 3.1.0.5) was used to perform paired or unpaired one-way analysis of variance (ANOVA). Differentially expressed gene lists were created using the following criteria: P-value <0.05, log signal intensity >2.8, >3.5 or >3.8 (referred to in each chapter as appropriate) and fold change of >1.5 or <-1.5. When possible, the Benjamini-Hochberg false discovery rate (FDR) correction was applied (described in the individual chapters) uncorrected analysis was performed in Chapters 3, 4 and 6 with this described in further detail in these chapters. Algorithm information for un-annotated transcript probes was found in TAC through an interface with the Affymetrix online browser. Probe sequence could then be copied and BLAST analysis performed on the online browser at http://www.ensembl.org to try and manually match the probe to a transcript. A transcript was considered matched to a probe sequence and could be manually annotated

when the E-score was $<1x10^{-20}$ [33, 150] and other suggested transcripts did not meet these criteria. Gene lists could then be used for gene enrichment analysis.

2.6 Gene enrichment analysis

The following gene enrichment platforms were used to explore the transcriptome of the normal and diseased valves and cells. Their basis and function are briefly described.

2.6.1 Miru

Miru (version 1.4), now called Graphia Pro (Kajeka, U.K.), is a network analysis tool that allows for the visualisation of large data matrixes on 3D or 2D graphs[270, 271]. Miru works to cluster data based on similarity, with nodes on the graph representing a data point and edges (the connecting lines between nodes) representing the relation between nodes past a selected threshold Pearson correlation coefficient, laid out with the Fruchterman-Reingold algorithm. In a transcript-to-transcript analysis, nodes represent the expression of a gene across a sample set, and genes with similar expression patterns will be placed close to each other in the network layout. In a sample-to-sample analysis, the data is transposed, and nodes represent the expression of all genes in a sample allowing the similarity of samples to be identified. Both the gene-to-gene and sample-to-sample analysis were performed with the Pearson correlation coefficient stated in each results chapter. To further delineate genes with similar expression in the network, Markov Clustering (MCL) with an inflation stated in each chapter and a minimum cluster size of 5 genes was used. The similarity of expression can then be used to infer possible functional roles of these clustered genes. Cluster data could then be exported as a text file for further analysis.

2.6.2 Database for Annotation, Visualization and Integrated Discovery

The Database for Annotation, Visualisation and Integrated Discovery (DAVID v6.8) (http://www.david.ncifcrf.gov) is a browser-based gene enrichment tool that takes gene lists and predicts the biological processes that are associated with the genes in the list using the gene ontology (GO) terms. Gene lists deriving from differential expression analysis (section 2.5.3) or Miru clustering (section 2.6.1) were uploaded to DAVID for analysis. Gene ontology (GO) terms were selected for biological processes (GOTERM_BP_DIRECT), cellular components (GOTERM_CC_DIRECT) and molecular function (GOTERM_MF_DIRECT) and summarised in the functional annotation chart with GO term, genes names associated with GO term, number of genes, P-value of association and FDR value of association recorded. These were the only GO terms selected to try and remove redundancy from DAVID analysis.

2.6.3 Ingenuity Pathway Analysis

Ingenuity Pathway Analysis (IPA) (Qiagen) is a commonly used tool to analyse transcriptomic data. Differentially expressed gene lists were uploaded with related fold change to the online IPA server where core analysis was performed. This compared the submitted genes to all published literature and assigned reported attributes and pathways to them. From these canonical pathways, upstream regulators, disease and biological functions, as well as other factors were inferred by the software. These results were generated based on the number of genes in the submitted list that matched the genes reported in the literature to be involved in a certain process, with a statistical association calculated. Core analysis was performed with default settings on filtered gene sets. In some instances, gene names were not accepted by IPA and alternative names had to be submitted; some genes (often encoding novel proteins) were not accepted by IPA.

2.6.4 Gene list comparisons

To identify genes that either shared or did not share differential expression in different datasets and in pathways the INDEX function provided by Microsoft Excel (Microsoft Corporation, U.S.A) was used. The function is as follows:

=INDEX($Column of Gene list A$First cell of Gene list A:$Column of Gene list A$Final cell of Gene list A,MATCH($Cell of Gene list B,$First cell of Gene list A:$Column of Gene list A$Final cell of Gene list A,0))

This function was repeated to cover all cells for Gene list B. Venn diagrams based on the shared and differential genes were then produced in Microsoft Powerpoint (Microsoft Corporation). Genes that were identified as being matches in both datasets could then also be used for further gene enrichment analysis as described in sections 2.6.2 and 2.6.3.

2.7 Real-time quantitative Polymerase Chain Reaction

2.7.1 Complementary Deoxyribose Nucleic Acid synthesis

Reverse transcription of mRNA to complementary DNA (cDNA) was performed using the Superscript™ III RT kit (Invitrogen) according to manufacturer's recommendations with RNaseOUT recombinant RNase inhibitor (Invitrogen) treatment to remove RNase contaminants. For each reaction, 1 μg of total RNA was mixed with 1 μl random primers (Invitrogen), 1 μl 10 mM dNTP mix (Invitrogen) and made to 10 μl with nuclease-free water in a nuclease-free micro-centrifuge tube. RNA secondary structure was denatured by incubating at 65°C for 5 minutes followed by 1 minute on ice. Four microliters of 5X first strand buffer (Invitrogen), 1 μL 100 mM DTT (Invitrogen), 1 μL RNaseOUT recombinant RNase inhibitor (Invitrogen) and 1 μL of Superscript III reverse transcriptase (RT) (200 units/μL) (Invitrogen) were added to each reaction tube, mixed by pipetting and briefly centrifuged.

Reactions were incubated at 25°C for 10 minutes, 50°C for 50 minutes and 85°C for 5 minutes. Synthesised cDNA was then separated into 5 µL aliquots and either used immediately for amplification by PCR or stored at -20°C.

2.7.2 Primer design

Expression levels determined by microarray were validated using Reverse transcription quantitative PCR (RT-qPCR). For genes of interest and reference genes, exon sequence transcripts were found using CanFam 3.1 genome assembly (http://www.ensembl.org). The cDNA sequence was copied into primer3 browser-based primer design tool (http://www.primer3.ut.ee) and parenthesis ([]) were inserted in the sequence at intron junctions (so that primers were located outside the bracketed area) to enable intron spanning primer selection. Parameters for primer design were kept as standard except that GC content set to 40-60% and product length set to 70-250bp. Primers of optimum suitability were selected from those suggested by primer3 and were BLAST searched against the CanFam 3.1 genome assembly to check for off-target binding sites. Primer sequence and amplicon size are provided in the following chapters. Suitable primers were ordered from Eurofins Scientific (Luxembourg).

2.7.3 RT-PCR

As an initial screen of the suitability of primers standard reverse transcription PCR (RT-PCR) was performed to allow for analysis of PCR product by gel electrophoresis (checking expected product length, primer dimerization and off-target products) and sequencing. Using the Hotstar *Taq* polymerase kit (Qiagen) a master mix containing; 3 µL 10X buffer, 1 µL 10 mM $MgCl_2$, 1 µL 10 mM dNTPs mix (Invitrogen) and 20.25 µL nuclease-free water per sample was made and mixed in a nuclease-free Eppendorf tube. This master mix was

pipetted (25.25 μL per tube) into thin-walled PCR tubes, and 1.5 μL of 10 mM forward and reverse primer mix, 3 μl of cDNA (section 2.7.1) and 0.25 μL Hotstar *Taq* polymerase was added and mixed; reaction tubes were briefly centrifuged before PCR. PCR reactions were performed using the G-storm thermal cycler (Labtech international, U.K.) and reaction conditions were as follows: 15 minutes 95°C, 32 cycles of 95°C for 30 seconds, 60°C for 30 seconds and 72°C for 20 seconds with a final extension at 72°C for 10 minutes. Samples were either stored at -20°C or used immediately for gel electrophoresis.

2.7.4 Gel electrophoresis

cDNA samples and a 100bp ladder (Promega, U.S.A.) were prepared for loading by mixing 5 μL with 1 μL 6X blue/orange loading dye (Promega). UltraPure™ Agarose (Invitrogen) was used to prepare a 2% gel by dissolving powder by heating in 1X TAE (40 mM Tris base, 2 mM sodium EDTA, pH 7.2 with glacial acetic acid solution. To visualise DNA, 1 μL/10 mL Gel red™ (Biotium, U.S.A.) was mixed with agarose prior to pouring the gel. When set, the gel was placed in a Horizon gel electrophoresis system gel tank (Life-technologies, U.S.A.) and covered with 1X TAE solution. Following this samples were loaded onto the gel and the tank was attached to the Bio-Rad model 200/2.0 power supply and run at 75 V (constant voltage) for one hour before visualisation and image capture under UV light on the Gel logic 200 imaging system (Kodak, U.S.A).

2.7.5 RT-qPCR and relative gene expression quantification

RT-qPCR was performed using the Takyon 2X low Rox SYBR green mastermix dTTP blue (Eurogentec, Belgium) following the manufacturer's recommendations. Positive assays were performed in triplicate with a no-template control for each sample on clear 96-well plates. Per well, 10 μL of

Takyon™ mastermix (see Eurogentec for reagent list), 4 µL of forward and reverse primer mix (final concentration 100 nM for each primer), 3.5 µL nuclease-free water and 2.5 µL cDNA (1:10 dilution of synthesised cDNA; section 2.7.1) were mixed. The plate was centrifuged at 453*g* for 3 minutes in the Eppendorf 5810R centrifuge (Thermo Fisher Scientific). qPCR was performed on the Stratagene MxPro MX3000p (Agilent Technologies) under the following conditions: 95°C activation for 10 minutes, 40 cycles of 10 seconds at 95°C, 20 seconds of primer specific temperature annealing and 20 seconds at 72°C. Results were analysed using MxPro version 4.1 software (Agilent Technologies) and Microsoft Office Excel 2013. In brief, a gene's expression was measured at the cycle at which the fluorescence from the SYBR green mastermix became detectable above the background Rox fluorescence. The relative expression for genes of interest was calculated using ΔΔCt method with normalisation to the reference genes *MRPS25*, *GAPDH* and *RPL32* geomean expression. The primer sequence, amplicon size, primer efficiency and TMºC (see section 2.7.6) for reference genes are given in **Table 2-1**.

Gene Symbol	Forward Primer Sequence	Reverse Primer Sequence	Product Length	Optimum TM ºC	Primer Efficiency %
GAPDH	5'GGGAAGATGTGGCGTGAC3'	5'GAAGGCCATGCCAGTGAG3'	123	59	102.1
MRPS25	5'TCTTGGGGAAGAACAAGGAA3'	5'AGTGGGCTGGGTGAGAAAG3'	72	60	107.6
RPL32	5'GCAGCATTGAAGTTAACCGC3'	5'TCTCCTTGCACACACCTTCTCA3'	147	60	103

Table 2-1 Reference gene primer sequences used for normalisation in this thesis.

2.7.6 Primer efficiency

To determine the suitability and optimum annealing temperature for each primer, primer efficiency reactions were performed. cDNA samples diluted 1:10, 1:100 and 1:1000, were set up in triplicate for each primer on 96 well plates

which allowed for the generation of a standard curve in MxPro version 4.1. Ct values were plotted on the Y-axis and cDNA dilution was plotted on a logarithmic scale on the X-axis. The slope generated from this was converted from Log to standard and efficiency rate calculated. All primers fell between 90 and 110% which is generally accepted as a suitable range.

2.8 Western blotting

2.8.1 Cell protein extraction

Cells were harvested either by displacement with TrypLE Express (Thermo Fisher Scientific) or by cell scraping, after which any excess media was removed and cells were suspended in 1 mL cold PBS in a 1.5 mL Eppendorf tube. Cells were pelleted by centrifugation at 2300*g* in the Eppendorf 5415R tabletop centrifuge. Supernatant was removed and the cells were either snap frozen and stored at -70ºC or processed immediately. Cells were lysed using urea lysis buffer (7 M urea (Sigma-Aldrich), 0.1 M DTT (ITW, U.S.A.), 0.05% (v/v) Triton X-100 (Sigma-Aldrich), 25 mM NaCl and 20 mM HEPES pH 7.6 (Sigma-Aldrich)) by mixing 30-100 µL with the cell pellet and incubating on ice for 15 minutes and then centrifuged for 15 minutes at 16,000*g* in an Eppendorf 5415R tabletop centrifuge. The protein-containing supernatant was then either stored at -70ºC or used immediately for analysis.

2.8.2 Protein quantification

Protein concentration was quantified using the quick start Bradford assay (Bio-Rad.). An eight-point dilution series of bovine serum albumin (BSA) (Bio-Rad) ranging from 2 mg/mL to blank dH_2O was made and pipetted in triplicate on a clear-bottomed 96 well plate in 5 µL aliquots. Protein samples were diluted 1:10 and then 5 µL aliquots were pipetted in duplicate onto the 96 well plate. 250 µL of 1X Bradford reagent (Bio-Rad) was added to wells

containing standard or sample and incubated at room temperature for 5 minutes. Absorbance was measured at 595 nm on the Victor3 V1420 Multilabel Plate Counter (Perkin Elmer, U.S.A.). Samples were quantified against the standard curve generated from absorbance reading from the BSA dilution series. Calculations were performed using Microsoft Office Excel software.

2.8.3 Gel Electrophoresis

Thirty micrograms of protein from the sample lysates was resolved by sodium dodecyl sulphate polyacrylamide gel electrophoresis (SDS-PAGE). Typically, 10% resolving gels were used in protein analysis. Gels were prepared using the Bio-Rad Protean III mini-gel system. After assembly of the gel casting apparatus, resolving gels were made with the following constituents 10% gels; 10% acrylamide/bis-acrylamide (National Diagnostics, U.S.A.), 375 mM Tris (pH 8.8) (Fisher Scientific), 0.1% SDS, 0.1% ammonium persulphate (APS) (Sigma-Aldrich) and 0.04% tetramethylethylenediamine (TEMED) (Sigma-Aldrich). APS and TEMED were added just before pouring to initialise polymerisation. Resolving gel was poured to leave an appropriate gap for the comb and 5% stacking gel. As the gel set, isopropanol (Fisher scientific) was poured on top of the resolving gels to create a level interface and to remove air bubbles. The stacking gel was made as follows; 5% acrylamide/bis-acrylamide, 126 mM Tris-HCl (pH 6.8), 0.1% SDS, 0.1% APS and 0.1% TEMED and was poured on top of the resolving gel once it had set and isopropanol had been removed. A well-forming comb was inserted into the stacking gel and the apparatus left for 20-30 minutes at room temperature. Following the stacking gel setting, the gel was removed from the casting stand, the comb was detached and the gel was placed in the running module and covered in SDS-PAGE running buffer (25 mM Tris, 0.1% (w/v) SDS and 192 mM glycine (Sigma-Aldrich) in dH_20). Prior to loading, the samples were heated at 95ºC

for 3 minutes to denature protein structure. Pre-stained protein ladder (Bio-Rad and GE Healthcare, U.K.) was added to at least one well and used to indicate protein size. Electrophoresis was performed at 180-200 volts for 45-60 minutes using the PowerPac Basic (Bio-rad).

2.8.4 Transfer

Following protein separation by electrophoresis, proteins were transferred onto Hybond enhanced chemiluminescence (ECL™) nitrocellulose membranes (GE Healthcare) using the mini trans-blot module (Bio-Rad). To correctly assemble the module, the following protocol was used: one sponge then one piece of blotting paper, the resolving gel, the nitrocellulose membrane, one piece of blotting paper, the final sponge. These were put together and submerged in 1X transfer buffer (25 mM Tris, 192 mM glycine and 20% methanol (Fisher Scientific) in dH_2O). The assembled cassette was inserted into the transfer holder ensuring the correct current direction was followed so that the protein transferred from the gel to the membrane. An ice block was placed in the transfer tank to prevent overheating and the tank was filled with transfer buffer. Transfers were performed for 1 hour at 100 volts.

2.8.5 Immunoblotting

To detect proteins of interest, the nitrocellulose membrane was removed from the cassette and washed for 5 minutes in 0.1% PBS Tween 20 (Scientific Laboratory Supplies, U.K.). Blocking was then performed with 5% milk powder (Sigma-Aldrich) 0.1% PBS Tween for 1 hour at room temperature. The primary antibody (mouse anti-αSMA (Sigma-Aldrich) 1:1,000 dilution, rabbit anti-SM22α (Abcam, U.K.) 1:2,000 dilution or mouse anti-β-actin (Abcam) 1:20,000 dilution) was diluted in blocking buffer and incubated with the membrane overnight at 4ºC. The membrane was then washed with 0.1% PBS

Tween for three X five minute washes and then incubated for 1 hour at room temperature with a horseradish peroxidase (HRP) conjugated secondary antibody directed against the primary antibody species (rabbit anti-mouse HRP (DAKO, Denmark) 1:1000 dilution and pig anti-rabbit HRP (DAKO) 1:2000 dilution) diluted in blocking buffer. The membrane was then washed as previously before application of Amersham™ ECL™ Western Blot Detection Reagent (GE Healthcare, Cat No. RPN2209) to allow for visualisation of the protein bands. This was incubated with the blots for 1-2 minutes before the membrane was placed in cling film with all air bubbles removed and then into a film cassette. To visualise the protein bands radiographic film (GE Healthcare) was loaded into the cassette in a dark room and incubated with the membrane for between 1 second to 2-3 minutes depending on the antibody. Radiographic films were developed in a SRX-101A radiographic processor (Konica Minolta, U.K.).

2.9 Enzyme-Linked Immunosorbent Assays

2.9.1 Tumour Necrosis Factor

A DuoSet canine tumour necrosis factor (TNF) Enzyme-Linked Immunosorbent Assay (ELISA) (R&D Systems, U.S.A.) was used to analyse the level of TNF secreted from VICs into media. Prior to the assay being performed, the capture antibody supplied with the kit was diluted 1:180 in PBS and used to coat the necessary number of wells in a high protein-binding capacity Maxisorp 96 well plate (Nunc, Denmark).To run the standard dilution series 50 μL of antibody was applied per well in triplicate. Once coated, plates were incubated overnight at room temperature, washed 5X with 0.05% PBS Tween 20 (Scientific Laboratory Supplies) in the Skanwasher 400 (Molecular Devices, U.S.A.), with all solution being completely aspirated off after the final wash. Reagent diluent (10% BSA) (R&D Systems) was diluted

1:10 with PBS to make a working solution. Three hundred microliters per well was used as a blocking buffer with a 1 hour incubation period at room temperature. Following this, the plate was washed as indicated previously. A dilution series of TNF standard was produced by first diluting 65 ng/mL recombinant canine TNF 1:65 in reagent diluent to get a 1000 pg/mL top standard. A 2 fold 7 point serial dilution series was then set up by diluting this standard in reagent diluent. 50 µL of sample media or standard dilution series was then pipetted into coated wells in triplicate and incubated for 2 hours at room temperature. The plate was then washed as previously. Stock 18 µg/mL biotinylated goat anti-canine TNF detection antibody was diluted 1:180 in reagent diluent for a working solution at 100 ng/mL. 50 µL of this per well was then pipetted onto the plate and incubated for 2 hours at room temperature before being washed as previously. Stock Streptavidin-HRP was then diluted 1:200 with reagent diluent and 50 µL per well was added to the plate, the plate was then protected from light with foil and incubated at room temperature for 20 minutes whilst being shaken gently on a Wellmix microplate shaker (Thermo Fisher Scientific). Following washing the plate as previously described, 50 µL of 1 step ultra TMB ELISA Highly Sensitive Substrate Solution (Thermo Scientific) was added to each well, protected from light and incubated using the Wellmix at room temperature for approximately 20 minutes or until a colour change was detected in the wells containing the TNF standard dilution series . Following this 25 µL of 1 M H_2SO_4 (sulphuric acid) was pipetted into each well using a multi-channel pipette, to stop the substrate solution reaction. Optical density at both 450 nm (wavelength of interest) and 540 nm (wavelength used to correct for imperfections on the plate by subtracting from the 450 nm reading) were read on the Cytation 3 imaging reader (BioTek, U.S.A.). Results were then exported to Microsoft office excel

and secreted TNF in each sample was calculated using the standard dilution series.

2.9.2 Interferon gamma

To detect interferon gamma (IFNγ) secreted into the media from VICs a DuoSet canine IFNγ ELISA (R&D systems) was utilised. This used the protocol described in 2.9.1 including the same dilution factors. However, the standard used was recombinant canine IFNγ and the capture antibody and detection antibody were targeted against canine IFNγ.

2.9.3 Transforming Growth Factor β1

A Human Quantikine® TGFβ1 ELISA (R&D Systems) was used to analyse secreted TGFβ1 from canine VICs as the dog and the human TGFβ1 share 100% homology at the protein level (http://www.ensembl.org). The ELISA was performed following the manufacturer's protocol. Prior to the assay being performed, all reagents were prepared as required. This included diluting calibrator diluent RD5-53 1:4 with dH_2O, making a 1:25 dilution of wash buffer concentrate with dH_2O and making 1 M HCl and 1.2 M NaOH/0.5 M HEPES solution. A dilution series of TGFβ1 standard (1:2 dilution at each step) from 2000 pg/mL to 31.3 pg/mL was performed with calibrator diluent RD5-53. To activate all latent TGFβ1 in the supernatants and expose the antibody-binding epitope, 20 µL of 1 M HCl was added to each 100 µL of the samples. Samples were then incubated for 10 minutes at room temperature and then neutralised with 20 µL of 1.2 M NaOH. Pre-coated microplate strips were treated with 50 µL of assay diluent RD1-73 with enough strips prepared for all samples and standards to be run in duplicate. Fifty microliters of standard or activated sample was added to each well and incubated at room temperature for 2 hours. All wells were gently aspirated and washed 3X with assay wash buffer

and 100 µL of TGFβ1 conjugate was then added to each well and the samples incubated at room temperature for 2 hours. All wells were washed as described above and 100 µL of substrate solution was added to each well. Wells were then protected from light and incubated at room temperature for 30 minutes. Finally, 100 µL of assay stop solution was added to each well and the optical densities for both 450 nm and 540 nm wavelengths were read on the Cytation 3 imaging reader. Results were then exported to Microsoft Office Excel and secreted TGFβ1 in each sample was calculated against the standard dilution series.

2.9.4 Transforming Growth Factor β2

A mouse/rat/canine/porcine TGFβ2 Quantikine® (R&D Systems) was used to analyse secreted TGFβ2 from canine VICs. The ELISA was performed following manufacturers instructions and followed the same protocol described in section 2.9.3 with the exception that the standard used was recombinant TGFβ2 and the capture and detection antibodies were targeted against TGFβ2. To activate all latent TGFβ2 in the supernatants and expose the antibody-binding epitope, 20 µL of 1 M HCl was added to each 100 µL of the samples.

2.9.5 Transforming Growth Factor β3

A human TGFβ3 (98% homology between human and canine TGFβ3 (http://www.ensembl.org)) DuoSet ELISA (R&D Systems) was used to analyse secreted TGFβ3 from canine VICs. The ELISA was performed following manufacturers instructions and followed the same protocol described in section 2.9.1 with the exception that the standard used was recombinant TGFβ3 and the capture and detection antibodies were targeted against TGFβ3.

To activate all latent TGFβ3 in the supernatants and expose the antibody-binding epitope, 20 μL of 1 M HCl was added to each 100 μL of the samples.

2.10 Proteoglycan assay

To assess proteoglycan changes in VIC media supernatants the sulphated glycosaminoglycan quantification assay (AMS Biotechnology Ltd, U.K.) was used following the manufacturer's instructions. Stock 100 μg/mL chondroitin sulphate was diluted 1:5 with the DLF media used to propagate VICs to obtain a 20 μg/mL top standard. A 2 fold 7 point dilution series was made from the top standard, again diluting in media. One hundred microliters of either standard dilution series or sample supernatant was pipetted in triplicate into wells of a clear 96 well plate. One hundred μL of assay dye was then added to each well, gently swirled to mix, and the optical density was measured at 515 nm on a Synergy HT plate reader (BioTek). Results were then exported to Microsoft Office Excel and secreted proteoglycan in each sample was calculated against the standard dilution series.

2.11 Cell culture treatment conditions

2.11.1 TGFβ1 and SB431542 cell culture conditions

To analyse the effect of TGFβ1 signalling and the TGFβ pathway in VICs, a microarray gene expression study was carried out on 3 biological replicates of quiescent VICs (qVICs) and VICs derived from diseased valves (aVICs) (all passage 3). All cells were grown in T25 cell culture flasks for the duration of the experiment. This approach was used to ensure that a high quantity and quality of RNA would be obtained from all samples. VICs were seeded at a density of 200,000 cells per flask. Cells were maintained in 5ml of DLF media (described in section 2.4) per flask. qVICs were treated with 5 ng/mL recombinant human TGFβ1 (Gibco Life Sciences, U.S.A.) dissolved in 4 mM

HCl, 0.1% BSA (Sigma-Aldrich) (concentration chosen upon personal communication with Dr. Karen Tan as well as previously being shown to induce activation in aortic VICs[117, 272]). aVICs were treated with 10 μM SB431542 (Sigma-Aldrich) dissolved in Dimethyl Sulfoxide (DMSO) (Sigma-Aldrich) (concentration chosen upon personal communication with Dr. Karen Tan). Control plates for all qVICs and aVICs were run concurrently, passage matched and with vehicle treatment of DMSO (1 μL/mL), and 4 mM HCl, 0.1% BSA (1 μL/mL) added. In addition, to account for vehicle effects in the treatment groups, DMSO (1 μL/mL) was added to the TGFβ1-treated qVICs and 4 mM HCl, 0.1% BSA (1 μL/mL) was added to the SB431542 treated aVICs. A diagram of the experimental approach is shown in **Figure 2-4**.

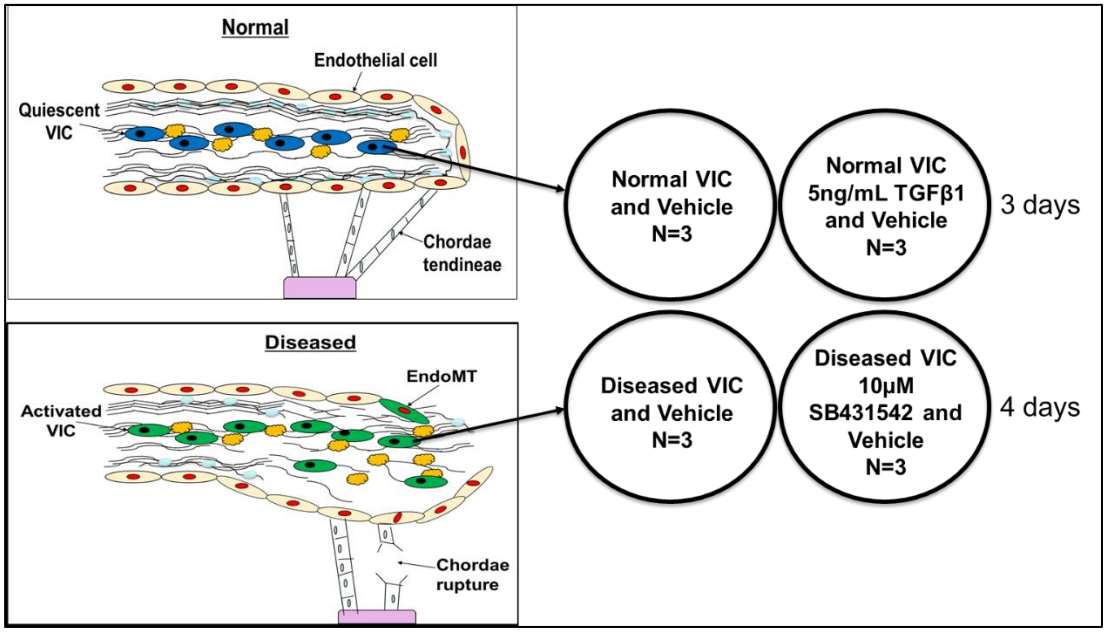

Figure 2-4 Summary of the experimental design used to derive samples for microarray analysis of TGFβ signalling in VICs.

Following 72 hours of treatment of the qVICs and 96 hours of treatment for the aVICs, cells were processed for storage and RNA extraction as described in section 2.3.2 with the exception that cells were counted on a haemocytometer prior to pelleting for storage. This was performed for later normalisation of

proteoglycan data from these cells (see Chapter 6). All cell media was stored in appropriately labelled bijou tubes at -20ºC for future analysis.

2.11.2 5HT and LY272015 cell culture conditions

To investigate the role of serotonin (5HT) signalling in VICs the following protocol was used. qVICs and aVICs were cultured in 35 mm^2 plastic cell culture dishes over the course of the experiment (qVICs ranged between passage 3-5, aVICS were all passage 3). As two time points (4 and 7 days) and both RNA and protein were being sampled, each primary cell culture was set up in quadruplicate with cells being cultured for 4 days seeded at 150,000 cells per well and cells cultured for 7 days seeded at 50,000 cells per well. Culture wells were supplemented with 5 mL DLF media and treatment every 48 hours. qVICs were treated with 1μM 5HT (Sigma-Aldrich) dissolved in sterile dH_2O (concentration was chosen upon personal communication with Dr. Karen Tan and for previous use in the literature[171]). aVICs were treated with either 100 nM or 1 μM of the selective 5HTR2B antagonist LY272015 (Santa Cruz Biotechnology, U.S.A.) dissolved in DMSO (100 nM selected as this concentration had previously been reported in the literature [171, 273] and 1 μM selected to check the effect of a high dose). To control for the effect of vehicle, media was supplemented to 1 μL/mL DMSO in the 5HT treated qVICs and the lower dose LY272015 treatment. As a control, DMSO treated (1 μL/mL) qVICs and aVICs were propagated concurrently with the treatment groups.

Cells were harvested after appropriate treatment times (see section 2.3.2) and went on to either have RNA (section 2.3.2) or protein (section 2.8.1) extracted. Media from day 7 cells intended for protein extraction was stored in appropriately labelled bijou tubes at -20ºC and used for proteoglycan analysis normalised to protein concentration (see Chapter 6).

2.12 Cell microscopy and image capture

Photomicrographs of cells were taken using a Zeiss Axiovert 40 CFL inverted microscope (Zeiss, Germany) at x10 magnification. Images had 100 μM scale bar attached in Axiovision software (version 4.7.2) and were exported as JPEG files.

2.13 Statistical analyses

Microarray statistical analysis was performed in the transcriptome analysis console as stated in section 2.5.3, all other statistical analysis was performed in Minitab17. When the data had a normal distribution, parametric tests were performed. Otherwise, a non-parametric test was performed. 2-sample T-tests, paired sample T-tests or Mann Whitney U-tests were performed with significant values being P-value <0.05.

Chapter 3 Grade dependent changes in MMVD

3.1 Introduction

As discussed in Chapter 1, myxomatous mitral valve disease (MMVD) causes a progressive deterioration in the structure and function of the mitral valve. The gross anatomy and histological features of the disease have been well characterised with a grading system (Whitney grading)[4]. This has been implemented to distinguish, broadly, the development of disease from early to end-stage (Chapter 1 section 1.2.2).

However, the molecular mechanisms underpinning and controlling disease development in the dog remain poorly understood. One reason for this is that the majority of previous studies have examined changes between normal (Grade 0) and end grade (Whitney grade 4) disease. This is particularly true of transcriptomic studies where presently only three studies (two microarrays, one RNAseq) in the dog have been performed and all have compared normal to highly diseased valves [33, 143, 150]. Although these studies have been informative in highlighting the fundamental transcriptomic differences between normal and diseased valves, they fail to distinguish which of these pathways may be causal and which may be consequential. To ascertain this requires contextualising transcriptomic changes as the disease progresses. Furthermore, by virtue of the natural history of the disease, these studies have compared older MMVD-affected dogs with younger disease-free dogs. The pathology of the condition (discussed in Chapter 1 section 1.2) means that it is unfeasible to propose a study into MMVD where the control group will be completely devoid of myxomatous lesions and be of the same age as an end grade diseased group[22]. This makes data analysis difficult as age cannot be removed as a confounding factor[22]. Tackling this problem can be partly

achieved by assessing disease in a grade-dependent manner. Although there will still be a difference between the control and end grade groups, the age of lower grade and control groups are likely to overlap, allowing for a distinction of which pathways solely associated with disease and those associated with senescence.

Another consideration is the effect of breed on the development of MMVD. All breeds of dog will likely develop some form of the disease by 10 years of age, however, the vast majority of these will not reach clinical significance[3, 4, 50]. As discussed in Chapter 1 section 1.6, it is well established that various small breed dogs, such as the Cavalier King Charles Spaniel (CKCS) and dachshund, are predisposed to developing the disease at an early age, making the eventual development of clinical symptoms more likely[24, 166, 222]. Although previous studies have looked at potential genetic variants responsible for this, none have been successful in establishing a single responsible variant [201, 219-221]. Previous microarray studies have both included at least one group containing just one breed with Oyama *et al* using exclusively beagles in their control group and Lu *et al* comparing beagles to CKCS [33, 150], allowing a possible breed bias to be introduced.

With this in mind, the aim of this study was to investigate the transcriptomic changes occurring as MMVD progresses. To minimise artefacts and bias related to age, breed and secondary effects of late disease, multiple breeds in control and grade 1-4 groups were used. This allows broader statements about the development of MMVD in the dog as a whole. Although new information about various aspects of end grade disease was expected, this study was particularly interested in separating cause and consequence pathways involved in the development of the disease.

3.2 Materials and methods

3.2.1 Tissue collection

For full details on tissue collection, see Chapter 2 section 2.2. Thirty valves were collected with full owner consent for this study. The description of these dogs is summarised in **Table 3-1**. Disease grade was assessed grossly by two investigators and scored using the Whitney grading system [4].

Sample ID	Date sampled	Dog Breed	Gender	Age	Whitney grade
B2G0	05/06/2015	BEAGLE	MALE	4y	0
B4G0	05/06/2015	BEAGLE	FEMALE	4y	0
PBT1G0	20/11/2015	PITBULL TERRIER' TYPE	MALE	2y9m	0
PBT3G0	01/04/2016	'PITBULL TERRIER' TYPE	MALE	1y9m	0
PBT2G0	27/11/2015	'PITBULL TERRIER' TYPE	MALE	3y	0
B26G0	26/10/2015	BEAGLE	MALE	3y	0
B5G1	09/04/2015	BEAGLE	FEMALE	4y1m	1
B3G1	09/04/2015	BEAGLE	MALE	3y10m	1
B1G1	09/04/2015	BEAGLE	MALE	4y1m	1
MG1	25/09/2015	MASTIFF	MALE	5y	1
SBT1	30/10/2015	STAFFORDHSIRE BULL TERRIER	FEMALE	6y	1
SBT2G1	24/06/2016	STAFFORDHSIRE BULL TERRIER	FEMALE	10y	1
B3G2	09/04/2015	BEAGLE	MALE	3y2m	2
B6G2	09/04/2015	BEAGLE	FEMALE	3y2m	2
RG2	23/10/2015	ROTTWEILLER	MALE	5y	2
ABDG2	05/02/2016	AMERICAN BULLDOG	MALE	6y	2
CG2	19/02/2016	BORDER COLLIE	MALE	5y	2
SBTG2	01/04/2016	STAFFORDHSIRE BULL TERRIER	FEMALE	7y	2
BTG3	29/01/2016	ENGLISH BULL TERRIER	FEMALE	10y	3
WHTG3	06/11/2015	WEST HIGHLAND TERRIER	MALE	10y	3
811M_024	16/01/2013	CAVALIER KING CHARLES SPANIEL	MALE	12y	3
811M_019	20/12/2012	CAVALIER KING CHARLES SPANIEL	MALE	11y	3
811M_023	16/01/2013	CAVALIER KING CHARLES SPANIEL	MALE	12y	3
811M_017	20/02/2013	CAVALIER KING CHARLES SPANIEL	FEMALE	10y	3
CKCSG4	21/03/2014	CAVALIER KING CHARLES SPANIEL	MALE	16y	4
JRG4	30/10/2015	JACK RUSSEL TERRIER	FEMALE	11y	4
C1G4	19/02/2016	BORDER COLLIE	MALE	13y	4
811M_016	20/12/2012	CAVALIER KING CHARLES SPANIEL	FEMALE	12y	4
811M_007	22/05/2012	CAVALIER KING CHARLES SPANIEL	MALE	14y	4
C2G4	08/07/2016	BORDER COLLIE	MALE	13y	4

Table 3-1 Description of the dogs used in this study.

3.2.2 RNA extraction, quantification and quality control for microarray

The extraction protocol followed for whole valve RNA extraction is detailed in Chapter 2 section 2.3.1. Almost all RNA extractions were performed by myself, with the exception of CKCS samples with the sample ID beginning 811M which were extracted by Dr. Chie Chien Lu prior to the start of this study. Quantification and quality control assessment of RNA for microarray analysis was performed as described in Chapter 2 section 2.3.3.

3.2.3 Affymetrix Canine Gene 1.1ST microarray analysis

For this study, microarray analysis was performed using two 16 well Affymetrix Canine Gene 1.1ST chips. RNA processing, hybridisation, post-hybridisation quality control, summarisation file creation and differential gene expression analysis was performed as described in section 2.5 of Chapter 2. Unless otherwise stated, this study relaxed the Benjamini-Hochberg false discovery rate (FDR) correction to allow the inclusion of a greater number of genes for gene enrichment analysis.

3.2.4 Gene enrichment analysis

The network analysis tool Miru (version 1.4) was utilised as described in Chapter 2 section 2.6.1. In this study, a pairwise gene-to-gene comparison was made using a Pearson correlation with the Fruchterman-Reingold algorithm threshold set at r=0.87 to allow the maximum number of nodes (genes) with the smallest number of edges (connections between genes). This calculation governs how nodes are plotted on the 3D graph, determining the stringency of the association of gene expression patterns with one another (topology). Markov clustering (MCL) inflation was set at 4.3.

The tools Database for Annotation, Visualisation and Integrated Discovery (DAVID) and Ingenuity Pathway Analysis (IPA) were used as stated in

Chapter 2 sections 2.6.2 and 2.6.3; default settings were used throughout. Gene list comparison was performed as outlined in Chapter 2 section 2.6.4.

3.2.5 cDNA synthesis and RT-qPCR

To validate the microarray analysis RNA samples were synthesised into complementary DNA (cDNA) and real-time quantitative polymerase chain reaction (RT-qPCR) was performed. For this analysis, all RNA samples except 811M_016 were reverse transcribed into cDNA as stated in Chapter 2 section 2.7.1. Sample 811M_016 was excluded due to a lack of remaining RNA. Primers used for validation are listed in **Table 3-2** and were designed and optimised following the protocol summarised in Chapter 2 section 2.7.2-2.7.6.

Gene Symbol	Forward Primer Sequence	Reverse Primer Sequence	Product Length	Optimum TM °C	Primer Efficiency %
ACTA2	5'CGGCTACTCCTTTGTGACG3'	5'CGTGGCCATCTCGTTCTC3'	100	58	102.2
HTR2B	5'CCAATCCAGGCCAATCAAAG3'	5'CAGGTGATGTTGCTTGGGTT3'	143	59	104.8
TAGLN	5'GACATGTTCCAGACCGTCGA3'	5'CAATGACGTGCTTTCCCTCC3'	199	59	106.7
ACTG2	5'TGCCAACAATGTCCTTTCCG3'	5'GCCTCCAATCCAGACTGAGT3'	148	60	93
SLIT3	5'CTGACAAGGACAACGGCATC3'	5'CCCATCATTCACCGTCTCCA3'	146	60	101
CDKN2A	5'CATGTTGGCTCAGAATCGGG3'	5'CTCACGTCCAAGGCACAAAA3'	125	60	90.6
SLC10A6	5'GCTGTTGGATGGGTTTCTCA3'	5'TCCAAGAAAGCACCAGTCTCT3'	147	58	101.7
CILP	5'TGCTCCAATTATACCGTGCG3'	5'CAGAACACTTGCTCCAGGGA3'	100	62	106.1
MMP12	5'GACACAATTCATGGACCCTGG3'	5'TCAAATACGTCAGGTCCTTGGA3'	129	63	110
ADAMTS5	5'GTTCCCAAATATGCAGGCGT3'	5'AGCTTCGAACCAATGATGCC3'	191	59	101.6
ADAMTS19	5' GGACGGTGAGGTGTACTAAC 3'	5'ACTGCATTCCTTTACCACAGG 3'	150	59	100.2

Table 3-2 Primers designed and optimised for the validation of whole valve microarray data.

RT-qPCR of the samples was performed following the protocol outlined in Chapter 2 section 2.7.7 with the optimum TMºC (**Table 3-2**) for each primer being used as the annealing temperature.

3.3 Results

3.3.1 Breed, gender and age analysis

The 30 tissue samples obtained for analysis in this study were from 11 different breeds of dogs (**Table 3-1**) with 2 or more different breeds of dog in each Whitney grade of disease. 10 females and 20 males were included in the study (**Table 3-1**) with at least 1 female being included in each Whitney grade of disease. The average age of the dogs in each grade of disease (n=6 per grade) is summarised in **Figure 3-1**. A significant difference in age of at least P-value <0.05 was reached between all groups with the exception of between normal and grade 1 and grade 1 and grade 2 valves.

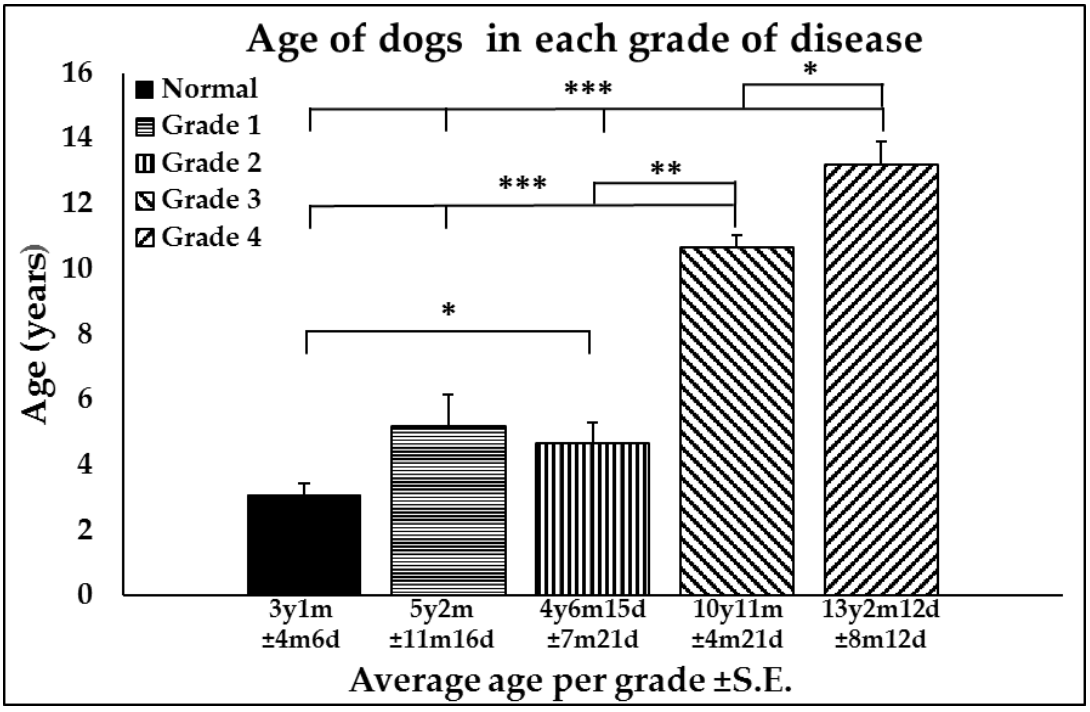

Figure 3-1 Average age of dogs sampled for microarray analysis. Significant differences between Whitney grades of disease are shown by * symbols with: * indicating P-value <0.05, ** P-value <0.01 and *** P-value <0.001.

3.3.2 RNA quality assessment

Post-extraction, the RNA concentrations from all RNA samples from the 30 valves were quantified. These along with 260/280 and 260/230 absorbance ratio readings and RNA integrity number (RIN) were recorded (**Table 3-3**). RNA concentration ranged from 192.3-1315.6 ng/μL. Absorbance ratios were all within the acceptable reference range (1.8-2.2) for both 260/280 and 260/230, indicating that the extractions did not contain contaminants. Gel electrophoresis images generated by the Agilent 2200 bioanalyser (**Figure 3-2**) visualised the 28S and 16S rRNA in each sample. The intensity for each of these was then semi-quantified and a ratio of 28S:16S was used to create the RIN for each sample[268]. The majority of samples passed the accepted RIN cut-off of >7 for microarray analysis. Samples MG1, C1G4 and 811M_007 had RINs below 7 (5.9, 6.5 and 6.3 respectively). Upon personal communication with Chieko Kontani (Edinburgh Genomics), it was decided that these samples would be included in the initial microarray analysis.

Sample ID	RNA concentraion [ng/µl]	260/280	260/230	RIN
B2G0	330.7	2.07	1.92	8.2
B4G0	416	1.96	1.99	8.5
PBT1G0	416.7	2.07	2.08	7.6
PBT3G0	307.6	2.13	1.98	8.2
PBT2G0	876.4	2.05	2.15	8.5
B26G0	825.2	2.02	2	7.7
B5G1	424.4	2.04	2.02	9.1
B3G1	372	2.03	2.15	7.9
B1G1	848.2	2.05	2.03	8.3
MG1	228.8	2.07	2.04	5.9
SBT1	652.2	2.06	1.98	7.6
SBT2G1	541.1	2.06	1.98	8.6
B3G2	281.1	2.08	1.9	9.3
B6G2	1026.6	2.03	2.15	8.7
RG2	631.2	2.11	2.31	7.8
ABDG2	998.9	2.09	2.04	8.4
CG2	826.4	2.03	2.05	8.2
SBTG2	522.9	2.1	2.22	7.7
BTG3	627.6	2.09	2.17	8.3
WHTG3	439.9	2.07	2.19	7
811M_024	303.5	2.05	2.16	8.6
811M_019	465.7	2.01	2.19	8.8
811M_023	351.6	2.06	2.04	7.2
811M_017	192.3	2.06	2.13	7.6
CKCSG4	806.5	2	2	7.9
JRG4	974	2.06	2.2	8.6
C1G4	1315.6	1.97	1.81	6.6
811M_016	265.7	2.07	2.18	8.9
811M_007	541.6	2.1	1.99	6.3
C2G4	1175.6	1.97	1.98	8.3

Table 3-3. Concentration, 260/280 and 260/230 absorbance readings and RIN for each valve sample.

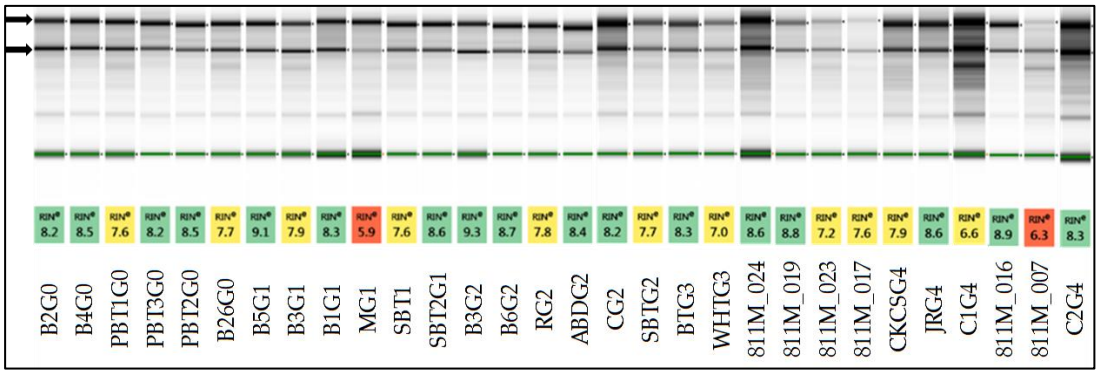

Figure 3-2. Gel electrophoresis images visualising the 28S (indicated by the top arrow) and 16S (indicated by the bottom) rRNA intensity in each sample. The RIN for each sample is shown and colour coded with >8 given a green colour, 6.5-8 given a yellow colour and <6.5 given a red colour.

3.3.3 Microarray post-hybridisation quality control

Post-hybridisation analysis was performed to assess the gene expression data from the microarray analysis of the submitted samples. All wells on the array showed the correct concentration of spike in and labelling controls indicating that the arrays had been performed correctly. After Robust Multi-array Average (RMA) and gene-level normalisation, log expression signal was plotted (**Figure 3-3**) in box plots with the majority of samples showing a similar profile relative to one another. Samples MG1 and 811M_007 showed a larger amount of variation compared to any other samples (highlighted in red). These two samples had the lowest RINs out of all samples.

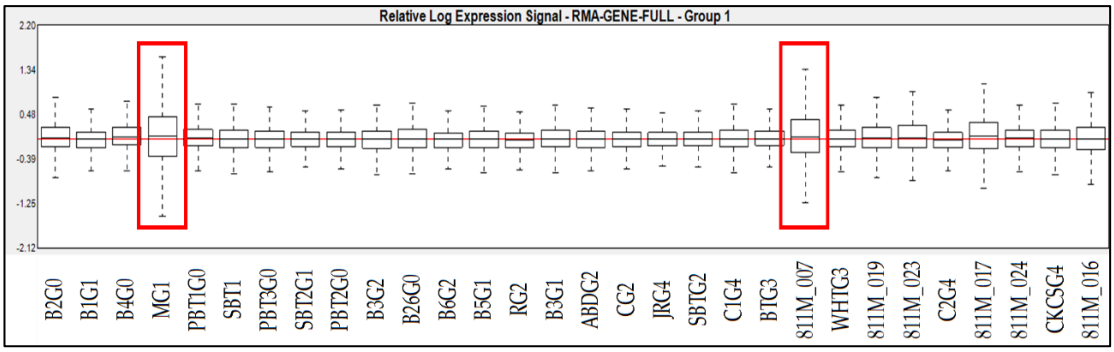

Figure 3-3. Post-RMA signal intensity boxplots for each sample. Highlighted in red are samples MG1 and 811M_007, which show the largest variation.

The sample-to-sample analysis in Miru (r=0.97) (**Figure 3-4**) highlighted samples 811M_007 and MG1 as clustering away from the main group of samples. This difference was also apparent in the PCoA plot (**Figure 3-5**). In transcript-to-transcript expression analysis, 9951 nodes (transcripts) were plotted with the two largest clusters being grouped based on the differential expression in samples 811M_007 and MG1 (**Figure 3-6**) (Pearson correlation r=0.85, MCL inflation 2.2). These samples had the lowest RINs of any samples and, as shown by these analyses, this was causing a detrimental effect on

microarray analysis of all samples. Therefore, these two samples were removed from the dataset for subsequent analyses.

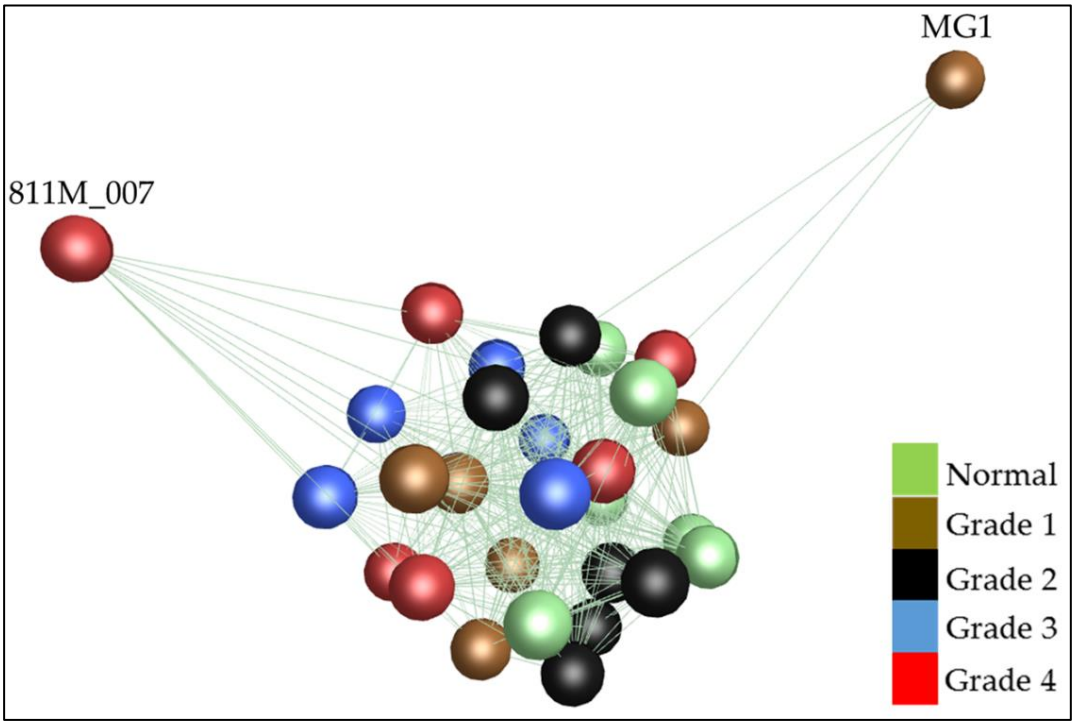

Figure 3-4. Sample-to-sample analysis of whole valve RNA submitted for microarray analysis. Normal valves are coloured green, grade 1 brown, grade 2 black, grade 3 blue and grade 4 red. Highlighted are samples 811M_007 and MG1 which are located away from the other samples.

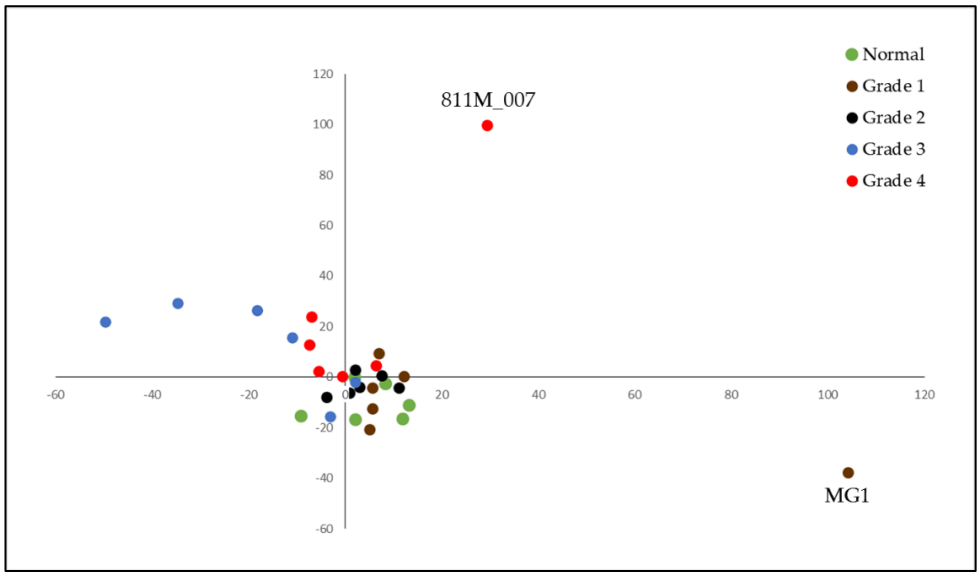

Figure 3-5. PCoA plot indicating the level of similarity in transcript expression between samples. Normal valves are coloured green, grade 1 brown, grade 2 black, grade 3 blue and grade 4 red. Highlighted are samples 811M_007 and MG1 are separated from the other samples.

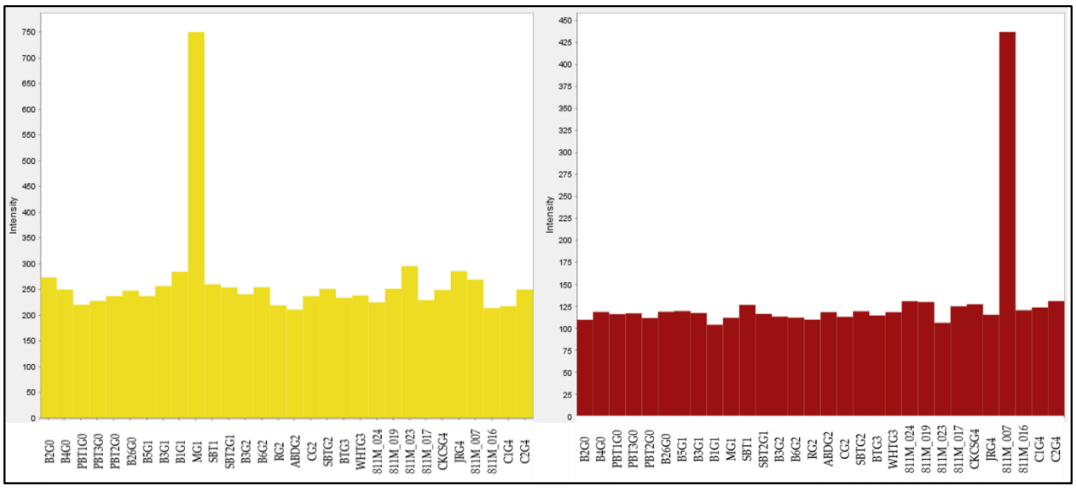

Figure 3-6. Bar charts of the average gene expression in the largest two gene clusters from transcript-to-transcript analysis of all 30 samples submitted for microarray analysis. Y-axis shows averaged normalised intensity. The yellow bar chart on the left highlights that the genes in this cluster are only highly expressed in the MG1 sample. The red bar chart on the right highlights that the genes in this cluster are only highly expressed in the 811M_007 sample.

After outlier removal, sample-to-sample analysis in Miru (r=0.97) showed a distribution with normal and lower grade valves clustering towards one side of the plot and higher grade 3 and 4 diseased valves clustering to on the other (**Figure 3-7**). This highlights a difference transcriptomically in these samples. Additionally, there is a slight breakaway group of grade 3 and 4 diseased valves away from the main cluster (highlighted in the red circle); this will be investigated further in Chapter 4.

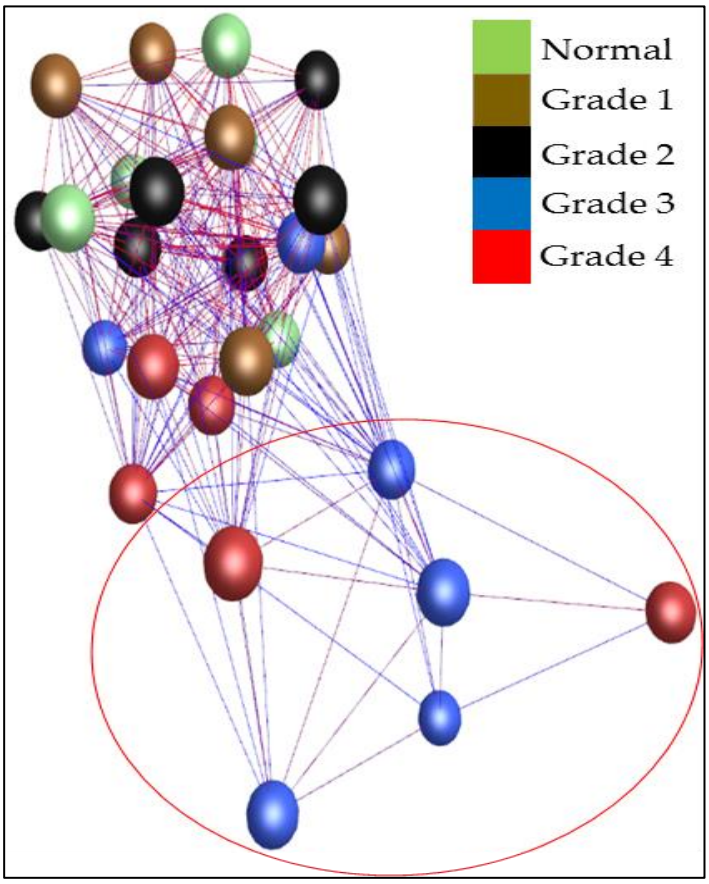

Figure 3-7. Sample-to-sample analysis with outliers removed showing samples coloured by grade of disease. (Normal samples are coloured green, grade 1 brown, grade 2 black, grade 3 blue and grade 4 red. Highlighted by a red circle is a set of grade 3 and 4 disease samples clustering away from the main group of samples.

Signal intensity distribution for each of the remaining samples was analysed and presented as a log2 signal histogram (**Figure 3-8**). This shows log signal intensity from 0-13.89 with a similar distribution pattern for all samples being exhibited, with an initial peak at 1.8 log signal (which is indicative of the inherent background signal associated with microarray). This peak declines and a plateau in the expression of genes is seen between 3.8-8 log signal intensity before a decline in genes expressing above this signal intensity until no genes being expressed at a greater intensity than 13.89. This figure shows that to remove the effect of background on this dataset genes expressed below 3.8 log signal intensity should be removed.

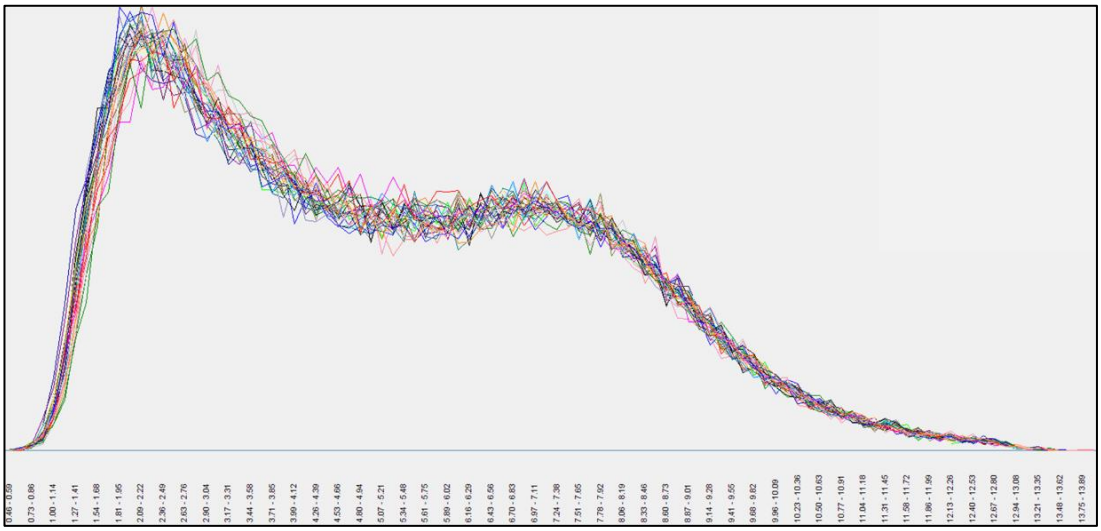

Figure 3-8. The Log2 signal line graph for samples. Each line represents a sample with the X-axis plotting signal intensity and Y-axis plotting the number of probes on the array with that signal intensity. The higher the line is on the Y-axis, the greater the number of probes are showing that signal intensity. A uniform pattern of expression can be seen here.

3.3.4 Differential expression of genes

With post-hybridisation quality control and outlier removal completed, differential expression of genes was calculated in the Affymetrix

Transcriptome Analysis Console. In total 1002 genes were differentially expressed (>1.5 or <1.5 fold change, p-value <0.05, >3.8 log2 signal intensity) in at least one grade of disease when compared to normal valve samples. This comprised 461 genes upregulated and 541 genes downregulated relative to normal valves. When expression in each grade of the diseased valves was compared to expression in normal valves, grade 1 valves had 71 differentially expressed genes, grade 2 had 59, grade 3 had 673 and grade 4 had 507 (full gene list can be found in **Appendix I: Chapter 3 Tables S1-4**). These results were exported as volcano plots (**Figure 3-9**). Points on these plots were generally equally distributed between up and down-regulated genes with 46 transcripts up-regulated and 25 down-regulated in grade 1, 39 up-regulated and 20 down-regulated in grade 2, 290 up-regulated and 383 down-regulated in grade 3 and 258 up-regulated and 248 down-regulated genes in grade 4. These gene lists were exported to Microsoft Excel and log2 signal intensity was transformed into raw signal intensity for later analysis.

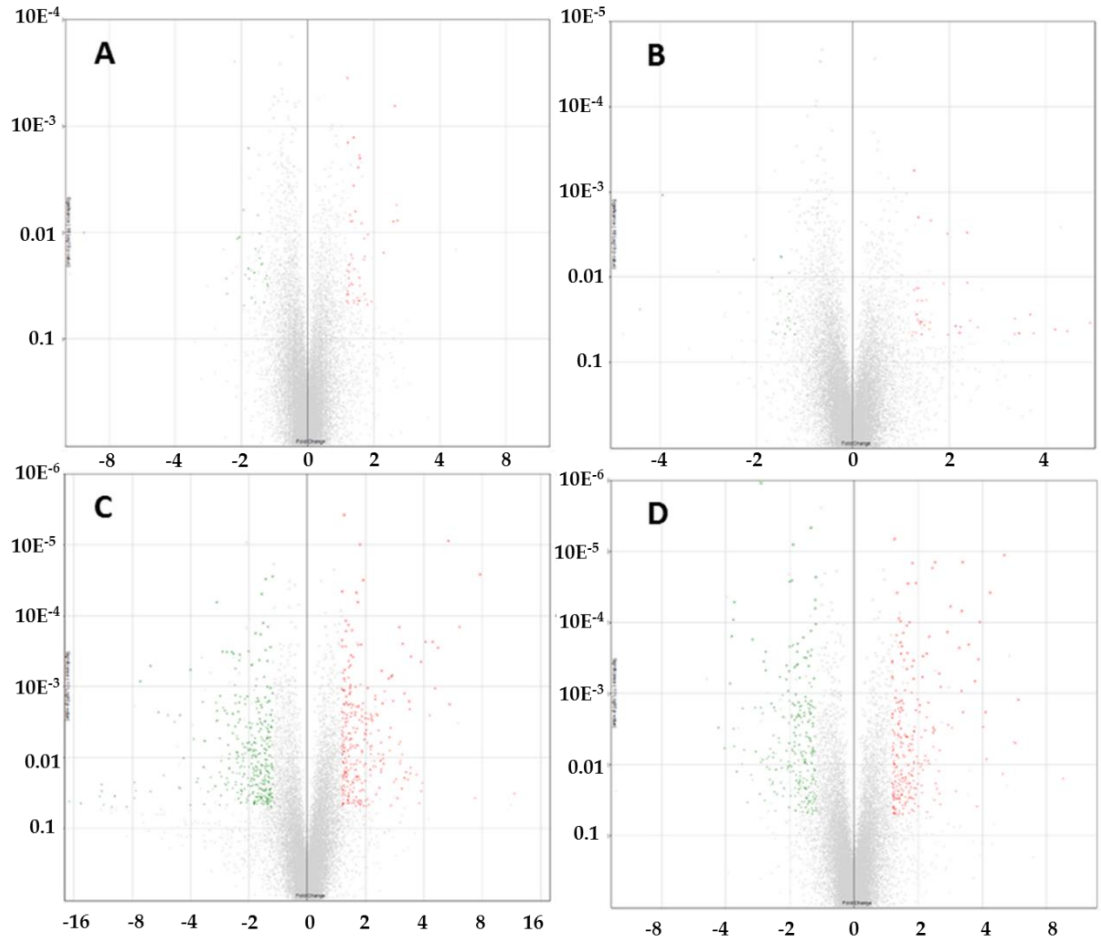

Figure 3-9. Volcano plots of each stage of disease compared against transcript expression in normal valves. A – grade 1; B – grade 2; C – grade 3; D – grade 4. The X-axis shows fold change value and Y-axis shows the P-value. Central vertical line shows 0 fold change with negative fold changes relative to normal on the left and positive fold changes on the right. Red are up-regulated transcripts (>1.5 fold) green are down-regulated transcripts (<-1.5 fold) and grey are transcripts which do not meet criteria for differential expression.

Higher stringency analysis was performed for all grades of disease, with the inclusion of a false discovery rate (FDR) of Q-value <0.1 as well as the criteria included above. Under these criteria, a total of 88 genes were differentially expressed with 18 being altered in grade 3 (12 up-regulated and 6 down-

regulated) and 70 being altered in grade 4 (37 up-regulated and 33 down-regulated). No genes were differentially expressed compared to normal in grades 1 and 2 with a FDR correction applied. Full gene lists for grades 3 and 4 with the FDR correction applied are shown in **Table 3-4** and **Table 3-5**.

Gene Symbol	Description	Fold Change	ANOVA p-value	FDR q-value
NT5E	5-nucleotidase, ecto (CD73)	-2.93	0.000065	0.088017
TANC2	tetratricopeptide repeat, ankyrin repeat and coiled-coil containing 2	-1.72	0.000049	0.080518
CCDC65	coiled-coil domain containing 65	-1.69	0.000126	0.098682
ENPP2	ectonucleotide pyrophosphatase/phosphodiesterase 2	-1.64	0.000031	0.075599
Uncharacterised		-1.6	0.000144	0.098682
LOC102152842	zinc finger protein 512-like	-1.51	0.000028	0.075599
LOC480571	septin-4	1.51	0.000045	0.080518
UBTD1	ubiquitin domain containing 1	1.55	0.000004	0.068246
FAM174A	family with sequence similarity 174, member A	1.58	0.000118	0.098682
ACYP2	acylphosphatase 2, muscle type	1.63	0.000135	0.098682
Uncharacterised		1.79	0.000047	0.080518
BNC2	basonuclin 2	1.82	0.000064	0.088017
NOV	nephroblastoma overexpressed	1.87	0.00001	0.068246
CDKN2B	cyclin-dependent kinase inhibitor 2B (p15, inhibits CDK4)	1.94	0.000032	0.075599
PLCXD3	phosphatidylinositol-specific phospholipase C, X domain containing 3	2.98	0.000145	0.098682
CDKN2A	cyclin-dependent kinase inhibitor 2A (melanoma, p16, inhibits CDK4)	5.34	0.000009	0.068246
LRRN1	leucine rich repeat neuronal 1	6.1	0.000143	0.098682
CDKN2A	cyclin-dependent kinase inhibitor 2A (melanoma, p16, inhibits CDK4)	7.79	0.000026	0.075599

Table 3-4. Differentially expressed genes between grade 3 and normal valves with high stringency criteria (FDR Q-value <0.1).

Gene Symbol	Description	Fold Change	ANOVA p-value	FDR q-value
Uncharacterised		-3.75	0.000157	0.073688
NKAIN2	Na+/K+ transporting ATPase interacting 2	-3.68	0.000092	0.060638
CILP	cartilage intermediate layer protein, nucleotide pyrophosphohydrolase	-3.64	0.000052	0.052298
NT5E	5-nucleotidase, ecto (CD73)	-2.99	0.000172	0.074864
TMEFF2	transmembrane protein with EGF-like and two follistatin-like domains 2	-2.73	0.000001	0.030355
ADCYAP1	adenylate cyclase activating polypeptide 1 (pituitary)	-2.65	0.000353	0.083815
WIF1	WNT inhibitory factor 1	-2.6	0.000472	0.094419
MIR218-1	microRNA mir-218-1	-2.6	0.000258	0.080548
KCNQ5	potassium channel, voltage gated KQT-like subfamily Q, member 5	-2.07	0.000405	0.090038
LRP1B	low density lipoprotein receptor-related protein 1B	-2.01	0.000487	0.094419
ALDH1A1	aldehyde dehydrogenase 1 family, member A1	-2	0.000027	0.039052
IGF2BP2	insulin-like growth factor 2 mRNA binding protein 2	-2	0.000219	0.076063
TMEFF2	transmembrane protein with EGF-like and two follistatin-like domains 2	-1.95	0.000026	0.039052
Uncharacterised		-1.94	0.00021	0.076063
CRISPLD2	cysteine-rich secretory protein LCCL domain containing 2	-1.93	0.000008	0.039052
AFF2	AF4/FMR2 family, member 2	-1.9	0.000428	0.090038
PTGFR	prostaglandin F receptor (FP)	-1.86	0.000404	0.090038
OVGP1	oviductal glycoprotein 1, 120kDa	-1.85	0.000258	0.080548
SCIN	scinderin	-1.84	0.000199	0.076063
ARGLU1	arginine and glutamate rich 1	-1.84	0.000386	0.08795
SNTB1	syntrophin, beta 1 (dystrophin-associated protein A1, 59kDa, basic component 1)	-1.73	0.000163	0.074067
KCNQ5	potassium channel, voltage gated KQT-like subfamily Q, member 5	-1.71	0.000311	0.081427
SLC1A3	solute carrier family 1 (glial high affinity glutamate transporter), member 3	-1.67	0.000316	0.081427
PDGFRL	platelet-derived growth factor receptor-like	-1.65	0.000258	0.080548
SNTB1	syntrophin, beta 1 (dystrophin-associated protein A1, 59kDa, basic component 1)	-1.63	0.000408	0.090038
CACNA2D1	calcium channel, voltage-dependent, alpha 2/delta subunit 1	-1.6	0.000293	0.081323
MPP6	membrane protein, palmitoylated 6 (MAGUK p55 subfamily member 6)	-1.59	0.000131	0.071504
SCARA5	scavenger receptor class A, member 5	-1.59	0.000005	0.039052
TYW3	tRNA-yW synthesizing protein 3 homolog (S. cerevisiae)	-1.58	0.000245	0.078947
MOB3B	MOB kinase activator 3B	-1.52	0.000048	0.051544
LOC489911	zinc finger protein 688-like; zinc finger protein 785; zinc finger protein 764	-1.52	0.000064	0.056956
ERBB4	erb-b2 receptor tyrosine kinase 4	-1.51	0.000023	0.039052
SRSF2	serine/arginine-rich splicing factor 2	-1.51	0.000106	0.060638
FAM174A	family with sequence similarity 174, member A	1.51	0.000349	0.083815
CDR2	cerebellar degeneration-related protein 2, 62kDa	1.51	0.000363	0.084496
RAI14	retinoic acid induced 14	1.55	0.000007	0.039052
CYR61	cysteine-rich, angiogenic inducer, 61	1.58	0.000152	0.073688
LOC479476	arachidonate 12-lipoxygenase, 12S-type	1.59	0.000038	0.046206
CDKN1A	cyclin-dependent kinase inhibitor 1A (p21, Cip1)	1.62	0.000088	0.060638
NOV	nephroblastoma overexpressed	1.65	0.000097	0.060638
NME1	non-metastatic cells 1, protein (NM23A) expressed in	1.65	0.000192	0.076063
COL4A1	collagen, type IV, alpha 1	1.66	0.000276	0.081323
LOC100856638	uridine phosphorylase 1-like; uridine phosphorylase 1	1.68	0.000217	0.076063
ADAM22	ADAM metallopeptidase domain 22	1.7	0.00014	0.072075
BNC2	basonuclin 2	1.72	0.000337	0.083815
LBH	limb bud and heart development	1.77	0.000451	0.09208
Uncharacterised		1.77	0.00011	0.061186
GAP43	growth associated protein 43	1.78	0.000269	0.081323
ARNTL2	aryl hydrocarbon receptor nuclear translocator-like 2	1.79	0.000028	0.039052
ATP8B1	ATPase, aminophospholipid transporter, class I, type 8B, member 1	1.82	0.000099	0.060638
GPER1	G protein-coupled estrogen receptor 1	1.87	0.000416	0.090038
ARAP2	ArfGAP with RhoGAP domain, ankyrin repeat and PH domain 2	1.88	0.000015	0.039052
MFSD2A	major facilitator superfamily domain containing 2A	1.9	0.000346	0.083815
CLEC3A	C-type lectin domain family 3, member A	1.95	0.000028	0.039052
Uncharacterised		2.1	0.000298	0.081427
BMP6	bone morphogenetic protein 6	2.19	0.000275	0.081323
KCNMB1	potassium channel subfamily M regulatory beta subunit 1	2.25	0.000159	0.073688
ANGPT1	angiopoietin 1	2.33	0.000017	0.039052
NTRK3	neurotrophic tyrosine kinase, receptor, type 3	2.4	0.000014	0.039052
NLGN4X	neuroligin 4, X-linked	2.51	0.000522	0.096567
LRRC3B	leucine rich repeat containing 3B	2.73	0.000137	0.072075
TPM2	tropomyosin 2 (beta)	2.83	0.000059	0.054713
HTR2B	5-hydroxytryptamine (serotonin) receptor 2B, G protein-coupled	3.11	0.000226	0.076063
Uncharacterised		3.2	0.000069	0.057543
CDKN2A	cyclin-dependent kinase inhibitor 2A (melanoma, p16, inhibits CDK4)	3.23	0.000014	0.039052
Uncharacterised		3.44	0.000205	0.076063
CCL13	chemokine (C-C motif) ligand 13	3.82	0.000329	0.083815
LRRN1	leucine rich repeat neuronal 1	3.89	0.000098	0.060638
SERPINE1	serpin peptidase inhibitor, clade E (nexin, plasminogen activator inhibitor type 1), member 1	4.34	0.000038	0.046206
CDKN2A	cyclin-dependent kinase inhibitor 2A (melanoma, p16, inhibits CDK4)	5.07	0.000011	0.039052

Table 3-5. Differentially expressed genes between grade 4 and normal valves with high stringency criteria (FDR Q-value <0.1).

3.3.5 Gene Network analysis

To understand expression trends throughout all grades of disease, the average gene expression level for each of 1002 differentially expressed genes (without FDR correction) found between all 4 grades of disease and normal valves were entered into Miru. Transcript-to-transcript analysis using a Pearson correlation coefficient of r=0.87 and default Markov Clustering (MCL) with inflation 2.2, pre-inflation 2.2 and a minimum cluster of 5 nodes only produced 12 clusters. The majority of genes were clustered as being either upregulated or downregulated in grade 3 and 4 of disease (395 and 457 genes respectively) without allowing for more specific trends in the data to be observed (**Figure 3-10A**). Optimisation of MCL clustering with an inflation of 4.3, pre-inflation of 2.2 and minimum cluster 5 produced 26 clusters of genes which could be investigated to find more specific trends in gene expression throughout all grades of disease (**Figure 3-10B**).

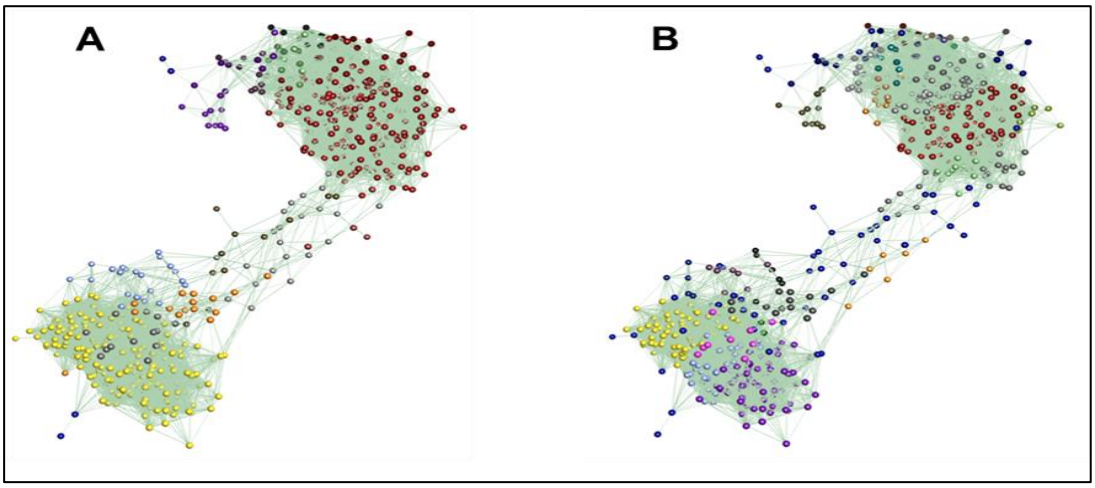

Figure 3-10. Miru cluster optimisation. (A) Default Miru MCL clustering of 1002 differentially expressed genes showing 12 clusters of genes with down-regulated genes on the right side of the plot (the majority of nodes red) and upregulated on the left side of the plot (the majority of nodes yellow. (B) Optimised MCL clustering (inflation of 4.3) of differentially expressed genes with 26 clusters identified.

The largest 5 gene clusters from the optimised MCL plot of differentially expressed genes were examined. Cluster 1 contained 233 genes (**Figure 3-11A**) and had an average signal profile where the gene changes between normal and grades 1 and 2 were not distinguishable, whereas grades 3 and 4 showed a distinct down-regulation, grade 3 slightly more so than 4, in comparison to the other graded valves (**Figure 3-11B**). Genes were submitted to DAVID 6.8 with 59 GO terms being associated with these genes. The 10 most significant terms listed (**Table 3-6**) were topped by proteinaceous extracellular matrix.

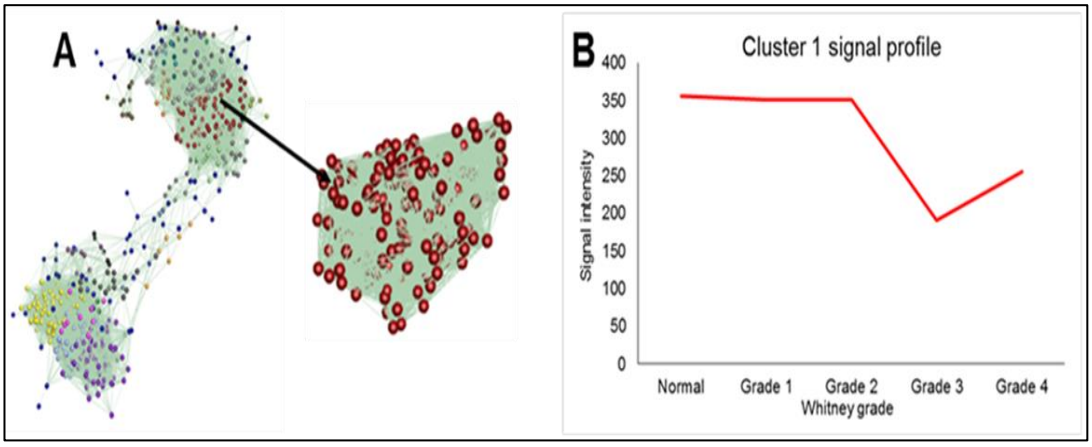

Figure 3-11. Miru clustering of differentially expressed genes – Cluster 1. (A) The position of Cluster 1. (B) Average signal profile of the 233 genes in Cluster 1.

Category	Term	Count	P-Value	FDR
GOTERM_CC_DIRECT	Proteinaceous extracellular matrix	14	8.49E-08	1.00E-04
GOTERM_BP_DIRECT	Semaphorin-plexin signaling pathway	6	9.11E-06	0.0137
GOTERM_MF_DIRECT	Semaphorin receptor binding	5	6.43E-05	0.07969
GOTERM_CC_DIRECT	Receptor complex	8	1.10E-04	0.13001
GOTERM_BP_DIRECT	Positive regulation of cell migration	9	1.25E-04	0.18806
GOTERM_CC_DIRECT	Extracellular space	24	1.32E-04	0.15553
GOTERM_MF_DIRECT	Chemorepellent activity	5	1.99E-04	0.2459
GOTERM_CC_DIRECT	Integral component of plasma membrane	22	2.19E-04	0.25831
GOTERM_BP_DIRECT	Negative regulation of axon extension involved in axon guidance	5	2.24E-04	0.33691
GOTERM_BP_DIRECT	Cell-matrix adhesion	6	7.03E-04	1.05167

Table 3-6. Functional analysis chart of the top 10 GO terms associated with cluster 1.

Cluster 2 contained 206 genes (**Figure 3-12A**) with an average signal profile indicating up-regulation of these genes in grade 3 and 4 valves (particularly grade 3) in comparison to normal, grade 1 and grade 2 valve groups (**Figure 3-12B**). 66 GO terms were associated with the genes from this cluster with 3 of top 10 (**Table 3-7**) connected to immune-related GO terms indicating that the involvement of immune-related pathways is important in late-stage disease.

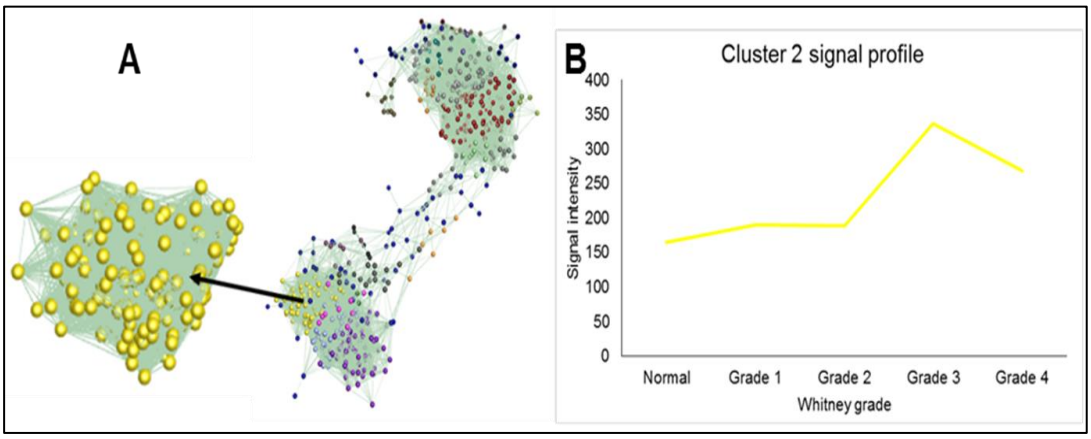

Figure 3-12. Miru clustering of differentially expressed genes – Cluster 2. (A) Miru clustering highlighting the position of Cluster 2. (B) Average signal profile of the 206 genes included in cluster 2.

Category	Term	Count	PValue	FDR
GOTERM_BP_DIRECT	Inflammatory response	14	6.09E-08	9.10E-05
GOTERM_BP_DIRECT	Positive regulation of inflammatory response	6	2.94E-05	0.04396
GOTERM_BP_DIRECT	Positive regulation of ERK1 and ERK2 cascade	9	6.82E-05	0.10185
GOTERM_BP_DIRECT	Immune response	10	9.66E-05	0.14432
GOTERM_BP_DIRECT	Cellular response to tumor necrosis factor	6	3.63E-04	0.54113
GOTERM_BP_DIRECT	Cell-cell signaling	6	6.22E-04	0.9261
GOTERM_BP_DIRECT	Positive regulation of GTPase activity	6	9.38E-04	1.39313
GOTERM_MF_DIRECT	CCR chemokine receptor binding	4	0.00125	1.5204
GOTERM_CC_DIRECT	External side of plasma membrane	8	0.00138	1.61382
GOTERM_BP_DIRECT	Neutrophil chemotaxis	5	0.00175	2.58195

Table 3-7. Functional analysis chart of the top 10 GO terms associated with cluster 2.

Cluster 3 contained 147 genes (**Figure 3-13A**) with an average signal profile showing a progressive decrease in gene expression. Grade 1 and 2 valves

showed a slight decrease in gene expression in comparison to normal valves and a larger decrease in signal was seen in grade 3 and 4 valves in comparison to other valves (**Figure 3-13B**). 30 GO terms were associated these genes. A recurring theme in the top 10 GO terms (**Table 3-8**) involves G-protein coupled receptor (GPCR) signalling related terms. In general clusters 3-5 illustrated gene trends which changed more gradually throughout disease in comparison to clusters 1 and 2.

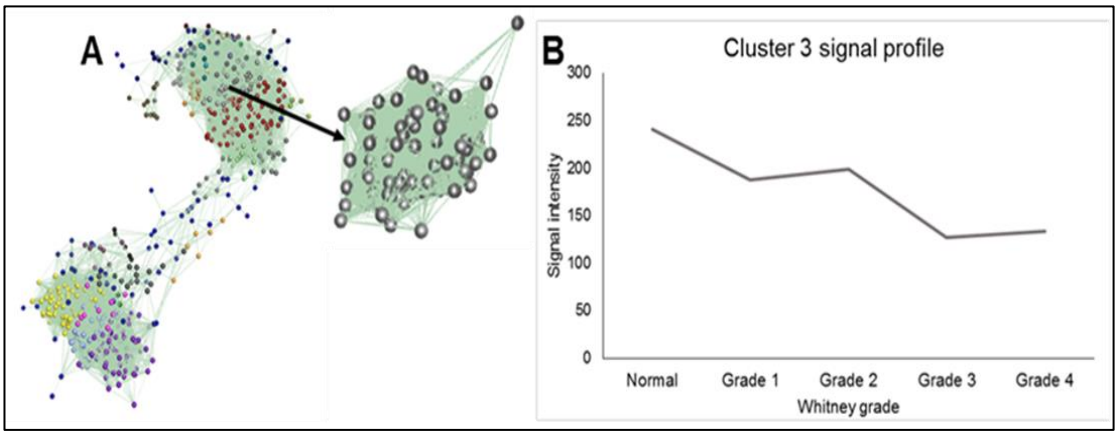

Figure 3-13. Miru clustering of differentially expressed genes – Cluster 3. (A) Miru clustering highlighting the position of cluster 3. (B) Average signal profile of the 147 genes in cluster 3.

Category	Term	Count	P-Value	FDR
GOTERM_MF_DIRECT	Heparin binding	6	1.53E-04	0.17588
GOTERM_CC_DIRECT	Cell surface	9	0.00102	1.09886
GOTERM_BP_DIRECT	Adenylate cyclase-activating GPCR signaling pathway	4	0.00114	1.58043
GOTERM_MF_DIRECT	G-protein coupled peptide receptor activity	3	0.00221	2.5091
GOTERM_MF_DIRECT	Calcium ion binding	10	0.0043	4.83464
GOTERM_CC_DIRECT	Integral component of membrane	34	0.00787	8.23544
GOTERM_BP_DIRECT	Adenylate cyclase-inhibiting GPCR signaling pathway	3	0.01624	20.4417
GOTERM_CC_DIRECT	Basolateral plasma membrane	4	0.01766	17.6233
GOTERM_CC_DIRECT	Proteinaceous extracellular matrix	5	0.01796	17.8929
GOTERM_BP_DIRECT	Phospholipase C-activating GPCR signaling pathway	3	0.02121	25.8816

Table 3-8. Functional analysis chart of the top 10 GO terms associated with cluster 3.

Cluster 4 contained 96 genes (**Figure 3-14A**) with an average signal intensity profile which increased in grade 3 and 4 of disease (**Figure 3-14B**). 24 GO terms

were related with all genes in cluster 4. GO terms in the top 10 GO terms associated with cluster 4 included osteoblast- and bone-related GO terms (**Table 3-9**).

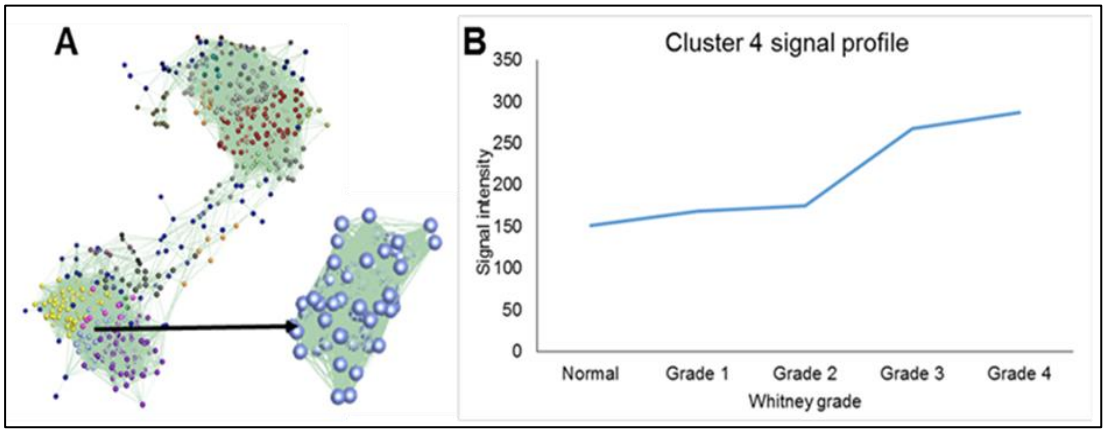

Figure 3-14. Miru clustering of differentially expressed genes – Cluster 4. (A) Miru clustering highlighting the position of cluster 4. (B) Average signal profile of the 96 genes in cluster 4.

Category	Term	Count	P-Value	FDR
GOTERM_BP_DIRECT	Positive regulation of angiogenesis	5	7.43E-04	1.03282
GOTERM_BP_DIRECT	Cellular response to lipopolysaccharide	4	0.00353	4.82258
GOTERM_BP_DIRECT	Bone morphogenesis	3	0.00574	7.7239
GOTERM_BP_DIRECT	Organelle fission	2	0.01036	13.5408
GOTERM_BP_DIRECT	Nucleoside triphosphate catabolic process	2	0.02062	25.2498
GOTERM_BP_DIRECT	Cellular response to hypoxia	3	0.02092	25.5695
GOTERM_BP_DIRECT	Positive regulation of osteoblast differentiation	3	0.02374	28.5099
GOTERM_BP_DIRECT	Neutrophil chemotaxis	3	0.0257	30.4915
GOTERM_MF_DIRECT	Ephrin receptor activity	2	0.0306	29.1705
GOTERM_BP_DIRECT	Innate immune response	4	0.03426	38.551

Table 3-9. Functional analysis chart of the top 10 GO terms associated with cluster 4.

Cluster 5 contained 80 genes (**Figure 3-15A**) with an average signal intensity profile which increased in a progressive manner reaching its peak in grade 4 disease (**Figure 3-15**B). 26 GO terms were assigned to these genes including metalloendopeptidase activity and stem cell differentiation (**Table 3-10**).

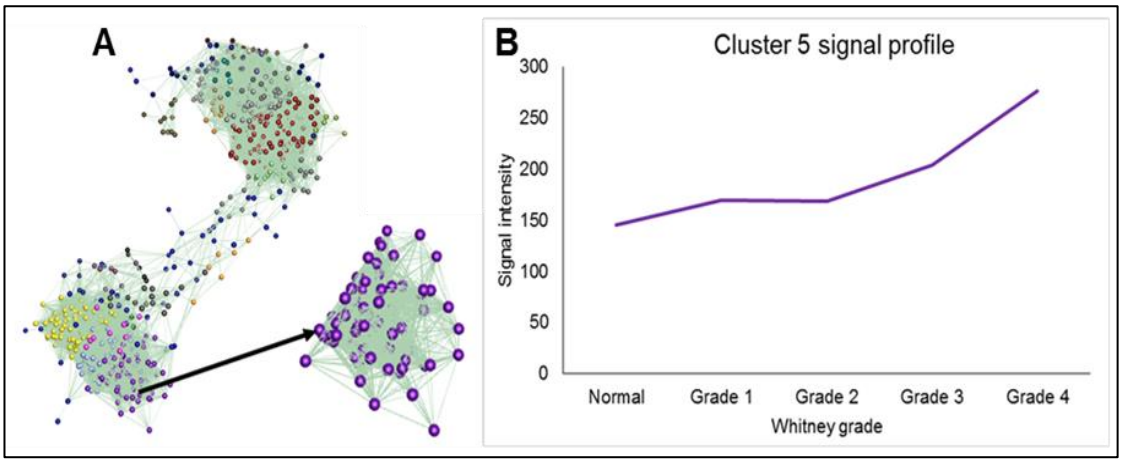

Figure 3-15. Miru clustering of differentially expressed genes – Cluster 5 (A) Miru clustering highlighting the position of cluster 5. (B) Average signal profile of the 80 genes in cluster 5.

Category	Term	Count	P-Value	FDR
GOTERM_MF_DIRECT	Metalloendopeptidase activity	5	6.63E-04	0.70482
GOTERM_BP_DIRECT	Stem cell differentiation	3	0.00327	4.53441
GOTERM_BP_DIRECT	Heart development	4	0.00708	9.58508
GOTERM_BP_DIRECT	Positive regulation of ERK1 and ERK2 cascade	4	0.0132	17.1765
GOTERM_BP_DIRECT	Positive regulation of endothelial cell proliferation	3	0.01437	18.5586
GOTERM_BP_DIRECT	Neutrophil chemotaxis	3	0.01496	19.2449
GOTERM_BP_DIRECT	Positive regulation of T cell differentiation in thymus	2	0.02315	28.2675
GOTERM_CC_DIRECT	Collagen type IV trimer	2	0.02559	23.4714
GOTERM_BP_DIRECT	Regulation of behavior	2	0.02696	32.1325
GOTERM_BP_DIRECT	Response to hypoxia	3	0.02955	34.6459

Table 3-10. Functional analysis chart of the top 10 GO terms associated with cluster 5.

To analyse trends for progressive down- and up-regulation of genes over the entire course of the disease, all clusters showing a down-regulation pattern or an up-regulation pattern were averaged and GO term analysis was performed. Collectively, these analyses indicated that genes that are changed significantly in one grade of disease follow a progressive pattern for change across all grades of disease. The down-regulated clusters contained 211 genes (**Figure 3-16A**) with the average signal intensity for genes in these clusters decreasing

by more than 2-fold by grade 4 disease (**Figure 3-16B**). 27 GO terms were associated with these clusters with the top 10 GO terms shown in **Table 3-11**.

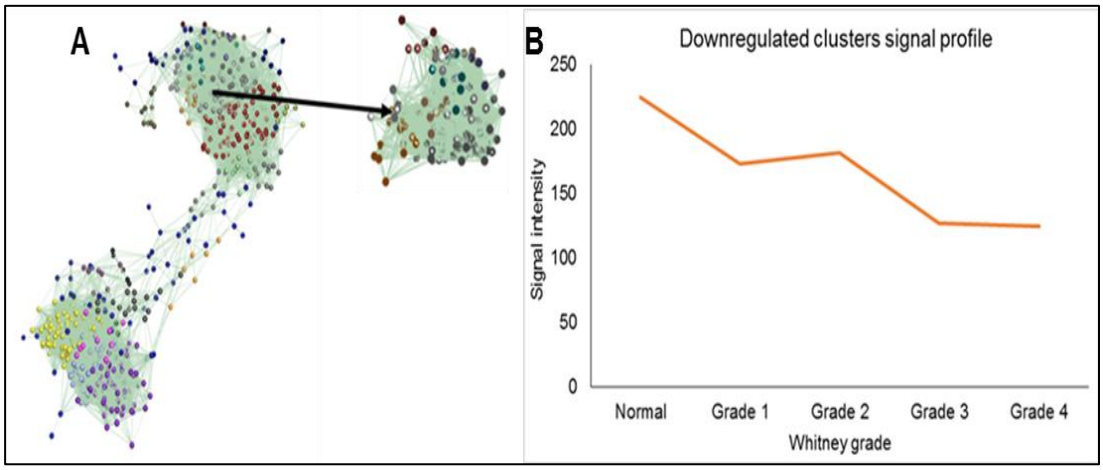

Figure 3-16. Analysis of all down-regulated genes. (A) The down-regulated genes in the network layout. (B) The average signal intensity for the 211 down-regulated genes in these clusters.

Category	Term	Count	P-Value	FDR
GOTERM_MF_DIRECT	Heparin binding	6	6.79E-04	0.82041
GOTERM_BP_DIRECT	Adenylate cyclase-activating GPCR signaling pathway	4	0.00236	3.33573
GOTERM_MF_DIRECT	G-protein coupled peptide receptor activity	3	0.00414	4.90597
GOTERM_MF_DIRECT	Calcium ion binding	12	0.0043	5.09472
GOTERM_CC_DIRECT	Cell surface	9	0.00594	6.42319
GOTERM_CC_DIRECT	Basolateral plasma membrane	5	0.00611	6.59806
GOTERM_BP_DIRECT	Adenylate cyclase-inhibiting GPCR signaling pathway	3	0.02608	31.596
GOTERM_BP_DIRECT	Negative regulation of kinase activity	2	0.03017	35.609
GOTERM_CC_DIRECT	Integral component of membrane	40	0.03166	30.122
GOTERM_BP_DIRECT	Phospholipase C-activating GPCR signaling pathway	3	0.03389	39.0643

Table 3-11. Functional analysis chart of the top 10 GO terms associated with the clusters associated with down-regulation in disease.

The up-regulated clusters contained 116 genes (**Figure 3-17A**) with the average signal intensity for genes in these clusters increasing by more than 2-fold by grade 4 disease (**Figure 3-17**B). 24 GO terms were associated with these clusters with the 10 most significant GO terms shown in **Table 3-12**.

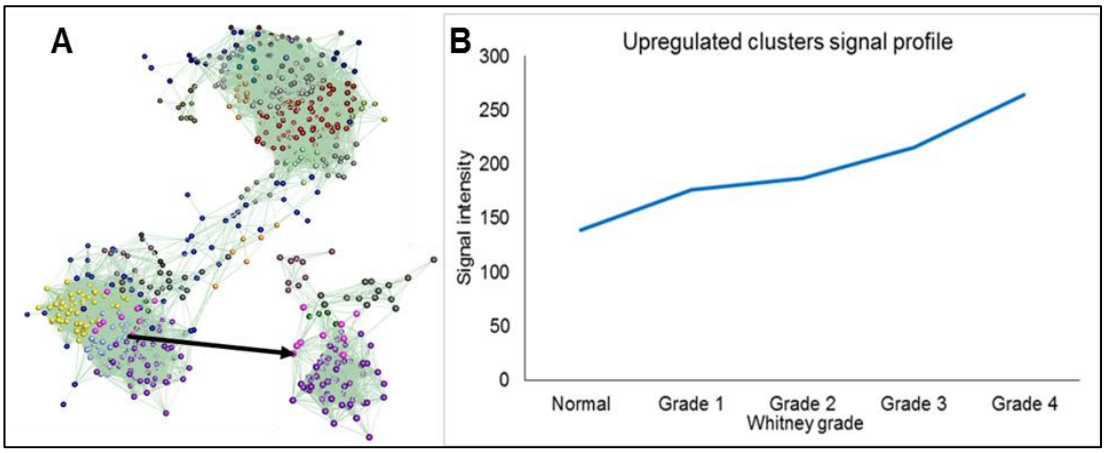

Figure 3-17. Analysis of all up-regulated genes. (A) Miru clustering of all genes showing a trend for up-regulation over the course of the disease. (B) Average signal intensity for the 116 genes in these clusters.

Category	Term	Count	P-Value	FDR
GOTERM_MF_DIRECT	Metalloendopeptidase activity	5	0.00149	1.64773
GOTERM_BP_DIRECT	Stem cell differentiation	3	0.00523	7.25952
GOTERM_BP_DIRECT	Heart development	4	0.01365	17.9351
GOTERM_BP_DIRECT	Positive regulation of endothelial cell proliferation	3	0.0226	28.0176
GOTERM_BP_DIRECT	Positive regulation of cell proliferation	5	0.02338	28.8392
GOTERM_BP_DIRECT	Neutrophil chemotaxis	3	0.0235	28.9738
GOTERM_BP_DIRECT	Positive regulation of ERK1 and ERK2 cascade	4	0.02495	30.4709
GOTERM_CC_DIRECT	Dendrite	4	0.02929	26.9821
GOTERM_BP_DIRECT	Positive regulation of T cell differentiation in thymus	2	0.02935	34.8472
GOTERM_CC_DIRECT	Collagen type IV trimer	2	0.0319	29.0338

Table 3-12. Functional analysis chart of the top 10 GO terms associated with the clusters associated with up-regulation in disease.

3.3.6 DAVID 6.8 gene enrichment between grades

The differentially expressed genes from each grade of disease (without FDR correction) were submitted to DAVID 6.8 for gene ontology enrichment. Due to the relatively low number of genes that were differentially expressed in grade 1 and 2 valves both up- and down-regulated genes had to be submitted together whereas the differentially expressed genes for grade 3 and 4 valves could be separated into GO terms associated with up- and down-regulation. The functional analysis charts for the GO terms associated with genes

differentially expressed in grade 1 valves are shown in **Table 3-13**. Nine GO terms were identified with the majority of terms suggesting that early pathogenic gene changes are related to membrane and extracellular matrix.

Category	Term	Count	PValue	FDR
GOTERM_BP_DIRECT	Regulation of ryanodine-sensitive calcium-release channel activity	2	0.0116	13.89
GOTERM_BP_DIRECT	Defense response to virus	3	0.0202	22.903
GOTERM_BP_DIRECT	Myoblast migration	2	0.0231	25.855
GOTERM_CC_DIRECT	Proteinaceous extracellular matrix	3	0.0822	56.851
GOTERM_CC_DIRECT	Integral component of membrane	16	0.0891	59.898
GOTERM_CC_DIRECT	Extracellular space	6	0.0892	59.946
GOTERM_BP_DIRECT	Negative regulation of protein kinase B signaling	2	0.0895	69.813
GOTERM_BP_DIRECT	Branching involved in ureteric bud morphogenesis	2	0.0948	71.993
GOTERM_MF_DIRECT	Calcium ion binding	5	0.0968	65.756

Table 3-13. Functional analysis chart summary of grade 1 related GO terms.

Functional analysis chart only identified two GO terms related for the genes differentially expressed in grade 2 valves (**Table 3-14**).

Category	Term	Count	P-Value	FDR
GOTERM_BP_DIRECT	Negative regulation of growth	2	0.0181198	19.636988
GOTERM_BP_DIRECT	Cellular response to hormone stimulus	2	0.0495574	45.537751

Table 3-14. Functional analysis chart summary of grade 2 related GO terms.

The functional analysis for grade 3 valve differentially expressed genes could be separated into up- and down-regulated genes, with 92 GO terms associated with up-regulated genes and 85 GO terms associated with down-regulated genes. The top 10 suggested terms are shown in **Table 3-15**.

	Category	Term	Count	PValue	FDR
Upregulated	GOTERM_BP_DIRECT	Inflammatory response	16	1.08E-07	1.70E-04
	GOTERM_BP_DIRECT	Positive regulation of angiogenesis	9	2.93E-05	0.0460492
	GOTERM_BP_DIRECT	Cell-cell signaling	8	5.68E-05	0.0890522
	GOTERM_BP_DIRECT	Positive regulation of ERK1 and ERK2 cascade	10	1.57E-04	0.2467334
	GOTERM_BP_DIRECT	Immune response	11	3.30E-04	0.5164762
	GOTERM_BP_DIRECT	Positive regulation of transcription from RNA polymerase II promoter involved in smooth muscle cell differentiation	3	7.10E-04	1.1086158
	GOTERM_BP_DIRECT	Neutrophil chemotaxis	6	8.47E-04	1.3217166
	GOTERM_BP_DIRECT	Regulation of cell growth	5	8.56E-04	1.3356317
	GOTERM_MF_DIRECT	Chemokine activity	5	0.0010917	1.3991207
	GOTERM_BP_DIRECT	Positive regulation of inflammatory response	5	0.0018038	2.7944106
Downregulated	GOTERM_CC_DIRECT	Proteinaceous extracellular matrix	19	1.42E-09	1.75E-06
	GOTERM_BP_DIRECT	Semaphorin-plexin signaling pathway	7	3.73E-06	0.0059178
	GOTERM_CC_DIRECT	Extracellular space	35	9.50E-06	0.0116947
	GOTERM_MF_DIRECT	Semaphorin receptor binding	6	1.70E-05	0.022432
	GOTERM_MF_DIRECT	Calcium ion binding	25	3.54E-05	0.0467482
	GOTERM_MF_DIRECT	Chemorepellent activity	6	7.12E-05	0.0938346
	GOTERM_BP_DIRECT	Negative regulation of axon extension involved in axon guidance	6	7.99E-05	0.1265495
	GOTERM_BP_DIRECT	Regulation of heart rate by cardiac conduction	6	9.74E-05	0.1543246
	GOTERM_MF_DIRECT	Heparin binding	9	1.53E-04	0.201529
	GOTERM_BP_DIRECT	Neural crest cell migration	7	1.85E-04	0.293209

Table 3-15. Functional analysis chart summary of grade 3 valves. GO terms associated with up- and down-regulated genes.

Functional analysis of the genes differentially expressed in grade 4 valves, likewise, was separated into terms associated with up- (107 GO terms) or down-regulated (40 GO terms) genes. The functional analysis chart of top 10 GO terms for both up- and down-regulated genes are shown in **Table 3-16**.

	Category	Term	Count	PValue	FDR
Upregulated	GOTERM_BP_DIRECT	Neutrophil chemotaxis	8	4.16E-06	0.00659
	GOTERM_CC_DIRECT	Extracellular space	29	8.42E-06	0.01006
	GOTERM_BP_DIRECT	Positive regulation of ERK1 and ERK2 cascade	11	1.11E-05	0.01758
	GOTERM_MF_DIRECT	Heparin binding	9	2.02E-05	0.02544
	GOTERM_BP_DIRECT	Cell-cell signaling	8	2.91E-05	0.04611
	GOTERM_MF_DIRECT	Integrin binding	5	8.47E-05	0.10658
	GOTERM_BP_DIRECT	Positive regulation of angiogenesis	8	1.14E-04	0.18042
	GOTERM_BP_DIRECT	Inflammatory response	11	1.96E-04	0.31029
	GOTERM_CC_DIRECT	Proteinaceous extracellular matrix	10	4.46E-04	0.53226
	GOTERM_BP_DIRECT	Positive regulation of endothelial cell proliferation	6	4.77E-04	0.75468
Downregulated	GOTERM_CC_DIRECT	Proteinaceous extracellular matrix	11	1.86E-05	0.02146
	GOTERM_BP_DIRECT	Receptor localization to synapse	3	0.00115	1.67606
	GOTERM_CC_DIRECT	Integral component of plasma membrane	19	0.00205	2.34731
	GOTERM_CC_DIRECT	Extracellular matrix	6	0.00557	6.25627
	GOTERM_BP_DIRECT	Adenylate cyclase-activating GPCR signaling pathway	4	0.00638	8.98655
	GOTERM_MF_DIRECT	G-protein coupled peptide receptor activity	3	0.00808	9.66805
	GOTERM_MF_DIRECT	Calcium ion binding	14	0.00905	10.7702
	GOTERM_BP_DIRECT	Positive regulation of phosphatidylinositol 3-kinase signaling	4	0.01439	19.1963
	GOTERM_CC_DIRECT	Cell surface	10	0.01516	16.191
	GOTERM_CC_DIRECT	Basolateral plasma membrane	5	0.0197	20.5581

Table 3-16. Functional analysis chart summary of grade 4 valves. Up-regulated genes associated with GO terms and down-regulated genes associated with GO terms.

Functional analysis was performed on the differentially expressed genes from the grade 3 and 4 valves with the higher stringency FDR cut off gene sets. Both the up- and down-regulated genes in these datasets had to be submitted together for each valve. The 18 genes differentially expressed in grade 3 valves only indicated one GO term associated with disease, negative regulation of inflammatory response (**Table 3-17**). The 70 genes differentially expressed in grade 4 valves had 19 GO terms associated with disease (**Table 3-18**) with several of the same GO terms (e.g. positive regulation of ERK1 and ERK2 cascade, proteinaceous extracellular matrix) found in the GO term analysis of the less stringent gene lists.

Category	Term	Count	PValue	FDR
GOTERM_BP_DIRECT	Negative regulation of inflammatory response	2	0.03391	29.1411

Table 3-17. Grade 3 valve GO term from FDR cut off gene set.

Category	Term	Count	P-Value	FDR
GOTERM_BP_DIRECT	Positive regulation of ERK1 and ERK2 cascade	5	4.40E-04	0.59452
GOTERM_BP_DIRECT	Negative regulation of cell death	3	0.00263	3.50626
GOTERM_BP_DIRECT	Positive regulation of phosphatidylinositol 3-kinase signaling	3	0.00782	10.09
GOTERM_BP_DIRECT	Negative regulation of inflammatory response	3	0.00987	12.5661
GOTERM_BP_DIRECT	Negative regulation of apoptotic process	4	0.0201	24.0395
GOTERM_BP_DIRECT	Positive regulation of cell proliferation	4	0.02416	28.1944
GOTERM_BP_DIRECT	Wound healing, spreading of cells	2	0.02529	29.3118
GOTERM_MF_DIRECT	Heparin binding	3	0.02607	23.665
GOTERM_BP_DIRECT	Regulation of blood coagulation	2	0.03358	37.0342
GOTERM_BP_DIRECT	Angiogenesis	3	0.03818	40.9749
GOTERM_BP_DIRECT	Positive regulation of cell migration	3	0.04679	47.7491
GOTERM_MF_DIRECT	Integrin binding	2	0.05142	41.712
GOTERM_BP_DIRECT	Negative regulation of endothelial cell apoptotic process	2	0.05535	53.7549
GOTERM_BP_DIRECT	Cell adhesion	3	0.06053	57.0748
GOTERM_CC_DIRECT	Cell surface	4	0.07811	55.4765
GOTERM_BP_DIRECT	Positive regulation of cell adhesion	2	0.08189	68.5664
GOTERM_BP_DIRECT	Cellular iron ion homeostasis	2	0.08451	69.7574
GOTERM_CC_DIRECT	Proteinaceous extracellular matrix	3	0.08569	58.9895
GOTERM_BP_DIRECT	Inflammatory response	3	0.09059	72.3672

Table 3-18. Grade 4 valve GO terms from FDR cut off gene set.

3.3.7 Ingenuity Pathway Analysis

The low stringency (no FDR correction) differentially expressed gene lists for each grade of disease was submitted into Ingenuity Pathway Analysis (IPA). Mapped genes were used for further analyses while unmapped genes were unable to be correctly identified and so not used for further analyses (**Table 3-19**).

Grade of disease	Mapped genes	Unmapped genes	Total genes
1	66	10	76
2	42	17	59
3	628	41	669
4	458	34	492

Table 3-19. Mapped, unmapped and total number of genes submitted into IPA for each grade of disease.

Canonical pathway analysis of each grade of disease showed an increasing number of pathways associated with disease (P-value <0.05) as the disease

progresses. The genes differentially expressed in grade 1 disease had eight canonical pathways attributed to them. Analysis of the genes differentially expressed in grade 2 disease showed an association of twelve pathways. Ninety-three pathways were associated with the differentially expressed genes in grade 3 disease. Finally, fifty-two pathways were associated with the differentially expressed genes in grade 4 disease. A summary of the top three canonical pathways associated with the differentially expressed genes in each grade of disease is shown in **Table 3-20**. This highlights the strength of the association of the gene list with the pathway (P-value) and the number of genes up- or down-regulated in each pathway. There was considerable overlap between the pathways for grade 3 and 4.

Grade of disease	Canonical Pathway	Up-regulated genes	Down-regulated genes	Genes changed in pathway	P-value
1	GPCR-Mediated Integration of Enteroendocrine Signalling	2	0	2/61	0.016218
	Lipid Rafts in the Pathogenesis of Influenza	0	1	1/6	0.019055
	Melanocyte Development and Pigmentation Signaling	1	1	2/91	0.033884
2	Aryl Hydrocarbon Receptor Signaling	2	1	3/115	0.002138
	Glycerol-3-phosphate Shuttle	0	1	1/3	0.006761
	Glycerol Degradation I	0	1	1/4	0.008913
3	Hepatic Fibrosis / Hepatic Stellate Cell Activation	10	15	25/183	3.16E-11
	Agranulocyte Adhesion and Diapedesis	8	13	21/189	5.13E-08
	Axonal Guidance Signaling	20	14	34/450	8.91E-08
4	Hepatic Fibrosis / Hepatic Stellate Cell Activation	3	14	17/183	2.29E-07
	Agranulocyte Adhesion and Diapedesis	2	14	16/189	1.78E-06
	Granulocyte Adhesion and Diapedesis	2	12	14/177	1.7E-05

Table 3-20. Summary of top three canonical pathways associated with each grade of disease. The number of genes up- and down-regulated in each pathway as well as the total number of genes changed in each pathway is shown. The P-value score shows the association of the gene list to the pathway (the lower the value indicates the stronger the association).

The upstream regulator analysis provided by IPA suggests which upstream transcriptional regulators are involved in the gene changes observed in a gene list. An increasing number of molecules were associated with each grade of disease and a stronger association for the top suggested molecules was also seen as the disease progresses. With a P-value cut-off (<0.05) 156 molecules were associated with the genes differentially expressed in grade 1 valves. 254 molecules were suggested as potential top upstream regulators in grade 2 disease. 1873 molecules were associated with the genes differentially expressed in grade 3 disease. 1961 molecules were suggested as potential upstream regulators for genes differentially expressed in grade 4 disease. **Table 3-21** summarises the top three upstream regulators associated with the differentially expressed genes in each grade of disease. Each regulator has the molecule type, the association of the gene list with the molecule (P-value) and prediction as to whether the molecule's pathway is being activated or inactivated (Z-score). Of particular note is the repeated association of the molecules Transforming Growth Factor β1 (TGFβ1) and Tumour Necrosis Factor (TNF).

Disease state	Upstream Regulator	Molecule Type	Activation Z-score	P-value
Grade 1	P2RY2	GPCR		0.0007
	Lithium	Chemical drug		0.00124
	Bucladesine	Chemical toxicant	1.131	0.00167
Grade 2	Mma_DMAG	Chemical		0.00067
	TNF	Cytokine	0.826	0.00089
	HOXB13	Transcription regulator		0.00122
Grade 3	TGFβ1	Growth factor	1.316	3.01E-22
	TNF	Cytokine	2.361	8.03E-18
	LPS	Chemical drug	3.874	3.00E-15
Grade 4	TGFβ1	Growth factor	2.589	6.22E-18
	TNF	Cytokine	3.313	1.17E-14
	IFNG	Cytokine	3.248	3.57E-14

Table 3-21. Summary of the top three upstream regulators associated with the differentially expressed genes lists for each grade of disease. For each upstream regulator, the molecule type, Z-score and P-value are given.

Forty-five downstream genes of TGFβ1 and TNF signalling pathways were shared in grade 4 diseased samples (**Figure 3-18**). Image networks produced for TGFβ1 (**Figure 3-19**) and TNF (**Figure 3-20**) indicate that, respectively, only 28 of 90 and 28 of 85 of the genes differentially expressed in grade 4 valves that are downstream targets for these molecules were inconsistent with previously published articles (yellow interrupted line).

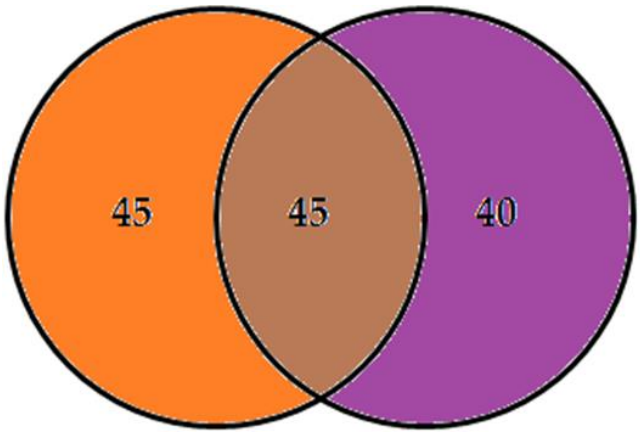

Figure 3-18. Venn diagram illustrating the number of genes shared between TGFβ1 and TNF pathways suggested by IPA upstream regulator analysis. The left orange circle shows the number of genes differentially expressed in grade 4 samples associated with TGFβ1 and not shared with TNF, in the right purple circle are the number of genes associated with TNF and not shared with TGFβ1 and in the centre brown area the number of shared genes between the two pathways are shown.

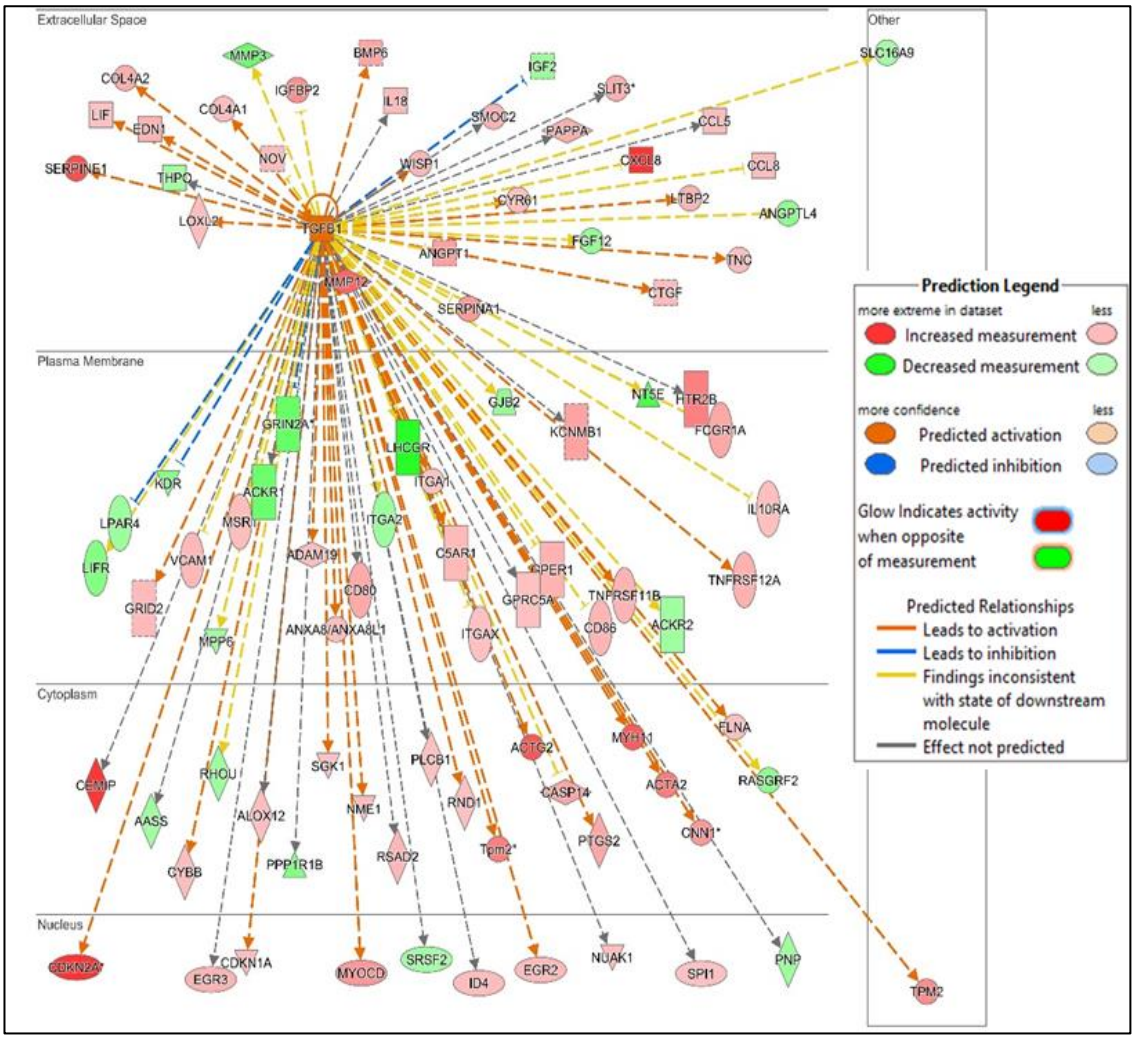

Figure 3-19. The network of genes that are differentially expressed in grade 4 valves that are downstream of TGFβ1 signalling. TGFβ1 is shown to have its effect from the extracellular space on the genes in their cellular location. Genes are coloured red and green to represent up- or down-regulation in the dataset. Dotted lines connecting TGFβ1 to these genes show the expected effect of TGFB signalling: orange - activation, blue - inhibition, yellow - result inconsistent and grey – effect not predicted.

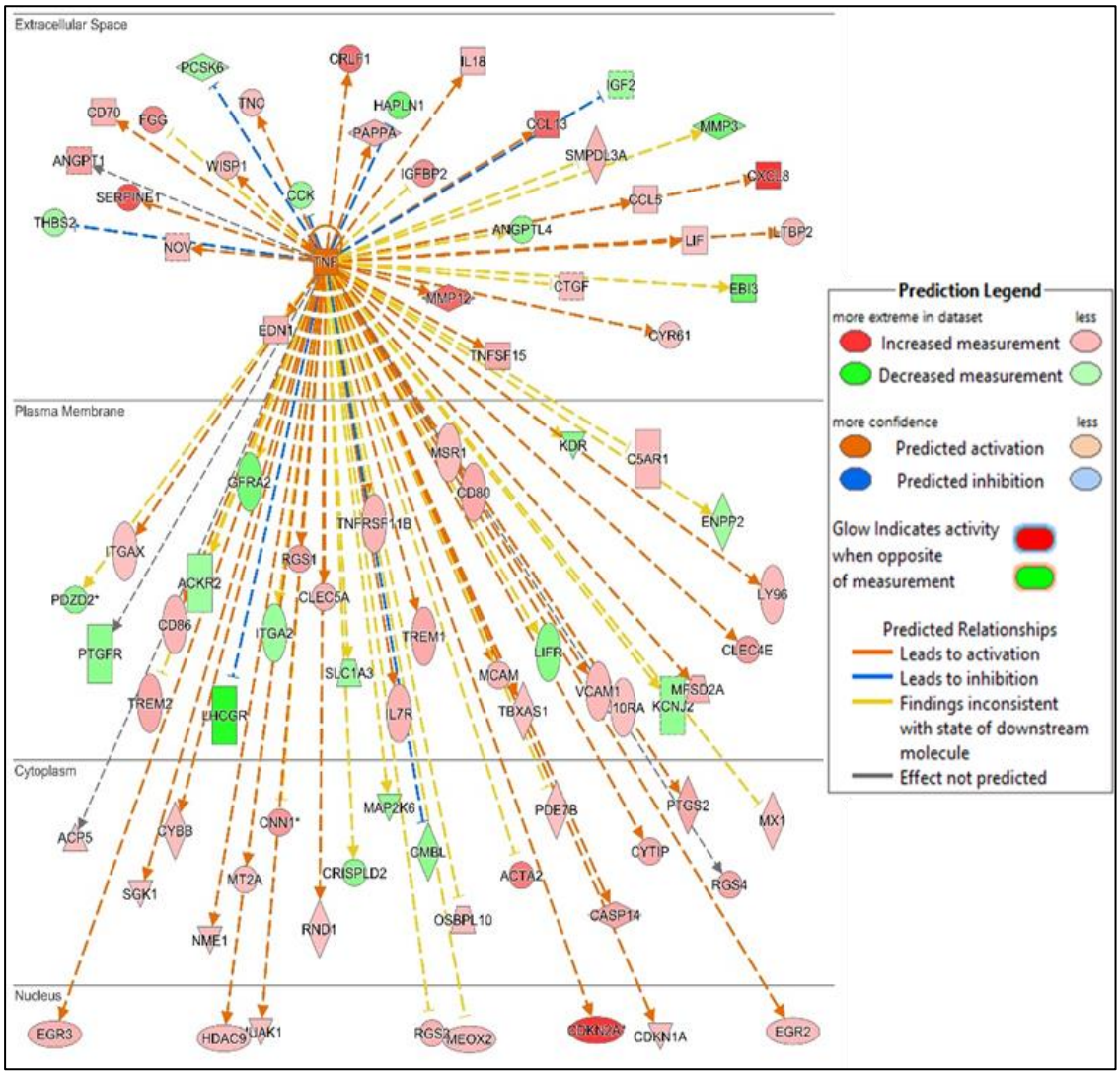

Figure 3-20. The network of genes that are differentially expressed in grade 4 valves that are downstream of TNF signalling. TNF is shown to have its effect from the extracellular space on the genes in their cellular location. Genes are coloured red and green to represent up- or down-regulation in the dataset. Dotted lines connecting TNF to these genes show the expected effect of TGFB signalling: orange - activation, blue - inhibition, yellow - result inconsistent and grey – effect not predicted.

Network analysis for the genes differentially expressed in each grade of disease highlights the disease and functional annotations assigned to each dataset. Four disease and function networks were associated with the genes

differentially expressed in grade 1 valves (**Table 3-22**). The top network in this analysis is visualised in **Figure 3-21**

Top disease and function
Cellular Movement, Hematological System Development and Function, Hypersensitivity Response
Cell Death and Survival, Cellular Development, Cellular Function and Maintenance
Cancer, Gastrointestinal Disease, Organismal Injury and Abnormalities
Cell Cycle, Cell Morphology, Cell-To-Cell Signaling and Interaction

Table 3-22. Summary of disease and function networks associated with differentially expressed genes in grade 1 disease. Underlined is the network that is visualised in Figure 3-21.

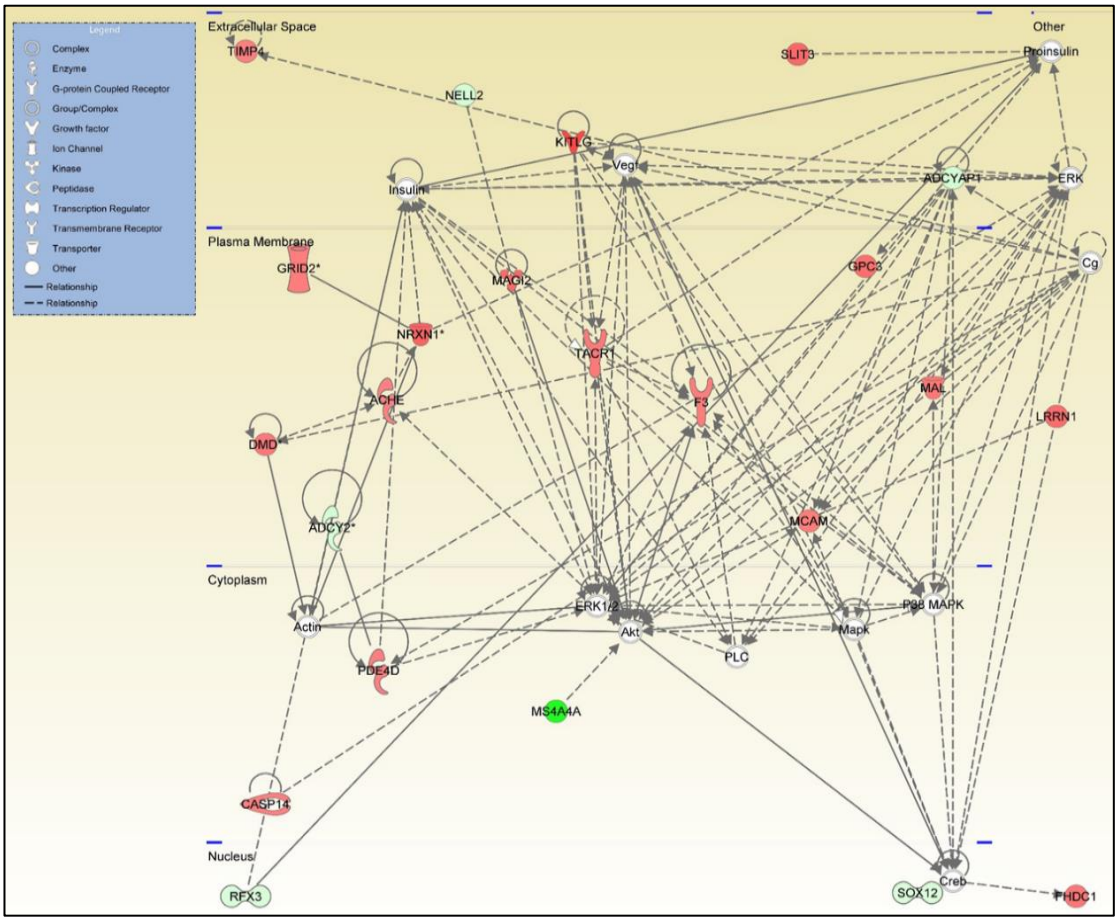

Figure 3-21. Schematic of the *Cellular movement, haematological system development and function, hypersensitivity response* disease and function network. Genes are shown in their protein cellular location with red indicating up-regulation, green down-regulation and un-coloured showing no change in the dataset.

Genes differentially expressed in grade 2 disease likewise were associated with four disease and function networks (**Table 3-23**). The *Cancer, organismal functions, organismal injury and abnormalities* network is schematised in **Figure 3-22**.

Top disease and function
Cancer, Organismal Functions, Organismal Injury and Abnormalities
Cell Death and Survival, Hematological System Development and Function, Gene expression
Cell Cycle, Developmental Disorder, Hereditary Disorder
Connective Tissue Disorders, Developmental Disorder, Gastrointestinal Disease

Table 3-23. Summary of disease and function networks associated with differentially expressed genes in grade 2 disease. Underlined is the network that is visualised in Figure 3-22.

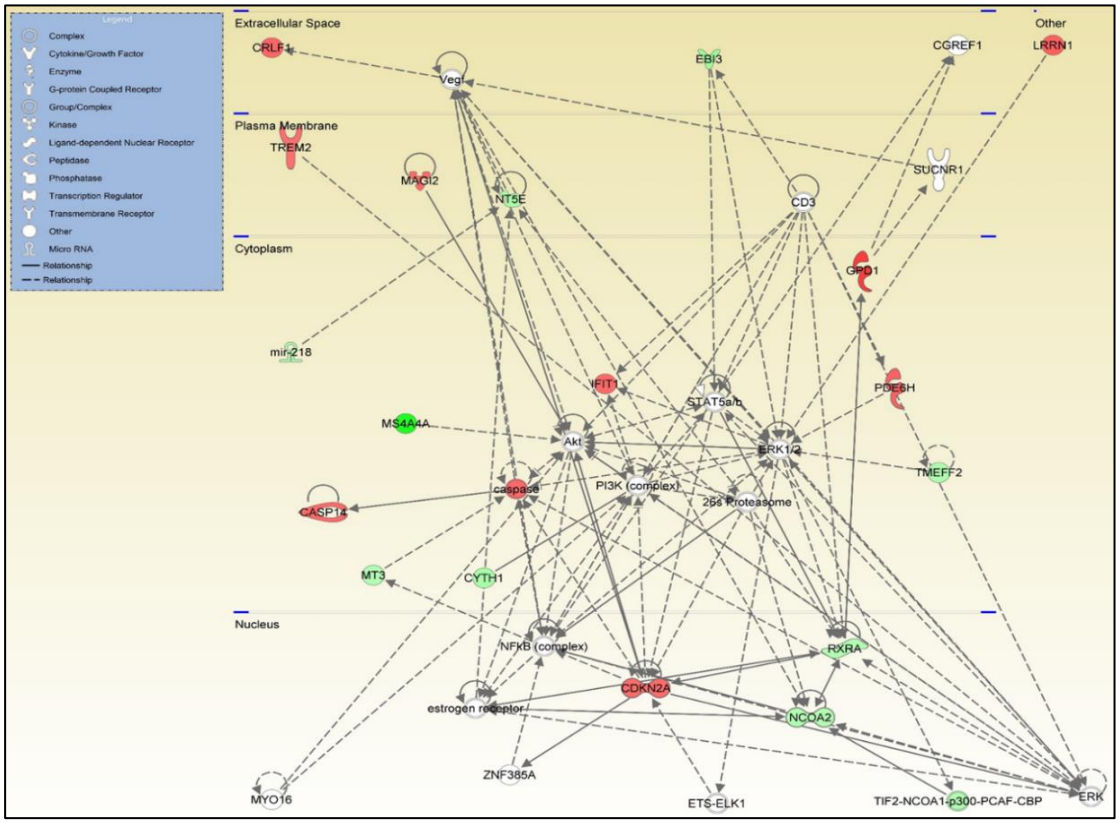

Figure 3-22. Schematic of the *Cancer, organismal functions, organismal injury and abnormalities* disease and function network. Genes are shown in their protein cellular location with red indicating up-regulation, green down-regulation and un-coloured showing no change in the dataset.

Genes differentially expressed in grade 3 disease were associated with ten disease and function networks (**Table 3-24**). The *Skeletal and muscular system development and function, cardiovascular system development and function, organ morphology* network is schematised in **Figure 3-23** as this was amongst the top networks and appeared to have biological relevance to disease.

Top disease and function
Cellular Function and Maintenance, Skeletal and Muscular System Development and Duncftion, Tissue Development
Skeletal and Muscular System Development and Function, Cardiovascular System Development and Function, Organ Morphology
Cancer, Organimsal Injury and Abnormalities, Tissue Morphology
Cellular Assembly and Organisation Cellular Function and Maintenance, Cellular Development
Cancer, Organimsal Injury and Abnormalities, Reproductive System Disease

Table 3-24. Summary of disease and function networks associated with differentially expressed genes in grade 3 disease. Underlined is the network that is visualised in Figure 3-23.

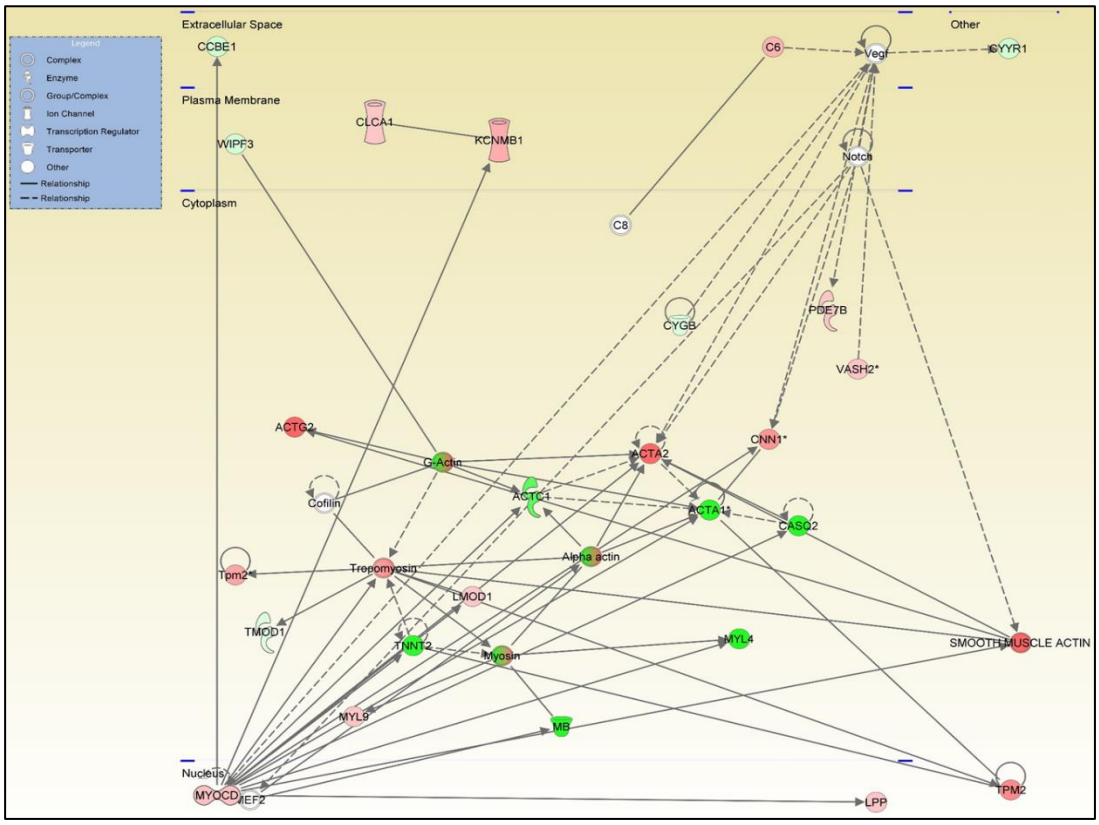

Figure 3-23. Schematic of the *Skeletal and muscular system development and function, cardiovascular system development and function, organ morphology* disease and function network. Genes are shown in their protein cellular location with red indicating up-regulation, green down-regulation and un-coloured showing no change in the dataset.

Genes differentially expressed in grade 4 disease were associated with ten disease and function networks (**Table 3-25**). The *Cardiovascular system development and function, organismal development and embryonic development* network are schematised in **Figure 3-24** as this was amongst the top networks and appeared to have biological relevance to disease.

Top disease and function
Cell Cycle, Cellular Development, Cellular Growth and Proliferation
Auditory Disease, Developmental Disorder, Hereditary Disorder
Cardiovascular System Development and Function, Organismal Development, Embryonic Development
Cell-To-Cell Signalling and Interaction, Hematological System Development and Function, Immune Cell Trafficking
Cell Death and Survival, Embryonic Development, Cellular Assembly and Organisation

Table 3-25. Summary of disease and function networks associated with differentially expressed genes in grade 4 disease. Underlined is the network that is visualised in Figure 3-24.

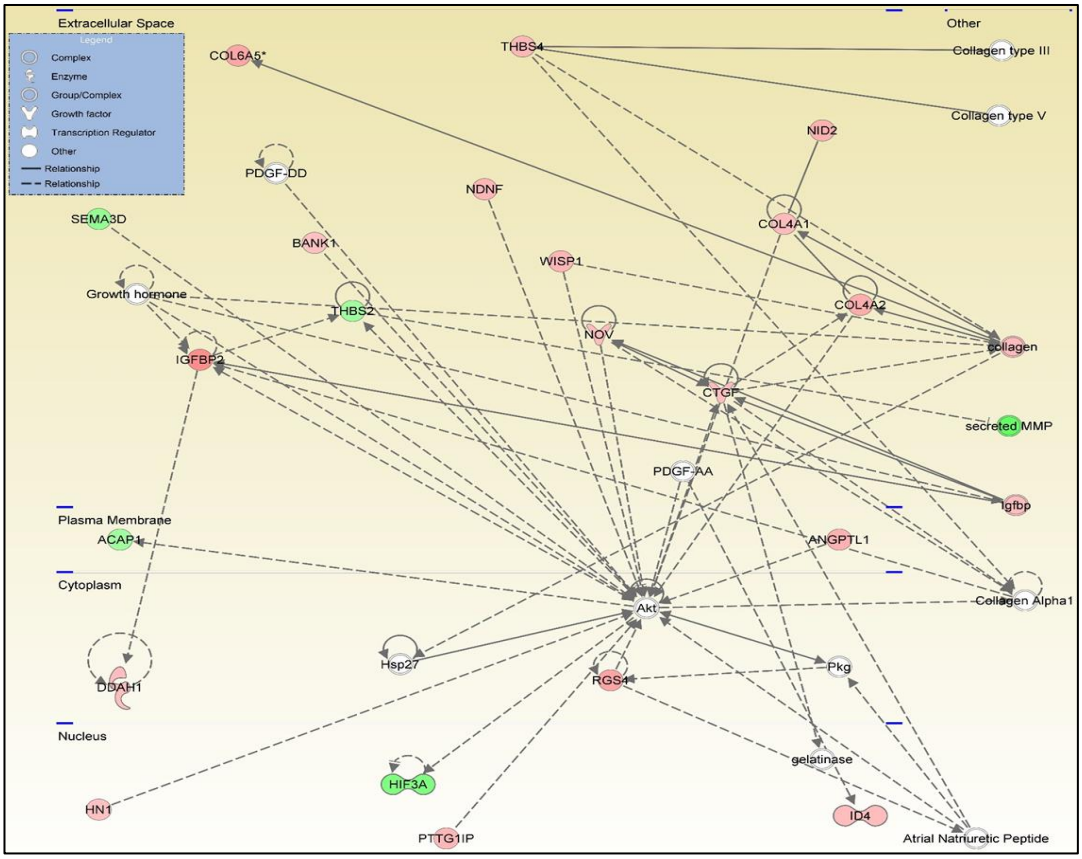

Figure 3-24. Schematic of the *Cardiovascular system development and function, organismal development and embryonic development* disease and function network. Genes are shown in their protein cellular location with red indicating up-regulation, green down-regulation and un-coloured showing no change in the dataset.

A noticeable effect in this analysis was that the milder grade 1 and 2 disease samples had considerably weaker associations (P-value) in all forms of analysis compared with the more severe grade 3 and 4 disease samples. This is due to the lower number of differentially expressed genes in each of these grades and the smaller fold change difference seen in these samples (as indicated in **Table 3-19**). As such, the results from the grade 3 and 4 diseased valve samples are more statistically credible. Additionally, there seems to be a level of agreement in the results returned for grade 3 and 4 diseased valve samples. This is exemplified by both the canonical pathway analysis and top upstream regulator analysis (**Table 3-20** and **Table 3-21**) suggested the same top two pathways.

To investigate the effect of the more stringent (Q-value >0.1) FDR correction applied to the genes differentially expressed in grade 4 disease. Grade 3 disease analysis was not performed due to the low number (18) genes differentially expressed when this correction is applied. Of the 64 genes accepted by IPA from the differentially expressed gene lists for grade 4 valves, 61 were mapped and 3 unmapped. Similarly, to the grade 1 and 2 analysis, the associations with this dataset are much lower than analysis without the FDR correction.

Eighteen canonical pathways were associated with this dataset (P>0.05) with the top five of these pathways shown in **Table 3-26**. These pathways differ with the canonical pathways associated with grade 4 disease without the FDR correction; however, the top suggested canonical pathway is the top canonical pathway suggested in grade 2 disease without the FDR correction (**Table 3-20**).

Canonical Pathway	Up-regulated genes	Down-regulated genes	Genes changed in pathway	P-value
Aryl Hydrocarbon Receptor Signaling	1	2	3/115	0.007244
Cell Cycle: G2/M DNA Damage Checkpoint Regulation	0	2	2/44	0.01
Melanoma Signaling	0	2	2/53	0.014454
Cell Cycle: G1/S Checkpoint Regulation	0	2	2/60	0.018197
STAT3 Pathway	0	2	2/68	0.022909

Table 3-26. Summary of the top five canonical pathways associated with genes differentially expressed in grade 4 of disease with the FDR correction (Q-value <0.1) applied. The number of genes up- and down-regulated in each pathway as well as the total number of genes changed in each pathway is shown.

The top five upstream regulators associated with the FDR corrected grade 4 disease dataset are shown in **Table 3-27**. In total 1201 molecules were associated with this dataset (P-value <0.05). The top suggested upstream regulator was TGFβ3 with TGFβ1 being the thirty-ninth upstream regulator (Z-score 0.672, P-value 0.000178). The gene interaction networks suggested by IPA for each of these factors are schematised in **Figure 3-25** and **Figure 3-26** respectively. TGFβ3 shows an interaction with three extracellular and two nuclear localised proteins, which are all increased in this dataset, in agreement with published literature as determined by IPA. TGFβ1 interacts with thirteen genes in the dataset but five of these changed their expression contradictory to what has been previously shown in the published literature. Although TGFβ3 had more genes whose expression was consistent with reports in the literature, TGFβ1 had not only more genes but the highest number of genes associated with it out of all pathways. Collectively this indicates an important role for both of these molecules in MMVD.

Upstream Regulator	Molecule Type	Activation Z-score	P-value
TGFβ3	Growth factor	2.156	1.00E-05
GRN510	Chemical reagent		1.17E-05
S100A11	Other		1.17E-05
ZFYVE16	transporter		1.17E-05
HIF1A	Transcription regulator	0.859	0.000017

Table 3-27. Summary of the top five upstream regulators associated with the differentially expressed genes lists for grade 4 disease with the FDR correction (Q-value>0.1) applied. For each upstream regulator, the molecule type, Z-score and P-value are given.

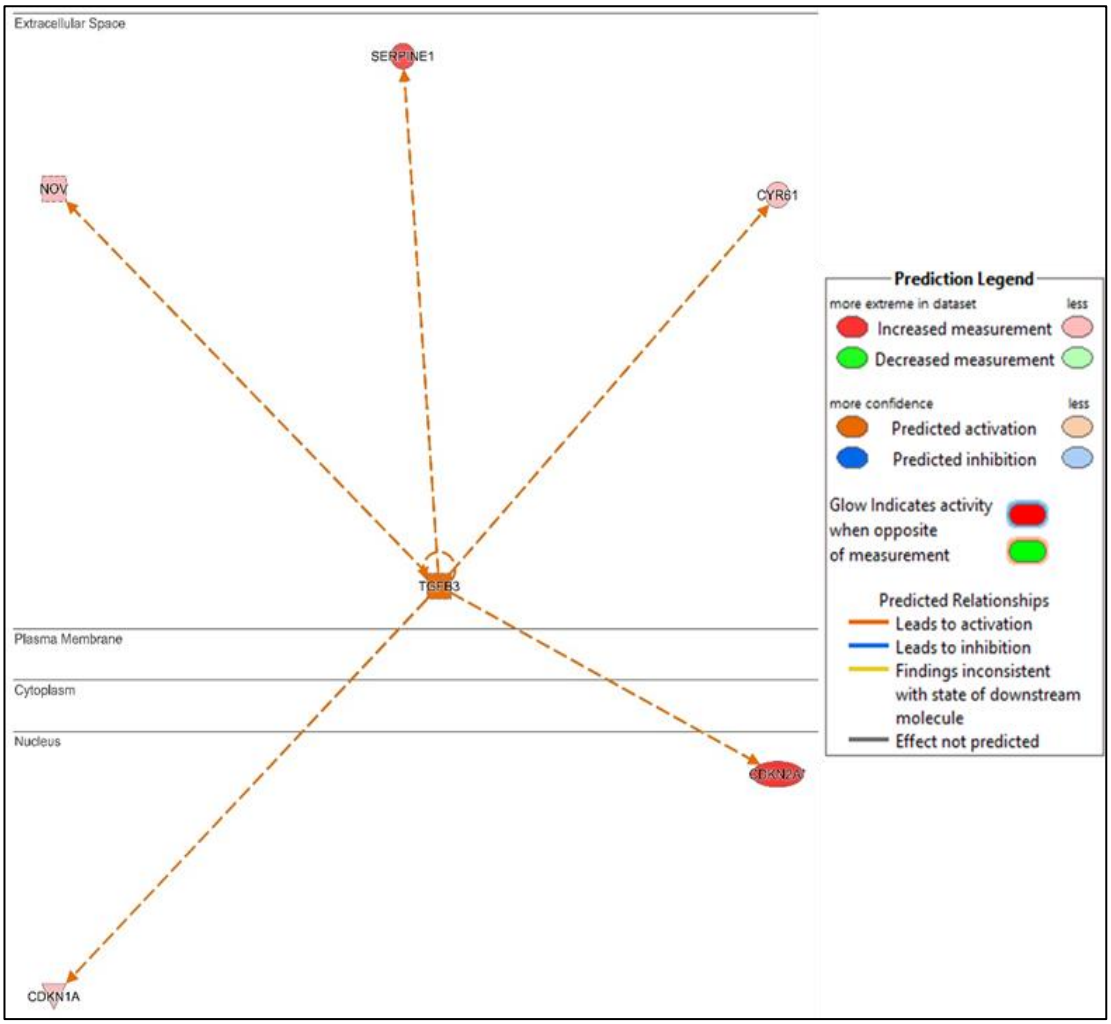

Figure 3-25. The network of genes that are differentially expressed in grade 4 disease with FDR correction (Q-value >0.1) that are downstream of TGFβ3 signalling. TGFβ3 is shown to have its effect from the extracellular space on the genes in their cellular location. Genes are coloured red to represent up-regulation in the dataset. Dotted lines connecting TGFβ3 to these genes are coloured orange to indicate activation of this gene.

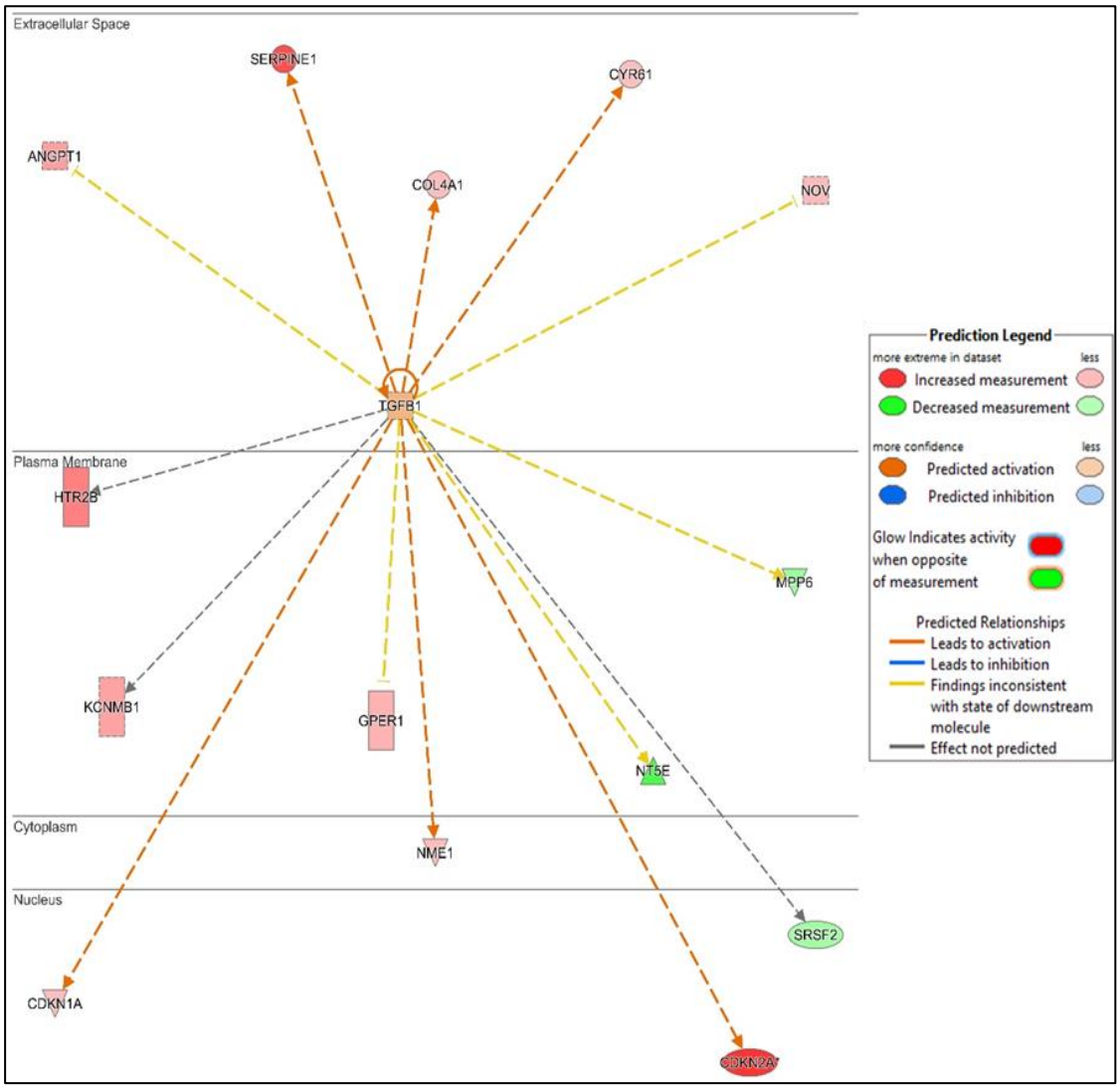

Figure 3-26. The network of genes that are differentially expressed in grade 4 disease with FDR correction (Q-value >0.1) that are downstream of TGFβ1 signalling. TGFβ1 is shown to have its effect from the extracellular space on the genes in their cellular location. Genes are coloured red and green to represent up- or down-regulation in the dataset. Dotted lines connecting TGFβ1 to these genes show the expected effect of TGFB signalling: orange - activation, yellow -result inconsistent and grey – effect not predicted.

Network analysis for the genes differentially expressed in this dataset was then performed using IPA. Six disease and function networks were associated with the genes differentially expressed in grade 4 disease with the FDR correction applied (**Table 3-28**). The top network in this analysis is visualised in **Figure 3-27**. This schematic also has the TGFβ signalling canonical pathway overlaid on it to show where this pathway would interact with the network.

Top disease and function
Cancer, Organismal Injury and Abnormalities, Cellular Development
Lipid Metabolism, Small Molecule Biochemistry, Molecular Transport
organismal Injury and Abnormalities, Post-Translational Modification, Cell Cycle
Cell Morphology, Cancer, organismal Injury and Abnormalities
Cell Signalling, Small Molecule Biochemistry, Cell-To-Cell Signalling and Interaction

Table 3-28. Summary of disease and function networks associated with differentially expressed genes in grade 4 disease. Underlined is the network that is visualised in Figure 3-27.

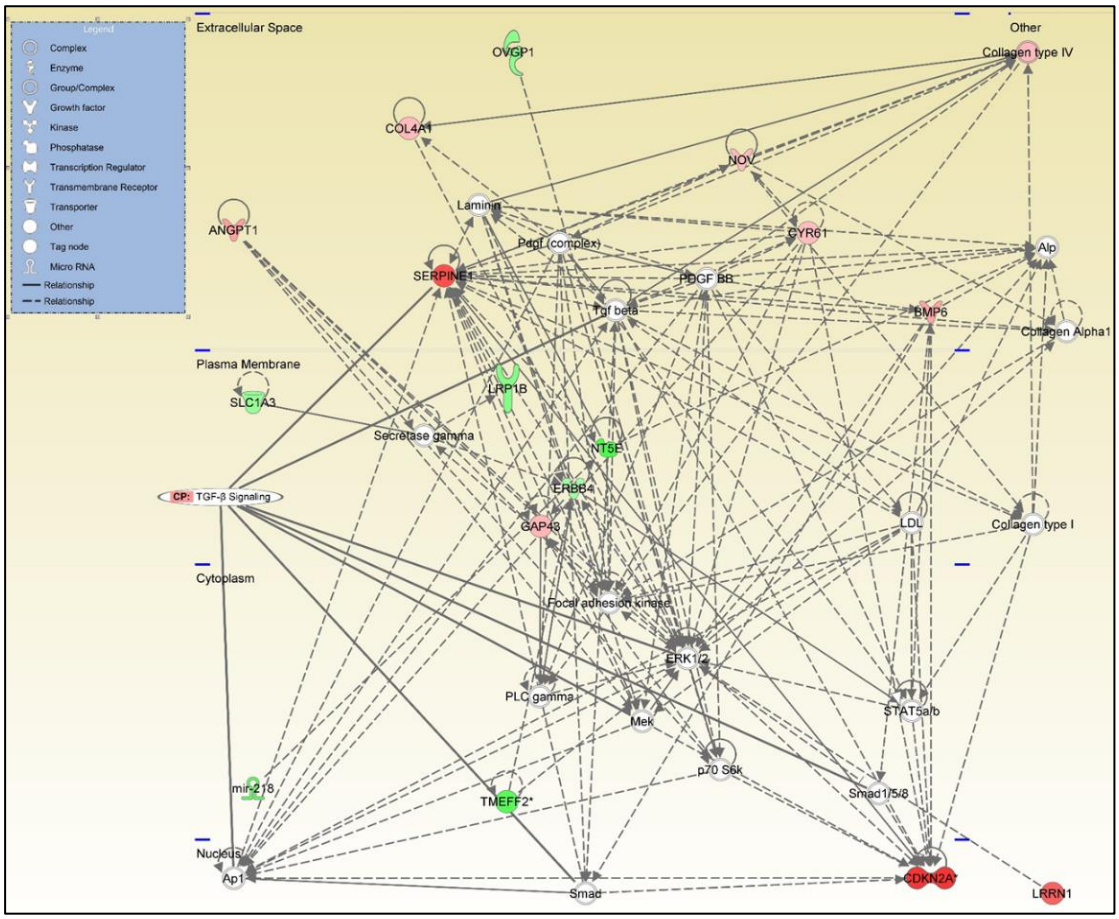

Figure 3-27. Schematic of the *Cancer, organismal injury and abnormalities disease and cellular development* network. Genes are shown in their protein cellular location with red indicating up-regulation, green down-regulation and un-coloured showing no change in the dataset. The canonical pathway TGFβ signalling is overlaid on this network indicating with black lines which genes it would interact within this network.

3.3.8 RT-qPCR validation of microarray analysis

To validate the microarray results RT-qPCR was performed on selected genes that were significantly altered in at least one grade of disease. These genes included known hallmarks of disease (*ACTA2* and *5HTR2B*), metalloproteinases (*MMP12, ADAMTS5* and *ADAMTS19*) and genes that changed in multiple grades of disease with high fold change differences

(*SLC10A6, CDKN2A, ACTG2, SLIT3* and *CILP*). The microarray results for these genes are shown in **Table 3-29** and the corresponding RT-qPCR results are shown in **Table 3-30**. Almost all results were in agreement between microarray and RT-qPCR with differences highlighted in yellow in the two tables. Results that did not agree all showed a significant difference in RT-qPCR but not by microarray. The direction of fold change movement matched for all genes.

Gene name	Grade 1		Grade 2		Grade 3		Grade 4	
	Fold change	P-value	Fold change	P-value	Fold change	P-value	Fold change	P-value
ACTA2	1.91	0.171	1.59	0.078	4.43	<0.001	3.24	0.001
HTR2B	1.2	0.53	1.2	0.387	2.14	0.002	3.11	<0.001
ADAMTS5	0	0.23	1.13	0.137	-1.81	0.035	-1.45	0.097
SLC10A6	1.1	0.544	-1.01	0.535	-2.01	<0.001	-1.67	0.003
CDKN2A	1.09	0.163	1.14	0.036	5.34	<0.001	3.23	<0.001
ACTG2	1.75	0.406	2.75	0.109	4.57	0.001	4.18	0.008
SLIT3	1.82	0.016	1.97	0.003	1.57	0.239	1.99	0.018
CILP	1.05	0.83	-1.16	0.556	-5.86	0.002	-3.64	<0.001
MMP12	1.52	0.809	2.92	0.097	2.87	0.02	3.77	0.038
ADAMTS19	-1	0.338	-1.33	0.155	-1.84	<0.001	-1.79	0.02

Table 3-29. Microarray fold change and P-value per grade of disease compared to normal valve samples for genes selected for microarray validation. Highlighted in yellow are instances where the significance of these results does not match with RT-qPCR validation.

Gene name	Grade 1		Grade 2		Grade 3		Grade 4	
	Fold change	P-value	Fold change	P-value	Fold change	P-value	Fold change	P-value
ACTA2	3.41	0.102	2.69	0.1	9.55	0.001	9.09	0.001
HTR2B	1.97	0.186	1.82	0.245	3.45	0.038	3.75	0.027
ADAMTS5	1.38	0.116	1.12	0.357	-1.83	0.036	-1.85	0.113
SLC10A6	-1.49	0.198	-1.64	0.013	-2.67	0.005	-6.25	0.003
CDKN2A	4.99	0.049	4.07	0.002	10.84	0.001	12.6	<0.001
ACTG2	6.05	0.068	6.94	0.001	15.75	<0.001	14.97	<0.001
SLIT3	3.35	0.002	4.07	0.001	1.876	0.14	5.2	0.001
CILP	-1.32	0.213	-2.71	0.001	-5.9	0.005	-14.27	0.014
MMP12	3.67	0.085	4.6	<0.001	12	<0.001	10.72	<0.001
ADAMTS19	-1.54	0.102	-2.32	0.005	-3.67	0.001	-9.01	<0.001

Table 3-30. RT-qPCR fold change and P-value per grade of disease compared to normal valve samples for genes selected for microarray validation. Highlighted in yellow are instances where the significance of these results do not match with microarray data. Normalised to *GAPDH, MRPS25* and *RPL32*.

3.4 Discussion

As outlined in section 3.1, this study primarily aimed to investigate the transcriptomic changes occurring in each Whitney grade of MMVD, examining a mix of breeds to make broad statements about the disease development and extrapolate cause and consequence pathways in disease. To do this, Affymetrix Canine 1.1ST arrays were utilised to analyse six samples of diseased valves per grade and compare them to six normal valve samples (thirty valves in total) with at least two breeds and both genders represented in each group. This builds and extends on previous microarray studies in the dog, from Oyama *et al* and Lu *et al*, which only examined normal and late-stage disease valves with n=4 and n=3 independent replicates used, respectively[33, 150]. Additionally, these studies did not use multiple breed groups, which may cause breed specific gene changes to be detected in the

dataset[33, 150]. Examining a mixed breed population and various grades of disease in the present study minimised some aspects of these biases in the dataset. One aspect that could not be completely eliminated is the effect of age. As summarised in **Figure 3-1**, there were significant differences between almost all groups except between grade 0/normal valve samples and grade 1 valves and between grade 1 valves and grade 2 valves, reflecting the age-dependent natural history of the disease[22]. This is something to be wary of when interpreting these results as the disease-related gene changes observed in the grade 3 and 4 valves may be an effect of age independent of disease. However, finding age (and breed) matched controls for a disease as prevalent as MMVD would be impractical[22].

An important factor to be aware of in any transcriptomic study is the quality of the RNA samples being examined. Low-quality RNA can compromise the results of downstream analysis nullifying findings[268]. The quality of RNA can be affected either by contamination of the sample or the breakdown of the RNA into smaller fragments. The presence of contaminants can be measured, as discussed in Chapter 2 section 2.3.1, and RNA breakdown can be quantified with RIN analysis. In this study, it was found that the vast majority of samples showed no contamination and little breakdown in RNA. However, as summarised in section 3.3.3, two samples in the microarray dataset were found to have degraded RNA that had a detrimental effect on the downstream analysis. These samples were removed from the dataset. This resulted in the grade 1 and 4 groups having five rather than six samples, however, this still represented an improvement on previous studies in the dog [33, 150].

As summarised in section 3.3.4, FDR correction resulted in a high degree of exclusion of differentially expressed genes. This contrasts with the previous studies in dogs were Oyama *et al* and Lu *et al* were able to establish 229 and

591 differentially expressed genes respectively with an FDR correction[33, 150]. Although in this study some genes were differentially expressed in the grade 3 and 4 diseased valve samples with an FDR correction applied, they only numbered 18 and 80 respectively. A reason for the lack of differential expression seen in grade 1 and 2 diseased valve samples could be related to how the disease develops in a region dependent manner[2, 4, 9]. Outside of the diseased areas of the grade 1 and 2 valves there is ostensibly normal tissue, which could be dampening any detectable gene changes[2]. In grade 3 and 4 diseased valves, the noticeably lower number of differentially expressed genes when using the FDR correction compared with the earlier studies could be, in part, because of the mixed breed approach used in this study[33, 150]. A variability in the baseline of expression of genes between breeds of dog within the same grade of disease could account for high standard deviation within the grade of disease. This, in turn, would make comparisons less likely to yield significant changes especially with the FDR correction applied. Of the five human transcriptomic studies performed on spontaneous mitral valve diseases (with four independent studies and one repeated analysis), two did not use an FDR correction, two used unconventional FDR approaches and one used an FDR correction of Q-value <0.1[27, 125, 131, 163, 171]. This supports the results presented here as the human population is genetically far more heterogeneous than a breed of dog so greater variability between individuals is expected, as is the case when mixing different dog breeds in the same group[274]. In future studies, two approaches could be used to allow for FDR correction to be applied to a dataset. The first would be to analyse samples from one breed of dog only. This would come with the caveat that any changes that were observed could be breed specific and would have to be confirmed in other breeds. The second would be to increase the number of valves in a mixed breed

analysis. The only publication describing human valve samples that were able to apply a standard FDR correction and still have over 2000 differentially expressed genes used n=11 valves for normal and affected groups[131]. Using similar numbers in a canine study would likely discount the variability between breeds. As important data could still be gathered from the datasets relaxed stringency analysis was performed and will be discussed going forward.

With the FDR requirement relaxed, differentially expressed genes were detectable in all grades of disease, with 1002 genes being differentially expressed in at least one grade of disease when compared to normal valve samples (section 3.3.4). When comparing these 1002 genes to the 592 differentially expressed genes in the study from Lu *et al* 125 genes were shared (data not shown) including genes such *HTR2B*, *CDK1NA* and *BMP6* which were also differentially expressed in the study of Oyama *et al*[33, 150]. Remarkably, this study is the first instance were *ACTA2*, the gene that encodes αSMA, was shown to be up-regulated in a microarray study (including both dog and human)[33, 125, 131, 150, 163, 171]. This is of interest as increased *ACTA2*/αSMA is seen as a hallmark of VIC activation into a myofibrotic phenotype and consequentially a hallmark for MMVD and is regularly used in other studies to indicate MMVD phenotype[45, 60, 121]. Although this result contrasts with previous transcriptomic data, in the context of the wider literature the up-regulation of *ACTA2* in this study is consistent with up-regulation of *ACTA2*/αSMA noted by both RT-qPCR and immunohistochemistry in a disease severity dependent manner[33, 43, 57].

As stated, the aim of this study was to try to identify gene and pathway transcriptomic changes that are causal in disease development. To do this it is important not just to focus on differently expressed genes in individual grades

of diseased valves, but also to identify trends in gene expression across all grades of disease. In this study, the tools Miru and DAVID were utilised to achieve this, as summarised in section 3.3.5 and 3.3.6.

GO term analysis consistently, both in Miru clusters and in by grade analysis (with or without FDR correction), showed that proteinaceous extracellular matrix was associated with down-regulated genes and inflammatory response and positive regulation of ERK1 and ERK2 cascade was associated with up-regulated genes. The down-regulation of some aspects proteinaceous extracellular matrix is expected in the context of disease, with the accumulation of proteoglycans and glycosaminoglycans in the matrix. Without an increase in the expression of these components seen in disease, it is proposed that a down-regulation of the proteinaceous proteins is required for this change to occur[17, 18, 125]. For example, genes highlighted in this GO term include members of the ADAMTS family of genes, specifically *ADAMTS2*, *5* and *19*. Down-regulation of *ADAMTS2* and *5* have previously been associated with disease phenotype. Mutation in *ADAMTS2* has been seen in Ehlers-Danlos syndrome with these patients having an increased risk of mitral valve prolapse. A knockout mouse lacking *ADAMTS5* developed myxomatous mitral valve disease as the down-regulation of this gene resulted in the deposition of proteoglycans[17, 78]. Furthermore, both *ADAMTS5* and *19* have been shown to change in previous transcriptomic studies on MMVD with down-regulation of *ADAMTS5* reported in human valves and down-regulation of *ADAMTS19* being shown in the Lu *et al* study[33, 131, 163]. Likewise, up-regulation of immune response and ERK1 and ERK2 cascade are also noted in the DAVID analysis of grade 3 and 4 disease samples. The activation of VICs during disease progression into a myofibrotic phenotype is likely to cause the release of cytokines and other immune-related factors, and ERK1 and ERK2

cascade signalling (amongst various roles) have been shown to be involved in αSMA production in myofibrotic VICs[45, 117, 275, 276]. In addition, ERK1 and ERK2 cascade is a downstream signalling component of both non-canonical TGFβ signalling and 5HT signalling both of which (as discussed in Chapter 1 sections 1.5.1 and 1.5.2) have previously been implicated in MMVD[171, 178, 203]. The results presented here are in support of these hypotheses.

Genes that showed a more gradual up-regulation during disease associated with GO terms including metalloendopeptidase activity, stem cell differentiation and heart development. The up-regulation of metalloendopeptidase activity may be counter-intuitive given the down-regulation of proteinaceous extracellular matrix; however, in the context of a disease where alteration of the extracellular matrix is fundamental, divergent expression of such genes is to be expected. For example, the down-regulation of *ADAMTS5*, which cleaves a proteoglycan called aggrecan, results in accumulation of the latter, contributing to the increased proteoglycan deposition seen in MMVD valves[17]. In contrast, concurrent up-regulation of *MMP12*, which encodes an elastase degrading elastin in the extracellular matrix, would be predicted as MMVD valves demonstrate disorganisation and cleavage of elastin, which could facilitate the migration of cells undergoing EndoMT[1, 2, 277, 278]. Up-regulation of the heart development pathway can, likewise, be attributed to the disease phenotype through the activation of developmental pathways such as EndoMT, a pathway significant in cardiac embryogenesis[33, 41, 57, 95].

Although genes may not be differentially expressed to a statistically significant level in each grade of disease, trend analysis allowed for the identification of disease-relevant GO-terms such as those discussed above. These insights would otherwise remain unclear as identification of disease-relevant GO

terms with believable P-value associations and the separation of genes into up- and down-regulated groups was not possible in lower grade 1-2 diseased valves (**Table 3-13** and **Table 3-14**). The identification of GO terms relevant to disease in trend analysis helps to show the advantage of this type of analysis over analysing genes changed by grade alone. Likewise, this study indicates that genes that can be detected as significantly altered in late-stage disease are changing in a progressive manner over the entire course of disease development. Furthermore, genes which show a progressive trend for change throughout disease and the GO terms associated with them are more likely to be involved in causing disease than those that are only associated with changes in gene expression in late grade valves. Thus this analysis helps to examine the study aim.

Analysis by grade using IPA helped to identify various interesting pathways associated with disease at different stages. Canonical pathway analysis indicated *Agranulocyte adhesion and diapedesi*s was the second and *Hepatic fibrosis/hepatic stellate cell activation* was the top pathway related to the gene lists submitted for grade 3 and 4 disease samples. The second suggested top upstream regulator in both grade 3 and 4 diseased samples, TNF, is involved in controlling agranulocyte adhesion and diapedesis [279, 280]. This pathway may also relate to the up-regulation of immune response noted in the DAVID GO term analysis. Likewise, TGFβ1, the top upstream regulator suggested for both grade 3 and 4 diseased valve samples, is involved in the control of *Hepatic fibrosis/hepatic stellate cell activation* pathway[184] and as a cytokine, it is linked with immune response pathways. Both TGFβ1 and TNF share many downstream targets making distinguishing which may be more important in disease pathogenesis difficult, although TGFβ1 does have the strongest associations. As described in Chapter 1 section 1.5.1, TGFβ signalling has

previously been implicated in the development of MMVD. TGFβ1 is commonly used to stimulate the activation of VICs into a myofibrotic phenotype *in vitro* [45, 60, 117]. Furthermore, TGFβ1 and 2 signalling have been implicated in the development of MMVD in both the dog and human. Increased *TGFB1* and *2* gene expression and increased phosphorylated SMAD2/3 protein (activated downstream TGFβ signalling molecule) have been detected in canine MMVD[124, 126]. Likewise, increased *TGFB1* gene expression and increased phosphorylated SMAD2/3 were observed in a human study and *TGFB2* has been implicated in two transcriptomic studies in humans[27, 125, 131, 176]. Interestingly, when analysing the genes differentially expressed in grade 4 diseased samples with the FDR correction applied, the top upstream regulator was another member of the TGFβ signalling family, TGFβ3. This evidence along with the data presented here helps support a role for TGFβ, in particular TGFβ1, signalling in MMVD development in dogs.

Network analysis associated the top disease and functions with each gene list for the different grades of disease. This indicated that the genes differentially expressed in grade 1 and 2 disease did not show any strong association with cardiovascular or tissue development functions, unlike grade 3 and 4 disease were these functions were both associated, suggesting cardiovascular development related pathways such as those involved in EndoMT are more relevant in late disease. This suggests that the changes to the cardiovascular system are a consequence rather than a cause of MMVD, since they only occur late in the progression of the disease. It did, however indicate that in all grades of disease as well as in the more stringent dataset analysis, there was an association with cell cycle or cell development, which could be related to the proliferation and transition of VICs into an activated phenotype discussed in Chapter 1 section 1.3.2.

As mentioned, one of the flaws in this study was the inability to use a suitable FDR correction for most analyses. Without it, there will be a higher rate of false positive error in the datasets. It was therefore imperative to validate the microarray results by an alternative method. The gold standard for this is by RT-qPCR which offers a wider dynamic range and the ability to detect lowly expressed genes[281, 282].

The RT-qPCR results validate the microarray results for the genes analysed and help to add credence to the other results obtained from this study despite the lack of FDR correction. As mentioned in section 3.3.8, the minority of genes that showed significant differential expression by RT-qPCR compared to microarray analysis indicated a change in expression that was in keeping with the other results for that gene i.e. up-regulation of a gene where it is up-regulated in all other grades of disease. This may be, due to the technical superiority of RT-qPCR being able to detect these more subtle changes, especially in the lower grade 1 and 2 valves.

To conclude, this study aimed to investigate transcriptomic changes occurring as MMVD progresses across all breeds of dogs and to identify pathways that are causal in disease progression. To that end, cluster analysis tools were utilised to identify genes associated with progressive changes throughout the disease. Perhaps most importantly, pathways involved in the upstream regulation of disease were identified.

Summary:

- Genes showing a progressive change in expression throughout disease (including some hallmarks of disease) were associated with pathways including ERK1 and ERK2 cascade, metalloendopeptidase activity and proteinaceous extracellular matrix.

- Using dogs from various breeds may cause greater variation within groups making distinguishing gene changes relevant to disease difficult when using an FDR corrected dataset
- By grade analysis identified TGFβ signalling as consistently important in disease regulation in later grade valves. In particular, TGFβ1 (which has previously been implicated in the literature) is suggested as the likely controller of disease.

This study has therefore succeeded in its aim and has provided valuable insight into the pathogenesis of MMVD. However, it was not possible to elucidate a better understanding of the early pathogenesis of MMVD. As stated, this is likely due to the approach of the study using whole valves, which in the lower grades still contain large amounts of normal valve tissue. This will have the effect of dampening any discreet gene changes occurring in the diseased sections of the valve. Gaining an understanding of the transcriptomic changes occurring in these lower grade valves is necessary for identifying factors, such as TGFβ1, which could be the primary drivers of disease pathogenesis from the onset. As such, the Chapter 5 aims to investigate this issue.

Another aspect that warrants further investigation is the effect of breed in MMVD development. Although using various breeds in this study posed its problems, it did allow for the identification of potential breed-specific differences in CKCSs. These results will be investigated further in Chapter 4.

(This page has been left intentionally blank)

Chapter 4 Transcriptomic changes in CKCS

4.1 Introduction

The clinical development of MMVD is associated typically with small breed dogs, notably the Cavalier King Charles Spaniel (CKCS), as the disease begins to develop earlier in these breeds allowing for clinical symptoms to develop at an earlier age[23, 24, 212, 222]. This early-onset of MMVD has been shown to be heritable and breeding programmes have shown some success in reducing the frequency of early-onset disease suggesting a genetic component is involved[222, 283, 284].

As discussed in Chapter 1 section 1.6, genome wide association studies (GWAS) studies investigating potential genetic variants related to MMVD development have been performed in the dog[219-221]. Two of these studies were performed on CKCSs comparing dogs with early-onset and late-onset disease[219, 220]. One was unable to identify any genomic regions that were consistently different between the two groups[219]. The other identified two loci with a total of thirty-one protein-coding genes within these regions that could be affected[220]. However, despite this study being published several years ago, no further developments have followed this study and the thirty-one genes identified have not been made public. It has therefore been proposed that a single variant is not responsible for disease and it is polygenic in its development[33, 210].

Furthermore, immunohistochemical analysis comparing CKCS to other breeds of dog with late-stage (grade 3-4) MMVD valve samples and to unaffected normal valves showed similar cellular changes in the two diseased groups[110]. This suggests that the resulting end-grade pathology of the disease is the same in CKCS as in other breeds. What is unknown is if there are different or

additional mechanisms responsible for the early development of MMVD in CKCSs.

In this study, we aim to investigate the transcriptomic profiles of diseased, Whitney grade 3 and 4, CKCS and other breeds of dog. It is hypothesised that differences will exist in CKCS but the hallmark gene changes in disease will not be different due to a level of shared pathogenesis. Both the CKCS group and the other breeds of dog group will be compared to normal valves as well as one another to identify any differences and similarities.

4.2 Materials and Methods

4.2.1 Tissue collection, RNA quantification and quality control

The valves used in this study are a subset of 17 valves used in Chapter 3 and are summarised in **Table 4-1**. For full details on tissue collection, see Chapter 2 section 2.2.

Sample ID	Date sampled	Dog Breed	Gender	Age	Whitney grade
B2G0	05/06/2015	BEAGLE	MALE	4y	0
B4G0	05/06/2015	BEAGLE	FEMALE	4y	0
PBT1G0	20/11/2015	'PITBULL TERRIER' TYPE	MALE	2y9m	0
PBT3G0	01/04/2016	'PITBULL TERRIER' TYPE	MALE	1y9m	0
PBT2G0	27/11/2015	'PITBULL TERRIER' TYPE	MALE	3y	0
B26G0	26/10/2015	BEAGLE	MALE	3y	0
BTG3	29/01/2016	BULL TERRIER	FEMALE	10y	3
WHTG3	06/11/2015	WEST HIGHLAND TERRIER	MALE	10y	3
JRG4	30/10/2015	JACK RUSSEL TERRIER	FEMALE	11y	4
C1G4	19/02/2016	BORDER COLLIE	MALE	13y	4
C2G4	08/07/2016	BORDER COLLIE	MALE	13y	4
811M_024	16/01/2013	CAVALIER KING CHARLES SPANIEL	MALE	12y	3
811M_019	20/12/2012	CAVALIER KING CHARLES SPANIEL	MALE	11y	3
811M_023	16/01/2013	CAVALIER KING CHARLES SPANIEL	MALE	12y	3
811M_017	20/02/2013	CAVALIER KING CHARLES SPANIEL	FEMALE	10y	3
CKCSG4	21/03/2014	CAVALIER KING CHARLES SPANIEL	MALE	16y	4
811M_016	20/12/2012	CAVALIER KING CHARLES SPANIEL	FEMALE	12y	4

Table 4-1. Description of dogs used in this study

4.2.2 RNA extraction, quantification and quality control

Full details of the protocols followed for RNA extraction, quantification and quality control can be found in Chapter 2 section 2.3.1 and 2.3.3 with the results of this analysis presented in Chapter 3 section 3.3.2. As mentioned in Chapter 3 section 3.2.2, almost all RNA extractions were performed by myself, with the exception of CKCS samples with the sample ID beginning 811M which were extracted by Dr. Chie Chien Lu prior to the start of this study.

4.2.3 Affymetrix Canine Gene 1.1ST microarray analysis

As in Chapter 3, microarray analysis was performed using two 16 well Affymetrix Canine Gene 1.1ST chips. RNA processing, hybridisation, post-hybridisation quality control, summarisation file creation and differential gene expression analysis was performed as described in section 2.5 of Chapter 2. A Benjamini-Hochberg false discovery rate (FDR) correction (Q-value <0.05) was applied to the comparisons of normal valves compared to CKCS valves and other breed diseased valves compared to CKCS valves. When comparing normal valves to the other breed diseased valves the FDR correction was relaxed to allow the inclusion of a greater number of genes for gene enrichment analysis.

4.2.4 Gene enrichment analysis

The network analysis tool Miru (version 1.4) was utilised as described in Chapter 2 section 2.6.1. A sample-to-sample comparison was performed with a Pearson correlation of r=0.97, this maximised the number of samples included whilst minimising the connection between samples. Meta-data (grade of disease, gender, breed etc.) applied to the dataset was then examined to see if this was having an effect on the association between samples.

The tools Database for Annotation, Visualisation and Integrated Discovery (DAVID) and Ingenuity Pathway Analysis (IPA) were used as stated in Chapter 2 sections 2.6.2 and 2.6.3; default settings were used throughout. Gene list comparison was performed as outlined in Chapter 2 section 2.6.4

4.3 Results

4.3.1 Transcriptomic differences in Cavalier King Charles Spaniels

The sample-to-sample analysis was performed in Miru (Pearson correlation r=0.97) and metadata was used to colour the nodes by grade of disease (**Figure 4-1A**), as presented in Chapter 3 section 3.3.3 (**Figure 3-7**). It was noted that, although an expected clustering of samples based on the grade of disease was observed, a subset of grade 3 and 4 disease samples was separating from the main cluster of samples. Colouring the nodes by breed (**Figure 4-1B**) of dog showed that all of the samples located away from the main cluster of samples were Cavalier King Charles Spaniels (CKCS).

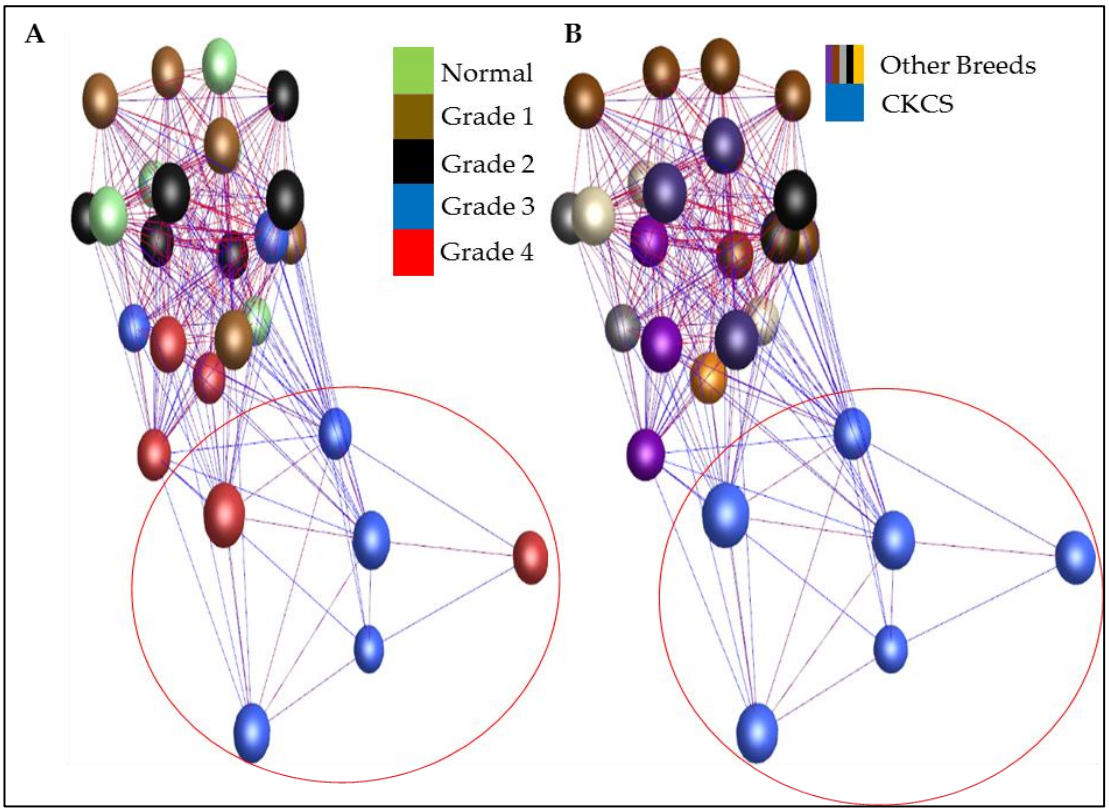

Figure 4-1. Sample-to-sample analysis showing samples coloured by grade of disease and by breed. (A) Normal samples are coloured green, grade 1 brown, grade 2 black, grade 3 blue and grade 4 red. Highlighted by a red circle is a set of grade 3 and 4 disease samples clustering away from the main group of samples. (B) Sample-to-sample analysis showing samples coloured by breed. Brown - beagle, dark purple - Staffordshire bull terriers, light purple - collies, light grey - west highland terrier, dark grey - Rottweiler, black - bull terriers, cream - Pitbull terriers, orange - Jack Russel terrier and blue - CKCSs. The red circle shows that all the CKCS samples in the analysis mapped away from the main group of samples.

4.3.2 CKCS differential gene expression

As CKCSs are a breed predisposed to the development of MMVD at an early age, further analysis of the differences between this breed and other breeds was carried out. There was no significant difference in age between the diseased valve groups in this analysis and a similar, but small, number of valves were split between groups (6 CKCS (3 in either grade) and 5 other breed dogs (2 in grade 3 and 3 in grade 4)). The CKCS and other breed grade 3 and 4 disease samples were separated and gene expression comparisons were performed with the normal valve samples for both groups. As well as this, comparison of the differential gene expression between the CKCS group and the other breed grade 3 and 4 disease samples was also performed. Using the same criteria as previously established (Chapter 3 section 3.2.3) without an FDR correction, 278 genes were differentially expressed (**Figure 4-2A**) between the other breed diseased and normal valve samples, with 165 up-regulated and 113 down-regulated. Comparing the CKCS samples to normal valves a FDR correction of Q-value <0.05 could be applied without the removal of all differentially expressed genes. With this criteria, 599 genes were differentially expressed (**Figure 4-2B**) between the CKCS and normal valve samples, with 270 up-regulated and 329 down-regulated. Finally, comparing CKCS to other breed grade 3 and 4 valves, with FDR correction (Q-value <0.05), found 161 genes differentially expressed (**Figure 4-2C**) with 27 genes up-regulated and 134 down-regulated in the CKCS breed. Full gene lists can be found in **Appendix II: Chapter 4 Tables S1-3**.

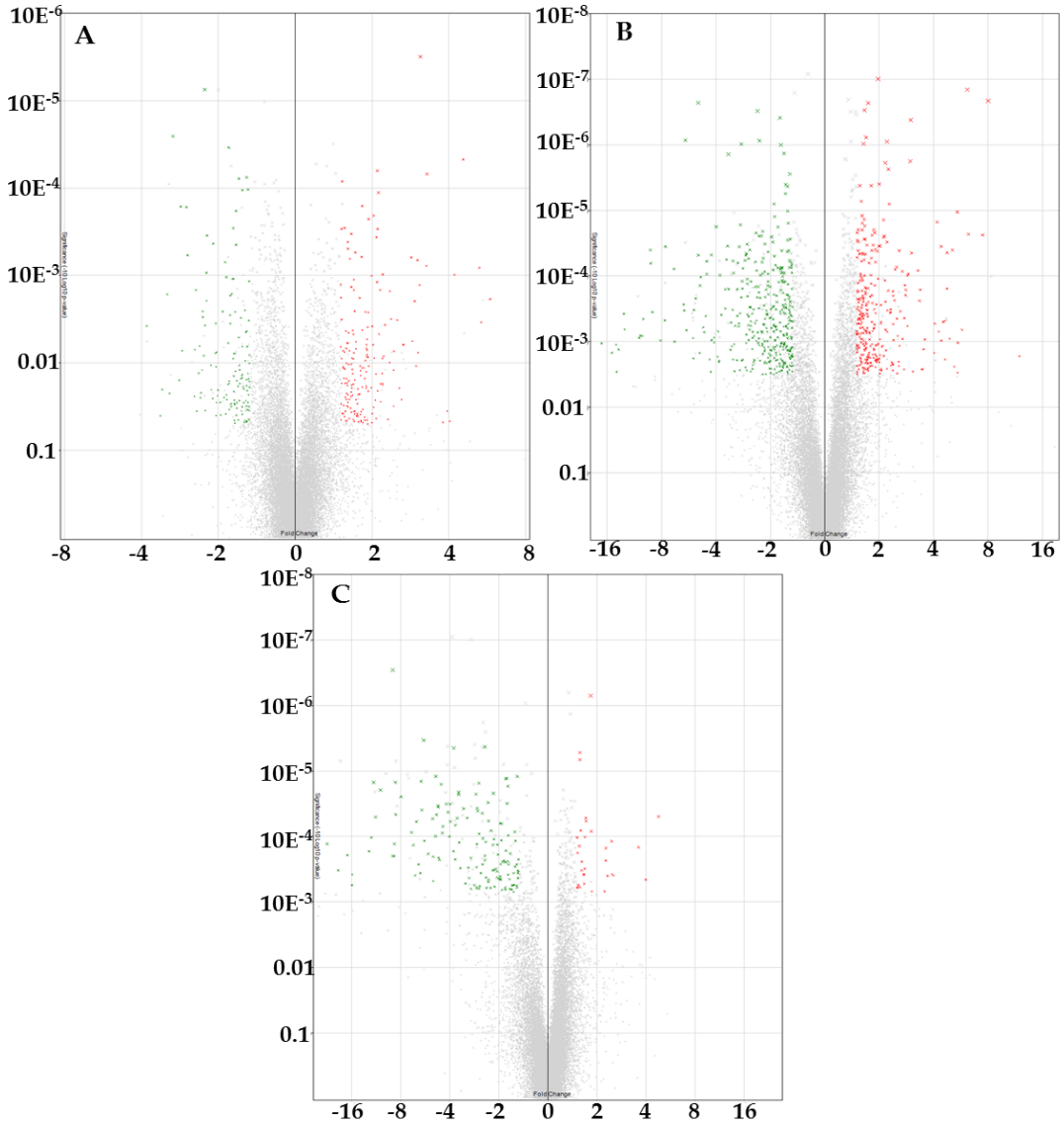

Figure 4-2. Volcano plots of differentially expressed genes in other breeds compared to normal samples, CKCS compared to normal samples and other breed compared to CKCS. Red dots represent genes that were up-regulated in disease, green represent genes that were down-regulated and uncoloured are genes which do not pass the differential expression criteria. The X-axis shows fold change value and the Y-axis shows P-value. (A) Differentially expressed genes in normal and other breed disease samples with no FDR correction. (B) Differentially expressed genes between CKCS samples and normal valve samples with FDR correction. (C) Differentially expressed genes between CKCS and other breed disease samples with FDR correction.

To investigate the level of similarity between the CKCS and the other breed grade 3 and 4 samples in comparison to normal valve samples, the number of genes that share differential expression was calculated (**Figure 4-3**). In total 120 of the genes differentially expressed when compared with normal valves were shared in both datasets. 158 genes were differentially expressed only in the other breed dataset and 479 genes were differentially expressed only in the CKCS dataset. Shared genes included known markers of disease phenotype such as *ACTA2* and *HTR2B,* which are up-regulated in both of these datasets and not different when comparing CKCS samples to the other breed grade 3 and 4 samples.

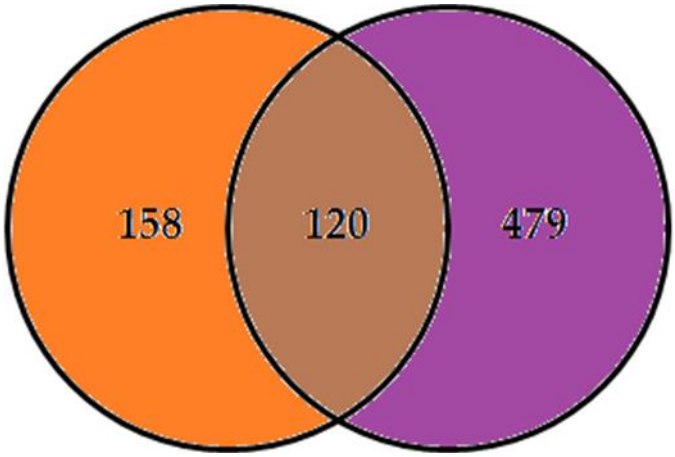

Figure 4-3. Venn diagram illustrating the number of shared differentially expressed genes in the CKCS and other breed grade 3 and 4 valves when compared to normal valves. In the left orange circle is the number of differentially expressed genes for other breed grade 3 and 4 valves compared to normal only, and not shared with the CKCS dataset. In the right purple circle the number of differentially expressed genes for CKCS samples compared to normal only and not shared with the other breed dataset is shown. In the centre, the number of shared differentially expressed genes between the two datasets is shown.

4.3.3 DAVID GO term analysis of breed-specific pathways

DAVID gene ontology enrichment was performed on each of the datasets with up- and down-regulated genes separated. When comparing other breed grade 3 and 4 disease samples to normal valve samples 59 GO terms were associated with up-regulated genes and 28 with down-regulated genes. The top ten GO terms for up- and down-regulated genes for this dataset are summarised in **Table 4-2** and included. CKCS samples compared to normal valve samples showed 49 GO terms associated with up-regulated genes and 96 with down-regulated genes. The top ten GO terms for up- and down-regulated genes for this dataset are summarised in **Table 4-3**. Finally, when comparing the CKCS samples to other breed grade 3 and 4 valve samples only one GO term was associated with up-regulated genes and 70 associated with down-regulated genes. The top ten GO terms for up- and down-regulated genes for this dataset are summarised in **Table 4-4**. The GO terms for the CKCS compared with normal had a greater emphasis on immune response in comparison to the other breed compared with normal analysis. However, three terms were shared in both analyses for up-regulated genes (extracellular space, cell-cell signalling and positive regulation of ERK1 and ERK2 cascade) and down-regulated genes (calcium ion binding, proteinaceous extracellular matrix and integral component of plasma membrane).

	Category	Term	Gene count	P-value	FDR
Up-regulated	GOTERM_MF_DIRECT	Calcium ion binding	14	9.81E-04	1.18887
	GOTERM_BP_DIRECT	Cardiac muscle fiber development	3	9.85E-04	1.49236
	GOTERM_BP_DIRECT	Positive regulation of angiogenesis	6	0.00118	1.79196
	GOTERM_BP_DIRECT	Positive regulation of ERK1 and ERK2 cascade	7	0.00177	2.66034
	GOTERM_BP_DIRECT	Cell-cell signaling	5	0.0039	5.78536
	GOTERM_MF_DIRECT	Structural constituent of muscle	3	0.00414	4.93182
	GOTERM_BP_DIRECT	Negative regulation of GPCR protein signalling	3	0.00521	7.65678
	GOTERM_BP_DIRECT	Positive regulation of cell proliferation	8	0.00679	9.87975
	GOTERM_CC_DIRECT	Extracellular space	16	0.00723	8.09541
	GOTERM_CC_DIRECT	Synapse	5	0.00996	10.9896
Down-regulated	GOTERM_CC_DIRECT	Proteinaceous extracellular matrix	8	3.65E-05	0.03795
	GOTERM_CC_DIRECT	Integral component of plasma membrane	14	2.27E-04	0.2357
	GOTERM_CC_DIRECT	Extracellular matrix	6	2.33E-04	0.24233
	GOTERM_MF_DIRECT	Calcium ion binding	12	2.96E-04	0.33195
	GOTERM_CC_DIRECT	Integral component of membrane	36	3.21E-04	0.33397
	GOTERM_BP_DIRECT	Adenylate cyclase-activating GPCR signalling	4	9.27E-04	1.28441
	GOTERM_MF_DIRECT	GPCR activity	3	0.00221	2.45393
	GOTERM_CC_DIRECT	Cell surface	7	0.01138	11.2334
	GOTERM_MF_DIRECT	Metalloendopeptidase activity	4	0.02209	22.2049
	GOTERM_BP_DIRECT	Positive regulation of mitochondrial depolarisation	2	0.03267	37.0447

Table 4-2. Functional analysis chart summary of other breed grade 3 and 4 disease samples compared to normal valves. The top 10 GO terms associated with genes up- and down-regulated in the other breed grade 3 and 4 disease samples compared to normal valves.

	Category	Term	Gene count	P-value	FDR
Up-regulated	GOTERM_BP_DIRECT	Cell-cell signalling	7	3.96E-04	0.61136
	GOTERM_BP_DIRECT	Immune response	10	1.15E-03	1.76196
	GOTERM_BP_DIRECT	Inflammatory response	10	0.00152	2.32542
	GOTERM_CC_DIRECT	Extracellular space	25	0.00155	1.89913
	GOTERM_BP_DIRECT	Positive regulation of inflammatory response	5	0.00164	2.50471
	GOTERM_BP_DIRECT	Positive regulation of ERK1 and ERK2 cascade	8	0.00311	4.71581
	GOTERM_MF_DIRECT	CCR chemokine receptor binding	4	0.00378	4.79573
	GOTERM_BP_DIRECT	Lymphocyte chemotaxis	4	0.0048	7.18014
	GOTERM_BP_DIRECT	Neutrophil chemotaxis	5	0.00583	8.65707
	GOTERM_BP_DIRECT	Eosinophil chemotaxis	3	0.00598	8.86813
Down-regulated	GOTERM_BP_DIRECT	cardiac muscle contraction	8	2.29E-07	3.64E-04
	GOTERM_BP_DIRECT	Regulation of heart rate by cardiac conduction	8	2.29E-07	3.64E-04
	GOTERM_CC_DIRECT	Z disc	9	1.65E-05	0.02048
	GOTERM_BP_DIRECT	Sarcomere organization	6	1.98E-05	0.03144
	GOTERM_CC_DIRECT	Voltage-gated calcium channel complex	6	3.48E-05	0.0432
	GOTERM_MF_DIRECT	Calcium ion binding	24	7.96E-05	0.10617
	GOTERM_BP_DIRECT	Regulation of ventricular cardiac muscle action potential	4	4.13E-04	0.65443
	GOTERM_BP_DIRECT	Regulation of the force of heart contraction	4	4.13E-04	0.65443
	GOTERM_CC_DIRECT	Proteinaceous extracellular matrix	11	6.32E-04	0.78217
	GOTERM_CC_DIRECT	Integral component of plasma membrane	26	0.00135	1.66305

Table 4-3. Functional analysis chart summary of CKCS disease samples compared to normal valves. The top 10 GO terms associated with genes up- and down-regulated in the CKCS disease samples compared to normal valves.

	Category	Term	Gene count	P-value	FDR
Up-regulated	GOTERM_BP_DIRECT	L-methionine biosynthetic process from methylthioadenosine	2	0.00607	6.03855
Down-regulated	GOTERM_CC_DIRECT	Z disc	9	2.90E-08	3.31E-05
	GOTERM_BP_DIRECT	Sarcomere organization	6	4.26E-07	6.17E-04
	GOTERM_BP_DIRECT	Regulation of heart rate	5	1.39E-05	0.02004
	GOTERM_BP_DIRECT	Cardiac muscle contraction	5	5.12E-05	0.07401
	GOTERM_CC_DIRECT	Sarcoplasmic reticulum membrane	4	2.30E-04	0.26205
	GOTERM_BP_DIRECT	Skeletal muscle thin filament assembly	3	3.79E-04	0.54748
	GOTERM_CC_DIRECT	Voltage-gated calcium channel complex	4	6.12E-04	0.69548
	GOTERM_CC_DIRECT	Intercalated disc	4	0.00113	1.28114
	GOTERM_BP_DIRECT	Regulation of heart rate by cardiac conduction	4	0.00114	1.64204
	GOTERM_BP_DIRECT	Regulation of cardiac muscle contraction by regulation of the release of sequestered calcium ion	3	0.00131	1.87449

Table 4-4. Functional analysis chart summary of CKCS compared to other breed grade 3 and 4 disease samples. The only GO term associated with genes up-regulated in the CKCS samples and the top 10 GO terms associated with down-regulated genes in the CKCS samples are shown.

4.3.4 IPA analysis of breed-specific pathways

Datasets were submitted to IPA for further analysis. The number of genes that the programme was able to map to published articles for each dataset is shown in **Table 4-5**.

Analysis	Mapped Genes	Unmapped genes	Total genes
Other breed Vs Normal	298	25	323
CKCS Vs Normal	645	36	681
CKCS Vs Other breed	150	10	160

Table 4-5. Mapped, unmapped and total number of genes submitted into IPA for each dataset.

Canonical pathway analysis of each dataset showed the pathways associated with each set of analysis (P-value <0.05). The genes differentially expressed between other breed grade 3 and 4 disease compared to normal valve samples had 58 canonical pathways attributed to them. Analysis of the genes differentially expressed in CKCS compared to normal valve samples showed an association of 77 pathways. Finally, 28 pathways were associated with the differentially expressed genes in CKCS compared to other breed grade 3 and 4 disease samples. A summary of the top three canonical pathways associated with the differentially expressed genes in each grade of disease is shown in **Table 4-6**. Other breed grade 3 and 4 valves compared to normal showed the same top canonical pathway as when samples were not separated by breed (Chapter 3 section 3.3.7), CKCS samples for both analyses showed calcium signalling as the top pathway.

Analysis	Canonical Pathway	Up-regulated genes	Down-regulated genes	Genes changed in pathway	P-value
Other breed Vs Normal	Hepatic Fibrosis / Hepatic Stellate Cell Activation	10	4	14/183	1.31826E-07
	Caveolar-mediated Endocytosis Signaling	6	1	7/71	3.80189E-05
	Agranulocyte Adhesion and Diapedesis	8	3	11/191	4.36516E-05
CKCS Vs Normal	Calcium Signaling	6	17	23/179	7.94328E-11
	Hepatic Fibrosis / Hepatic Stellate Cell Activation	8	12	20/183	2.39883E-08
	Axonal Guidance Signaling	11	16	27/452	1.99526E-05
CKCS Vs Other breed	Calcium Signaling	0	10	10/179	6.45654E-06
	LPS/IL-1 Mediated Inhibition of RXR Function	2	5	7/168	0.000977237
	Gluconeogenesis I	0	3	3/22	0.001071519

Table 4-6. Summary of top three canonical pathways associated with each dataset. The number of genes up- and down-regulated in each pathway as well as the total number of genes changed in each pathway is shown. The P-value score shows the association of the gene list to the pathway.

Upstream regulator analysis for each dataset comparing the effect of the CKCS breed was performed with a P-value cut-off (<0.05). The top four upstream regulators for each dataset analysed are summarised in **Table 4-7**. Z-scores for this showed that when comparing the diseased valve datasets to normal valve samples there was an activation of pathways whereas comparing CKCS to other breed grade 3 and 4 samples suggested an inhibition of pathways. There were 1937 molecules associated with the genes differentially expressed in other breed grade 3 and 4 disease samples when compared to normal valve samples. The molecule with the strongest association was again TGFβ1 with 65 genes in the dataset being associated with this pathway and only 20 of these showing an inconsistent change in expression to what has previously been published (**Figure 4-4**). There were 1831 molecules suggested as potential top upstream regulators in CKCS samples compared to normal valve samples. The top upstream regulator here was F2 (prothrombin) which is later cleaved into

thrombin in the blood clotting cascade. 29 genes in the dataset were associated with this pathway (10 of these were inconsistent with the literature) (**Figure 4-5**). Of note in this analysis is the presence of TNF and TGFβ1 in the top four upstream regulators. There were 377 molecules associated with the genes differentially expressed in CKCS samples compared to other breed grade 3 and 4 disease samples. The top upstream regulator here was Myocyte-specific enhancer factor 2C (MEF2C), which is an important gene in the control of myogenesis and cardiac muscle cells development. A total of 11 genes in the dataset were associated with this pathway with all genes matching the change of expression expected in the literature (**Figure 4-6**).

Analysis	Upstream Regulator	Molecule Type	Activation Z-score	P-value
Other breed Vs Normal	TGFB1	Growth factor	2.228	1.69E-15
	SRF	Transcription regulator	3.769	3.43E-12
	Cg	Complex	1.358	1.36E-11
	AGT	Growth factor	2.307	5.26E-11
CKCS Vs Normal	F2	Peptidase	1.503	2.2E-12
	TNF	Cytokine	1.892	2.18E-11
	AGT	Growth factor	2.018	1.15E-10
	TGFB1	Growth factor	1.486	9.03E-10
CKCS Vs Other breed	MEF2C	Transcription regulator	-3.087	1.11E-09
	MYOCD	Transcription regulator	-2.768	1.33E-07
	2,3 butanedione monoxime	Chemical drug	-1.4	3.71E-07
	DNMT3A	Enzyme	1.667	6.27E-07

Table 4-7. Summary of the top four upstream regulators associated with the differentially expressed genes lists for each dataset. For each upstream regulator, the molecule type, Z-score and P-value are given.

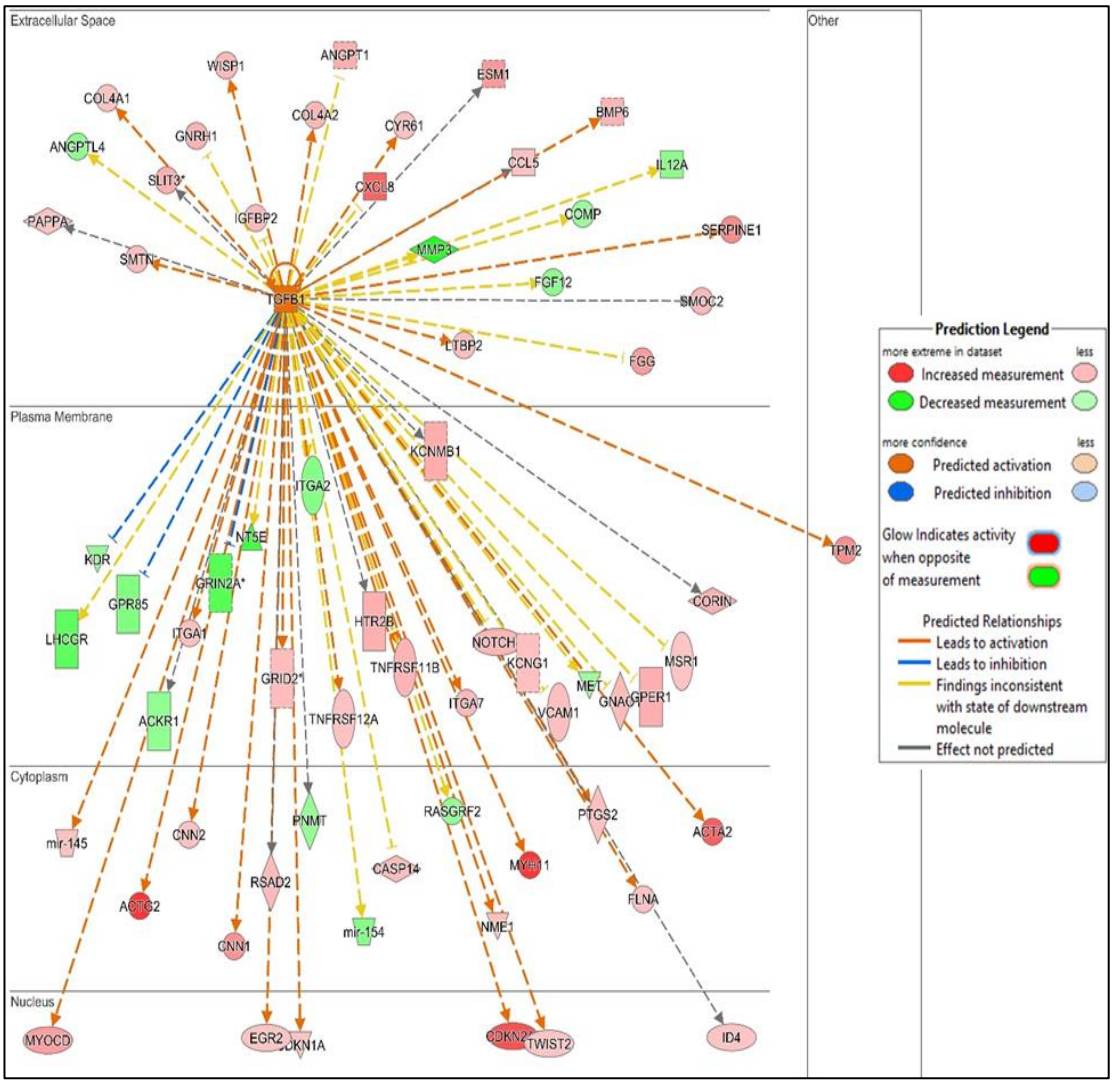

Figure 4-4. The network of genes that are differentially expressed in other breed grade 3 and 4 disease samples compared to normal valve samples that are downstream of TGFβ1 signalling. TGFβ1 is shown to have its effect from the extracellular space on the genes in their cellular location. Genes are coloured red and green to represent up- or down-regulation in the dataset. Dotted lines connecting TGFβ1 to these genes show the expected effect of TGFB signalling: orange - activation, blue - inhibition, yellow -result inconsistent and grey – effect not predicted.

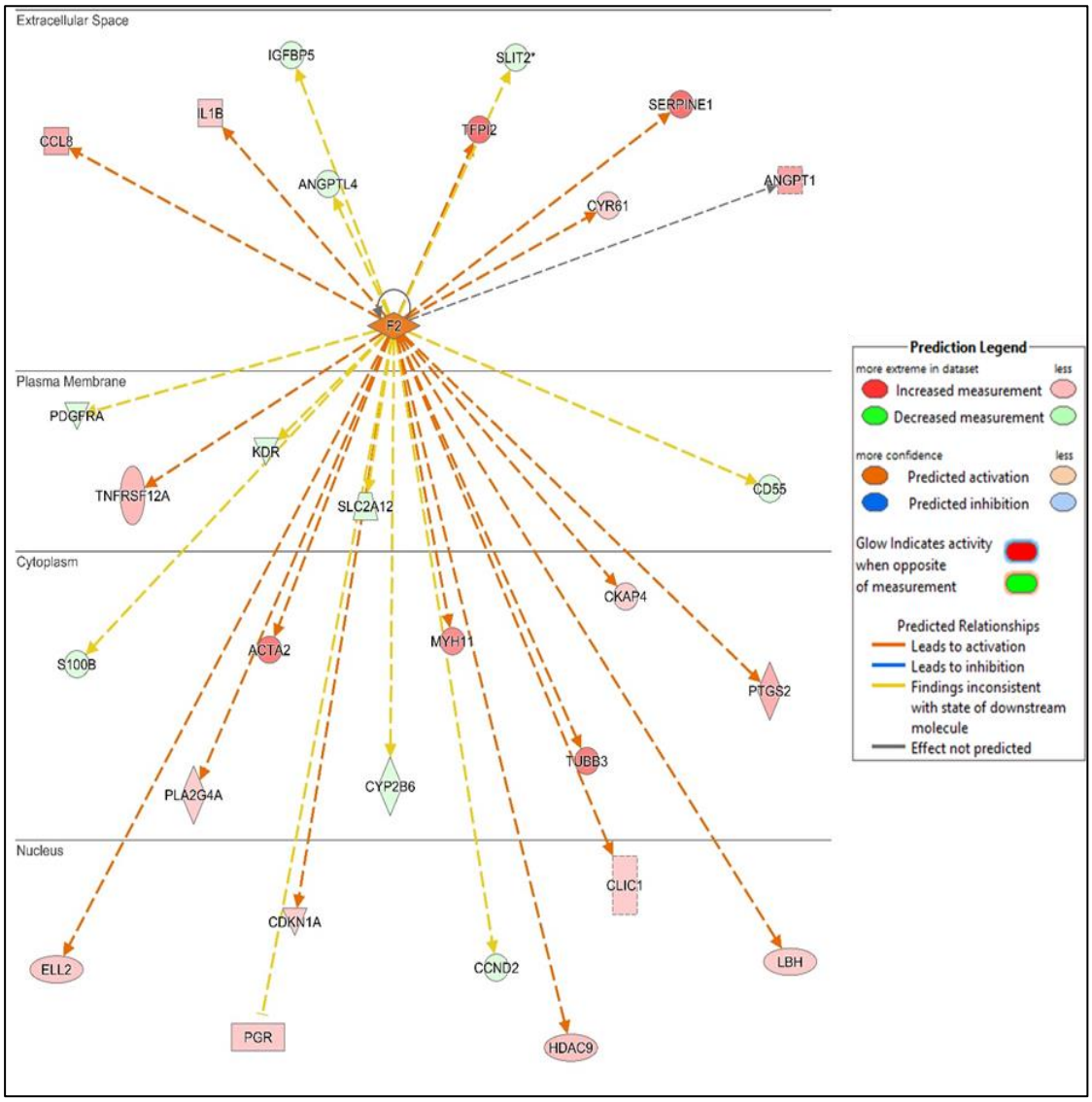

Figure 4-5. The network of genes that are differentially expressed in CKCS samples compared to normal valve samples that are downstream of F2 signalling. F2 is shown to have its effect from the extracellular space on the genes in their cellular location. Genes are coloured red and green to represent up- or down-regulation in the dataset. Dotted lines connecting F2 to these genes show the expected effect of F2 signalling: orange - activation, yellow -result inconsistent and grey – effect not predicted.

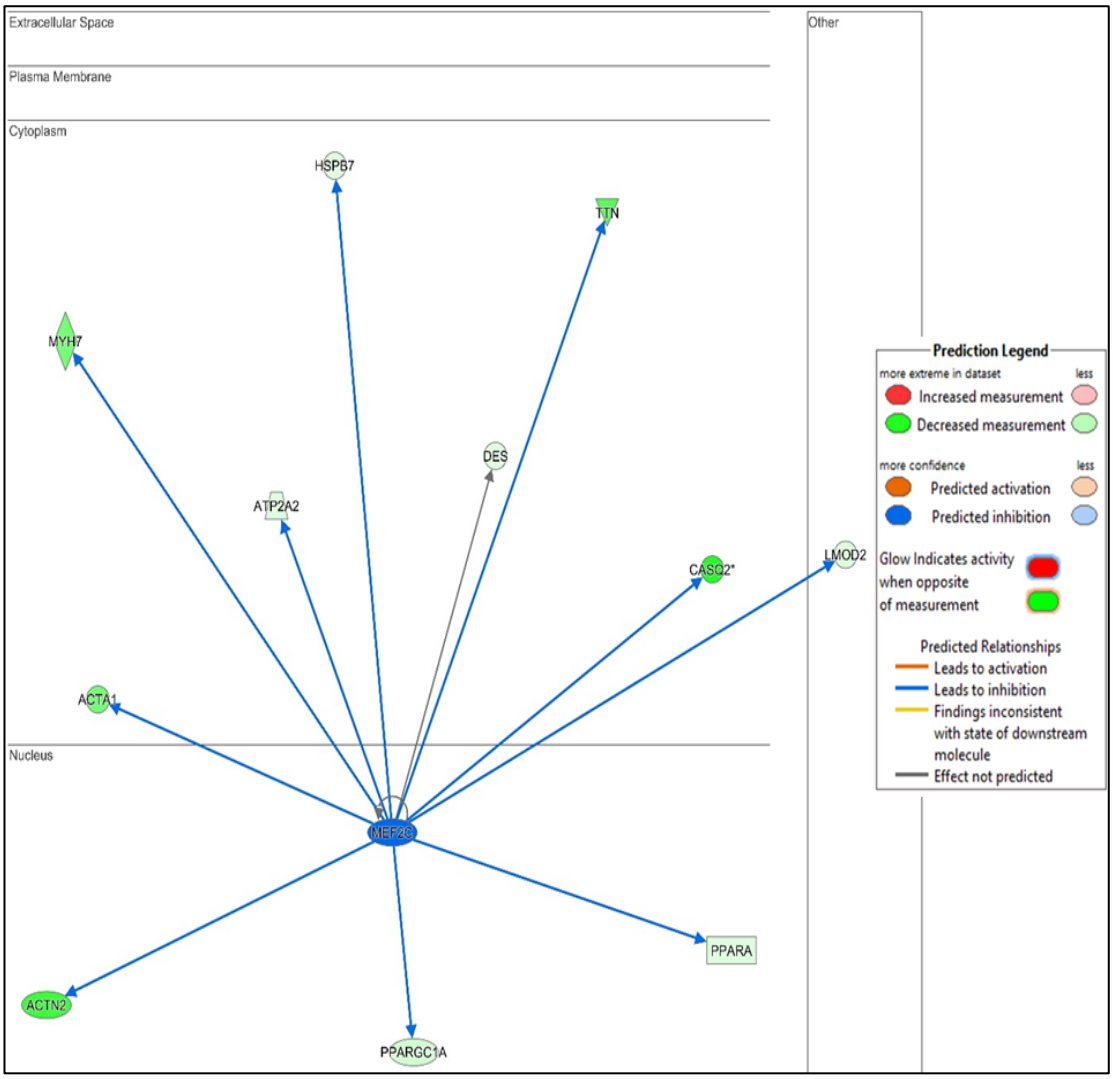

Figure 4-6. The network of genes that are differentially expressed in CKCS compared to other breed grade 3 and 4 disease samples valves that are downstream of MEF2C signalling. MEF2C is shown to have its effect from the extracellular space on the genes in their cellular location. Genes are coloured red and green to represent up- or down-regulation in the dataset. Dotted lines connecting MEF2C to these genes show the expected effect of MEF2C signalling: blue – inhibition and grey – effect not predicted.

Network analysis for the genes differentially expressed in other breed grade 3 and 4 disease samples compared to normal samples highlighted top five disease and functions annotations assigned to this dataset (**Table 4-8**). The top network in this analysis is visualised in **Figure 4-7**.

Top disease and function
Organismal Injury and Abnormalities, Renal and Urological Disease, Behavior
Cancer, Organismal Injury and Abnormalities, Reproductive System Disease
Cell Morphology, Cellular Movement, Hair and Skin Development and Function
Skeletal and Muscular System Development and Function, Cardiovascular System Development and Function, Organ Development
Cell-To-Cell Signaling and Interaction, Tissue Development, Cardiovascular Disease

Table 4-8. Summary of disease and function networks associated with differentially expressed genes in other breed grade 3 and 4 disease samples compared to normal samples. Underlined is the network that is visualised in Figure 4-7.

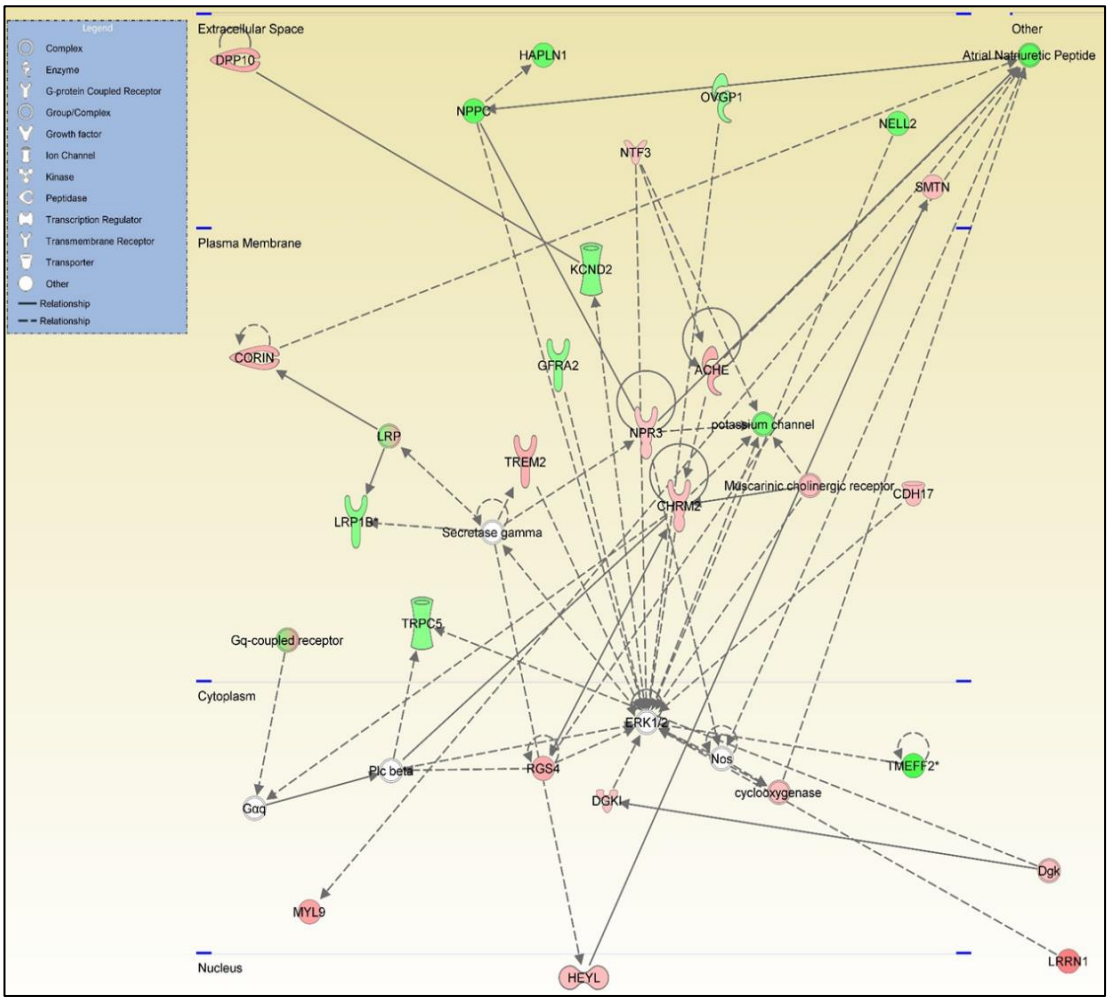

Figure 4-7. Schematic of the *Organismal injury and abnormalities, renal and urological disease and behaviour* network. Genes are shown in their protein cellular location with red indicating up-regulation, green down-regulation and un-coloured showing no change in the dataset.

Network analysis for the genes differentially expressed in CKCS samples compared to normal samples highlighted the top five disease and functions annotations assigned to this dataset (**Table 4-9**). Amongst these were several networks that involved cardiovascular pathways. The third pathway in this analysis is visualised in **Figure 4-8**.

Top disease and function
Cell Death and Survival, Cell Cycle, Cellular Movement
Cardiovascular System Development and Function, Cell Morphology, Organ Morphology
Cardiovascular Disease, Cell Death and Survival, Connective Tissue Disorders
DNA Replication, Recombination, and Repair, Cellular Movement, Cellular Assembly and Organization
Connective Tissue Disorders, Organismal Injury and Abnormalities, Skeletal and Muscular Disorders

Table 4-9. Summary of disease and function networks associated with differentially expressed genes in CKCS samples compared to normal samples. Underlined is the network that is visualised in Figure 4-8.

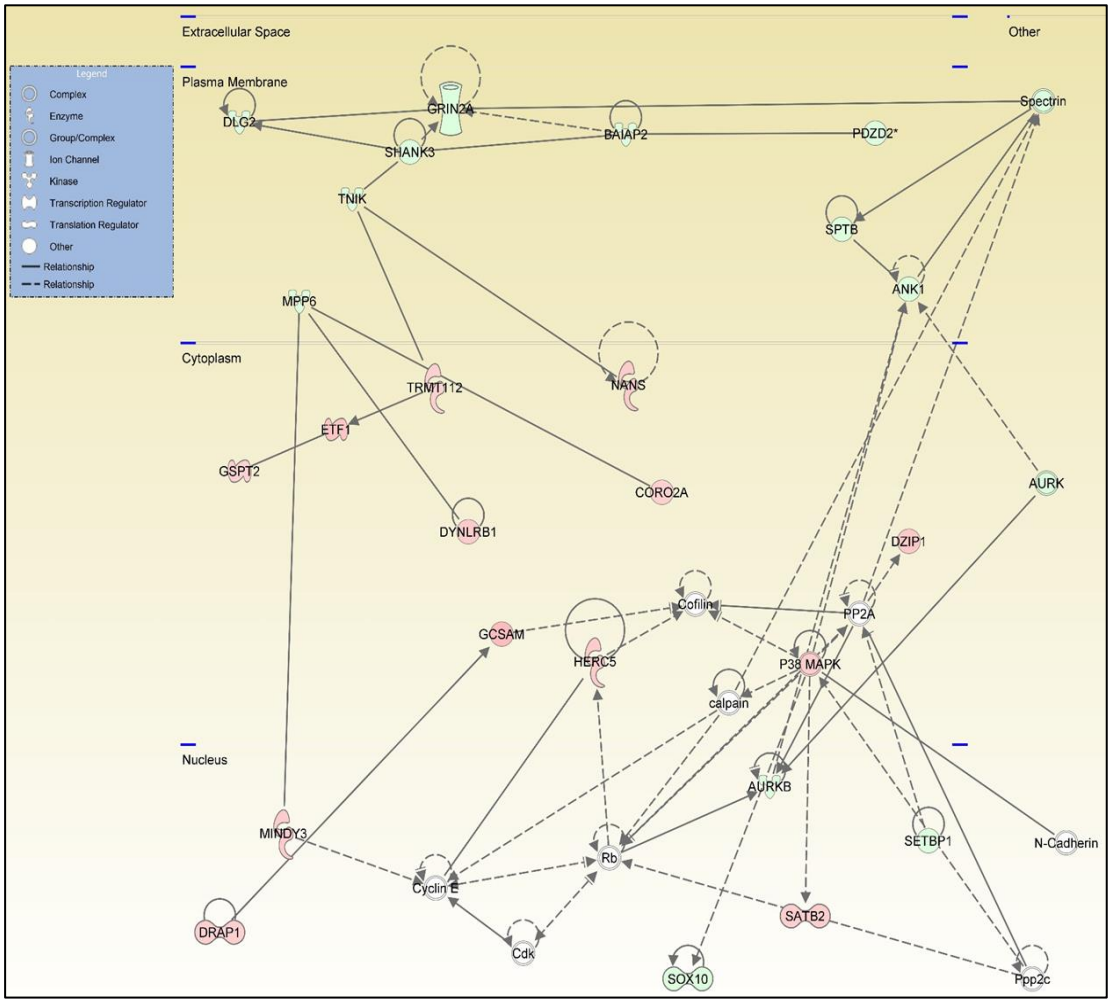

Figure 4-8. Schematic of the *Cardiovascular disease, cell death and survival and connective tissue disorders* network. Genes are shown in their protein cellular location with red indicating up-regulation, green down-regulation and un-coloured showing no change in the dataset.

Network analysis for the genes differentially expressed in CKCS samples compared to other breed grade 3 and 4 disease samples highlighted the top five disease and functions annotations assigned to the dataset (**Table 4-10**). The top pathway in this analysis is visualised in **Figure 4-9**.

Top disease and function
Skeletal and Muscular Disorders, Developmental Disorder, Hereditary Disorder
Carbohydrate Metabolism, Energy Production, Small Molecule Biochemistry
Lipid Metabolism, Small Molecule Biochemistry, Molecular Transport
Cellular Development, Cellular Growth and Proliferation, Organ Development
Cellular Function and Maintenance, Cardiovascular Disease, Hereditary Disorder

Table 4-10. Summary of disease and function networks associated with differentially expressed genes in CKCS samples compared to other breed grade 3 and 4 disease samples. Underlined is the network that is visualised in Figure 4-9.

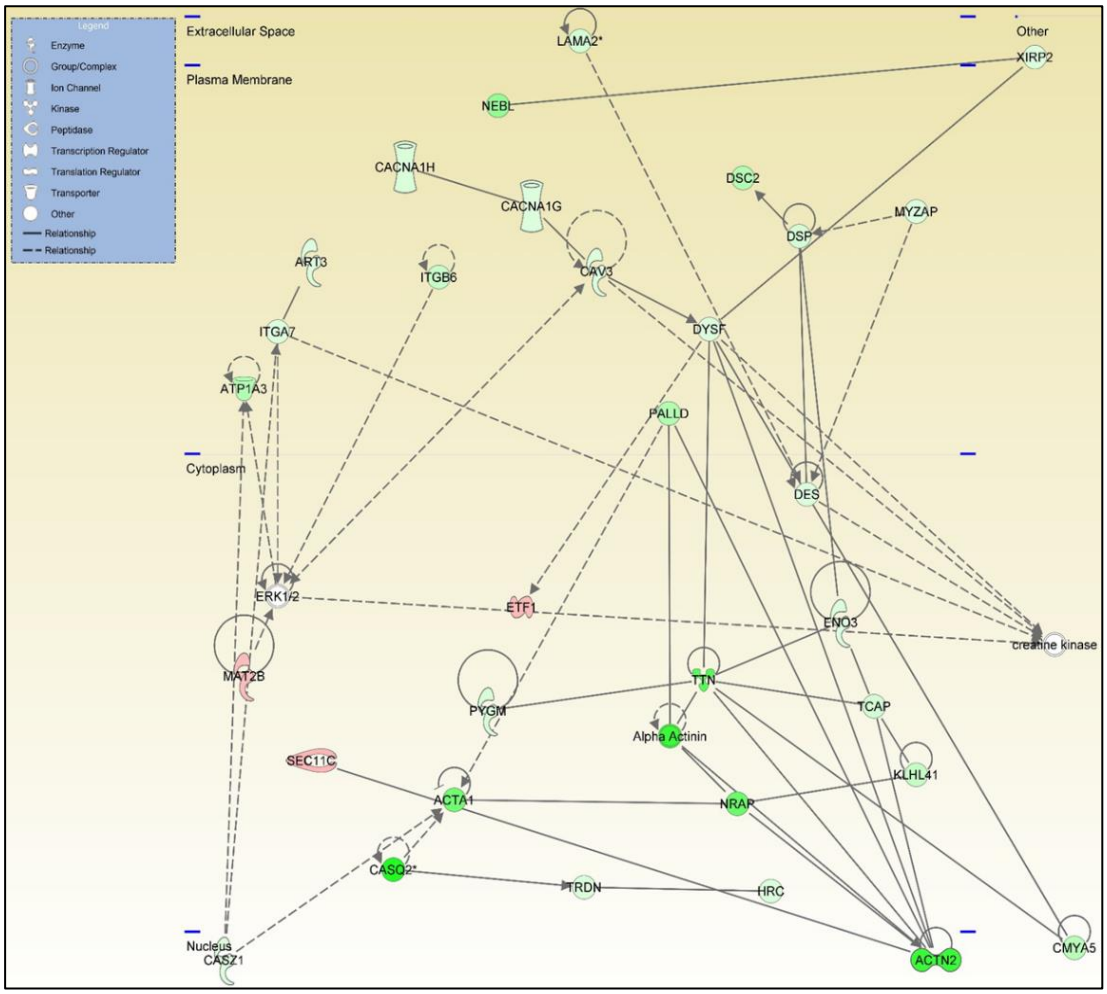

Figure 4-9. Schematic of the *Skeletal and muscular disorders and developmental disorder and hereditary disorder* network. Genes are shown in their protein cellular location with red indicating up-regulation, green down-regulation and un-coloured showing no change in the dataset.

4.4 Discussion

This study aimed to investigate the transcriptomic similarities and differences between CKCS diseased valve samples and other breed diseased valve samples. It is worth noting that almost all CKCS RNA samples in this analysis were isolated for a previous study (as stated in section 4.2.2) and the RNA had been stored at -80 C for several years. This may have played a role in the removal of one of the CKCS samples prior to analysis in this study (detailed

in Chapter 3 section 3.3). However, one of the CKCS samples, although from an older stored valve, was extracted for the current study and still clustered with the other CKCS valve samples away from the other samples. Additionally, the protocol for valve tissue extraction, tissue preparation and RNA extraction were performed using the same protocol as the previous student. It is therefore unlikely this caused the differences seen, but should be accepted as a potential flaw in the following analysis.

It was initially hypothesised (Chapter 3 section 3.1) that by looking at multiple breeds, transcriptomic changes that occur in each grade of MMVD could be elucidated without breed bias. Breed specific differences were hypothesised not affect the analyses as previous studies have indicated that MMVD is polygenic in its development and broadly follows the same pathogenesis in all breeds[1, 2, 33, 110, 219]. Conflicting GWAS results have been published in CKCS with one small study of 18 cases and 18 controls unable to associate any genome region with MMVD and the other weakly associating two loci. A study in whippets also found two loci (different from those in CKCS) associated with disease[219-221]. Immunohistochemical analysis of CKCS MMVD samples compared to other breed MMVD samples and to unaffected other breed normal valves showed no difference between the two diseased groups suggesting there is shared pathology between breeds[110]. However, some reports have indicated there may be a genetic basis for CKCS developing disease earlier in life with a greater heritability of early onset (age 4-5 years) clinically significant MMVD found in CKCS[23, 222, 285]. Recent reports on Swedish and UK breeding programmes have shown that the prevalence of MMVD or at least the prevalence of early-onset MMVD can be reduced in CKCS following a breeding programme[283, 284]. Given this, the results reported in this study may be enlightening.

Comparing the genes differentially expressed in diseased valve samples from other breeds and the CKCS diseased valve samples to normal valve samples, a number of the same genes were found to be differentially expressed (section 4.3.2). Of note were many of the genes described as hallmarks of MMVD (as discussed in Chapter 3 section 3.4) such as *ACTA2* and *HTR2B,* giving credence to the previous report that the central pathology of MMVD in all breeds is the same[2, 110]. Supporting this view, similarities were observed in the gene enrichment analysis performed for these two datasets. DAVID analysis indicated four (two up-regulated and two down-regulated) GO terms were shared in the top 10 lists for each dataset compared to normal valves. These included GO terms previously associated with analysis, in Chapter 3 section 3.3.5 and 3.3.6, for their relevance to disease; positive regulation of ERK1 and ERK2 cascade and down-regulation of proteinaceous extracellular matrix. Similarly, in IPA analysis of the diseased valve datasets compared to normal valve samples, matching pathways are seen in both the canonical pathway and top upstream regulator analysis. In agreement with the by grade analysis, in Chapter 3 section 3.3.7, the top canonical pathway suggested was the *hepatic fibrosis/hepatic stellate cell activation* pathway, this was the most significant pathway in the comparison with other breed samples and second in the CKCS analysis with *calcium signalling* being top. Interestingly, the second suggested canonical pathway in other breed samples was the up-regulation of genes in the *Caveolar-mediated endocytosis signalling* but this was not seen in CKCS. As this pathway is associated with the inhibition of TGFβ-activation of fibroblasts this may have some bearing on early development of disease in CKCS[164, 165]. TGFβ1 was also the top upstream regulator in the other breed analysis and the fourth most significant for the CKCS dataset. TNF was also implicated but F2 (prothrombin) was suggested as the top upstream regulator. In network

analysis, there were also various disease functions that matched between these two analyses. This included those involved in cardiovascular development and dysfunction although these functions were suggested far more in the CKCS analysis. Overall, the similarities between CKCS and other breed grade 3 and 4 suggest that there is a shared pathogenesis in the disease development (likely mediated by TGFβ1), in agreement with the previous literature[33, 110]. However, some differences in these datasets do exist and may be important.

The immune-related GO terms in the by grade analysis (Chapter 3 section 3.3.5 and 3.3.6) were only observed to be enriched in the CKCS compared to normal valve samples dataset, suggesting that this is enhanced in CKCS valve samples. This may be of interest as there is some evidence to suggest that CKCS are also pre-disposed to some inflammatory conditions such as inflammatory bowel disease and pancreatitis[286, 287]. However, what role this play in the early development of MMVD is highly speculative as the role of immune cells in MMVD is yet unknown[44]. As mentioned earlier, the top upstream regulator in the CKCS comparison to normal valve samples was the activation of prothrombin. Prothrombin is a factor related to blood coagulation, but it has a role in pro-inflammatory mediation as well as having downstream signalling activity in endothelial, smooth muscle and fibroblast cell types which can be related to MMVD[288]. Likewise, thrombin has also been shown to both induce and inhibit TGFβ1 signalling depending on the context[289, 290] However, prothrombin's role in blood coagulation may be most relevant to MMVD development. As discussed in Chapter 1 section 1.6.1, CKCS are predisposed to platelet dysfunction and macro-thrombocytopenia, which has been associated with early MMVD development in humans[225, 226, 228]. Prothrombin's role as a top upstream regulator in CKCS valves may indicate a presence or role for platelet interaction with the valve. If this were the case it would allow

for 5HT signalling to be enhanced in the valve which could lead to MMVD development, something which has been stipulated in the literature[171, 173, 229]. Additionally in this analysis, there is an enrichment for muscle conduction and muscle related GO terms in the down-regulated CKCS differentially expressed genes. This involvement of conduction and cardiac muscle related pathways was also seen in the IPA analysis with *Calcium signalling* being seen as the top canonical pathway in the CKCS dataset. Interestingly, differences in *Calcium signalling* and *Cardiac muscle* pathways were also seen when comparing CKCS to the other breeds in the grade 3 and 4 valve samples.

When considering the results generated from comparing the CKCS to the other breed diseased valves, in agreement with the previous analysis, genes that are typical of disease were not differentially expressed between groups, further supporting a central pathogenesis shared between all dogs[110]. This includes the MMVD markers *ACTA2* and *HTR2B*[2]. DAVID analysis centred around down-regulated GO terms with all involving muscle contractility and calcium signalling related pathways. This theme continued in IPA analysis with *Calcium signalling* again being the top canonical pathway suggested form this dataset. The top upstream regulator's list for this dataset is dominated by the down-regulation of the activity of factors involved in cardiac muscle contraction control and differentiation[291-293]. Understanding how down-regulation of cardiac muscle, smooth muscle related and calcium binding pathways relate to the early on-set or advanced progression of MMVD in CKCSs may provide clues to the early pathogenesis in CKCS and hence to possible breed-specific therapies. The consistent implication of a role of calcium binding and calcium signalling could be of interest when considering the role it may play in 5HT signalling. 5HT typically signals through G-protein q coupled receptors (such as 5HTR2B) which cause an influx of calcium into

the cell as part of their downstream signalling[172]. The heightened number of genes down-regulated in calcium related pathways may be indicative of either increased calcium signalling (potentially through 5HT signalling) through negative feedback of these genes in CKCS samples or that CKCS valves have something fundamentally different in capacity for calcium signalling. Both of these could result in downstream signalling that could enhance or cause early MMVD development. This is especially interesting given the recent reports implicating higher circulating 5HT in the platelets of CKCS compared to most other breeds and, as discussed, the potential role of dysfunctional platelets[225, 226, 229]. However, more in-depth studies would be required to confirm this. It may also be that, although a transcriptomic difference exists, it is not related to disease pathogenesis, but this seems unlikely due to the heritability of early-onset disease in this breed and the relevance that transcriptomic differences between breeds of dogs would have[222].

The drug predominantly used to treat the symptoms of MMVD, pimobendan, is a calcium sensitiser and inotrope[259, 294]. Pimobendan primarily acts by reducing the size of the heart and having peripheral vasodilatory effects, resulting in a prolonged period before congestive heart failure takes effect[35, 260, 294]. Given the implied involvement of calcium signalling in CKCS disease, it may be that reduced or enhanced calcium sensitisation and contractility in CKCS valves are involved in the early development or rapid progression of disease in this breed. Likewise, these changes could be symptomatic of a single or several unidentified change/s that have additional non-transcriptomic effects on the valve. These questions remain unanswerable with this current analysis which involved relatively small numbers, particularly of breeds other than CKCS with severe disease. Appreciation of what these results mean will require a far more in-depth analysis beyond the scope of this study. It would

be useful to have control CKCS unaffected samples, preferably age-matched, to compare with normal valves from other breeds as well as to the diseased valve samples. From this, further –omic or cell culture studies could be performed to generate hypotheses into the molecular reasons for early disease development, which might inform breeding programmes, or the development of appropriate therapies for at-risk dogs. In this context studies investigating if similar transcriptomic differences are present in the valves of other breeds predisposed to developing early-onset disease, such as the dachshund, would be beneficial [166].

In conclusion, this study has analysed the transcriptomic similarities and differences between CKCS and other breed dogs with grade 3 and 4 disease. In doing so, potentially key pathways that may be important in the early development of MMVD in CKCS have been identified.

Summary:

- Transcriptomic differences exist between CKCS and other breed dogs with grade 3 and 4 disease

- There is a shared central pathology in the development of MMVD regardless of breed

-calcium signalling, muscle contraction and prothrombin may be important in the early development of MMVD in CKCS

This study has therefore achieved its aim and established potentially important pathways that may cause the increased predisposition for MMVD in CKCS. However, there is a level of shared pathology across all breeds of disease implying the pathways identified are more enhancers rather than central drivers of disease pathogenesis. It may be the case that CKCS have

several of these pathways enhanced leading to early development. Regardless, investigating the central pathogenesis of disease shared in all dogs especially in early disease pathogenesis. As mentioned in Chapter 3, Chapter 5 aims to investigate this issue.

(This page has been left intentionally blank)

Chapter 5 Region dependent changes in early MMVD

5.1 Introduction

The development of myxomatous mitral valve disease (MMVD) begins in discreet areas of the valve (that can be macroscopically identified), typically towards the free edge, that expands eventually encompassing the entire valve by end-stage disease[2, 4, 36]. A neglected area of MMVD research is that which focusses on events in early disease progression (Whitney grade 1 and 2). This makes discerning causal pathways responsible for MMVD difficult. As highlighted in Chapter 3, analysis of early disease is confounded by the presence of high proportions of normal tissue that can mask MMVD-specific pathways when the whole valve is included in the analysis. In this study, this issue is circumvented by separating the areas of overtly diseased and normal tissue from the same grade 2 valves. It is hypothesised here, that by comparing the transcriptome of the normal and diseased tissue regions, pathways involved in the early development of MMVD will be observed.

This approach offers benefits over whole valve analysis as diseased valve tissue is compared directly to the normal tissue from the same valve in a paired analysis. This minimises the effect of confounding factors such as age and breed, as well as any differences in baseline expression of genes between individual animals. Additionally, this is a novel approach in MMVD research in any species. To my knowledge, only one previous study has used a dissection approach, similar to the one proposed here, in valve research. Nagy *et al* macroscopically dissected human aortic valves into normal, thickened and calcified regions before assessing gene expression by RT-qPCR[295]. This study was able to successfully show gene expression differences between the normal and thickened diseased areas or calcified diseased areas of the valve

and correlated gene expression with disease severity. This helps to justify the use of dissection as an appropriate technique to interrogate early disease development[295].

This chapter aims to investigate transcriptomic profiles of diseased and normal areas of Whitney grade 2 valves from the dog and identify differences that may be important in the early development of MMVD. Additionally, this study aims to investigate if the normal regions of diseased valves are similar or different to the whole normal valves samples.

5.2 Materials and methods

5.2.1 Tissue collection

For full details on tissue collection and dissection, see Chapter 2 section 2.2. Seven Whitney grade 2 valves were collected and the diseased and normal areas of the valve were macroscopically dissected. An additional four normal (grade 0) valves were collected and dissected following the same protocol with areas towards the free edge of the valve (were diseased lesions would typically begin to form) separated to compare to the rest of the valve tissue. Myself and another investigator in unison performed dissection and identification of diseased lesions on the valve. The description of the dogs used in this study is summarised in **Table *5-1***.

Sample ID	Date sampled	Dog Breed	Gender	Age	Whitney grade
SBT1G0	05/06/2017	STAFFORDHSIRE BULL TERRIER	MALE	1y	0
JRG0	23/03/2018	JACK RUSSEL TERRIER	MALE	4y	0
SBT2G0	04/05/2018	STAFFORDHSIRE BULL TERRIER	MALE	6y	0
GSG0	18/05/2018	GERMAN SHEPHERD	FEMALE	5y	0
JRG2	28/06/2016	JACK RUSSEL TERRIER	MALE	3y	2
BCG2	07/10/2016	BORDER COLLIE	MALE	3y	2
GSG2	26/08/2016	GERMAN SHEPHERD	FEMALE	4y1m	2
SBT1G2	05/08/2016	STAFFORDHSIRE BULL TERRIER	MALE	3y10m	2
SBT2G2	13/10/2017	STAFFORDHSIRE BULL TERRIER	MALE	4y1m	2
ROTG2	22/09/2017	MASTIFF	MALE	5y	2
BG2	14/04/2014	BEAGLE	FEMALE	6y	2

Table 5-1. Summary of the dogs used in this study.

5.2.2 RNA extraction, quantification and quality control for microarray

The extraction protocol followed for dissected valve RNA extraction is detailed in section 2.3.1 of Chapter 2. Quantification and quality control assessment of RNA for microarray analysis was performed as described in Chapter 2 section 2.3.3. RNA integrity numbers (RIN) were not assessed in the normal valve dissected samples as these were not used in microarray analysis.

5.2.3 Affymetrix Canine Gene 1.1ST microarray analysis

In this study, the majority of microarray analysis was performed on a single 24 well Affymetrix Canine Gene 1.1ST chip, the remaining 12 wells on this chip were used in the study discussed in Chapter 6. The normal and diseased tissue samples from sample BG2 were analysed by microarray on one of the 16 well Affymetrix Canine Gene 1.1ST chips used in the analysis described in chapter 3. RNA processing, hybridisation, post-hybridisation quality control, summarisation file creation and differential gene expression analysis was performed as described in section 2.5 of Chapter 2. Statistical analysis used paired sample analysis of variance (ANOVA) with differential gene expression determined as having a >±1.5 fold change difference in expression a >2.5 log signal intensity and with an adjusted P-value (Q-value) using a Benjamini-Hochberg false discovery rate (FDR) correction (Q-value <0.05).

5.2.4 Gene enrichment analysis

The network analysis tool Miru (version 1.4) was utilised as described in Chapter 2 section 2.6.1. A sample-to-sample comparison was performed with a Pearson correlation of r=0.9, this maximised the number of samples included whilst minimising the connection between samples. The tools Database for Annotation, Visualisation and Integrated Discovery (DAVID) version 6.8 and Ingenuity Pathway Analysis (IPA) were used as stated in Chapter 2 sections

2.6.2 and 2.6.3. Gene list comparison was performed as described in Chapter 2 section 2.6.4.

5.2.5 cDNA synthesis and RT-qPCR

To validate the microarray analysis and the expression of genes of interest in normal valve samples that have been dissected, RNA samples were synthesised into complementary DNA (cDNA) and real-time quantitative polymerase chain reaction (RT-qPCR) was performed (Chapter 2 section 2.7). The primers used are listed in **Table 5-2** and were designed and optimised following the protocol summarised in Chapter 2 section 2.7.2-2.7.6. All gene quantification was normalised to *MRPS25*, *RPL32* and *GAPDH*. Statistical analysis used paired sample T-tests as detailed in Chapter 2 section 2.13.

Gene Symbol	Forward Primer Sequence	Reverse Primer Sequence	Product Length	Optimum TM °C	Primer Efficiency %
ACTA2	5'CGGCTACTCCTTTGTGACG3'	5'CGTGGCCATCTCGTTCTC3'	100	58	102.2
HTR2B	5'CCAATCCAGGCCAATCAAAG3'	5'CAGGTGATGTTGCTTGGGTT3'	143	59	104.8
TAGLN	5'GACATGTTCCAGACCGTCGA3'	5'CAATGACGTGCTTTCCCTCC3'	199	59	106.7
ACTG2	5'TGCCAACAATGTCCTTTCCG3'	5'GCCTCCAATCCAGACTGAGT3'	148	60	93
HBEGF	5'CTGTGGTGCTGTCATCTGTC3'	5'TGGGAAGTAGTCATGCCTAACT3'	124	61	103.8
CDKN2A	5'CATGTTGGCTCAGAATCGGG3'	5'CTCACGTCCAAGGCACAAAA3'	125	60	90.6
SLC10A6	5'GCTGTTGGATGGGTTTCTCA3'	5'TCCAAGAAAGCACCAGTCTCT3'	147	58	101.7
CILP	5'TGCTCCAATTATACCGTGCG3'	5'CAGAACACTTGCTCCAGGGA3'	100	62	106.1
MMP12	5'GACACAATTCATGGACCCTGG3'	5'TCAAATACGTCAGGTCCTTGGA3'	129	63	110
ADAMTS5	5'GTTCCCAAATATGCAGGCGT3'	5'AGCTTCGAACCAATGATGCC3'	191	59	101.6
ADAMTS9	5'CACCGTGTCCTCTCTATGCT3'	5'AACCTCATTGCCTTTGTCCG3'	119	60	100

Table 5-2. Primers designed and optimised for use in this study.

5.3 Results

5.3.1 RNA quality assessment

Extracted RNA samples from dissected regions of valve tissue were quantified and their concentrations, 260/280 and 260/230 ratio and RNA integrity numbers (RIN) were recorded and summarised in **Table 5-3**. RNA

concentration ranged 157.4-2183.2 ng/µl. When comparing the RNA concentrations of 'normal' (mean: 1140 ng/µL ±247 S.E.) to 'diseased' (mean: 1360 ng/µL ±299 S.E.) regions of tissue from the normal valves did not demonstrate a statistical difference (P-value 0.117). Comparing the RNA concentration of 'normal' (mean: 854 ng/µL ±140 S.E.) and 'diseased' (mean: 554 ng/µL ±93 S.E.) regions of tissue from the grade 2 valves, a statistical difference in concentrations was identified (P-value 0.034). Absorbance reading ratios were all within the acceptable reference range (>1.8) for both 260/280 and 260/230, indicating uncontaminated RNA extractions. Gel electrophoresis images (**Figure 5-1**) display the 28S and 16S rRNA in each sample alongside the quantified RIN values. The majority of samples passed the accepted cut-off of RIN>7 for microarray analysis. Sample SBT1G2 'normal' had a RIN of 6.6 but was deemed acceptable for analysis by Edinburgh Genomics (personal communication with Chieko Kontani).

Sample ID	RNA [ng/μL]	260/280	260/230	RIN
SBT1G0 'normal'	978.9	2.1	2.22	-
SBT1G0 'diseased'	1157.3	2.1	2.27	-
JRG0 'normal'	806	2.11	2.22	-
JRG0 'diseased'	766.5	2.09	2.15	-
SBT2G0 'normal'	903.3	2.1	2.25	-
SBT2G0 'diseased'	1331.8	2.1	2.26	-
GSG0 'normal'	1873.1	2.07	2.23	-
GSG0 'diseased'	2183.2	2.06	2.23	-
JRG2 'normal'	649.97	2.12	2.22	8.4
JRG2 'diseased'	343.78	2.06	2.14	8.6
BCG2 'normal'	1178.93	2.09	2.2	7.7
BCG2 'diseased'	686.65	2.09	2.19	8
GSG2 'normal'	916.19	1.89	2.21	7.3
GSG2 'diseased'	532.2	2.11	2.16	8.6
SBT1G2 'normal'	616.95	2.12	2.04	6.6
SBT1G2 'diseased'	851.63	2.1	2.2	7.1
SBT2G2 'normal'	1235.56	2.09	2.21	8.3
SBT2G2 'diseased'	781.24	2.1	2.22	8.5
ROTG2 'normal'	1147.54	2.09	2.24	7.4
ROTG2 'diseased'	521.9	2.09	2.2	8.1
BG2 'normal'	235	2.09	2.15	8
BG2 'diseased'	157.4	2.08	2.15	7.1

Table 5-3. Concentration, 260/280 and 260/230 ratios and RIN for each 'diseased' and 'normal' region of valve tissue.

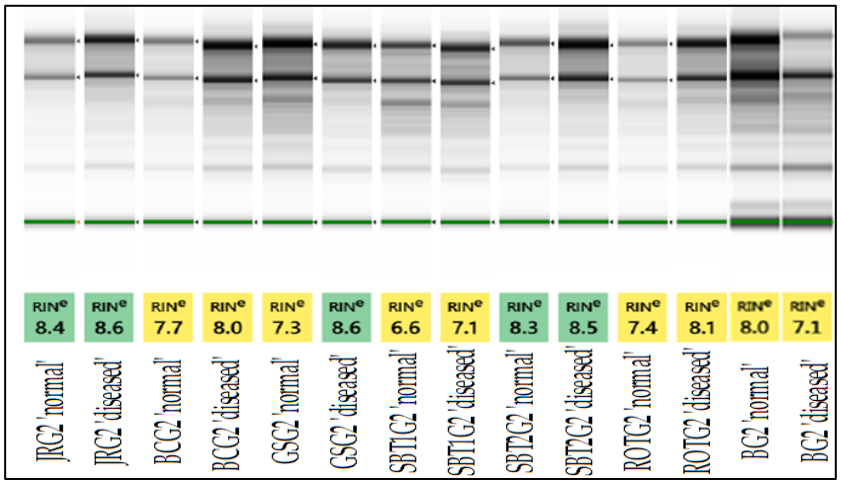

Figure 5-1. Gel electrophoresis images displaying the 28S (top band) and 16S (bottom band) rRNA intensities in each sample. The RIN for each sample is shown and colour coded with >8.2 given a green colour and 6.5-8.2 given a yellow colour.

5.3.2 Microarray post-hybridisation quality control

All wells on the array showed the correct concentration of spike in hybridisation and labelling controls indicated that no technical errors occurred on the plate. After Robust Multi-array Average (RMA) and gene-level normalisation, the log expression signal for the dissected normal, dissected diseased and whole valve normal samples are shown in **Figure 5-2**. The sample with the largest variability in the log expression signal was BG2 'normal'. Signal intensity distribution for these samples is shown as the log2 signal line graph in **Figure 5-3**. A similar signal distribution pattern was seen for all samples ranging from 0-13.69. The initial peak, indicative of background noise, ranges from 0.93-2.5. This figure shows that to remove the effect of background on this dataset, genes expressed below 2.5 log signal intensity should be removed.

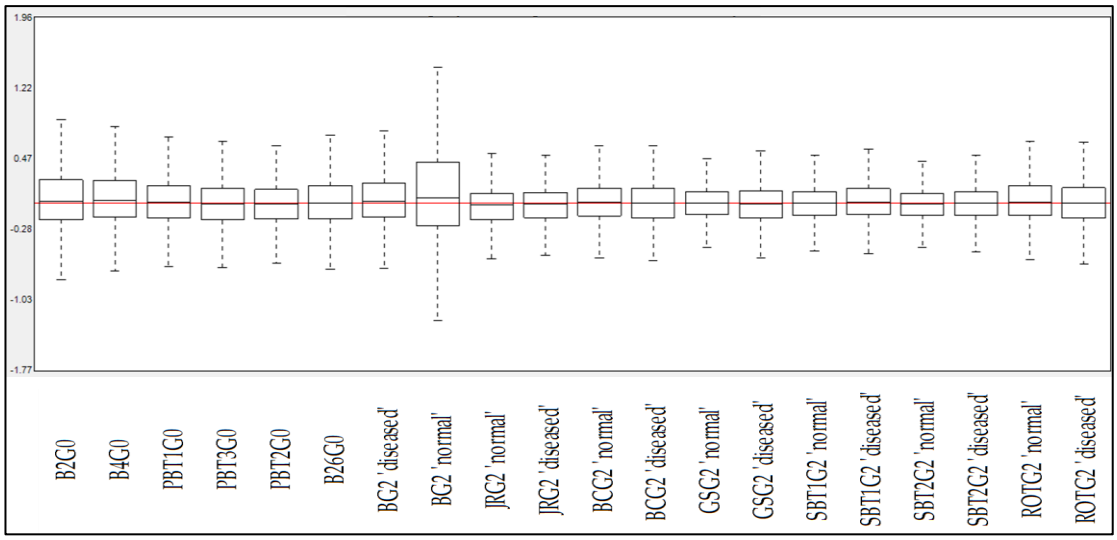

Figure 5-2. Post-RMA signal intensity boxplots.

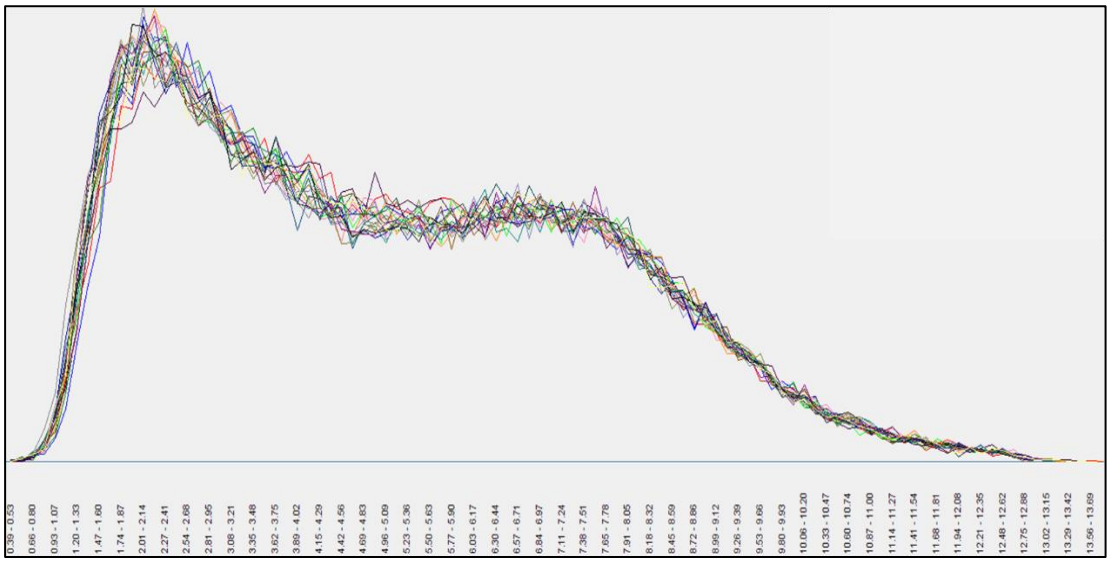

Figure 5-3. Log2 signal line graph for samples. Each line represents a sample and a uniform pattern of expression can be seen here.

Principal component analysis (PCA) in Affymetrix expression console and sample-to-sample analysis in Miru (r=0.9) was performed. Samples from 'normal' and 'diseased' regions of the valve clustered away from one another (**Figure 5-4**). The dissected valve samples analysed on the microarray chip used in Chapter 3 (yellow squares) clustered away from the samples analysed on the chip described in this chapter (red and blue squares) indicative of a potential batch effect. Comparing the normal whole valve samples to the 'normal' dissected valve regions, by PCA, indicated a slight difference between these two groups (**Figure 5-5**). Sample BG2 'normal', the sample which had the largest variability in the log expression signal, was plotted the furthest away from the other samples, suggesting there may be an issue with the samples use. However, the sample-to-sample analysis in Miru showed that samples clustered together based on whether they were the whole normal valve, dissected 'normal' regions or dissected 'diseased' regions (**Figure 5-6**). Normal whole valve and dissected 'normal' samples shared more edges with each other than the normal whole valve and dissected diseased valve. BG2

'normal' in this analysis clustered with other dissected 'normal' samples. This coupled with the sample having a relatively good RIN value (7.1) it was decided not to remove this sample from the dataset. Ultimately, PCA and sample-to-sample analysis highlighted that there were transcriptomic differences between both the diseased regions and normal regions of grade 2 valves as well as, to a lesser extent, between normal regions of grade 2 valves and whole normal valve samples.

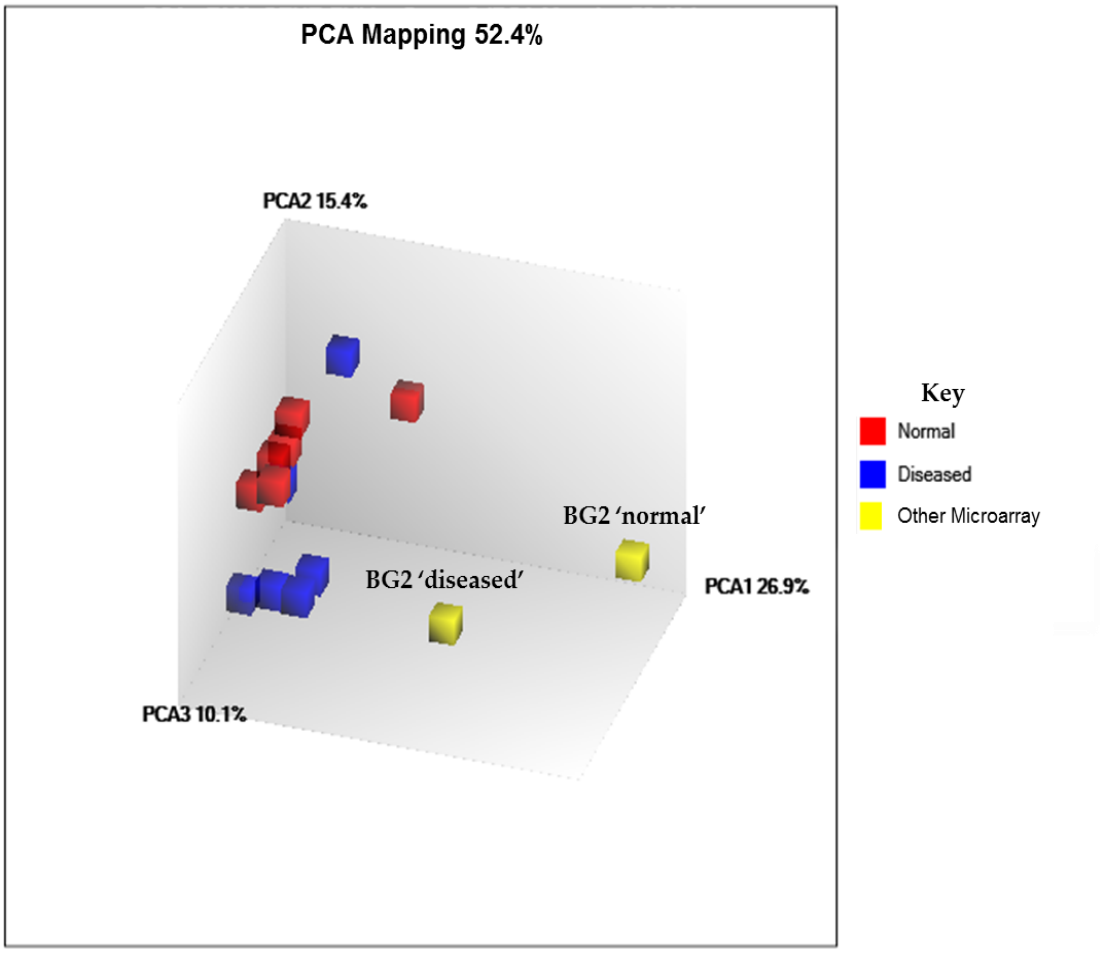

Figure 5-4. PCA plot comparing dissected 'normal' and dissected 'diseased' regions of the valve. Red squares represent 'normal' samples, blue squares represent 'diseased' regions and the yellow squares represent the dissected valve samples analysed in the previous array.

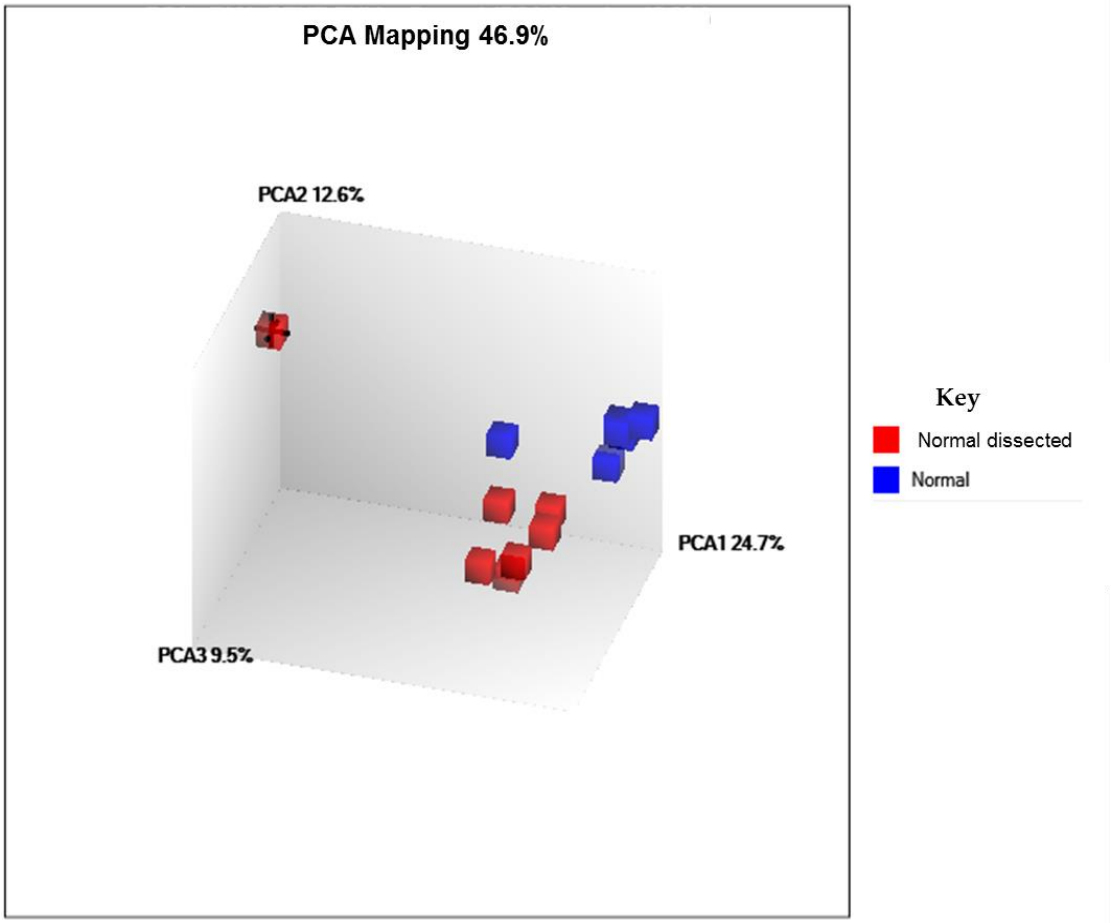

Figure 5-5. PCA plot comparing dissected 'normal' regions and normal whole valve samples. Red squares represent dissected 'normal' samples and blue squares represent normal whole valve samples. The red square with a black cross through it is the dissected 'normal' valve region from the previous array.

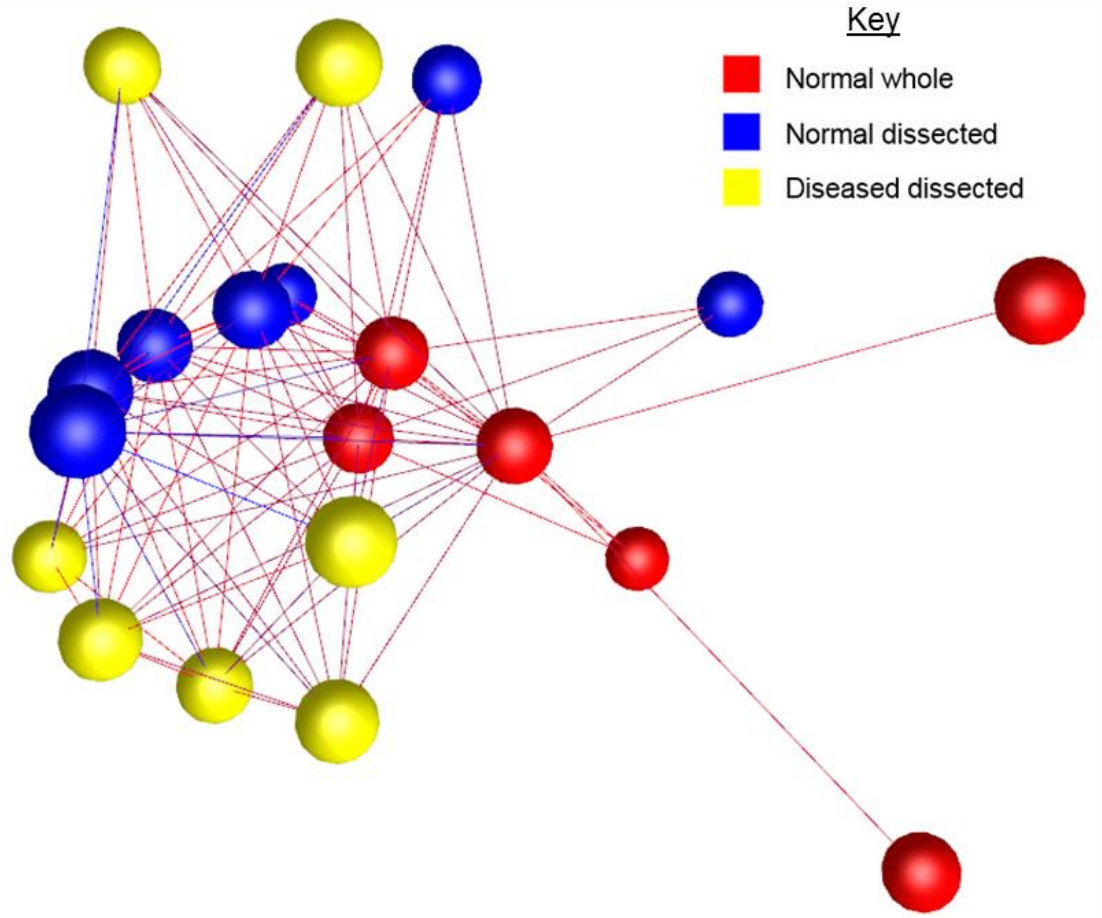

Figure 5-6. Sample-to-sample correlation (r=0.9) of dissected 'normal', dissected 'diseased' and whole normal valve. Red nodes represent whole normal valve samples, blue nodes represent dissected 'normal' regions of valve samples and yellow nodes represent the dissected 'diseased' regions of whole valve samples.

5.3.3 Differential expression of genes

315 probes which could be assigned to 289 genes were found to be differentially expressed between dissected 'normal' and dissected 'diseased' regions of the valve samples (>1.5 or <-1.5 fold change, Q-value <0.05, >2.8 log2 signal intensity). 170 genes were down-regulated and 119 genes were up-regulated in dissected 'diseased' regions when compared to the dissected 'normal' regions. When comparing the dissected 'normal' regions of valve to

normal whole valve samples, 238 probes which could be assigned to 202 genes were differentially expressed. 157 genes were up-regulated and 45 genes were down-regulated in dissected 'normal' regions compared to the normal whole valve samples. These two datasets are summarised in volcano plots in **Figure 5-7** and full gene lists can be found in **Appendix III: Chapter 5 Tables S1 and 2**.

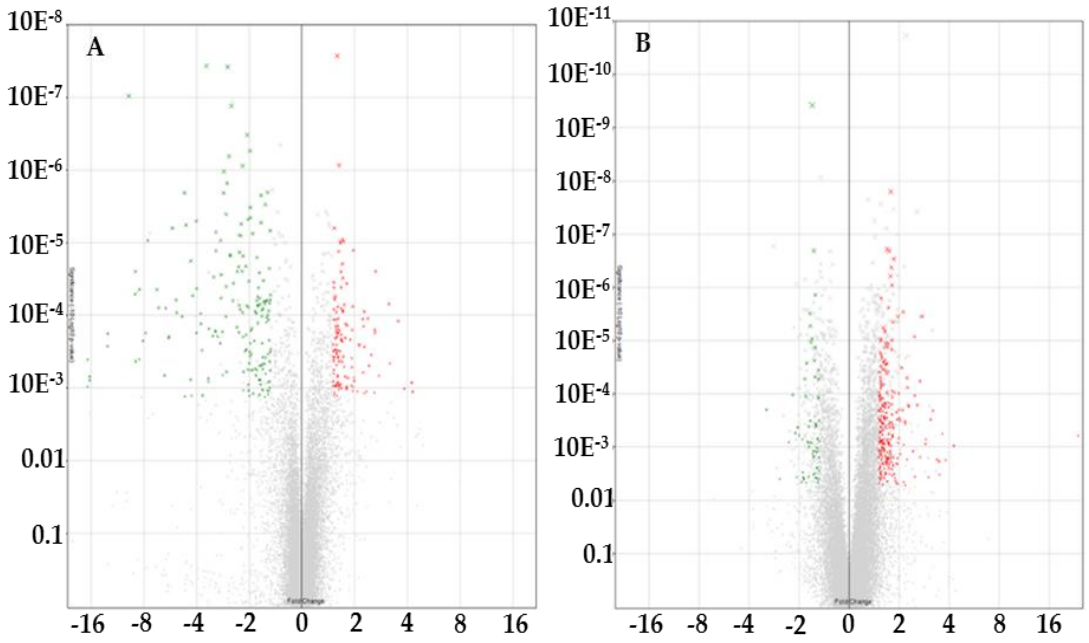

Figure 5-7. Volcano plots showing differential expression of genes in dissected and whole valve samples. (A) Genes differentially expressed between dissected 'normal' and 'diseased' regions. (B) Genes differentially expressed between 'normal' dissected regions of valve and normal whole valve samples.

To investigate the level of similarity between the two-dataset comparisons, the number of genes that shared differential expression was calculated. Out of the combined 472 genes differentially expressed in both datasets, 19 were found to be shared. This is illustrated in a Venn diagram in **Figure 5-8**. Of the

nineteen shared genes (listed in **Table 5-4**), only three shared whether they were up- or down-regulated in the two datasets.

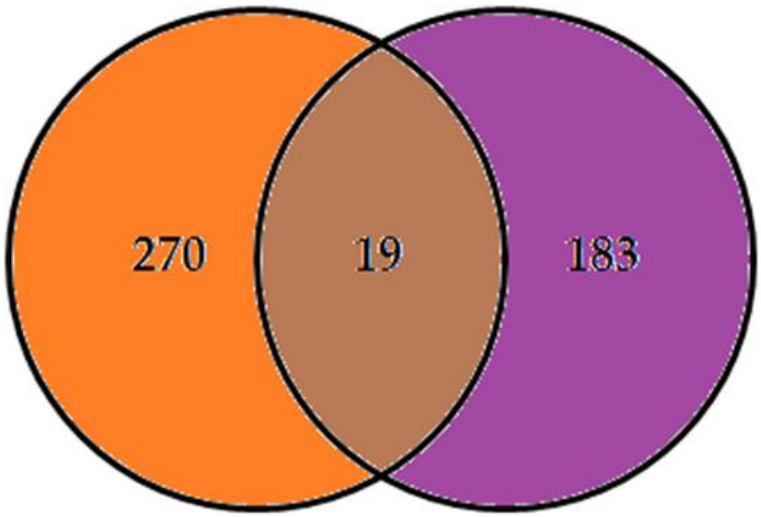

Figure 5-8. Venn diagram illustrating the number of shared differentially expressed genes in the two datasets. In the left orange circle, the number of differentially expressed genes for dissected 'normal' and dissected 'diseased' regions of the valve samples is shown. In the right purple circle, the number of differentially expressed genes for dissected 'normal' regions of the diseased valves and normal whole valve samples is shown. In the centre, the number of shared genes between the two datasets is shown.

Gene name	Fold change in dissected valves	Fold change in normal tissues
ALOX5AP	1.6	-1.52
INSIG1	-1.91	1.53
SLC10A6	-1.61	1.54
ADIPOR2	-1.98	1.6
LPAR3	1.72	1.63
CLEC5A	1.8	1.67
IGFBP6	-1.53	1.67
GREM2	-1.74	1.7
PLA2G16	-1.69	1.73
MYBL1	-1.81	1.77
MAL	-3.19	1.92
WISP1	1.67	1.93
NMUR2	-2.2	2.18
CIDEA	-7.59	2.18
LEPR	-1.78	2.29
CALB2	-2.89	2.49
F3	-12.87	2.88
DGAT2	-8.9	3.5
LYZF2	-2.83	3.63

Table 5-4. Shared differentially expressed genes in the two datasets. Genes in yellow share up- or down-regulation in both datasets.

5.3.4 DAVID 6.8 gene enrichment

DAVID GO term enrichment was performed on the up- and down-regulated genes from both of the datasets. The top ten GO terms suggested for the up- and down-regulated genes comparing dissected 'normal' and dissected 'diseased' regions of valve samples are summarised in **Table 5-5**. The top ten up-regulated and the one down-regulated GO terms associated with genes differentially expressed between dissected 'normal' regions of valve and normal whole valve samples are summarised in **Table 5-6**. No shared GO terms were suggested between these two datasets and the degree of association of the GO terms in this analysis have was much lower, indicated by the higher P-value and FDR values.

	Category	Term	Gene count	P-value	FDR
Up-regulated	GOTERM_BP_DIRECT	Immune response	11	3.25E-07	4.66E-04
	GOTERM_BP_DIRECT	Neutrophil chemotaxis	7	1.01E-06	0.00145
	GOTERM_BP_DIRECT	Eosinophil chemotaxis	4	1.86E-05	0.02665
	GOTERM_CC_DIRECT	Integral component of membrane	44	5.14E-05	0.05463
	GOTERM_CC_DIRECT	External side of plasma membrane	8	1.13E-04	0.12021
	GOTERM_BP_DIRECT	Chemokine-mediated signaling pathway	5	1.28E-04	0.18394
	GOTERM_MF_DIRECT	CCR chemokine receptor binding	4	3.04E-04	0.34272
	GOTERM_BP_DIRECT	Lymphocyte chemotaxis	4	5.44E-04	0.77798
	GOTERM_MF_DIRECT	Chemokine activity	4	8.90E-04	1.00101
	GOTERM_BP_DIRECT	Monocyte chemotaxis	4	9.81E-04	1.39882
Down-regulated	GOTERM_CC_DIRECT	Extracellular space	28	1.25E-08	1.37E-05
	GOTERM_CC_DIRECT	Lipid particle	6	6.16E-05	0.06733
	GOTERM_MF_DIRECT	Heparin binding	7	1.76E-04	0.21874
	GOTERM_CC_DIRECT	Integral component of membrane	53	7.60E-04	0.8275
	GOTERM_CC_DIRECT	Extracellular exosome	35	0.0012	1.29825
	GOTERM_BP_DIRECT	Response to insulin	4	0.00161	2.38306
	GOTERM_BP_DIRECT	Lipid storage	4	0.00181	2.68488
	GOTERM_BP_DIRECT	Low-density lipoprotein particle clearance	3	0.00195	2.87493
	GOTERM_CC_DIRECT	Proteinaceous extracellular matrix	7	0.00478	5.1044
	GOTERM_BP_DIRECT	Glucose homeostasis	5	0.00755	10.7315

Table 5-5. Functional analysis chart summary of GO terms associated with up- and down-regulated genes differentially expressed in the 'diseased' regions of valve compared to 'normal' regions.

	Category	Term	Gene count	P-value	FDR
Up-regulated	GOTERM_BP_DIRECT	Translation	7	0.00274	3.81602
	GOTERM_MF_DIRECT	Structural constituent of ribosome	7	0.00669	7.56247
	GOTERM_BP_DIRECT	Intracellular protein transport	6	0.0136	17.6462
	GOTERM_CC_DIRECT	Cytosolic large ribosomal subunit	4	0.01496	15.6621
	GOTERM_BP_DIRECT	Transcytosis	2	0.03993	43.8971
	GOTERM_BP_DIRECT	Negative regulation of angiogenesis	3	0.04748	49.8405
	GOTERM_CC_DIRECT	Synaptic vesicle	3	0.05136	44.8855
	GOTERM_BP_DIRECT	Regulation of cellular senescence	2	0.05546	55.4804
	GOTERM_BP_DIRECT	Nucleoside triphosphate biosynthetic process	2	0.05546	55.4804
	GOTERM_BP_DIRECT	Angiogenesis	4	0.05882	57.6713
Down-regulated	GOTERM_MF_DIRECT	Nucleotide binding	3	8.90E-02	0.98149

Table 5-6. Functional analysis chart summary of GO terms associated with up- and down-regulated genes differentially expressed in the dissected 'normal' regions of valve compared to normal whole valve samples.

5.3.5 Ingenuity Pathway Analysis

Both datasets were submitted for analysis in IPA with the number of mapped and unmapped genes in each dataset summarised in **Table 5-7**.

Dataset	Mapped genes	Unmapped genes	Total genes
Dissected valve sample comparison	270	19	289
Normal valve sample comparison	181	21	202

Table 5-7. Mapped, unmapped and total number of genes submitted into IPA for each dataset.

Canonical pathway analysis was performed and sixty-two and twenty-seven pathways respectively were associated with genes differentially expressed in 'diseased' regions compared to 'normal' regions and 'normal' regions of dissected valve compared to normal whole valve samples (P-value <0.05). Comparing the two sets of analysis, it is apparent that stronger associations were obtained for the 'normal' and 'diseased' dissected regions comparison dataset. The top three canonical pathways associated with both sets of comparison are summarised in **Table 5-8**.

Dataset	Canonical Pathway	Up-regulated genes	Down-regulated genes	Genes pathway	P-value
Dissected valve sample comparison	Hepatic Fibrosis/Hepatic Stellate Cell Activation	7	14	21/160	3.9811E-09
	Granulocyte Adhesion and Diapedesis	11	6	17/132	1.6218E-07
	Agranulocyte Adhesion and Diapedesis	10	6	16/135	1.1749E-06
Normal valve sample comparison	TREM1 Signaling	5	0	5/75	0.00038905
	Toll-like Receptor Signaling	5	0	5/76	0.00040738
	Serine Biosynthesis	1	1	2/5	0.00066069

Table 5-8. Summary of top three canonical pathways associated with each dataset. The number of genes up- and down-regulated in each pathway as well as the total number of genes changed in each pathway is shown. The P-value score shows the association of the gene list to the pathway.

Upstream regulator analysis associated 2156 molecules with the 'normal' and 'diseased' dissected regions dataset and 290 molecules with the 'normal' dissected regions of valve and normal whole valve samples dataset (P-value <0.05). The top three molecules for each dataset are summarised in **Table 5-9** with Tumour Necrosis Factor (TNF) and Reproductive Homeobox 5 (RHOX5) respectively being suggested as the most likely upstream regulator for genes differentially expressed in 'diseased' compared to 'normal' regions and 'normal' regions of valve compared to normal whole valve. The genes downstream of TNF are summarised in **Figure 5-9**. One hundred and seven genes were associated with the pathway with eighty genes being differentially expressed in accordance with the literature and twenty-two not. One of the other pathways of interest in this dataset was the TGFβ1 signalling pathway, with the genes downstream of this molecule summarised in **Figure 5-10**. One hundred and one differentially expressed genes from the dataset were associated with this pathway with 75 of these changing their expression with what would be expected from the literature and 26 showing an unexpected change. Only four differentially expressed downstream genes were associated with RHOX5, three of which did not match the change in expression expected from the literature (**Figure 5-11**).

Dataset	Upstream Regulator	Molecule Type	Activation Z-score	P-value
Dissected valve sample comparison	TNF	Cytokine	3.544	4.02E-26
	TGFB1	Growth factor	0.926	1.79E-19
	IFNG	Cytokine	2.233	2.19E-18
Normal valve sample comparison	Rhox5	Transcription regulator	0.277	7.54E-06
	POLG	Enzyme		0.0000495
	ADCY7	Enzyme		0.0000635

Table 5-9. Summary of the top three upstream regulators associated with each dataset. For each upstream regulator, the molecule type, Z-score and P-value are given.

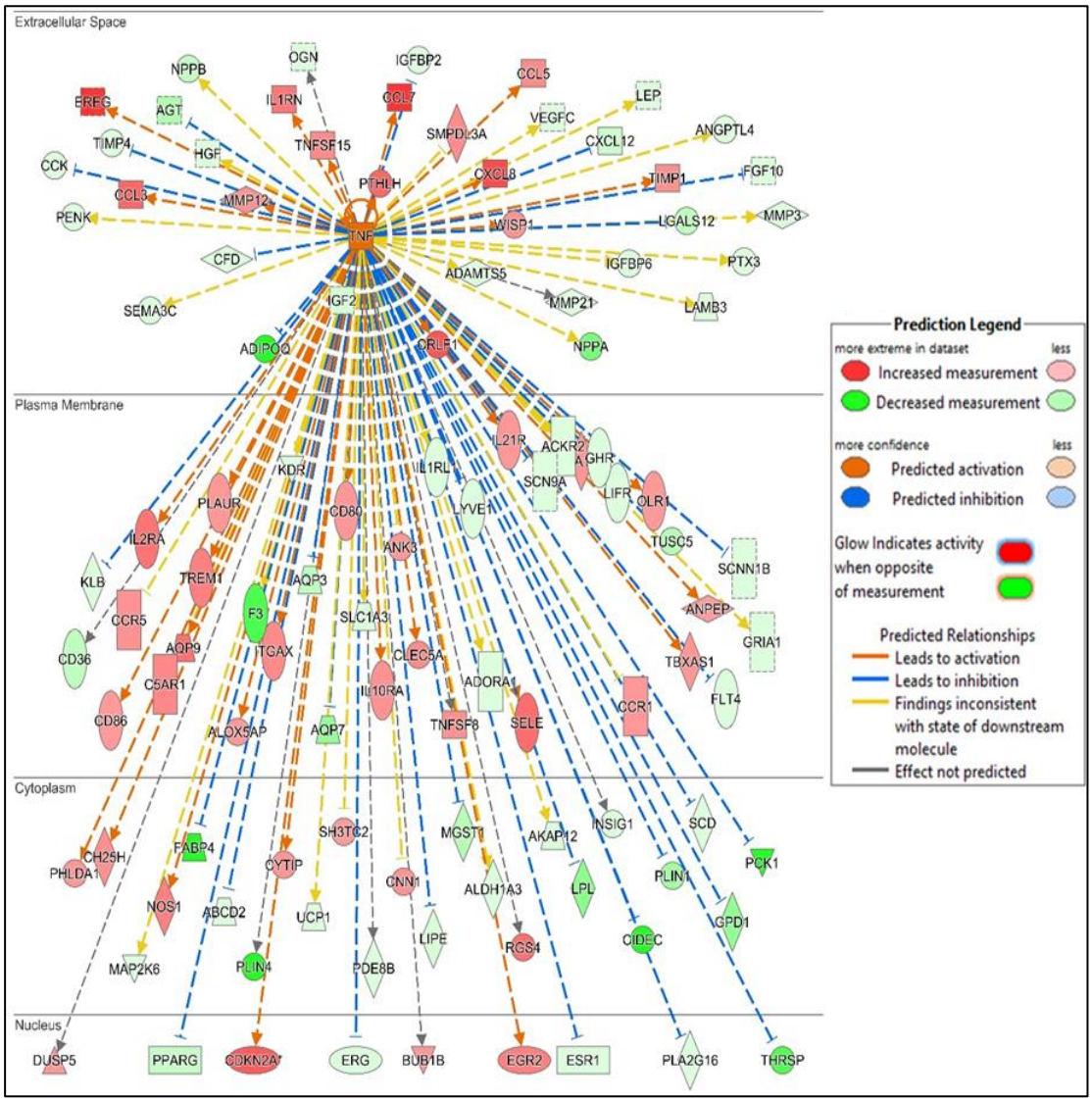

Figure 5-9. The network of genes that are differentially expressed in 'diseased' compared to 'normal' regions that are downstream of TNF signalling. TNF is shown to have its effect from the extracellular space on the genes in their cellular location. Genes are coloured red and green to represent up- or down-regulation in the dataset. Dotted lines connecting TNF to these genes show the expected effect of TNF signalling: orange - activation, blue - inhibition, yellow -result inconsistent and grey – effect not predicted.

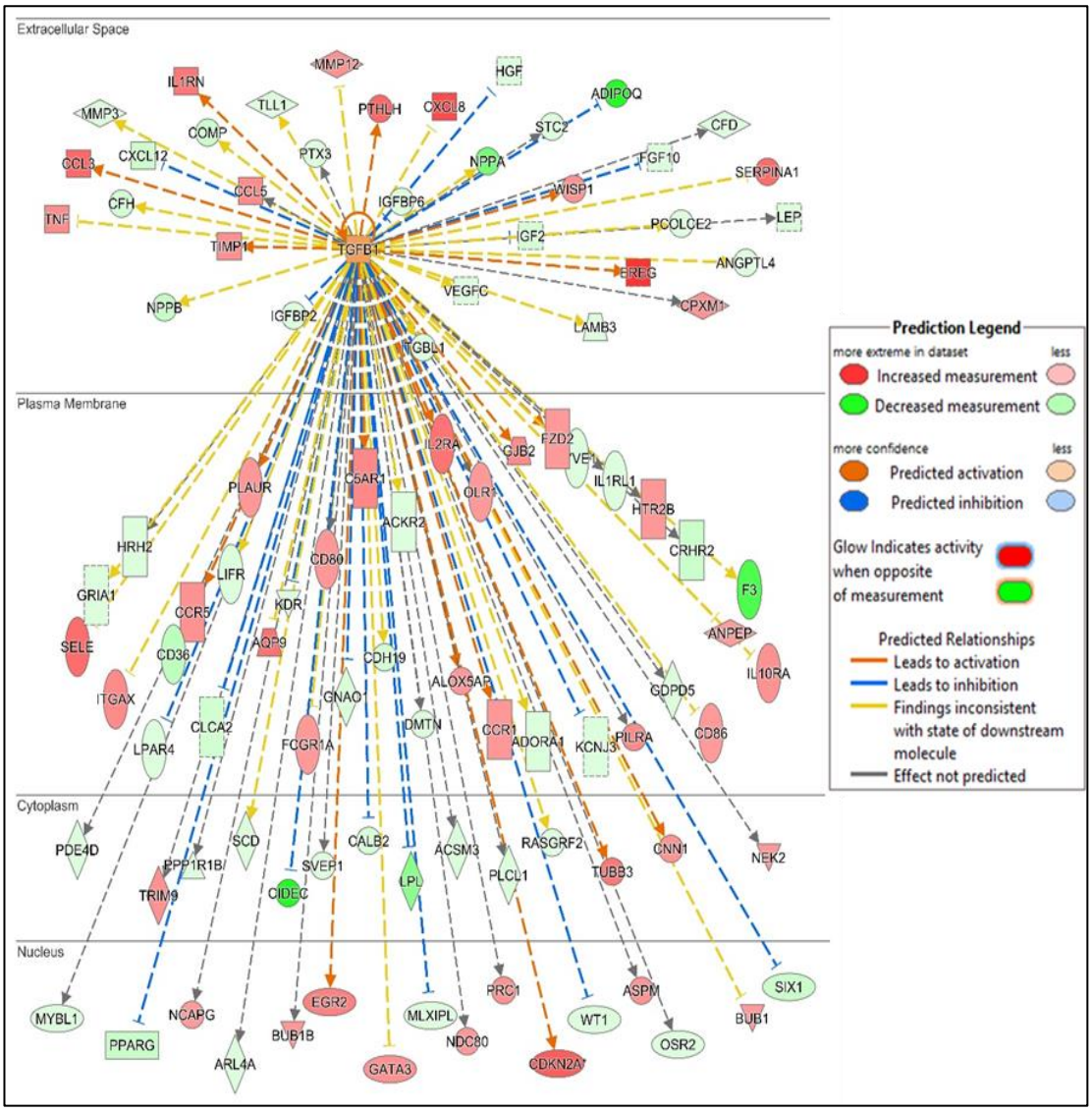

Figure 5-10. The network of genes that are differentially expressed in 'diseased' compared to 'normal' regions that are downstream of TGFβ1 signalling. TGFβ1 is shown to have its effect from the extracellular space on the genes in their cellular location. Genes are coloured red and green to represent up- or down-regulation in the dataset. Dotted lines connecting TGFβ1 to these genes show the expected effect of TGFβ signalling: orange - activation, blue - inhibition, yellow -result inconsistent and grey – effect not predicted.

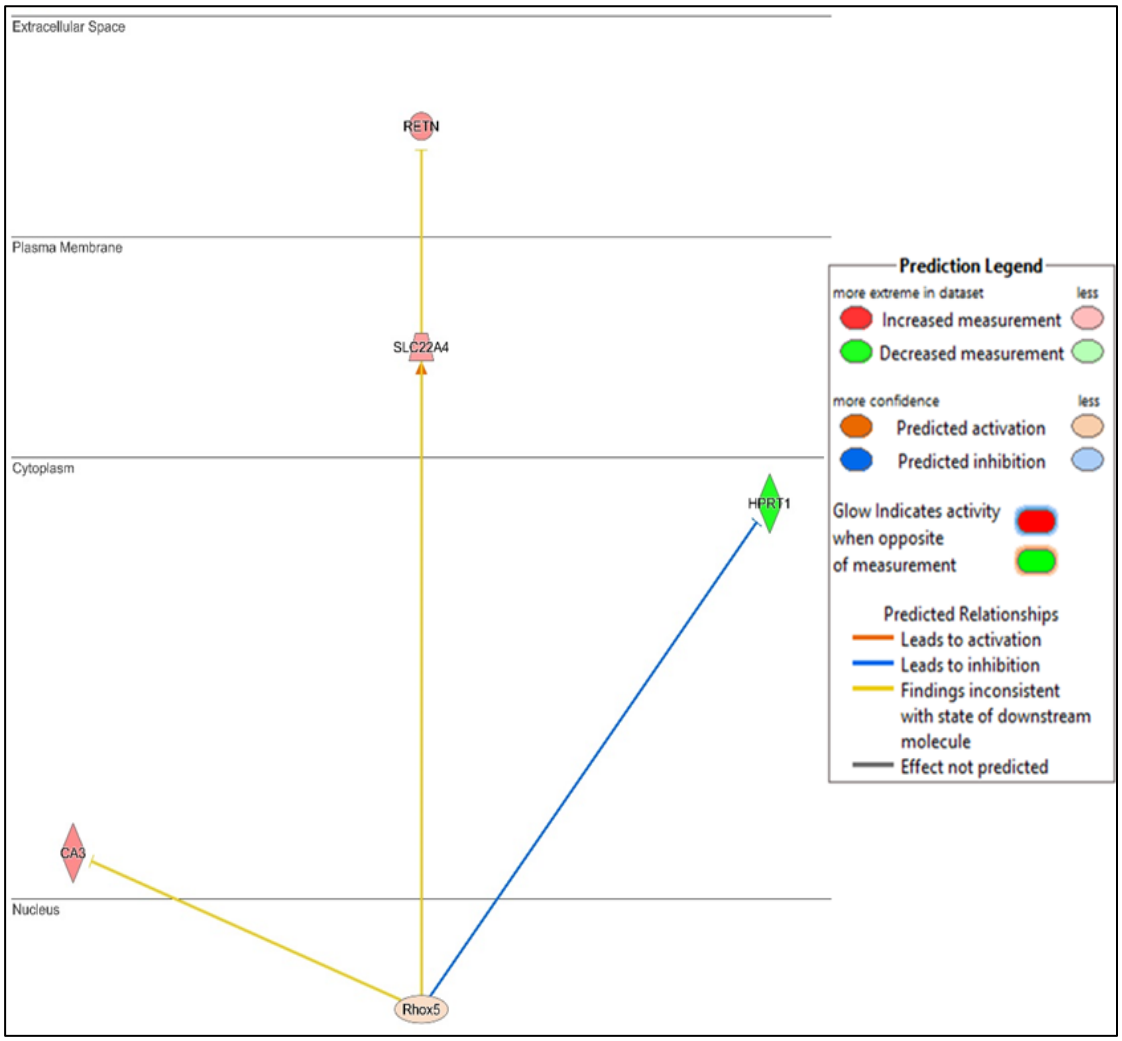

Figure 5-11. The network of genes that are differentially expressed in 'normal' regions of dissected valve compared to normal whole valve samples that are downstream of RHOX5 signalling. RHOX5 is shown to have its effect from the nucleus on the genes in their cellular location. Genes are coloured red and green to represent up- or down-regulation in the dataset respectively. Dotted lines connecting RHOX5 to these genes show the expected effect of RHOX5 signalling: blue – inhibition and yellow - result inconsistent.

The signal intensity values from the microarray analysis for each of the three top upstream regulators suggested for the 'diseased' compared to 'normal' dissected regions dataset are shown in **Table 5-10**. TGFβ1 has approximately

a ten-fold greater signal intensity than TNF or IFNG. These results were corroborated when examining these factors expression in the whole valve analysis (**Table 5-11**).

Upstream Regulator	Microarray signal intensity	
	Normal	Diseased
TNF	11.87	14.32
TGFβ1	176.06	192.67
IFNG	3.97	3.45

Table 5-10. Signal intensity values for each of the top upstream regulators for the dissected 'normal' compared to dissected 'diseased' regions dataset.

Upstream Regulator	Microarray signal intensity				
	Normal	Grade 1	Grade 2	Grade 3	Grade 4
TNF	15.56	15.03	16.56	19.02	12.64
TGFβ1	121.09	143.01	134.36	139.1	142.02
IFNG	4.95	5.24	4.89	4.75	5.09

Table 5-11. Signal intensity values for each of the top upstream regulators for the dissected 'normal' compared to dissected 'diseased' regions dataset in each grade of disease in whole valve analysis

Network analysis was performed and highlighted the disease and function annotations associated with the genes differentially expressed for both datasets. The top three groups of disease and functions are summarised for both datasets in **Table 5-12**. The top groups for each dataset are also visualised in **Figure 5-12** and **Figure 5-13**.

Dataset	Top Diseases and Functions
Dissected valve sample comparison	Tissue Morphology, Connective Tissue Development and Function, Lipid Metabolism Connective Tissue Disorders, Organismal Injury and Abnormalities, Skeletal and Muscular Disorders Cell-To-Cell Signaling and Interaction, Cell Signaling, Molecular Transport
Normal valve sample comparison	Organismal Injury and Abnormalities, Renal and Urological Disease, Connective Tissue Disorders Connective Tissue Disorders, Developmental Disorder, Hereditary Disorder Cellular Function and Maintenance, Hematological System Development and Function, Humoral Immune Response

Table 5-12. Summary of disease and function networks for both datasets.

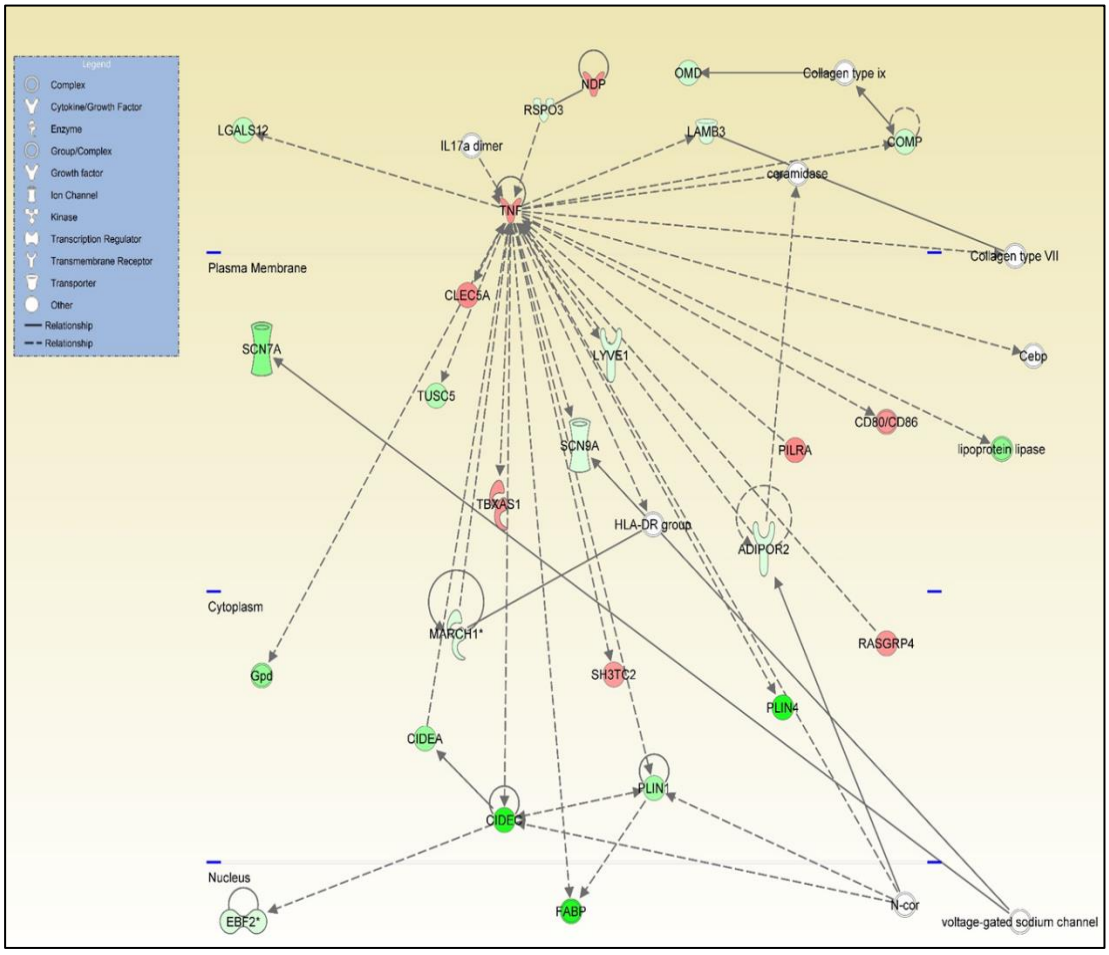

Figure 5-12. Schematic of the *Tissue morphology, connective tissue development and function lipid metabolism* disease and function network. Genes are shown in their protein cellular location with red indicating up-regulation, green down-regulation and un-coloured showing no change in the dataset.

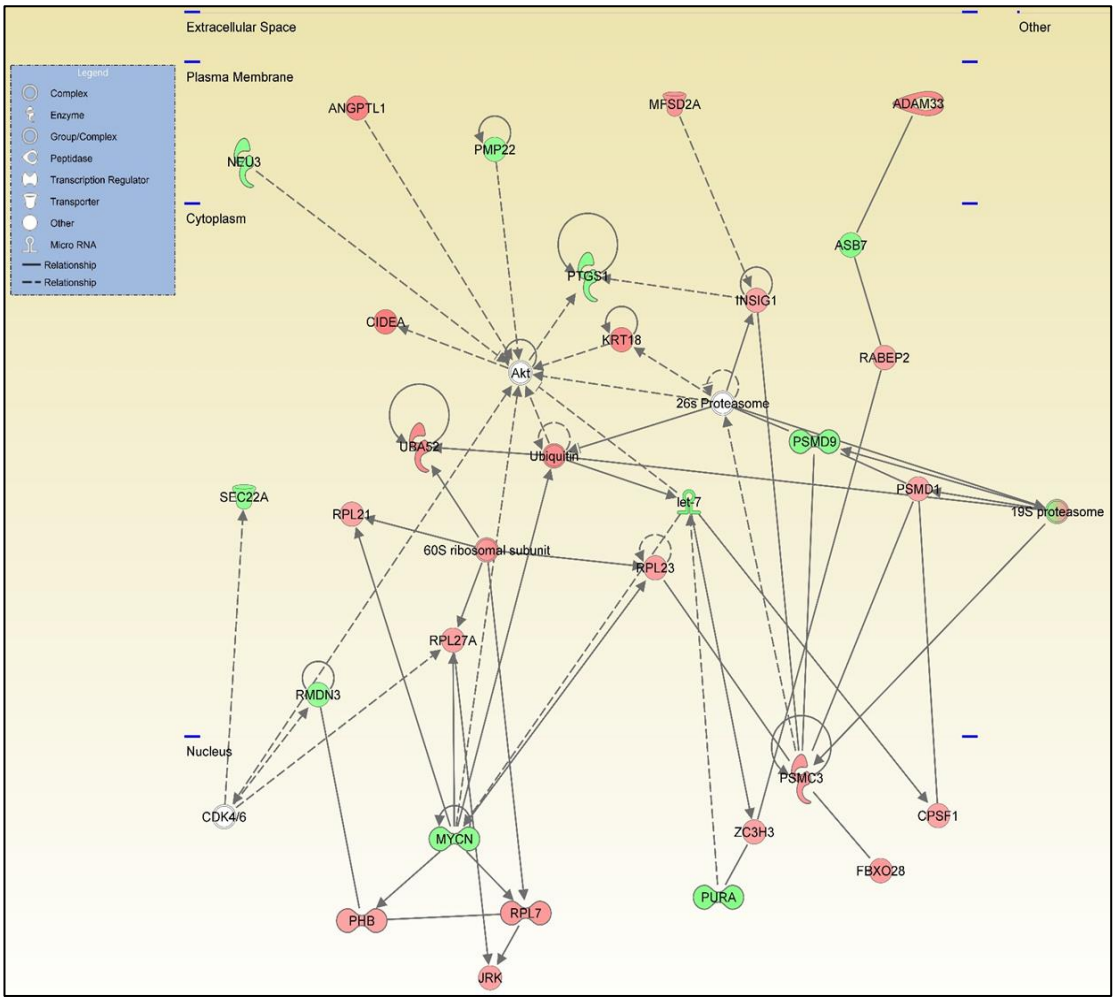

Figure 5-13. Schematic of the *Organismal injury and abnormalities, renal and urological disease and connective tissue disorders* disease and function network. Genes are shown in their protein cellular location with red indicating up-regulation, green down-regulation and un-coloured showing no change in the dataset.

5.3.6 RT-qPCR validation of microarray analysis

Validation of the microarray results was performed with RT-qPCR on selected genes of interest. The majority of these genes surpassed the FDR corrected Q-value cut-off of <0.05, with the exception of *ADAMTS5* and *ACTG2* which were selected for their differential expression in the whole valve analysis, had surpassed ±1.5 fold change and had a Q-value <0.1. Additionally, RT-qPCR

was performed for these same genes of interest on samples from the dissected tissue of normal valves. This analysis compares the expression of these genes from areas where the disease would typically develop (towards the edge of the leaflet) to the rest of the valve. Fold change data for this analysis is summarised in **Table 5-13**. All RT-qPCR data comparing 'diseased' and 'normal' valve regions were in agreement with the corresponding fold changes observed in the microarray analysis. There was no significant difference detected between the different normal regions of valve dissected out of the normal valves for any of these genes.

Gene name	qPCR 'Diseased' compared to 'Normal'		Microarray 'Diseased' compared to 'Normal'		qPCR Normal valve dissection	
	Fold change	P-value	Fold change	Q-value	Fold change	P-value
ACTA2	3.12	0.001	1.79	0.043	2.44	0.157
HTR2B	2.64	<0.001	1.57	0.031	-2.64	0.982
ADAMTS5	-2.28	0.004	-1.6	0.072	3.39	0.186
ADAMTS9	-2.54	0.002	-1.56	0.013	2.29	0.112
SLC10A6	-1.92	0.004	-1.67	0.013	2.01	0.56
CDK2NA	4.96	0.034	1.99	0.04	-1.38	0.215
ACTG2	3.31	<0.001	1.93	0.065	-1.16	0.4
HBEGF	2.34	0.008	1.9	0.042	1.76	0.547
CILP	-5.89	<0.001	-5.77	0.02	3.3	0.079
MMP12	2.59	0.002	1.67	0.019	1.65	0.724

Table 5-13. Summary of Microarray validation by RT-qPCR of the 'diseased' compared to 'normal' regions of the valve and RT-qPCR performed on dissected normal valves. Data presented as fold change compared to normal and associated P/Q-value. Normalised to *GAPDH, MRPS25* and *RPL32*.

5.4 Discussion

This study aimed to investigate the transcriptomic profiles of overtly diseased and normal regions of Whitney grade 2 MMVD valves. It was hypothesised

that differences in expression of genes between these two groups would give an indication to which pathways are fundamentally important in early disease development. Furthermore, this study attempted to compare the transcriptome of seemingly normal regions of Whitney grade 2 valves to that of the whole normal valve, to establish whether the normal regions from the dissected valves were also expressing genes related to disease pathogenesis. Additionally, to eliminate the possibility that the gene changes observed were purely based on regional differences in expression in the valve, dissections were performed on completely normal unaffected valves mimicking the dissections performed in the Whitney grade 2 valves. RNA extracted from these dissected normal valves was then assessed by RT-qPCR for genes differentially expressed between the diseased and normal regions of valves, serving as controls for the diseased dissected valve analyses.

Prior to transcriptomic analysis, it was noted that there was significantly less RNA extracted from diseased regions of Whitney grade 2 valves compared to the normal regions of the same valve (section 5.3.1). This may be because the amount of diseased tissue from these valves was smaller than the remaining normal tissue. However, this difference in RNA concentration was not observed in the dissected normal valves, where the upmost effort was made to use similar sized pieces of tissue in each group as the Whitney grade 2 valves. If the difference observed was caused by disease rather than a difference in tissue size it could be attributed to cells in this region producing less RNA, a decrease in the number of cells in this region or a combination of both. Previous reports in the literature indicate that even in myxoid regions of the spongiosa from early diseased valves, there is an overall decrease in cell number compared to the same regions in normal valves[44, 49]. However there is an increase in cell number in the sub-endothelial areas (atrialis and fibrosa)

so it may be the case that total cell number remains the same[48, 153]. Regardless of this potential difference, the concentration of as well as the quality of RNA extracted from dissected valves was adequate for further study, with all samples passing post-hybridisation quality control. This indicates that this is a feasible approach for future research.

An advantage that this study has over the whole valve analysis of disease is that by comparing samples from the same valve, paired analysis can be performed. This minimises the effect of confounding factors such as breed and age of dog as well as baseline differences in gene expression between individual dogs within groups, which was shown to have an effect in Chapters 3 and 4. This allowed for the more stringent FDR corrected Q-value to be used in this analysis, minimising the effect of false positives due to multiple-comparisons[296]. The FDR corrected gene list produced for the comparison between regions of diseased and normal tissue included some hallmarks of disease, also noted in Chapter 3 and 4, such as *ACTA2* and *HTR2B*, supporting the hypothesis that differentially expressed genes that are related to disease progression are detectable in the overtly diseased regions of valve[1, 2]. Furthermore, when comparing the normal regions of the diseased valves to whole normal valves, although differences did exist, these hallmark genes were not differentially expressed. In fact, only nineteen genes were differentially expressed in both datasets with only three sharing up-or down-regulation in expression (all up-regulated) (section 5.3.3). This supports the view that the majority of genes differentially expressed in the normal regions of valve compared to whole normal valve samples were not diseased related. These findings help to support the hypothesis of this study and show that this approach is of use in future studies.

Nonetheless, differential gene expression was detected between the normal regions of dissected valves and the normal whole valve samples. This may indicate that normal regions of valve from Whitney grade 2 valves are different from completely unaffected valves. However, it is important to consider other factors that may be responsible for the differences observed. For example, batch effects, such as analysis being performed at different times on different array plates with different batches of reagents could be have been shown to have an effect on microarray analysis[297, 298]. The normal regions of dissected valve and normal whole valve samples were run on the same Affymetrix Canine Gene 1.1ST array platform on two separate occasions so batch effects could be responsible for differential expression. Methods do exist to account for these batch effects but were beyond the scope of this study[299, 300]. Aside from batch effects, it is conceivable that the differentially expressed genes are due to regional differences in cell type and gene expression between normal regions from diseased valves and whole normal valves. For example, it is established that there is a greater number of adipose cells towards the proximal side of the valve[36]. The removal of the diseased region, which is typically located on the free edge of the valve, would allow for a stronger signal from these cells to be detected. In future studies, performing transcriptomic analysis comparing the normal regions from dissected diseased valves and the regions same valvular regions dissected from completely normal valves would help to clarify what genes are differentially expressed due to region and which are due to disease development. To investigate the gene changes detected in both datasets further and establish their potential role in disease gene enrichment analysis was performed.

DAVID GO term analysis of the up- and down-regulated genes in the diseased regions of valve compared to the normal regions of valve indicated a role for

up-regulation of immune-related pathways and down-regulation of lipid and metabolism-related pathways in the diseased regions. As mentioned in Chapter 3, the up-regulation of immune-related genes may be attributed to the immune-cell-like qualities of the activated VIC population[45, 117]. Additionally, the mast cells present in the valve migrate to the periphery of the diseased region of the valve, although it is not known how if they contribute to disease[30]. The down-regulation of lipid and metabolism-related genes could be, as discussed earlier, due to the regional differences in the valve with a reduced presence of adipocytes towards the free edge of the valve[36]. Genes related to the GO term proteinaceous extracellular matrix were down-regulated in this analysis similar to what was seen in the analysis of whole valves (Chapter 3). Comparing these GO terms to the GO terms associated with the genes differentially expressed between normal regions of diseased valves with normal whole valve samples showed there was no similarity. Interpreting what the GO terms associated with the normal sample comparison is problematic, as there does not appear to be a coherent set of similar GO terms suggested. This indicates that the gene differences detected in this comparison are not being caused by a specific stimulus but may, as suggested earlier, be a result of a technical effect such as batch effects.

The analysis in IPA of both datasets (section 5.3.5) likewise garnered interesting results. Canonical pathway analysis of the genes differentially expressed in diseased regions of valve showed that the top three pathways matched with the top three pathways identified for grade 4 valve samples in Chapter 3, with *hepatic fibrosis/hepatic stellate cell activation* being the most significant. As discussed in Chapter 3, the involvement of these pathways in disease is not immediately clear, however, it can be related to the top upstream regulators TGFβ1 and TNF[184, 279, 280]. These were also the top upstream

regulators suggested for this dataset and will be discussed further later. Comparing these results to those suggested for normal regions of valve compared to normal whole valves, as with DAVID analysis, there was a marked decrease in the association of pathways with the differentially expressed genes in this dataset, as well as the number of genes associated with each pathway. The top two pathways suggested for this analysis are associated with the up-regulation of genes in immune-related pathways. This may suggest that the normal regions of the diseased valves are undergoing some form of immune response, which was not highlighted in the GO term analysis. However, due to the relatively low number of genes (5 each) associated with these pathways it is difficult to infer biological significance. As mentioned, the top three upstream regulators associated with the genes differentially expressed in the diseased regions of valve included TNF and TGFβ1 as well as IFNG. This, like the canonical pathway analysis, showed a similarity with the grade 3 and 4 analysis presented in Chapter 3. As discussed, there is a relevance for both molecules in disease progression, in particular TGFβ signalling[45, 60, 78, 117, 124-126, 131, 176]. However, the top upstream regulator was TNF with TGFβ1 suggested as the second most likely candidate. TNF also has a potential role in disease development with some indications it could act on valvular endothelial cells to induce endothelial-to-mesenchymal transition and so could contribute to the VIC population of the valve[90, 91]. In this study, the microarray signal intensities (section 5.3.5) for each of the top three upstream regulators in disease indicates that only *TGFB1* is expressed at a biologically relevant level with signals for *IFNG* and *TNF* indistinguishable from background fluorescence. Likewise, this was also the case in the by grade analysis. Additionally, there has been no indication in the literature of increases in circulating TNF in dogs affected by MMVD[301, 302]. However, signal

intensity does not necessarily relate to the amount of active protein in the valve with this warranting further investigation (see Chapter 6). All of these observations support a more credible role for TGFβ1 in disease regulation.

Upstream analysis of the normal regions of dissected valves compared to normal whole valve samples again showed less association of suggested pathways to the differentially expressed genes in the dataset. This can be seen with the top upstream regulator, RHOX5, only having an effect on four differentially expressed genes in the dataset, three of which did not change in a way predicted by the literature. Similarly to the previous gene enrichment analyses, it is difficult to attribute any of the suggested molecules to a function in disease progression. In contrast, in network analysis the normal regions of dissected diseased valves compared to normal whole valve samples, pathways that could be related to disease development were associated. This includes functions such as *connective tissue disorder*. This could suggest that the transcriptomic differences between normal regions of the Whitney grade 2 valves and normal whole valves are diseased related implying that disease relevant changes are occurring in the grossly normal tissue. However, taking into account the previous gene enrichment analysis and the lack of shared differentially expressed genes between the two datasets this does not appear to be the case. It appears far more likely that, as previously asserted, the gene changes between the two normal tissue samples are caused by something other than disease progression, such as regional differences or batch effect. This analysis helps to address an aim of this study, showing support that normal regions of diseased valves do not appear to be undergoing transcriptomic changes reminiscent of disease progression.

Network analysis, as with the DAVID analysis, highlighted a role for the down-regulation of *lipid metabolism* as part of the first group of disease and

functions group. Alongside this, disease and functions such as *tissue morphology* and *connective tissue development* were also associated with the diseased regions of valve. Disease and functions such as these can be related with the extracellular matrix remodelling that occurs in disease. The majority of these functions seem to be controlled by TNF adding support to a role for this molecule in disease. However, these changes likewise could be being controlled by other factors and influences. For example, TGFβ1 as previously discussed (Chapter 1 section 1.5.1) is also heavily involved in tissue morphological changes and extracellular matrix development, specifically in valves[107, 179, 181]. Equally, down-regulation of *lipid metabolism* is likely being associated, as previously discussed, due to a reduced presence of adipocytes in the regions typically were disease develops rather than due to the influence of TNF[36]. Additionally, TGFβ signalling has been shown to induce a reduction in lipid metabolism as well as other metabolic processes in murine hepatocytes *in vitro* which may implicate it in the results established here[303].

Finally, RT-qPCR on genes of interest selected from the differentially expressed genes in diseased areas was performed to validate the microarray data. Included in these selected genes was *ADAMTS9* which, like its family member *ADAMTS5,* cleaves proteoglycans and has previously been implicated in the development of MMVD[17, 18]. Eight of the eleven genes analysed here were also used to validate the whole valve microarray analysis (Chapter 3). RT-qPCR confirmed the up- and down-regulation of the genes of interest in the RNA used for microarray analysis, validating the microarray analysis and gene enrichment discussed in this study.

The RT-qPCR analysis comparing dissected regions of normal valves indicated that there was no significantly differentially expressed genes of interest in the free edge regions of the normal valve. This indicates that gene

changes present in diseased regions of valve are disease-related and not due to regional differences that exist in the normal valve. This helps to support the contention that the differentially expressed genes detected in the ostensibly diseased regions of the valve are truly representative of early disease development. However, this analysis is only being performed on a small number of genes of interest, which are associated with the disease. Ideally, in future studies, these dissected normal valves would also be examined transcriptomically allowing for the elimination of genes that may be only differentially expressed due to regional differences.

To conclude, this study has met its aims by:

- Establishing transcriptomic differences that are relevant to disease progression in diseased regions of Whitney grade 2 valves compared to normal regions of the same valve
- Showing that the normal regions of the valve do not show transcriptomic changes that are disease relevant when compared to normal whole valves, indicating they are suitable for comparison with the diseased regions
- Validating that gene changes in the diseased regions are not caused by regional differences that would be observed in the context of a normal valve
- Showing that the dissection approach is feasible for more in-depth research of early disease development

This study has therefore been able to elucidate transcriptomic changes occurring in early disease development. Furthermore, these changes are broadly in agreement with changes in the late-grade diseased valves established in Chapter 3. Of particular interest is the role of TGFβ1, which is

implicated as the leading candidate as a potential upstream regulator of disease in the studies presented in this thesis. As such, this factor warrants further investigation to establish its role in disease development.

(This page has been left intentionally blank)

Chapter 6 Transcriptomic profiling of VICs and the effect of TGFβ1 signalling

6.1 Introduction

Mitral valves comprise of layers of multiple cell types and cell composition can change drastically in MMVD due to events like EndoMT and the activation of valvular interstitial cells (VICs). As discussed in Chapter 1 section 1.3.2, VICs are the predominant cell type in mitral valves and VICs are proposed to play a pivotal role in the development of MMVD[45, 117, 304, 305]. Studying cells in 2D culture is an inexpensive, easy to use and reproducible method that allows for interrogation of the molecular and signalling aspects identified in tissue study[186]. In this study, *in vitro* analyses were conducted using VICs isolated from both normal and diseased mitral valves.

It has been shown that in MMVD the normally quiescent VICs (qVICs) are activated into a myofibrotic-like phenotype (aVICs) which are responsible for perpetrating many of the pathological signs of disease, including the deposition of extracellular matrix components such as proteoglycans[2, 43-45, 60, 61]. When activated aVICs begin to express markers including *ACTA2*/αSMA, *MYH10*/SMemb and *TAGLN*/SM22 (*gene*/protein) [43, 45, 60, 114-116]. Additionally, morphological differences are apparent between the two cell types *in vitro* with qVICs organised in an orthogonal, honeycomb-like pattern with an elongated spindle morphology and aVICs adopting a far more disorganised structure with varying morphologies including a large rhomboid and a hyper-elongated morphology [45, 113]. Using proteoglycan deposition, activation markers and morphological characteristics to define the qVIC and aVIC populations allow for comparison studies to be performed in culture on qVICs isolated from normal valves and aVICs isolated from diseased valves.

However, previous *in vitro* VIC studies have been hampered by the spontaneous activation of qVICs into aVICs under standard culture conditions in 10% FBS[45, 121, 306]. Recently, an optimised protocol for human aortic VICs using a low serum (2%) and FGF2 supplemented medium was shown to be able to maintain qVIC phenotype in 2D culture[138]. If this protocol is also successful for canine VICs, a better fundamental understanding of the differences between these two phenotypes could be achieved and the effect of molecules hypothesised to be involved in disease can be assessed.

From the work so far presented in this thesis, roles for TGFβ signalling, TNF and IFNγ in the upstream regulation of early disease have been proposed (Chapters 3-5). In particular, TGFβ1 signalling has been consistently implicated in disease progression. TGFβ signalling, notably via TGFβ1, has been identified as an activator of qVICs into an aVIC phenotype, not only in culture but also potentially in MMVD[43, 122, 125, 126, 131, 133, 174, 177]. Serotonin (5HT), as discussed in Chapter 1 section 1.5.2, has been associated with MMVD, both through the induction of disease in the presence of hyper-physiological levels of 5HT and the consistent up-regulation of aspects of the 5HT signalling mechanism such as 5HTR2B (consistently up-regulated in the canine disease)[33, 71, 133, 150, 170-173]. However, the exact mechanism through which these signalling pathways may be induced in MMVD and the downstream signalling consequences are not fully understood. Therefore, these are prime targets to be investigated further *in vitro*.

This study aimed to investigate VICs from normal (qVICs) and diseased (aVICs) valves, which are cultured according to the optimised human cell culture protocol[138]. VIC phenotype and activation status would be determined by the expression of activation hallmark genes/proteins, deposition of proteoglycans and morphology. The secretion of TGFβ, TNF and

IFNγ molecules from VICs would be examined by ELISA, to determine the functional protein expression of these potential upstream regulators of MMVD. Furthermore, this study aimed to assess the effect of TGFβ1 and 5HT signalling in VICs by treating qVICs with each of these factors and treating aVICs with inhibitors of these pathways and observing the effect on phenotype. If these factors contribute to the development of MMVD, it was expected that treated qVICs would acquire the aVIC phenotype, while inhibitor-treated aVICs would revert to the qVIC phenotype. Finally, as the previous tissue microarray analysis indicated that TGFβ1 is the most important signalling molecule in the development of MMVD, transcriptomic profile analysis of four groups, qVICs, aVICs, qVICs +TGFβ1 and aVICs + TGFβRI kinase inhibitor (SB431542) (which inhibits canonical SMAD2/3 signalling) would be performed[307, 308].

6.2 Materials and Methods

6.2.1 Tissue collection and cell extraction

Tissue collection and VIC extraction were performed as described in Chapter 2 section 2.2.1, 2.2.2 and 2.4. The animals used in this study are shown in **Table 6-1**. The majority (4/6) of samples were collected and cells extracted by Dr. Mengmeng Liu before this study began[121].

Sample ID	Date sampled	Dog Breed	Gender	Age	Whitney grade	Sampler
B09	09/04/2015	BEAGLE	FEMALE	2y7m	0	Dr. M. Liu
B10	09/04/2015	BEAGLE	MALE	2y	0	Dr. M. Liu
B12	09/11/2015	BEAGLE	MALE	2y9m	0	Dr. M. Liu
D1	-	LABRADOR	MALE	6y	2	Dr. M. Liu
D2	03/12/2017	COLLIE	MALE	10y	3	G. Markby
D3	07/12/2016	CAVALIER KING CHARLES SPANIEL	MALE	15y	4	G. Markby

Table 6-1. Description of VICs used in this study.

6.2.2 Cell culture conditions and treatments

Cells were maintained in DLF media, following the protocol of Latif *et al*, as described in Chapter 2 section 2.4[138]. The treatment of cells for the assessment of TGFβ1 and 5HT signalling was performed as described in Chapter 2 sections 2.11.1 and 2.11.2 respectively. VICs used for microarray analysis were all passage 3, for other experiments VICs were between passage 2 and 6.

6.2.3 RNA extraction and quantification and quality control

RNA extraction from cells was performed following the protocol detailed in Chapter 2 section 2.3.2. RNA quantification and quality assessment were performed on all samples as described in Chapter 2 section 2.3.3, quality control for microarray by assessment of 28S and 18S rRNA and calculation of RIN was reserved for the samples used in the transcriptomic analysis.

6.2.4 Affymetrix Canine Gene 1.1ST microarray analysis

This study was performed on the remaining 12 wells of the 24 well Affymetrix Canine Gene 1.1ST chip also used in Chapter 5 section 5.2.3. RNA processing, hybridisation, post-hybridisation quality control, summarisation file creation and differential gene expression was performed as described in Chapter 2 section 2.5. Statistical analysis was performed using unpaired (between qVIC and aVIC phenotype) and paired (within phenotype with or without treatment) ANOVA with differential gene expression determined as having $\geq \pm 1.5$ fold change in expression and P-value <0.05. No FDR adjustment was applied to the transcriptomic data in this chapter.

6.2.5 Gene Enrichment analysis

The network analysis tool Miru (version 1.4) was utilised as described in Chapter 2 section 2.6.1. A sample-to-sample comparison was performed with

a Pearson correlation of r=0.97, this maximised the number of samples included whilst minimising the connection between samples. The tools Database for Annotation, Visualisation and Integrated Discovery (DAVID) version 6.8 and Ingenuity Pathway Analysis (IPA) were used as stated in Chapter 2 sections 2.6.2 and 2.6.3, default settings were used throughout. Gene list comparison was performed as described in Chapter 2 section 2.6.4.

6.2.6 cDNA synthesis and RT-qPCR

cDNA synthesis and RT-qPCR was performed as described in Chapter 2 section 2.7.2-2.7.6. The primers used to investigate genes of interest in this study are summarised in **Table 6-2**. *ACTA2*, *HTR2B*, *TAGLN* and *MYH10* were used for VIC characterisation and assessment of 5HT signalling. For microarray validation, all genes of interest were investigated. All gene quantification was normalised to *MRPS25*, *RPL32* and *GAPDH*.

Gene Symbol	Forward Primer Sequence	Reverse Primer Sequence	Product Length	Optimum TM ºC	Primer Efficiency %
ACTA2	5'CGGCTACTCCTTTGTGACG3'	5'CGTGGCCATCTCGTTCTC3'	100	58	102.2
HTR2B	5'CCAATCCAGGCCAATCAAAG3'	5'CAGGTGATGTTGCTTGGGTT3'	143	59	104.8
TAGLN	5'GACATGTTCCAGACCGTCGA3'	5'CAATGACGTGCTTTCCCTCC3'	199	59	106.7
MYH10	5'TGCCAACAATGTCCTTTCCG3'	5'GCCTCCAATCCAGACTGAGT3'	148	59	93
HBEGF	5'CTGTGGTGCTGTCATCTGTC3'	5'TGGGAAGTAGTCATGCCTAACT3'	124	61	103.8
MAL	5'CTGCCCTGTTTTACCTCAGC3'	5'GGACCACGTACAGCAGAGT3'	141	61	99.1
BMPER	5'TTTCTGGCATATACTCGGGC3'	5'CAGTTGTCACAGGTCTTGGC3'	143	60	105.2
VCAM	5'GATGCGGGAGTGTACGAATG3'	5'GCACAATAAAGCACGAGTAGTTC3'	131	60	97.1
PDK4	5'CCAATTTCTCGTCTCTATGCCA3'	5'GGCTGATTTGTTAAAGACTGGGA3'	144	60	95.6
FAP	5'TCAAATGTGGGATAGCAGTGG3'	5'GGAGGCCCATGAATCGTTCT3'	81	60	106.3
SLC10A6	5'GCTGTTGGATGGGTTTCTCA3'	5'TCCAAGAAAGCACCAGTCTCT3'	147	58	101.7

Table 6-2. Primers designed and optimised for use in this study.

6.2.7 Protein extraction and quantification and western blotting

Protein extraction from cells, protein quantification and western blot assessment of αSMA, SM22 and β-actin expression were performed as described in Chapter 2 section 1.8.

6.2.8 ELISAs

Enzyme-linked immunosorbent assays (ELISAs) were performed on the media supernatants from cells cultured for 72 hours prior to collection. qVICs and aVICs were approximately 60-70% confluent when first plated and 80-90% confluent when supernatants were collected for assessment. The ELISA protocols for TNF, IFNγ, TGFβ1, 2 and 3 are described in Chapter 2 section 2.9 (sub-sections 2.9.1-5 respectively) with values normalised to total cellular protein (per μg), measured by the Quick Start Bradford protein assay (Bio-Rad, Cat. No. 5000201) of the cell sample, from which the supernatant was obtained. A TGFβ1 assay was performed by Dr. Karen Tan, using the same method, except that the cells had been in culture for 120 hours.

6.2.9 Proteoglycan assay

Quantification of proteoglycan deposition in supernatants from cells in this study was performed as described in Chapter 2 section 2.10. Supernatants were collected from cells cultured for 72 hours. Where possible, values were normalised to the total cellular protein (μg) of the cell sample from which the supernatant was collected (sections 6.3.1 and 6.3.10). When samples were used for downstream microarray analysis, values were normalised to cell numbers (cellx10^5) of the sample from which the supernatant was collected (section 6.3.9).

6.2.10 Microscopy and image capture

Microscopy and cell imaging were performed as described in Chapter 2 section 2.12.

6.3 Results

6.3.1 qVIC and aVIC characterisation

VICs isolated from normal valves (expected to be primarily composed of qVICs) and from diseased valves (expected to be mostly aVICs), were assessed for gene and protein level expression of activation markers (hallmarks of disease) as well as for the deposition of proteoglycans and cell morphology. Expression of *ACTA2*, *TAGLN* and *MYH10* genes was assessed by RT-qPCR for the presumed qVICs and aVICs. All genes were found to be significantly up-regulated in the presumed aVICs in comparison to the presumed qVICs with a 40.7 fold increase in expression for *ACTA2* (P-value 0.006) (**Figure 6-1A**), 4.3 fold increase for *TAGLN* (P-value 0.006) (**Figure 6-1B**) and 4 fold increase for *MYH10* (P-value 0.047) (**Figure 6-1C**). Protein expression of αSMA (*ACTA2*), SM22 (*TAGLN*) and β-actin were assessed by western blot (**Figure 6-1D**). Bands were detectable for αSMA in the three presumed aVIC samples (particularly D3); likewise, bands were detectable for SM22 in all samples, strongly in D2 and D3, but also in B09. β-Actin expression indicated equal loading between samples. Proteoglycan (PG) deposition was significantly greater in the media of presumed aVICs compared to qVICS (P-value 0.002) (**Figure 6-1E**). Morphological assessment of the presumed qVICs (**Figure 6-1F**) and aVICs (**Figure 6-1G**) identified differences in morphology consistent with the phenotypes previously reported[45, 113], with the presumed qVICs being more spindle-like and having a more uniform honeycomb-like distribution, and the presumed aVICs having a disorganised structure with larger rhomboid and hyper-elongated cells present. Collectively, these differences were consistent with the literature and indicate that the cells in culture recapitulate the cells *in vivo*[2, 45, 113, 121]. Henceforth these cultured cells will be referred to as qVICs and aVICs respectively.

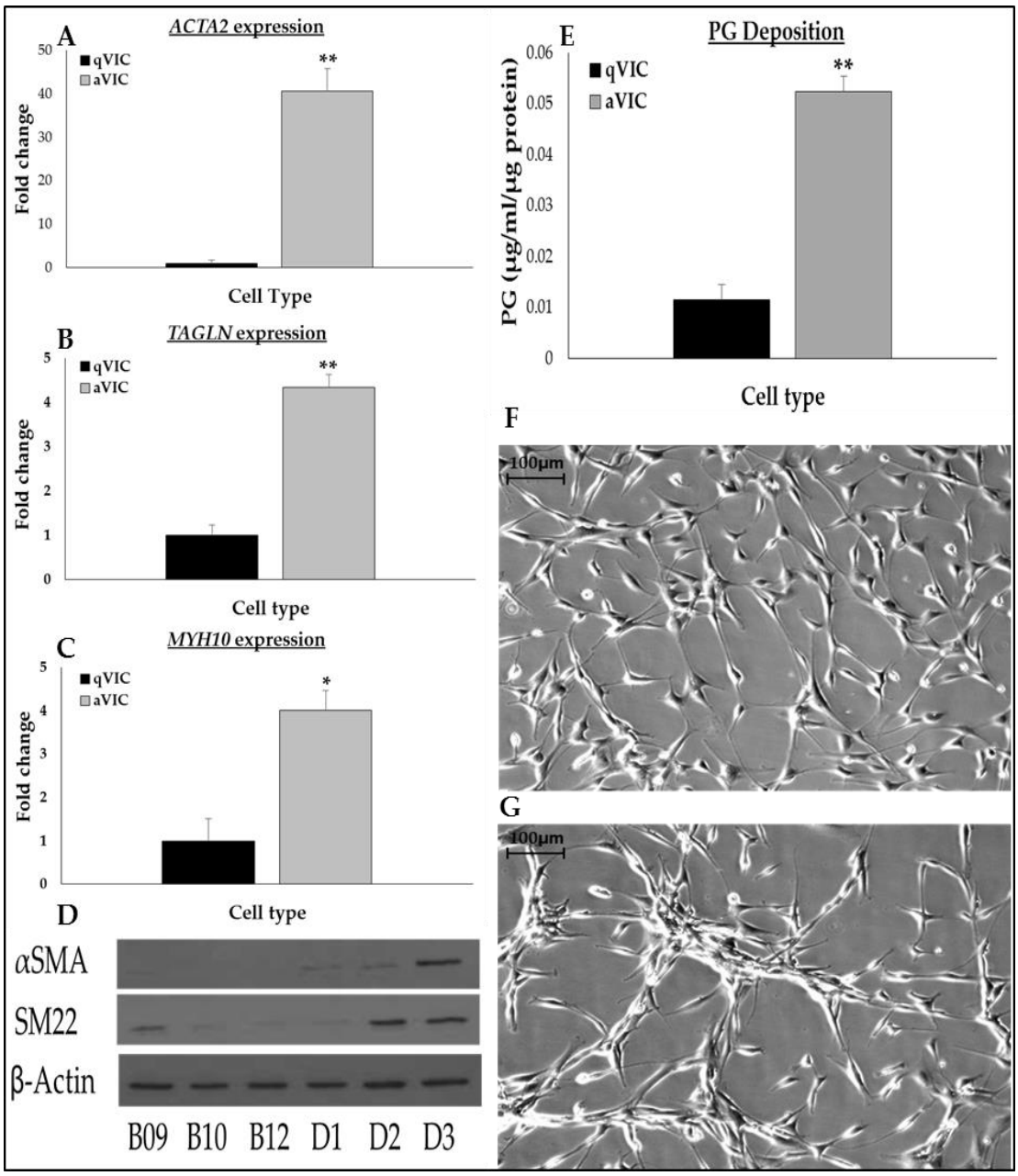

Figure 6-1. qVIC and aVIC characterisation. (A) Relative fold change expression in *ACTA2*. (B) Relative fold change expression in *TAGLN*. (C) Relative fold change expression in *MYH10*. (D) Western blot images for αSMA, SM22 and β-Actin in the qVICs (B09, B10 and B12) and aVICs (D1-3). (E) Comparison of proteoglycan (PG) deposition between qVICs and aVICs. (F) Representative morphology image of qVICs. (G) Representative morphology image of aVICs. * = P-value <0.05, ** = P-Value <0.01, scale bar = 100µm. n=3 per group.

6.3.2 qVIC and aVIC secretion of TGFβ1-3, TNF and IFNγ

ELISAs were performed on the supernatants from qVICs and aVICs, after 72 hours in culture, to detect IFNγ, TNF, TGFβ1, TGFβ2 and TGFβ3. IFNγ was at an undetectable level, below the sensitivity of the assay, in both qVIC and aVIC supernatants suggesting little to no secretion of this factor from VICs. There was no significant difference in TNF, TGFβ1, TGFβ2 and TGFβ3 expression comparing qVICs and aVICs (**Table 6-3**). However, the TGFβ1 level exceeded any of the other molecules assessed. A TGFβ1 ELISA performed on the same primary lines of VICs after 120 hours by Dr Karen Tan showed a significant increase (P-value 0.024) of TGFβ1 deposited by aVICs (9.78 pg/mL/μg protein ±0.43 S.E.) in the supernatant compared to qVICs (3.19 pg/mL/μg protein ±0.26 S.E.) (**Figure 6-2**).

Molecule	qVICs [pg/ml/μg protein]	aVICs [pg/ml/μg protein]	P-value
TNF	0.14 ±0.0084 S.E.	0.11±0.029 S.E.	0.43
TGFβ1	1.12 ±0.14 S.E	1.8 ±0.51 S.E.	0.331
TGFβ2	0.31 ±0.0084 S.E.	0.4 ±0.12 S.E.	0.526
TGFβ3	0.05 ±0.0064 S.E.	0.04 ±0.0095 S.E.	0.372

Table 6-3. Summary of ELISA data. Quantification of the concentration of TNF and TGFβ1-3 in the supernatants of qVICs and aVICs. n=3 per group.

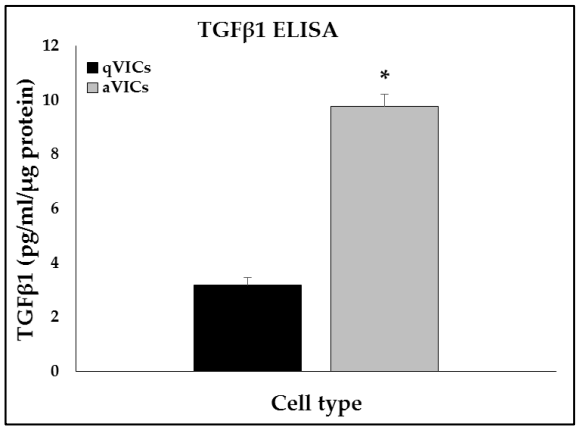

Figure 6-2. Bar chart of TGFβ1 ELISA performed after 120 hours in culture. n=3 per group. * = P-value <0.05

6.3.3 RNA quantification and quality assessment for microarray

RNA to be used for microarray analysis of VICs was extracted from cells and quantified. The concentrations along with 260/280 and 260/230 absorbance ratios and RNA integrity number (RIN), were recorded in **Table 6-4**. RNA concentration ranged from 369.5 to 1358.5 ng/μL. A statistical difference was found when comparing average RNA concentrations of qVICs + vehicle (434.6 ±76 ng/μL) with qVICs + TGFβ1 (638.7 ±75.6 ng/μL) using a paired t-test (P-value 0.015). However, no significant difference was observed when performing a t-test comparing qVICs + vehicle with aVICs + vehicle (993 ±187 ng/μL) (P-value 0.109) or comparing aVICs + vehicle with aVICS + SB431542 (1081 ±145 ng/μL) (P-value 0.481). Absorbance ratios were all within the acceptable reference range (>1.8) for both 260/280 and 260/230, indicating that the extractions did not contain contaminants. Gel electrophoresis images (**Figure 6-3**) displayed the 28S and 16S rRNA in each sample with RIN calculated and shown. All samples passed >7 cut-off for microarray analysis.

Sample ID	RNA [ng/μl]	260/280	260/230	RIN
B09 + Vehicle	586.1	2.1	2.06	10
B10 + Vehicle	369.5	2.04	1.96	10
B12 + Vehicle	348.1	2.06	1.96	10
B09 + TGFβ1	777.2	2.09	2.2	9.8
B10 + TGFβ1	621.7	2.1	2.08	10
B12 + TGFβ1	517.1	2.12	2.07	10
D1 + Vehicle	878.2	2.08	2.02	9.6
D2 + Vehicle	1358.5	2.08	2.1	9.3
D3 + Vehicle	742.6	2.1	1.93	10
D1 + SB431542	1157.9	2.09	2.19	10
D2 + SB431542	1285.2	2.08	1.96	10
D3 + SB431542	801.2	2.1	2.14	10

Table 6-4. Concentration, 260/280 and 260/230 absorbance reading and RIN for each VIC sample.

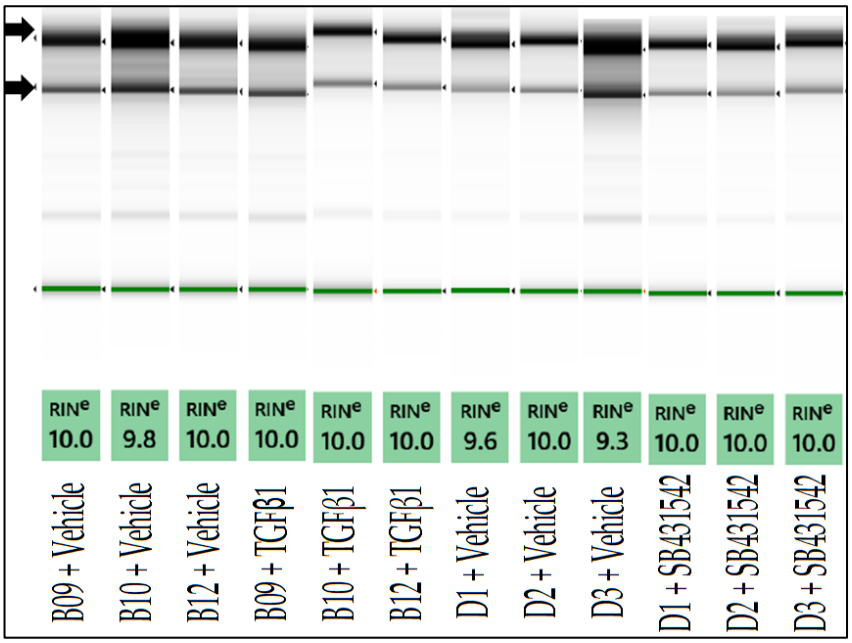

Figure 6-3. Gel electrophoresis images visualising the 28S (indicated by the top arrow) and 16S (indicated by the bottom) rRNA intensity in each sample.

6.3.4 Microarray post-hybridisation quality control

Post-hybridisation analysis was performed to assess the quality of gene expression data generated from microarray analysis of the submitted samples. All wells on the array showed the correct concentration of spike in and labelling controls indicated that the arrays had been performed correctly. After Robust MultiArray Average (RMA) and gene-level normalisation, log expression signal was plotted (**Figure 6-4**). All samples showed a similar log expression signal. Signal intensity distribution for each of the samples was analysed and presented as a log2 signal line graph (**Figure 6-5**). This shows log signal intensity from 0-13.62 with a similar distribution pattern exhibited for all samples. There was a peak between 2-3.5 log signal intensity before a decline in genes expressing above this signal intensity until no genes were being expressed at a greater intensity than 13.62. This figure shows that to remove the effect of background on this dataset, genes expressed below 3.5 log signal intensity should be removed.

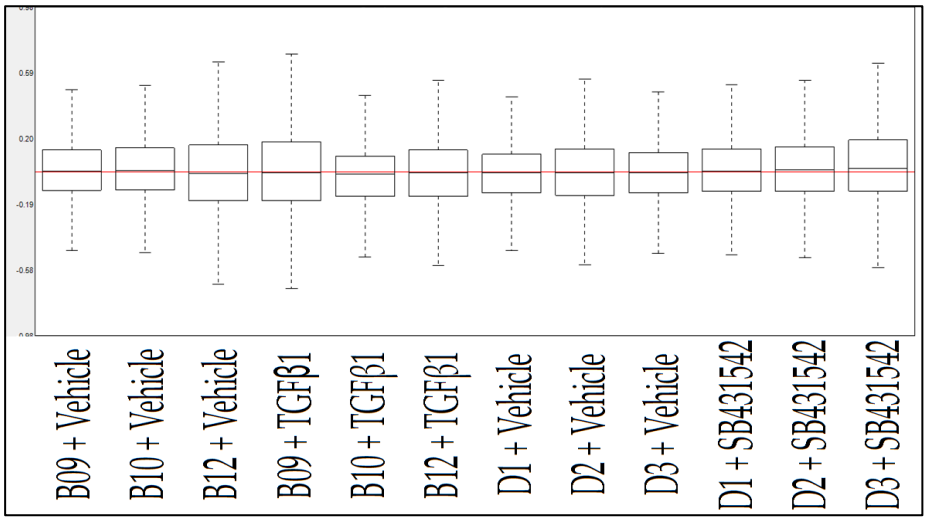

Figure 6-4. Post-RMA signal intensity boxplots for each sample.

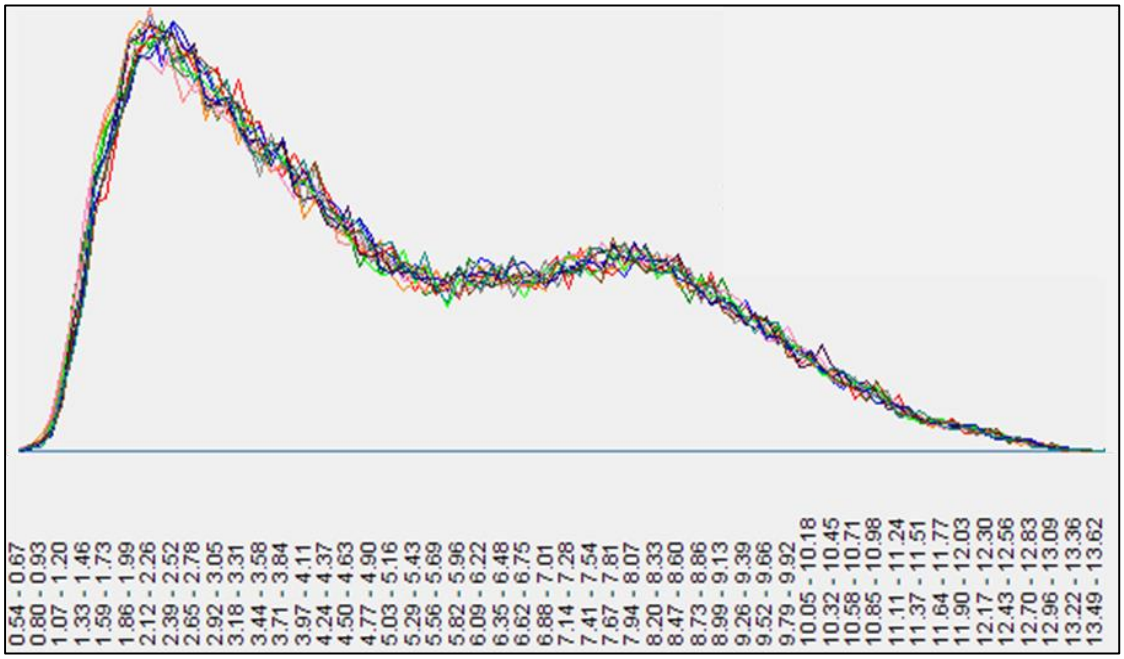

Figure 6-5. Log2 signal line graph for samples. Each line represents an RNA sample with the X-axis plotting signal intensity and Y-axis plotting the number of probes on the array with that signal intensity. The higher the line is on the Y-axis, the greater the number of probes showing that signal intensity. A uniform pattern of expression can be seen here.

Principal component analysis (PCA) and sample-to-sample analysis in Miru (r=0.97) were performed. In PCA analysis (**Figure 6-6**), qVICS + vehicle (red squares) and aVICs + vehicle (yellow squares) clustered the furthest apart for all samples. Treatment with TGFβ1 or SB431542 (TGFβRI kinase inhibitor) caused a change in the transcriptomic profile in the VICs with qVICs treated with TGFβ1 (blue squares) shifting towards aVIC + vehicle side of the plot and aVICs treated with SB431542 (green squares) shifting towards the qVIC + vehicle side of the plot. Likewise, in the sample-to-sample analysis (**Figure 6-7**), a similar distribution of the samples can be seen with samples within treatment and cell phenotype groups clustering together. Collectively these results indicate that all samples are suitable for downstream analysis.

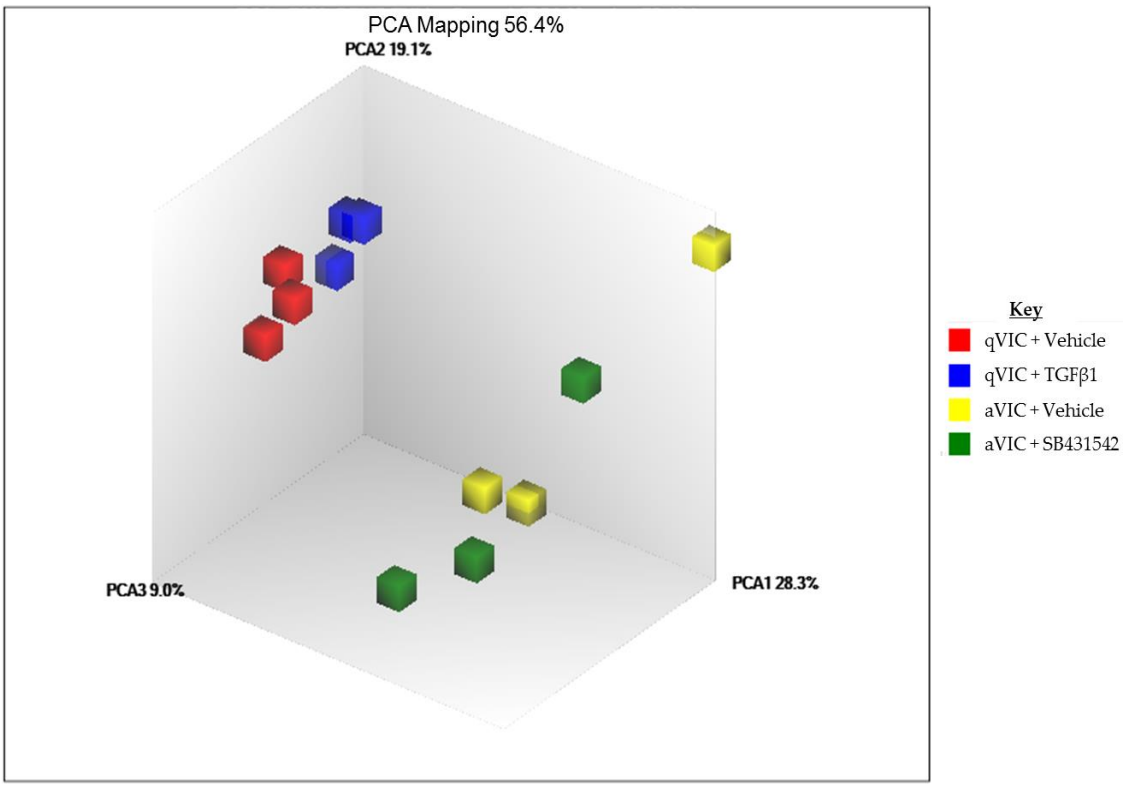

Figure 6-6. PCA plot comparing qVIC and aVIC samples with and without treatment. Red squares represent qVICs + vehicle, yellow squares represent aVICs + vehicle, blue squares represent qVICs + TGFβ1 and green squares represent aVICs + SB431542.

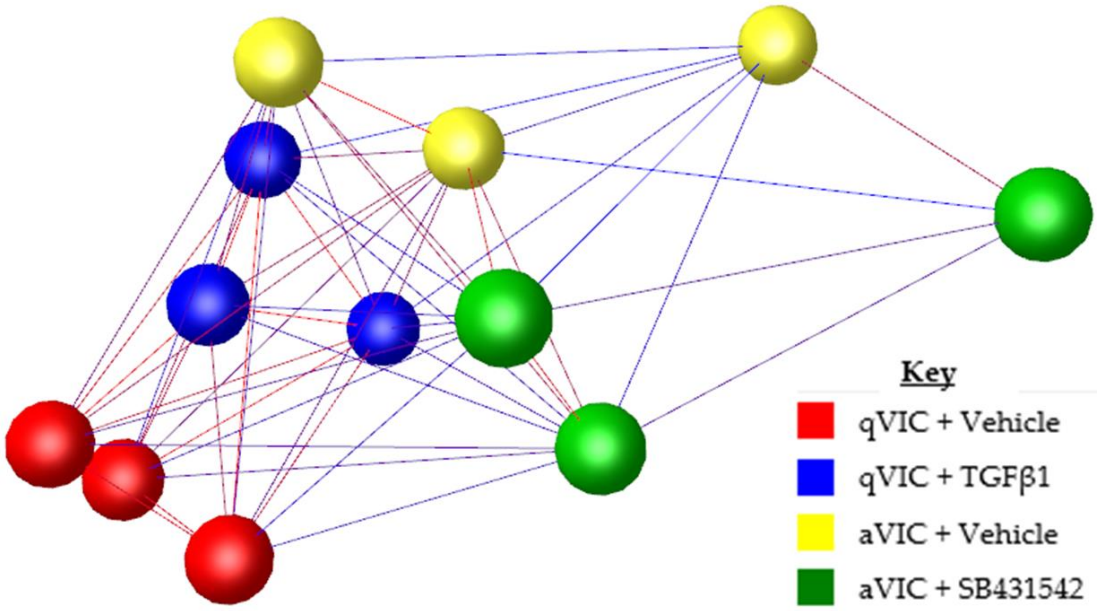

Figure 6-7. Sample-to-sample correlation (r=0.97) of qVICs and aVICs with and without treatment. Red nodes represent qVICs + vehicle, yellow nodes represent aVICs + vehicle, blue nodes represent qVICs + TGFβ1 and green nodes represent aVICs + SB431542.

6.3.5 Differential expression of genes

Although various comparisons could be made between groups, the most pertinent for this study were between qVICs and aVICs and on the effect of TGFβ1 treatment or SB431542 treatment on qVICs and aVICs respectively. Differential gene expression for these groups is illustrated in **Figure 6-8**. There were 275 genes differentially expressed between qVICs treated with TGFβ1 and qVICs with vehicle (144 down-regulated with TGFβ1 treatment and 131 up-regulated) (**Figure 6-8A**). a total of 236 genes showed altered expression in aVICs treated with SB431542 compared to aVICs with vehicle (115 down-regulated with SB431542 treatment and 121 up-regulated) (**Figure 6-8B**). there were 902 genes differentially expressed in aVICs compared to qVICs (406

down-regulated in aVICs and 496 up-regulated) (**Figure 6-8C**). The full gene lists for these analyses can be found in **Appendix IV: Chapter 6 Tables S1-3**.

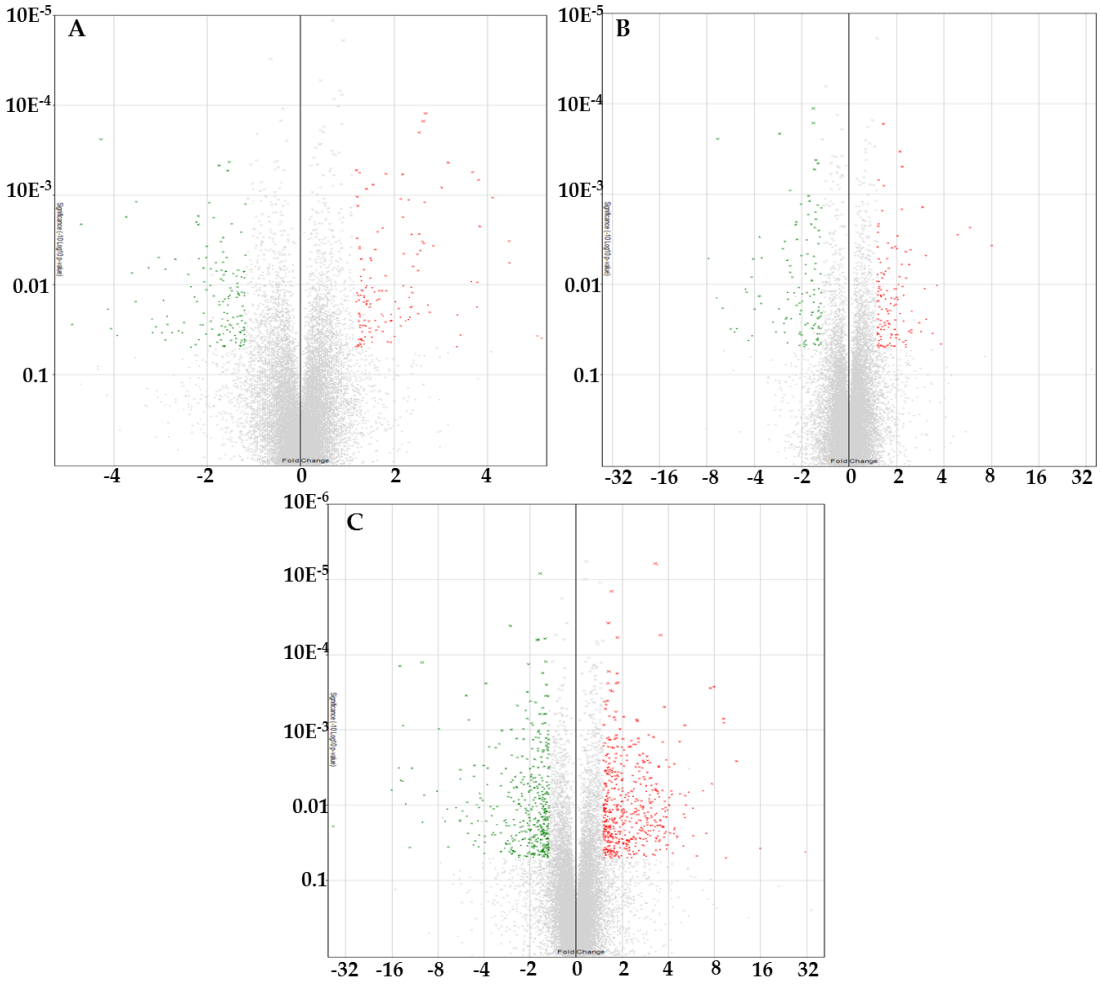

Figure 6-8. Volcano plots comparing qVICs to aVICs and the effect of treatments on VICs. Red dots represent up-regulated genes, green represent genes that were down-regulated and uncoloured are genes which do not pass the differential expression criteria. The X-axis shows fold change value and the Y-axis shows the P-value. (A) Genes differentially expressed between qVICs + vehicle and qVICs treated with TGFβ1. (B) Genes differentially expressed between aVICs + vehicle and aVICs treated with SB431542. C, Differentially expressed genes between qVICs and aVICs.

To investigate the similarity between genes differentially expressed in qVICs treated with TGFβ1 and aVICs with vehicle (both compared to qVICs with vehicle) gene lists were compared to one another. There were 102 genes found to be shared between the two datasets (**Figure 6-9**) with only one of these not showing the same direction of fold change (mastermind-like domain-containing protein 1 (*MAMLD1*), down-regulated -1.52 fold in qVICs treated with TGFβ1 and up-regulated 1.56 fold in aVICs).

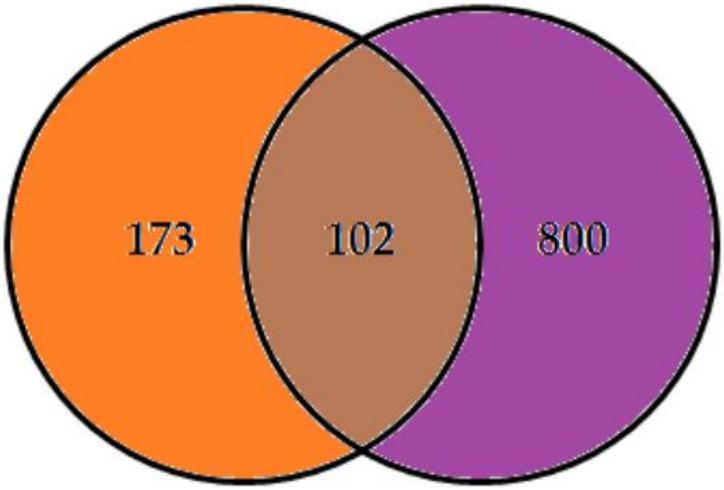

Figure 6-9. Venn diagram illustrating the number of shared differentially expressed genes in qVICs treated with TGFβ1 and aVICs with vehicle. In the left orange circle, the number of differentially expressed genes for qVICs treated with TGFβ1 and not shared with aVICs is shown. In the right purple circle, the number of differentially expressed for aVICs samples and not shared with qVICs treated with TGFβ1 is shown. In the centre, the number of shared genes between the two datasets is shown.

To complement the ELISA data presented earlier (section 6.3.2) further, the gene signal intensities of TNF, IFNγ and TGFβ1-3 were examined for each cell type and treatment and the raw signal intensity are presented in **Table 6-5**.

Molecule	Microarray signal intensity			
	qVIC + vehicle	qVIC + TGFβ1	aVIC + vehicle	aVIC + SB431542
TNF	4.89	4.72	4.5	4.78
IFNG	5.16	7.26	4.85	5.13
TGFβ1	296.11	385.34	359.53	344.89
TGFβ2	537.45	442.64	359.53	250.73
TGFβ3	744.43	776.04	809	326.28

Table 6-5. Signal intensity values for each molecule examined by ELISA.

6.3.6 DAVID GO term analysis

DAVID GO term enrichment analysis of the gene lists derived was performed. The top ten GO terms for up- and down-regulated genes for qVICs treated with TGFβ1 compared to qVICs and vehicle are summarised in **Table 6-6**, highlighting a role for extracellular matrix regulation by these genes. The top ten GO terms for up- and down-regulated genes for aVICs treated with SB431542 compared to aVICs and vehicle is summarised in **Table 6-7**, highlighting a downregulation of mesenchymal related GO-terms. The top ten GO terms for up- and down-regulated genes for aVICs and vehicle compared to qVICs and vehicle are summarised in **Table 6-8** highlighting an up-regulation in DNA replication. Finally, the top ten GO terms for up-regulated genes and the one GO term associated with down-regulated genes for the shared genes in aVICs and TGFβ1 treated qVICs is summarised in **Table 6-9**, highlighting that the shared genes are associated with extracellular space and smooth muscle cell proliferation amongst other GO terms.

	Category	Term	Gene count	P-value	FDR
Up-regulated	GOTERM_BP_DIRECT	Positive regulation of release of cytochrome c from mitochondria	4	2.64E-04	0.38132
	GOTERM_CC_DIRECT	Extracellular matrix	5	0.00387	4.2409
	GOTERM_CC_DIRECT	Extracellular space	12	0.01687	17.3279
	GOTERM_BP_DIRECT	Cholesterol metabolic process	3	0.01837	23.5133
	GOTERM_BP_DIRECT	Osteoblast differentiation	4	0.01841	23.5522
	GOTERM_MF_DIRECT	Acylglycerophosphocholine O-acyltransferase activity	2	0.02591	26.6683
	GOTERM_MF_DIRECT	GTPase activator activity	5	0.02659	27.2671
	GOTERM_CC_DIRECT	Extracellular exosome	22	0.02729	26.6109
	GOTERM_CC_DIRECT	Collagen trimer	3	0.03073	29.4616
	GOTERM_CC_DIRECT	Cytoplasm	25	0.03698	34.3791
Down-regulated	GOTERM_BP_DIRECT	Actomyosin structure organization	4	7.14E-04	1.05707
	GOTERM_CC_DIRECT	Cell surface	10	8.44E-04	0.96142
	GOTERM_CC_DIRECT	Integral component of plasma membrane	15	0.00108	1.23267
	GOTERM_BP_DIRECT	Positive regulation of Ras protein signal transduction	3	0.0048	6.90528
	GOTERM_BP_DIRECT	Cardiac conduction system development	2	0.01617	21.529
	GOTERM_MF_DIRECT	E-box binding	3	0.01709	18.5306
	GOTERM_CC_DIRECT	Extracellular space	13	0.01817	18.9324
	GOTERM_BP_DIRECT	Positive regulation of ERK1 and ERK2 cascade	5	0.01976	25.684
	GOTERM_CC_DIRECT	Cell body	3	0.02099	21.5577
	GOTERM_BP_DIRECT	Outflow tract morphogenesis	3	0.02296	29.2174

Table 6-6. Functional analysis chart summary of the top ten GO terms associated with up- or down-regulated genes in qVICs treated with TGFβ1 compared to qVICs and vehicle.

	Category	Term	Gene count	P-value	FDR
Up-regulated	GOTERM_CC_DIRECT	Lysosome	6	0.001142	1.24282
	GOTERM_BP_DIRECT	Angiogenesis	5	0.00706	9.51341
	GOTERM_BP_DIRECT	Positive regulation of TOR signaling	3	0.01016	13.4181
	GOTERM_BP_DIRECT	Nephron tubule epithelial cell differentiation	2	0.013912	17.9349
	GOTERM_CC_DIRECT	Mitochondrial membrane	3	0.01667	16.8095
	GOTERM_MF_DIRECT	Creatine kinase activity	2	0.019243	20.4883
	GOTERM_CC_DIRECT	Gtr1-Gtr2 GTPase complex	2	0.0197	19.5725
	GOTERM_BP_DIRECT	Renal tubule morphogenesis	2	0.020796	25.6583
	GOTERM_BP_DIRECT	Epithelial cell proliferation involved in renal tubule morphogenesis	2	0.020796	25.6583
	GOTERM_BP_DIRECT	Glomerulus morphogenesis	2	0.020796	25.6583
Down-regulated	GOTERM_BP_DIRECT	Collagen fibril organization	6	1.28E-06	0.00187
	GOTERM_MF_DIRECT	Extracellular matrix structural constituent	5	6.49E-05	0.07331
	GOTERM_BP_DIRECT	Positive regulation of epithelial to mesenchymal transition	4	6.09E-04	0.88332
	GOTERM_CC_DIRECT	Extracellular space	14	0.001122	1.25424
	GOTERM_CC_DIRECT	Stress fiber	4	0.001916	2.13231
	GOTERM_CC_DIRECT	Extracellular matrix	5	0.002899	3.21056
	GOTERM_BP_DIRECT	Transforming growth factor beta receptor signaling pathway	4	0.004864	6.85297
	GOTERM_BP_DIRECT	Positive regulation of release of cytochrome c from mitochondria	3	0.007117	9.87749
	GOTERM_CC_DIRECT	Focal adhesion	7	0.008523	9.17272
	GOTERM_BP_DIRECT	Positive regulation of cell migration	5	0.009217	12.6128

Table 6-7. Functional analysis chart summary of the top ten GO terms associated with up- or down-regulated genes in aVICs treated with SB431542 compared to aVICs and vehicle.

	Category	Term	Gene count	P-value	FDR
Up-regulated	GOTERM_MF_DIRECT	ATP binding	73	8.12E-13	1.13E-09
	GOTERM_BP_DIRECT	DNA replication initiation	11	8.27E-11	1.33E-07
	GOTERM_BP_DIRECT	Chromosome segregation	14	1.53E-10	2.45E-07
	GOTERM_CC_DIRECT	Kinesin complex	13	3.38E-09	4.46E-06
	GOTERM_BP_DIRECT	Mitotic sister chromatid segregation	9	1.37E-08	2.20E-05
	GOTERM_BP_DIRECT	Microtubule-based movement	14	1.54E-08	2.47E-05
	GOTERM_CC_DIRECT	Midbody	15	3.16E-08	4.17E-05
	GOTERM_CC_DIRECT	Nuclear chromosome, telomeric region	15	9.51E-08	1.26E-04
	GOTERM_CC_DIRECT	Nucleoplasm	67	2.13E-07	2.82E-04
	GOTERM_BP_DIRECT	Cell division	11	5.07E-07	8.14E-04
Down-regulated	GOTERM_CC_DIRECT	Intracellular	36	3.71E-06	0.00466
	GOTERM_CC_DIRECT	Lysosome	12	6.38E-05	0.08019
	GOTERM_BP_DIRECT	Small GTPase mediated signal transduction	15	7.56E-05	0.12256
	GOTERM_BP_DIRECT	PDGF receptor signaling pathway	6	9.44E-05	0.15311
	GOTERM_BP_DIRECT	intracellular signal transduction	18	1.61E-04	0.26021
	GOTERM_MF_DIRECT	Guanyl-nucleotide exchange factor activity	7	9.98E-04	1.33324
	GOTERM_MF_DIRECT	Semaphorin receptor activity	4	0.00208	2.753
	GOTERM_BP_DIRECT	Vasculogenesis	6	0.00263	4.18228
	GOTERM_MF_DIRECT	Rho guanyl-nucleotide exchange factor activity	7	0.00295	3.88544
	GOTERM_CC_DIRECT	Endosome	9	0.00815	9.77246

Table 6-8. Functional analysis chart summary of the top ten GO terms associated with up- or down-regulated genes in aVICs and vehicle compared to qVICs and vehicle.

	Category	Term	Gene count	P-value	FDR
Up-regulated	GOTERM_BP_DIRECT	Retina vasculature morphogenesis in camera-type eye	2	0.01613	19.6781
	GOTERM_CC_DIRECT	Cell surface	5	0.02198	20.9497
	GOTERM_BP_DIRECT	Insulin-like growth factor receptor signaling pathway	2	0.02569	29.5769
	GOTERM_CC_DIRECT	Plasma membrane	11	0.04139	36.0558
	GOTERM_CC_DIRECT	Microtubule	3	0.04523	38.7122
	GOTERM_CC_DIRECT	Extracellular space	7	0.04575	39.0637
	GOTERM_BP_DIRECT	Positive regulation of smooth muscle cell proliferation	2	0.06301	58.3991
	GOTERM_BP_DIRECT	Regulation of multicellular organism growth	2	0.06606	60.1855
	GOTERM_CC_DIRECT	Intracellular	6	0.07053	53.8688
	GOTERM_BP_DIRECT	Response to heat	2	0.07212	63.5318
Down-regulated	GOTERM_CC_DIRECT	Collagen trimer	2	0.08399	57.2015

Table 6-9. Functional analysis chart summary of the top ten GO terms associated with up-regulated genes and the GO term associated with down-regulated genes shared in aVICs with vehicle and TGFβ1 treated qVICs.

6.3.7 IPA analysis

IPA analysis was performed on TGFβ1-treated qVICs compared to vehicle-treated qVICs, the SB431542-treated aVICs compared to aVICs and vehicle, aVICs and vehicle compared to qVICs and vehicle and the shared genes in the aVIC and TGFβ1-treated qVICs datasets. In the shared analysis, both fold change differences associated with each gene was uploaded in the same analysis (i.e. fold change associated with aVICs and fold change associated with TGFβ1-treated qVICs). The numbers of mapped and unmapped genes in these analyses are summarised in **Table 6-10**.

Analysis	Mapped Genes	Unmapped genes	Total genes
TGFβ1 treated qVICs	273	2	275
SB431542 treated aVICs	200	36	236
aVICs compared to qVICs	855	47	902
Shared aVICs and TGFβ1 treated qVICs	92	10	102

Table 6-10. Mapped unmapped and total number of genes submitted to IPA for analysis for each dataset.

Canonical pathway analysis was performed with 29, 37, 32 and 44 pathways being statistically significantly (P-value <0.05) associated with the TGFβ1-treated qVICs compared to qVICs and vehicle, the SB431542-treated aVICs compared to aVICs and vehicle, aVICs with vehicle compared to qVICs with vehicle and the shared genes in the aVIC and TGFβ1-treated qVICs datasets, respectively. The top three pathways associated with each of the four datasets are shown in **Table 6-11**.

Analysis	Canonical Pathway	Up-regulated genes	Down-regulated genes	Genes changed in pathway	P-value
TGFβ1 treated qVICs	Hepatic Fibrosis/Hepatic Stellate Cell Activation	6	4	10/160	0.00076
	Integrin Signaling	3	8	11/196	0.00102
	Role of Tissue Factor in Cancer	2	6	8/112	0.00107
SB431542 treated aVICs	Superpathway of Cholesterol Biosynthesis	10	0	10/22	1E-12
	Cholesterol Biosynthesis I	0	7	7/11	1.3E-10
	Cholesterol Biosynthesis II	0	7	7/11	1.3E-10
aVICs compared to qVICs	Cell Cycle Control of Chromosomal Replication	15	0	15/49	1.7E-09
	Role of BRCA1 in DNA Damage Response	15	0	15/73	5.9E-07
	Mitotic Roles of Polo-Like Kinase	12	1	13/60	1.7E-06
Shared aVICs and TGFβ1 treated qVICs	Superpathway of Cholesterol Biosynthesis	3	0	3/28	0.0002
	Zymosterol Biosynthesis	2	0	2/6	0.00025
	Axonal Guidance Signaling	4	4	8/457	0.00059

Table 6-11. Summary of top three canonical pathways associated with each dataset. The number of genes up- and down-regulated in each pathway as well as the total number of genes changed in each pathway is given. The P-value score gives the association of the gene list to the pathway.

Upstream regulator analysis likewise found an association for 1015, 837, 991 and 1034 molecules with the TGFβ1-treated qVICs compared to qVICs and vehicle, the SB431542-treated aVICs compared to aVICs and vehicle, aVICs and vehicle compared to qVICs and vehicle and the shared genes in the aVICs and TGFβ1-treated qVICs datasets respectively (P-value <0.05). The top three molecules associated with each dataset are shown in **Table 6-12**. In both treatment datasets, the top predicted upstream regulator was TGFβ1, with its activation seen in the qVICs treated with TGFβ1 and inhibition observed in the aVICs treated with SB431542. These two pathways are schematised in **Figure 6-10** and **Figure 6-11**. The top upstream regulators in aVICs compared to qVICs are predominately involved in cell cycle control and apoptosis, including E2F4 (number 1), CDKN1A (number 2) and TP53 (number 5). E2F4 was predicted as the top upstream regulator and is schematised in **Figure 6-12**, but no predictions could be made as to the effect it would have on genes in the

dataset. CDKN1A was also schematised (**Figure 6-13**) illustrating an overall inhibition of this pathway. The upstream regulators associated with genes shared in the aVICs and TGFβ1-treated qVICs showed TNF and TGFβ1 to be among the top suggested pathways. TNF showed a slight inhibition (-0.244 Z-score) whereas TGFβ1 showed an activation (2.009 Z-score), and this pathway is illustrated in **Figure 6-14**.

Analysis	Upstream Regulator	Molecule Type	Activation Z-score	P-value
TGFβ1 treated qVICs	TGFB1	Growth factor	4.029	2.04E-12
	TNF	Cytokine	1.18	1.38E-11
	HGF	Growth factor	-0.623	1.47E-11
SB431542 treated aVICs	TGFB1	Growth factor	-3.946	3.06E-12
	GATA4	Transcription regulator	1.525	4.95E-10
	AGT	Growth factor	-0.808	1.48E-09
aVICs compared to qVICs	E2F4	Transcription regulator		5.85E-33
	CDKN1A	Kinase	-2.669	2.75E-28
	dextran sulfate	Chemical drug	0.422	3.98E-28
Shared aVICs and TGFβ1 treated qVICs	TNF	cytokine	-0.244	1.31E-08
	TGFB1	growth factor	2.009	1.39E-08
	dexamethasone	chemical drug	0.861	3.52E-08

Table 6-12. Summary of the top three upstream regulators associated with the differentially expressed genes lists for each dataset. For each upstream regulator, the molecule type, Z-score and P-value are given.

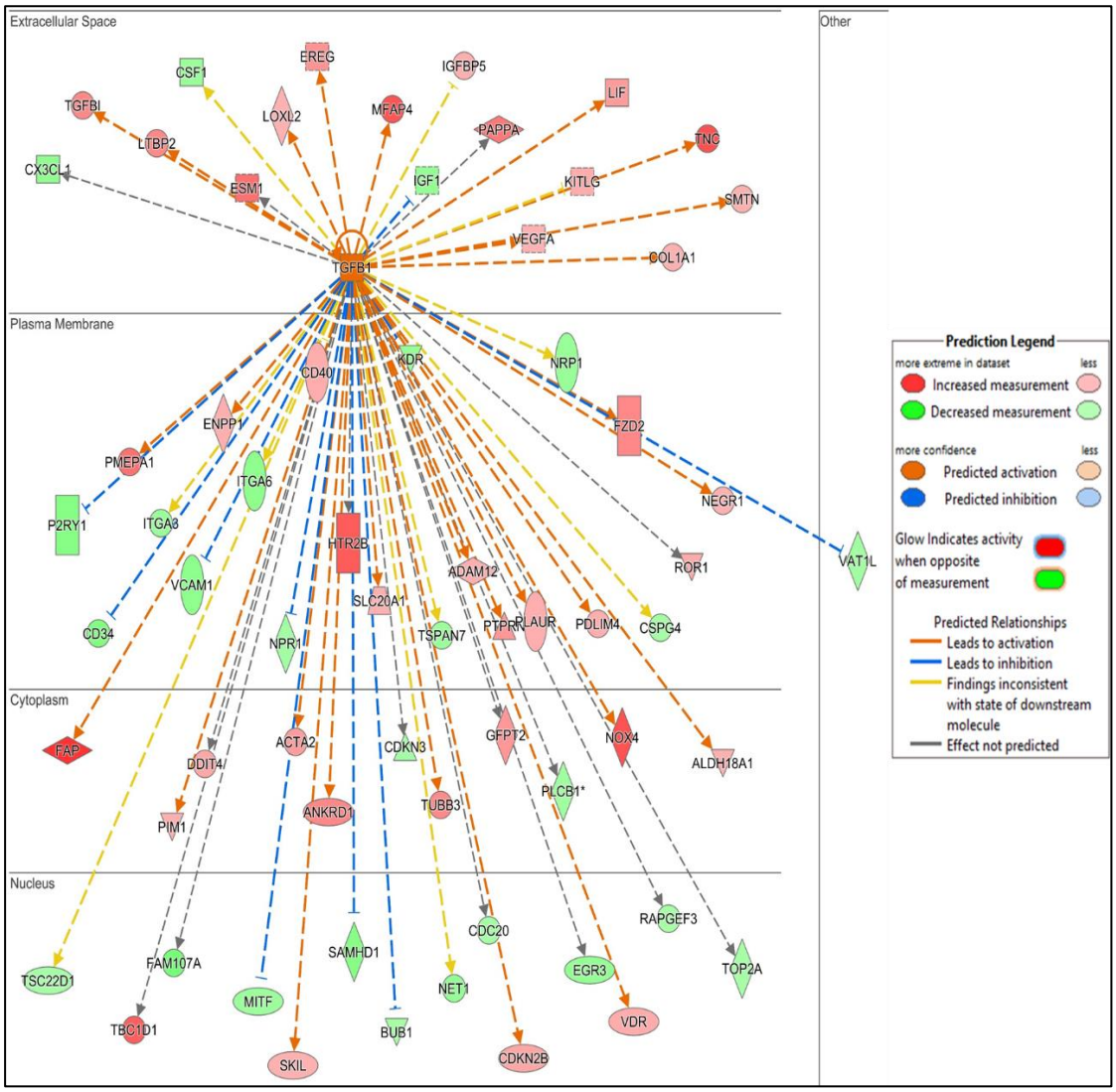

Figure 6-10. The network of genes that are differentially expressed in qVICs treated with TGFβ1 compared to qVICs and vehicle that are downstream of TGFβ1 signalling. TGFβ1 is shown to have its effect from the extracellular space on the genes in their cellular location. Genes are coloured red and green to represent up- or down-regulation in the dataset. Dotted lines connecting TGFβ1 to these genes show the expected effect of TGFβ1 signalling: orange - activation, blue - inhibition, yellow - result inconsistent and grey – effect not predicted.

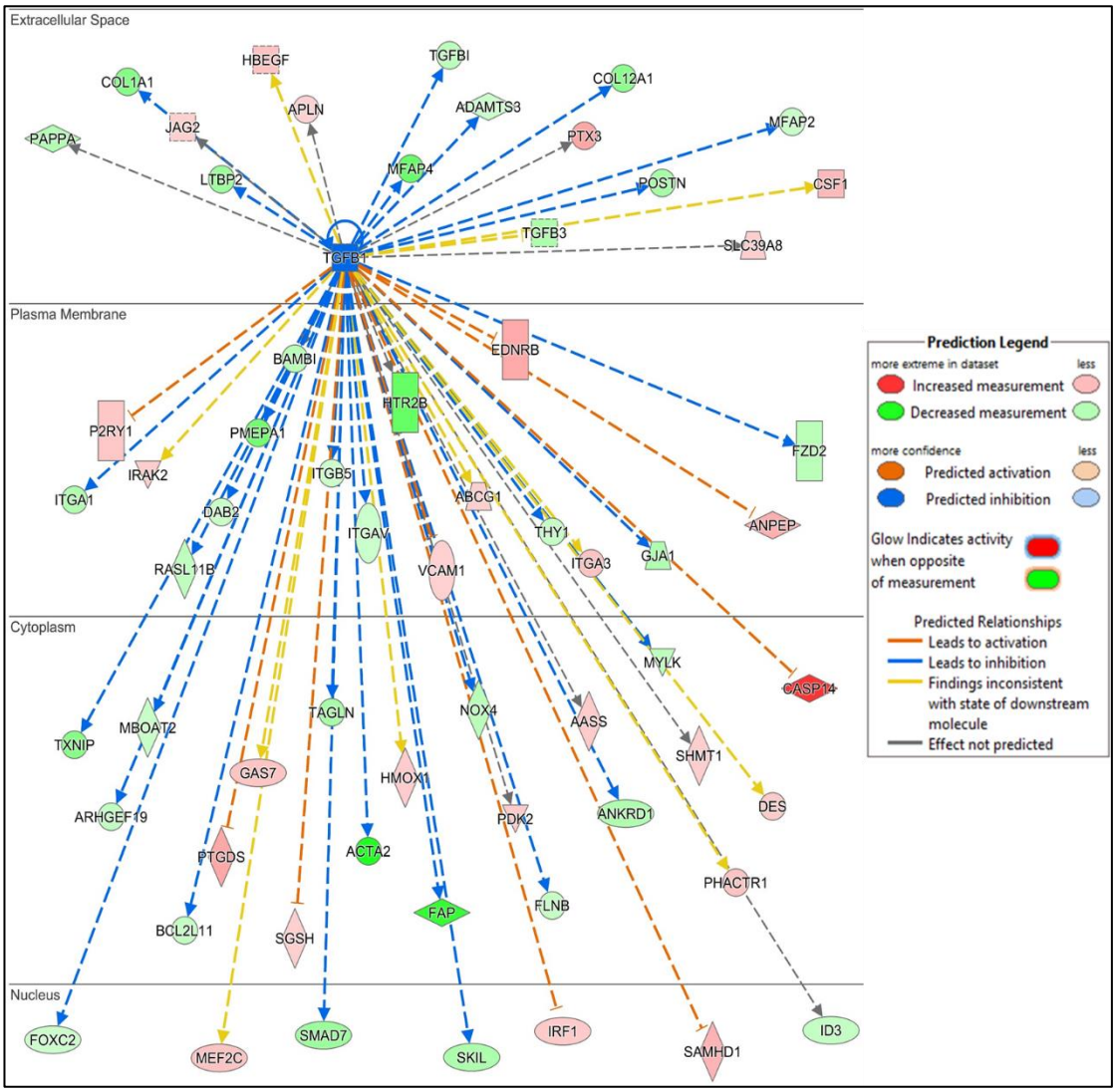

Figure 6-11. The network of genes that are differentially expressed in aVICs treated with SB431542 compared to aVICs with vehicle that are downstream of TGFβ1 signalling. TGFβ1 is shown to have its effect from the extracellular space on the genes in their cellular location. Genes are coloured red and green to represent up- or down-regulation in the dataset. Dotted lines connecting TGFβ1 to these genes show the expected effect of TGFβ1 signalling: orange - activation, blue - inhibition, yellow - result inconsistent and grey – effect not predicted.

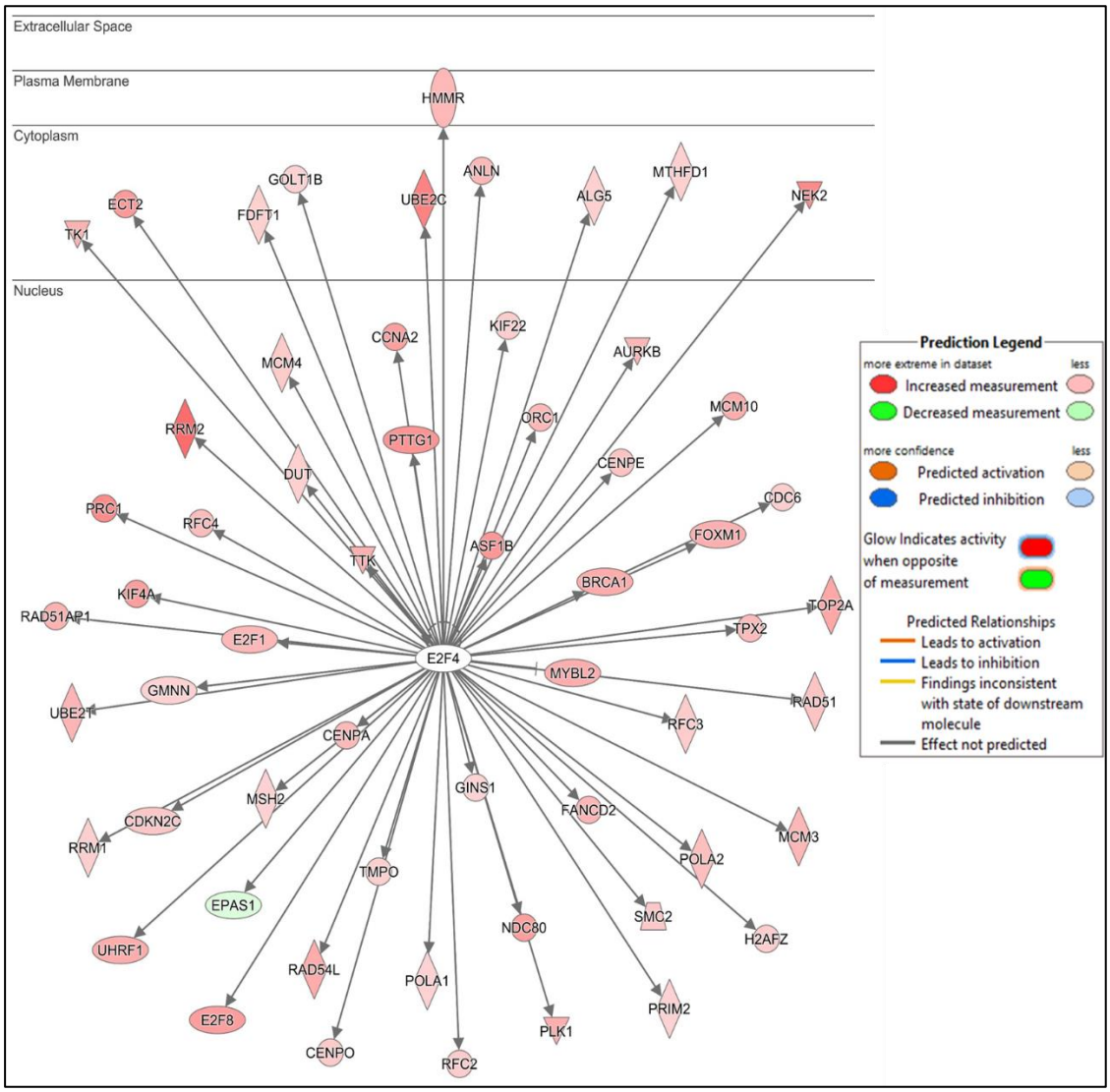

Figure 6-12. The network of genes that are differentially expressed in aVICs with vehicle compared to qVICs with vehicle that are downstream of E2F4. E2F4 is shown to have its effect from the nucleus on the genes in their cellular location. Genes are coloured red and green to represent up- or down-regulation in the dataset. Grey lines connecting E2F4 to these genes show that no effect is predicted for the effect of E2F4 on any of these genes.

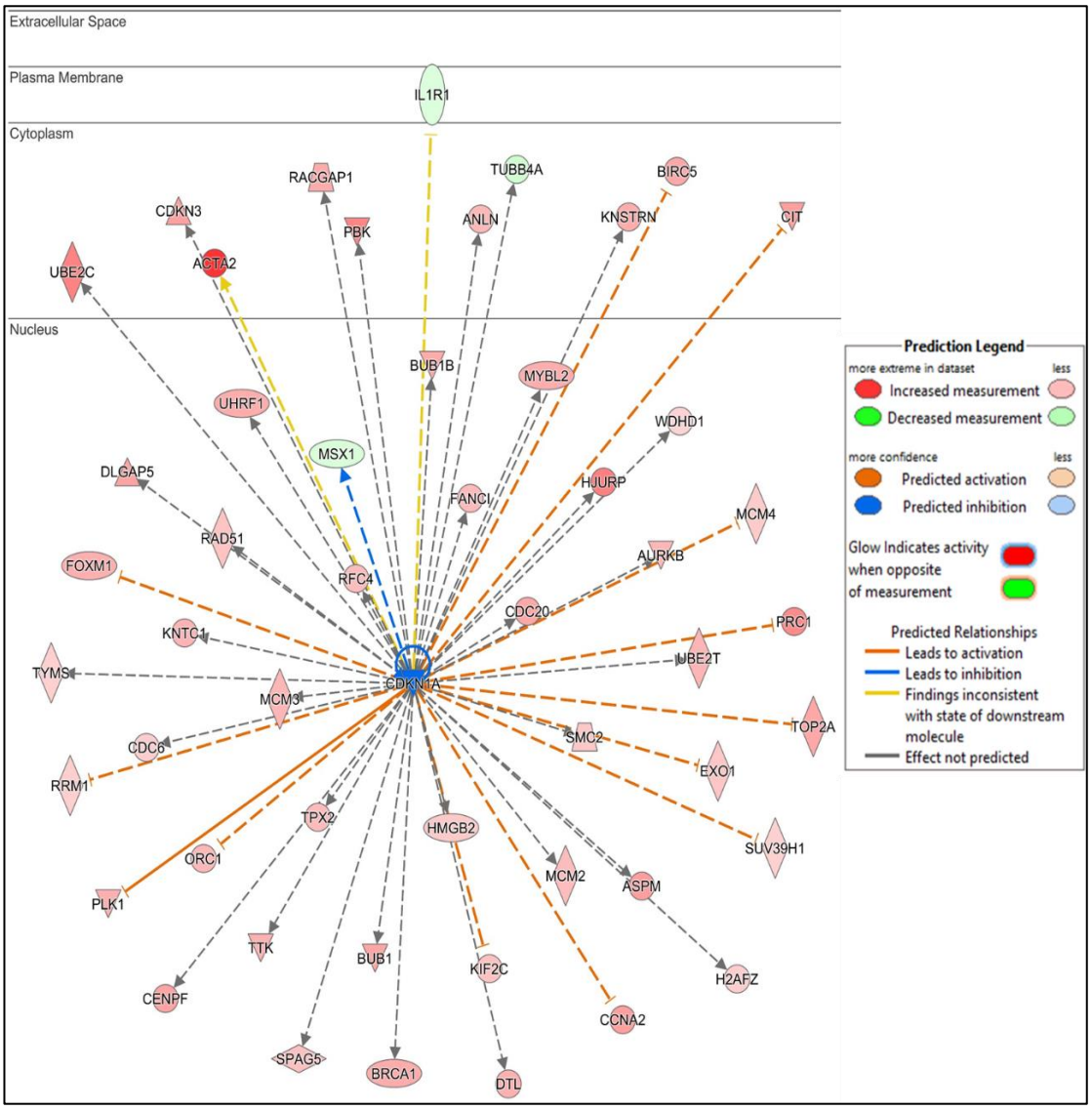

Figure 6-13. The network of genes that are differentially expressed in aVICs with vehicle compared to qVICs with vehicle that are downstream of CDKN1A. CDKN1A is shown to have its effect from the nucleus on the genes in their cellular location. Genes are coloured red and green to represent up- or down-regulation in the dataset. Lines connecting CDKN1A to these genes show the expected effect of CDKN1A signalling: orange - activation, blue - inhibition, yellow - result inconsistent and grey – effect not predicted.

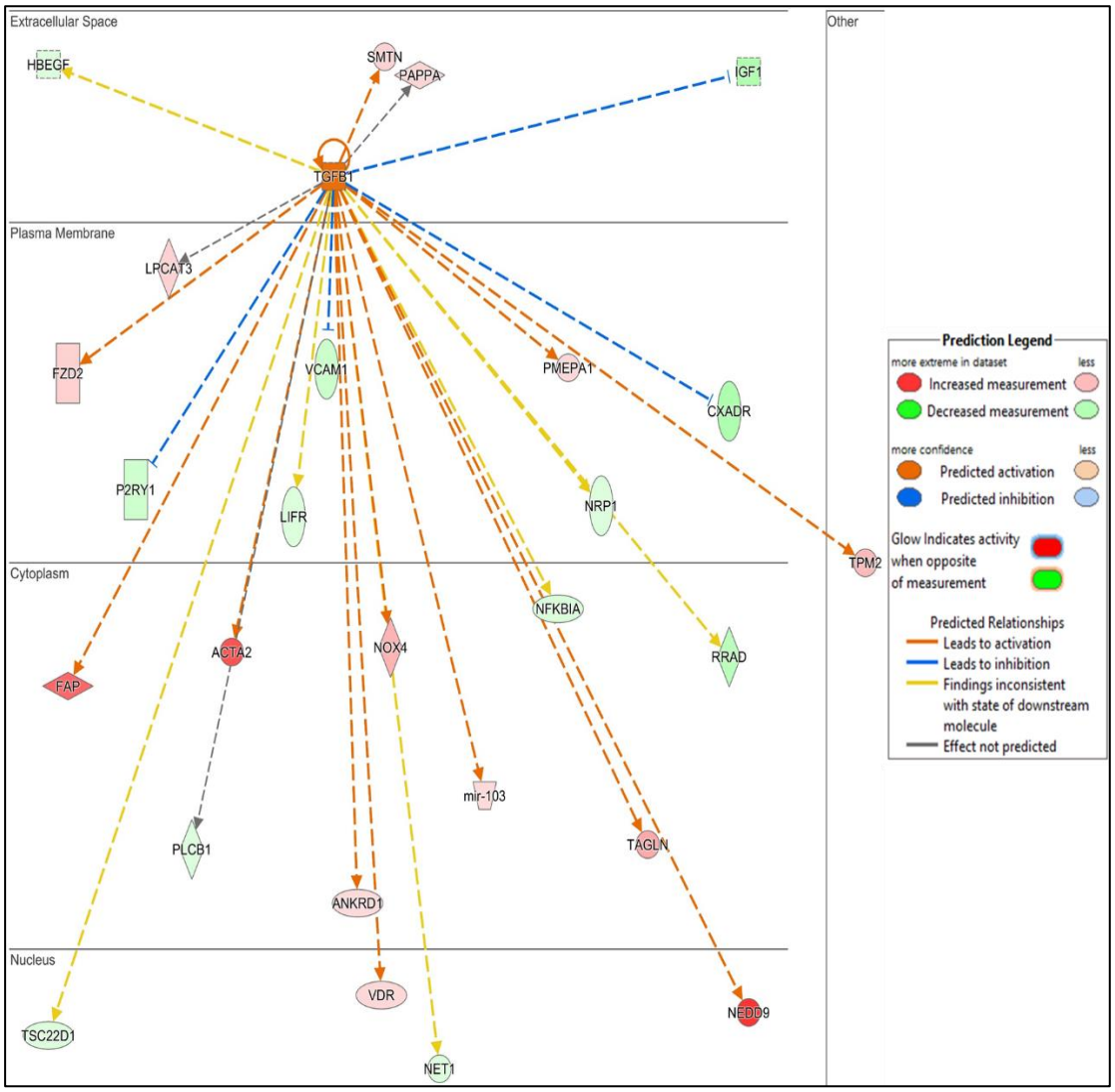

Figure 6-14. The network of genes that are shared in aVICs with vehicle and qVICs treated with TGFβ1 that are downstream of TGFβ1 signalling. TGFβ1 is shown to have its effect from the extracellular space on the genes in their cellular location. Genes are coloured red and green to represent up- or down-regulation in the dataset. Dotted lines connecting TGFβ1 to these genes show the expected effect of TGFβ1 signalling: orange - activation, blue - inhibition, yellow - result inconsistent and grey – effect not predicted.

The network analysis highlighted the disease and function annotations associated with each of the datasets. The top five associated with the genes differentially expressed between TGFβ1-treated qVICs compared to qVICs with vehicle are shown in **Table 6-13**. The *Cellular movement, cardiac arrhythmia and cardiovascular disease* functions are also schematised in **Figure 6-15**. The top five disease and function networks associated with the genes differentially expressed between aVICs treated with SB431542 compared to aVICs with vehicle are given in **Table 6-14**, and the *cardiovascular disease, hereditary disorder, organismal injury and abnormalities disease* function are further schematised in **Figure 6-16**. The top five networks associated with the genes differentially expressed between aVICs with vehicle and qVICs with vehicle are shown in **Table 6-15**, with *cell cycle, cellular movement and Cancer* schematised in **Figure 6-17**. Lastly, the top five disease and function networks associated with genes shared between aVICs with vehicle and qVICs treated with TGFβ1 and are shown in **Table 6-16**, and *cell morphology, cardiovascular disease and development disorder* shown in **Figure 6-18**.

Top disease and function
Cancer, Endocrine System Disorders, Organismal Injury and Abnormalities
Cellular Movement, Organismal Survival, Cancer
Cellular Movement, Cardiac Arrythmia, Cardiovascular Disease
Cancer, Organismal Injury and Abnormalities, Reproductive System Disease
Cardiac Enlargement, Cardiovascular Disease, Cardiovascular System Development and Function

Table 6-13. Summary of the top five disease and function networks associated with the genes differentially expressed between TGFβ1 treated qVICs compared to qVICs with vehicle.

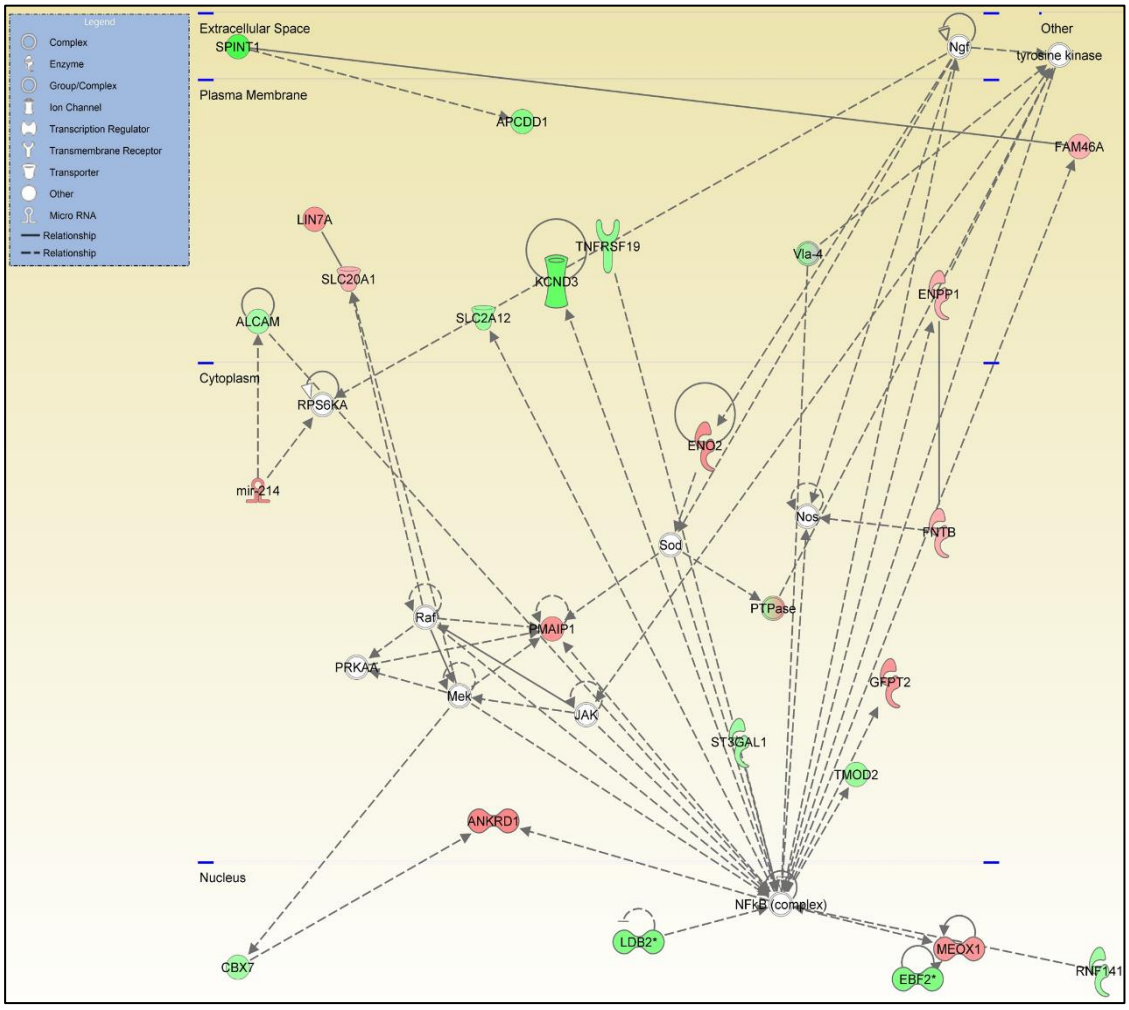

Figure 6-15. Schematic of the *Cellular movement, cardiac arrhythmia and cardiovascular disease* function network. Genes are shown in their protein cellular location with red indicating up-regulation, green down-regulation and un-coloured showing no change in the dataset.

Top disease and function
Dermatological Diseases and Conditions, Inflammatory Disease, Organismal Injury and Abnormalities
Drug Metabolism, Small Molecule Biochemistry, Cellular Assembly and Organization
Cardiovascular Disease, Hereditary Disorder, Organismal Injury and Abnormalities
Cell Morphology, Glomerular Injury, Organ Morphology
Developmental Disorder, Ophthalmic Disease, Organismal Injury and Abnormalities

Table 6-14. Summary of the top five disease and function networks associated with the genes differentially expressed between SB431542 treated aVICs compared to aVICs with vehicle.

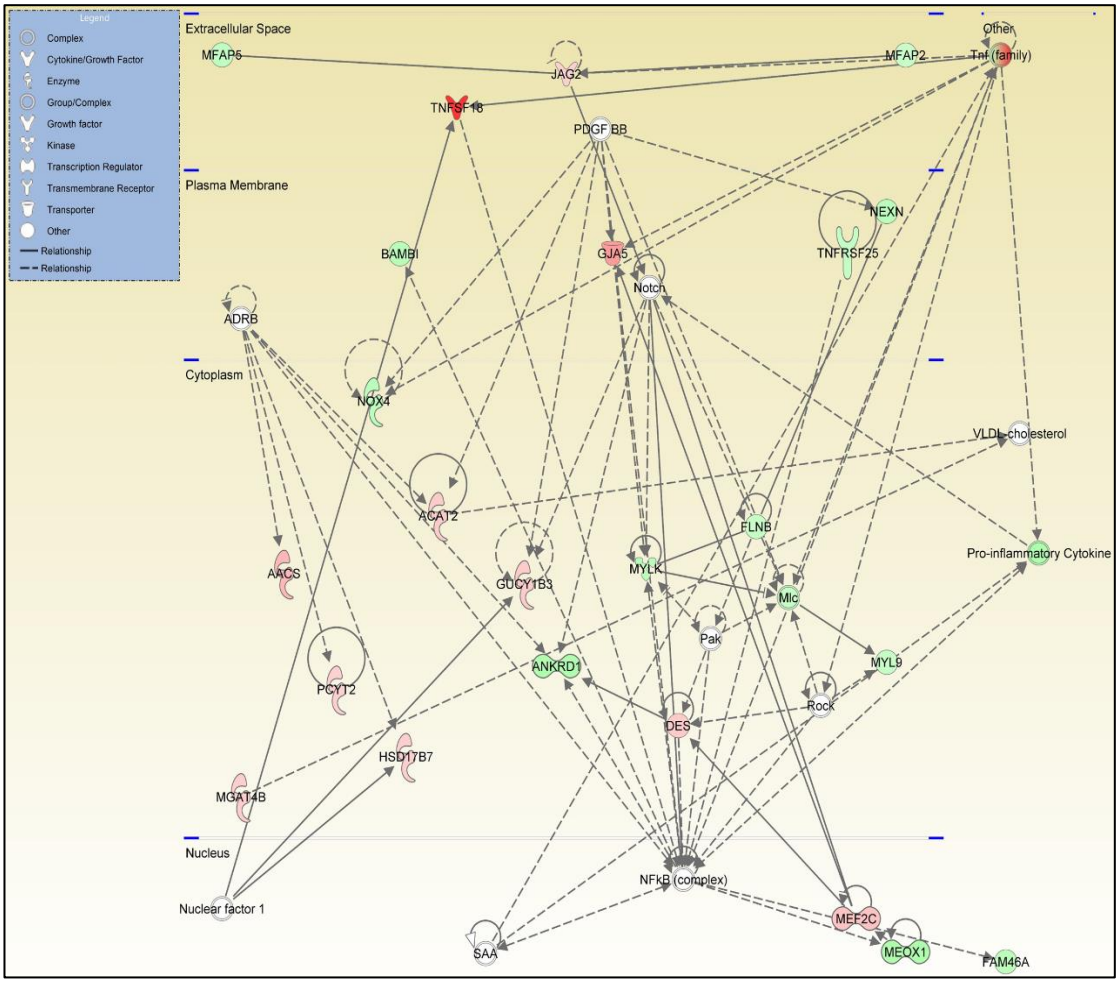

Figure 6-16. Schematic of the *Cardiovascular disease, hereditary disorder, organismal injury and abnormalities* function network. Genes are shown in their protein cellular location with red indicating up-regulation, green down-regulation and un-coloured showing no change in the dataset.

Top disease and function
Cell Cycle, Cellular Movement, Cancer
Cell Cycle, Reproductive System Development and Function, Cellular Assembly and Organization
Cellular Assembly and Organization, Connective Tissue Disorders, Developmental Disorder
Cellular Assembly and Organization, DNA Replication, Recombination, and Repair, Cell Cycle
Cell Cycle, DNA Replication, Recombination, and Repair, Cancer

Table 6-15. Summary of the top five disease and function networks associated with the genes differentially expressed between aVICs with vehicle compared to qVICs with vehicle.

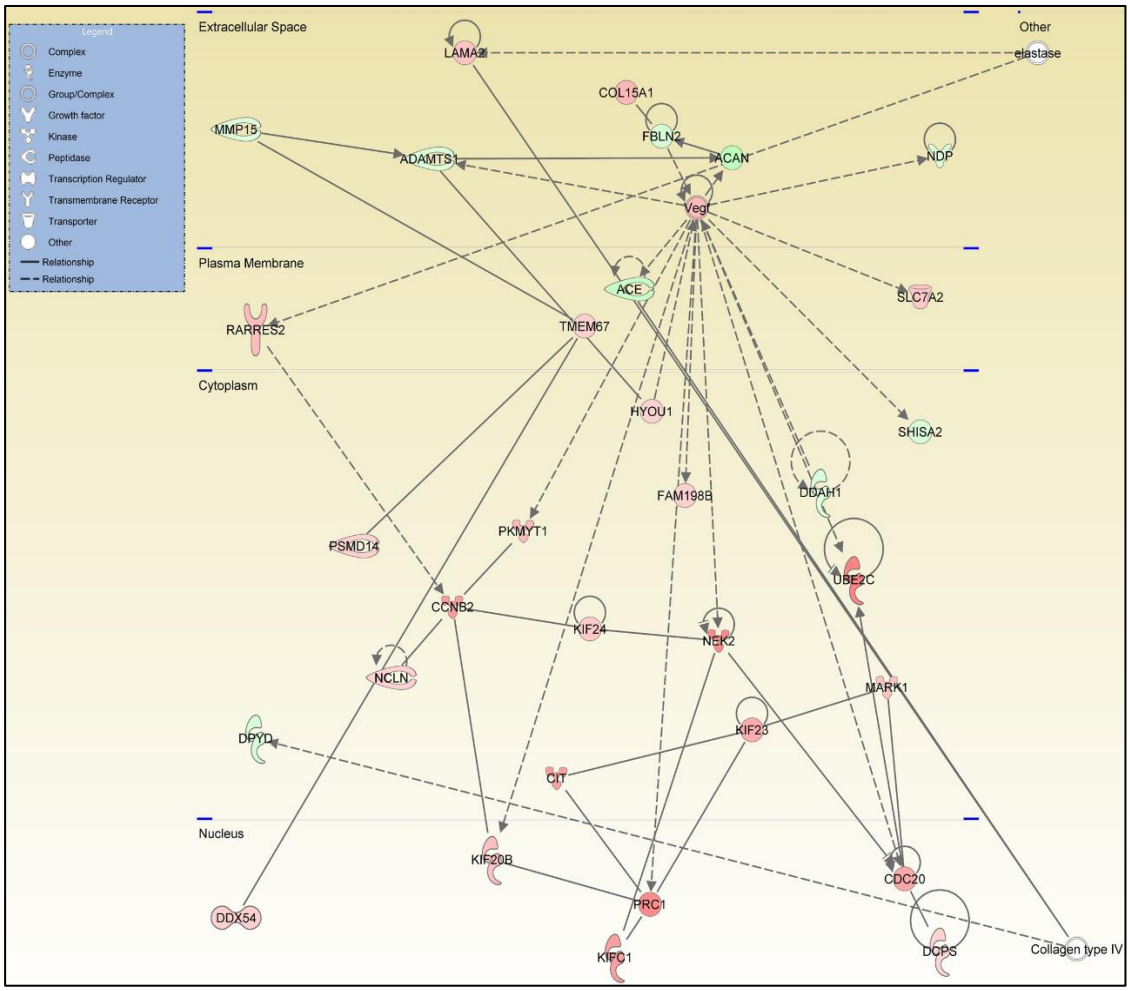

Figure 6-17. Schematic of the *Cell cycle, cellular movement and Cancer* function network. Genes are shown in their protein cellular location with red indicating up-regulation, green down-regulation and un-coloured showing no change in the dataset.

Top disease and function
Cell Morphology, Cardiovascular Disease, Developmental Disorder
Cancer, Endocrine System Disorders, Organismal Injury and Abnormalities
Connective Tissue Disorders, Organismal Injury and Abnormalities, Cell Death and Survival
Cellular Movement, Cellular Development, Cellular Growth and Proliferation
Cell-To-Cell Signaling, Hematological System Development and Function, Hematopoiesis

Table 6-16. Summary of the top five disease and function networks associated with the genes shared between aVICs with vehicle and qVICs treated with TGFβ1.

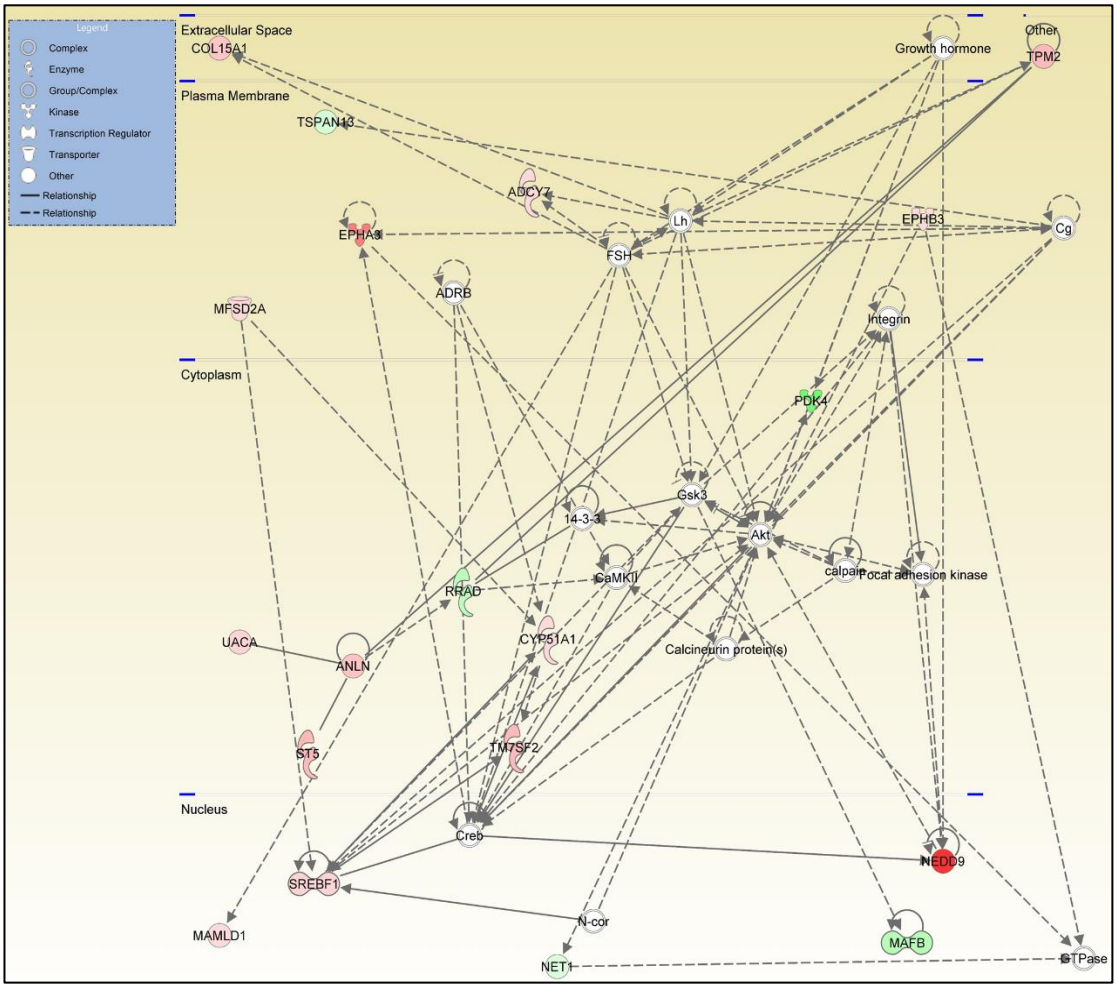

Figure 6-18. Schematic of the *Cell morphology, cardiovascular disease and development disorder* disease and function network. Genes are shown in their protein cellular location with red indicating up-regulation, green down-regulation and un-coloured showing no change in the dataset

6.3.8 RT-qPCR microarray validation

Validation of the microarray results by RT-qPCR was performed on selected genes of interest that showed a significantly different expression in at least one of the comparisons performed in the microarray analysis. Genes were selected based on their relevance to the disease myofibroblastic phenotype and activation (*ACTA2*, *TAGLN* and *MYH10*), differential expression described in the previous chapters (*HTR2B*, *HBEGF* and *SLC10A6*) or relative high fold change difference (*BMPER, VCAM1, PDK4* and *FAP*). The microarray results for these genes are shown in **Table 6-17** and the corresponding RT-qPCR results are shown in **Table 6-18**. Almost all results were in agreement between microarray and RT-qPCR with differences only seen in aVICs compared to qVICs, which are highlighted in yellow in the two tables. The *HTR2B* expression did not reach significance in the microarray analysis but did by RT-qPCR. *BMPER* did the opposite with significance reached in microarray analysis but not in RT-qPCR analysis.

Gene name	qVIC treated with TGFβ1		aVIC treated with SB431542		aVIC compared to qVIC	
	Fold change	P-value	Fold change	P-value	Fold change	P-value
ACTA2	1.95	0.0437	-6.36	0.0184	7.69	0.0051
TAGLN	2.1	0.0228	-2.58	0.034	3.78	0.0088
MYH10	-1.13	0.7948	-1.34	0.5271	2.18	0.0297
HTR2B	3.71	0.0176	-5.16	0.0308	3.35	0.1184
HBEGF	-1.73	0.0209	2.1	0.0003	-1.67	0.0085
BMPER	-3.09	0.0064	1.6	0.4142	-3.98	0.0257
VCAM1	-1.83	0.0004	1.59	0.1007	-2.79	0.0076
PDK4	-5.11	0.0021	-1.78	0.2011	-7.89	0.0009
FAP	4.71	0.0032	-6.94	0.0141	6.73	0.0063
SLC10A6	-1.96	0.0481	-1.17	0.993	-2.14	0.0109

Table 6-17. Microarray fold change and P-value for genes selected for microarray validation. Highlighted in yellow are instances where the significance of these results did not match with RT-qPCR validation.

Gene name	qVIC treated with TGFβ1		aVIC treated with SB431542		aVIC compared to qVIC	
	Fold change	P-value	Fold change	P-value	Fold change	P-value
ACTA2	6.01	0.03	-22.36	0.021	37.4	0.003
TAGLN	2.84	0.043	-2.72	0.042	3.92	0.028
MYH10	-1.74	0.086	-1.07	0.572	2.9	0.05
HTR2B	2.43	0.043	-9.34	0.042	2.33	0.029
HBEGF	-2.69	0.44	2.95	0.035	-2.5	0.021
BMPER	-5.28	0.008	2.31	0.12	-4.2	0.092
VCAM1	-2.83	0.049	2.78	0.065	-6.93	0.007
PDK4	-6.88	0.005	3.89	0.09	-74.07	0.012
FAP	7.64	0.002	-5.71	0.001	8.54	0.026
SLC10A6	-2.65	0.013	2.07	0.237	-4.53	0.042

Table 6-18. RT-qPCR fold change and P-value for genes selected for microarray validation. Highlighted in yellow are instances where the significance of these results did not match with microarray data. Normalised to *GAPDH, MRPS25* and *RPL32*.

6.3.9 Cell morphology and proteoglycan deposition in samples submitted for microarray

To further characterise the effects of TGFβ1 and SB431452 on the VIC phenotypes, cell morphology and proteoglycan deposition were assessed. Morphologically, qVICs treated with TGFβ1 (**Figure 6-19B**) showed a far more disorganised, clustered structure and hyper-elongated morphology (reminiscent of the aVIC morphology observed in section 6.3.1) compared to qVICs treated with vehicle (**Figure 6-19A**). aVICs treated with SB431452 (**Figure 6-19D**) showed a more organised structure and less elongation of cells (reminiscent of the qVIC morphology observed in section 6.3.1) compared to the aVICs treated with vehicle (**Figure 6-19C**). Proteoglycan deposition was increased significantly in qVICs treated with TGFβ1 compared to qVICs with vehicle (5.13 fold increase, P-value 0.02) (**Figure 6-20A**). Likewise, aVICs treated with SB431542 showed a significant decrease in proteoglycan

deposition compared to aVICs with vehicle (2.82 fold decrease, P-value 0.012) (**Figure 6-20B**). Comparing aVICs with vehicle to qVICs with vehicle a significant difference was also found in proteoglycan deposition (3.03 fold increase, P-value 0.42) (**Figure 6-20C**). The data show treatment of qVICs with TGFβ1 promotes the aVIC phenotype while treatment of aVICs with the TGFβRI kinase inhibitor reverses activation and supports a reversion to the qVIC phenotype.

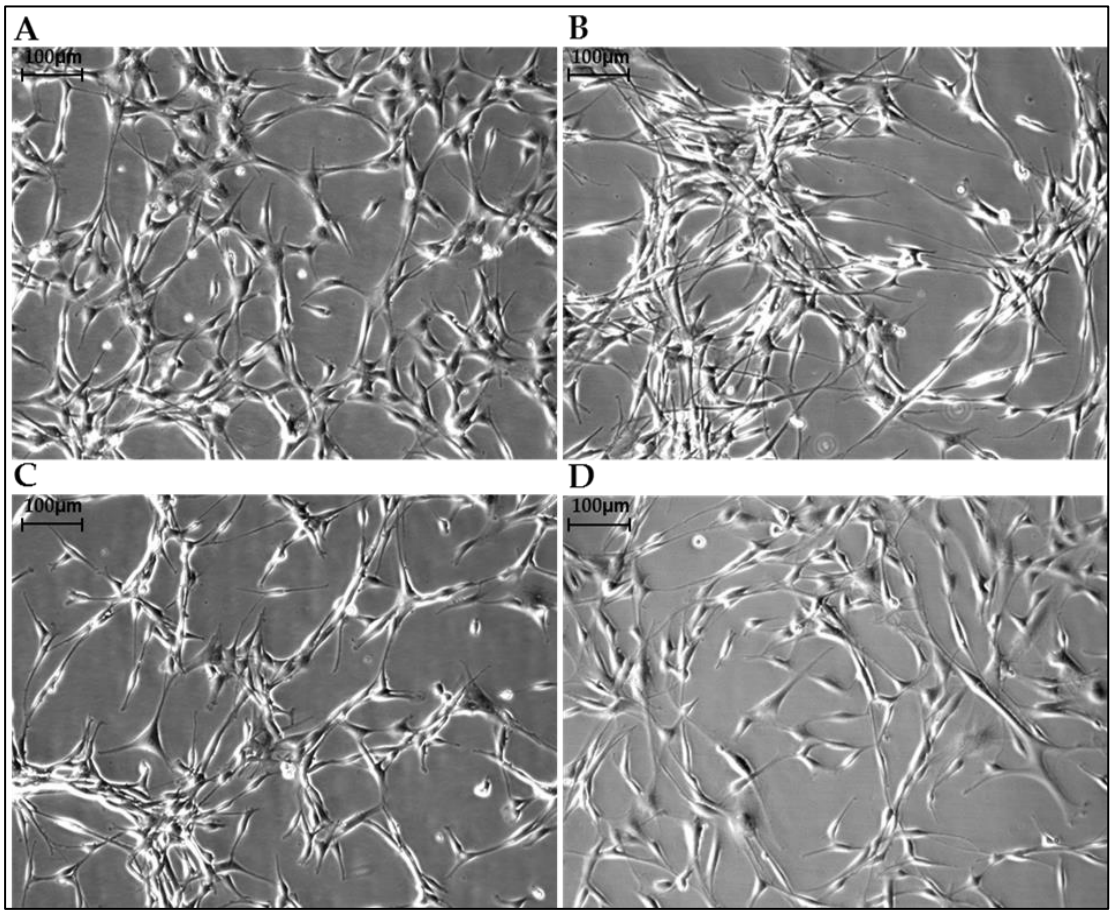

Figure 6-19. Cell Morphology of VIC phenotypes under treatment of TGFβ1 or SB431542. (A) Representative image of qVICs treated with vehicle. (B) Representative image of qVICs treated with TGFβ1. (C) Representative image of aVICs treated with vehicle. (D) Representative image of aVICs treated with SB431542. Scale bar = 100µm

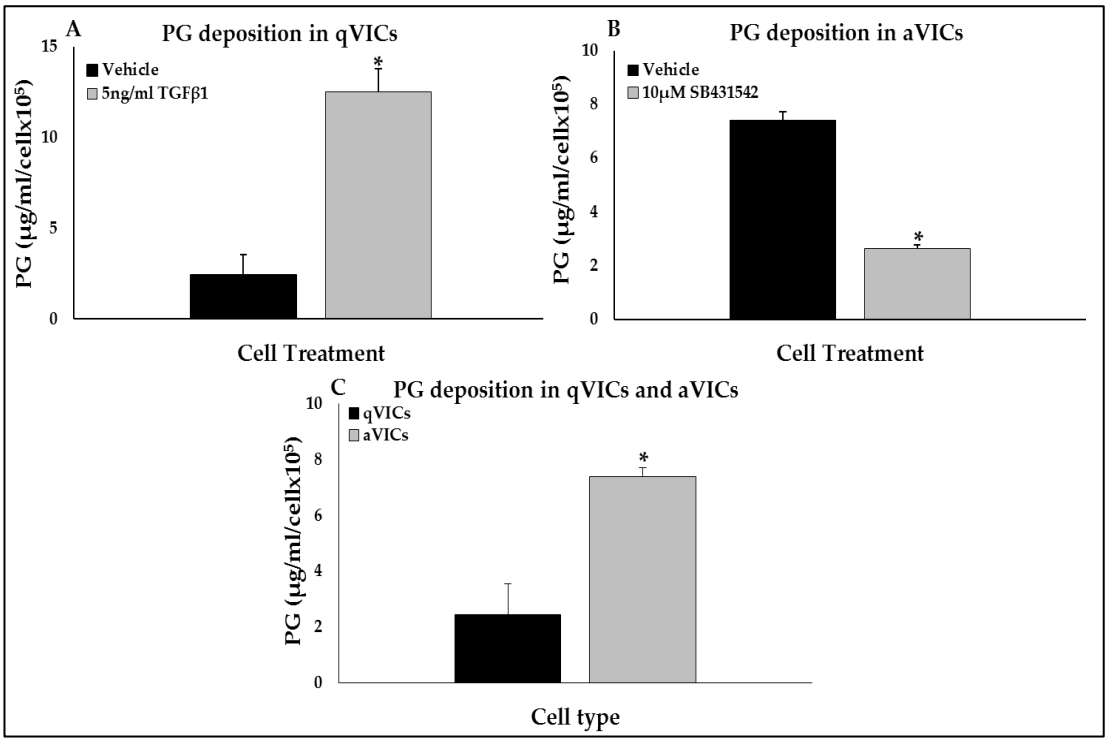

Figure 6-20. Proteoglycan deposition in VICs under treatment of TGFβ1 or SB431542. (A) Effect of TGFβ1 treatment of qVICs on proteoglycan deposition compared to qVICs with vehicle. (B) Effect of SB431542 treatment of aVICs on proteoglycan deposition compared to aVICs with vehicle. (C) Comparison of proteoglycan deposition between qVICs with vehicle and aVICs with vehicle. * = P-value <0.05. n=3 per group.

6.3.10 5HT signalling effect on gene expression and proteoglycan deposition

To assess the effect of 5HT signalling in VICs, qVICs were treated with 5HT and aVICs were treated with two different concentrations of the 5HTR2B antagonist LY272015. Two-time points (4 days and 7 days) were assessed for the gene expression of myofibroblast markers and *HTR2B*. Additionally, proteoglycan deposition was measured at 7 days. At day 4, gene expression for all conditions was not significantly different apart from an unexpected 1.9 fold increase (P-value 0.025) in *HTR2B* expression in the aVICs treated with

100 nM LY272015 (**Table 6-19**). At day 7, *HTR2B* expression was increased by 2.09 and 2.84 fold (P-value 0.024 and 0.003) in aVICs treated with 100 nM and 1 μM LY272015 respectively (**Table 6-20**). Likewise, an increase in expression of *MYH10* was seen for both concentrations of LY272015 at this time point reflecting a 1.52 fold (P-value 0.009) and 2.84 fold (P-value 0.001) change for 100 nM and 1 μM respectively. No significant changes were observed for 5HT (P-value 0.653), 100 nM (P-value 0.936) and 1 μM (P-value 0.458) LY272015 treatment in the deposition of proteoglycans from VICs on day 7 (**Figure 6-21**).

Gene	qVICs treated with 5HT		aVICs treated with 100nm LY272015		aVICs treated with 1μM LY272015	
	Fold change	P-Value	Fold change	P-Value	Fold change	P-Value
ACTA2	-1.42	0.728	1.05	0.713	-2.6	0.341
TAGLN	1.33	0.662	1.08	0.871	1.17	0.621
MYH10	-1.59	0.242	2.31	0.167	1.53	0.428
HTR2B	1.13	0.811	1.9	0.025	2.07	0.383

Table 6-19. Gene expression in 5HT signalling on day 4. Fold change and associated P-value for genes of interest in qVICs treated with 1 μM 5HT, aVICs treated with 100 nM LY272015 and aVICs treated with 1 μM LY272015.

Gene	qVICs treated with 5HT		aVICs treated with 100nm LY272015		aVICs treated with 1μM LY272015	
	Fold change	P-Value	Fold change	P-Value	Fold change	P-Value
ACTA2	1.97	0.289	-2.26	0.244	-1.39	0.575
TAGLN	2.91	0.093	-1.27	0.217	-1.24	0.61
MYH10	1.07	0.9	1.52	0.009	2.84	0.001
HTR2B	1.54	0.421	2.09	0.024	2.84	0.003

Table 6-20. Gene expression in 5HT signalling on day 7. Fold change and associated P-value for genes of interest in qVICs treated with 1 μM 5HT, aVICs treated with 100 nM LY272015 and aVICs treated with 1 μM LY272015.

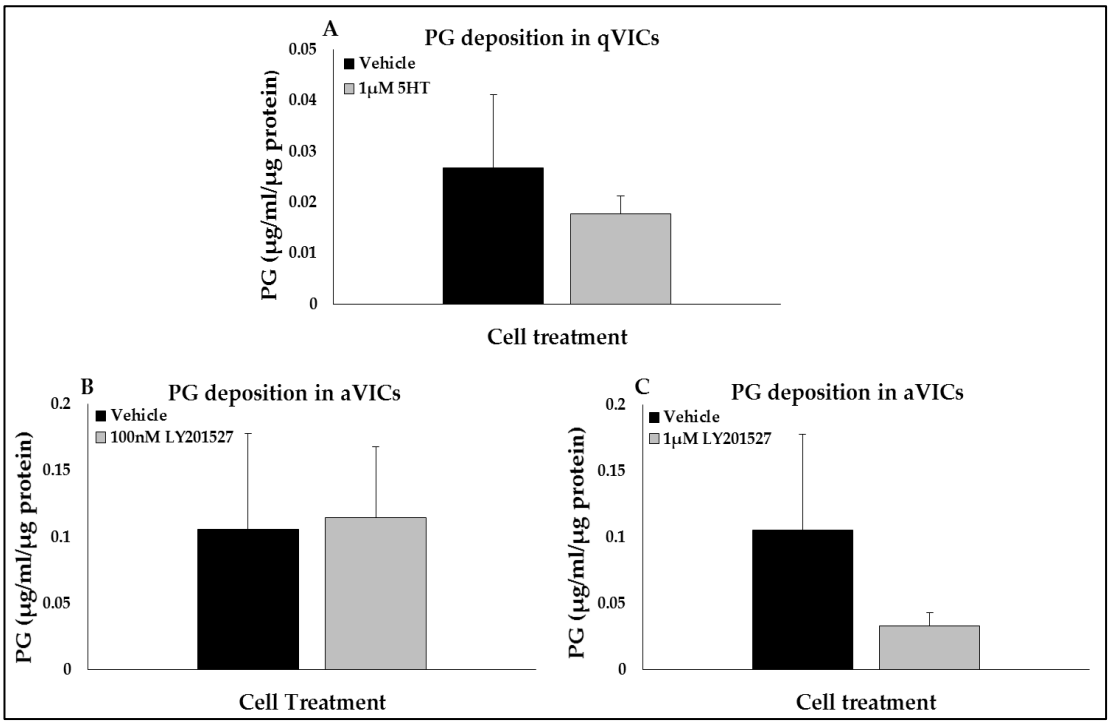

Figure 6-21. Proteoglycan deposition in VICs under treatment of 5HT or LY272015. (A) Effect of 5HT treatment of qVICs on proteoglycan deposition compared to qVICs with vehicle. (B) Effect of 100 nM LY272015 treatment of aVICs on proteoglycan deposition compared to aVICs with vehicle. (C) Effect of 1 μM LY272015 treatment of aVICs on proteoglycan deposition compared to aVICs with vehicle.

6.4 Discussion

This study aimed to build upon data presented in previous chapters and investigate MMVD *in vitro*. Myxomatous mitral valves present with activated VICs[2, 43, 57]. Using monocultures of primary VICs, proposed to be the main drivers of MMVD progression, examining VIC molecular events and signalling pathways can be achieved[1, 2, 43, 60]. In this study, both qVICs from normal valves and aVICs from diseased valves were cultured in a low serum culture system that has previously been shown to maintain these phenotypes in human aortic VIC cultures[138]. As the importance of TGFβ1 signalling was

identified in the valve tissue studies, investigation of the effects of exogenous TGFβ1 on qVICs and the inhibition of TGFβ signalling in aVICs with the TGFβRI kinase inhibitor SB431542 was undertaken. In addition, the role of 5HT signalling in MMVD was investigated in a similar way with the exogenous delivery of 5HT to qVICs and the inhibition of the 5HTR2B signalling with LY272015.

Initially, it was important to establish the phenotype of VICs isolated from normal and diseased valves. This was performed by examining the gene and protein expression of hallmarks of MMVD, proteoglycan deposition and cell morphology (section 6.3.1)[43, 45, 113]. It was shown that all of these markers indicated that qVICs from the normal valves and aVICs from the diseased valves had been isolated. Furthermore, their phenotype could be maintained in culture for several passages (at least passage 6) with the use of the optimised media conditions, which had previously not been possible[45, 138].

ELISAs for TNF and IFNγ, both previously implicated in disease pathogenesis (Chapter 3 and 5), indicated they were secreted from both populations of VICs at very low levels with IFNγ below the detection limits of the ELISA kit. This is in agreement with the gene expression detected for these factors both in VICs (section 6.3.2) and in tissue (Chapter 5 section 5.3.5), indicating that gene and protein level are similar. Together, these results indicate that TNF and IFNγ are only present at a minimal level in the valve. This is in spite of some reports indicating TNF has potential as an EndoMT stimulating factor[90]. However, these results, coupled with reports in the literature indicating that there is no association for an increase in the circulation of these molecules in MMVD dogs, makes it unlikely that they play an important role in disease development[301, 302]. It is more likely that their prominence in the analysis, in

particular TNF, is due to a cross-over in similar downstream targets to TGFβ signalling, as indicated in Chapter 3 section 3.3.7.

TGFβ1 ELISA data from qVICs and aVICs showed it to have the highest level of secretion out of the three TGFβs, and although not significant after 72 hours in culture, after 120 hours a significant increase in TGFβ1 was detected (data provided by Dr. Karen Tan). Supporting these data, TGFβ1 gene expression was detected at a level well above the background cut-off in VICs (section 6.3.5) and in tissue (Chapter 5 section 5.3.5). Comparative ELISA data for both TGFβ2 and TGFβ3 found a much lower secretion than TGFβ1, with no significant difference detected between qVICs and aVICs at 72 hours or 120 hours (pers. comm. Dr. Karen Tan; data not shown). Surprisingly, the gene expression intensity for these two factors was at a similar or slightly higher level to that for *TGFB1*. This suggests that either post-transcriptional/post-translational events are preventing the translation or secretion of these factors from the cell, or that they are being cleared from the supernatant and extracellular space at a far greater rate than TGFβ1. TGFβ1-3 undergo several post-translational events prior to their secretion in a latent form bound to latent TGFβ binding proteins (LTBPs)[180]. It may be events during this process are involved in the reduced secretion of TGFβ2 and TGFβ3. What relevance, if any, this disparity between gene level and protein secretion may have to MMVD is unknown and warrants future research. However, this is beyond the current scope of this study to investigate. It could also be argued that the higher secretion of TGFβ1 is because of its relevance to valve homeostasis as it is the activation of the extracellular latent forms of TGFβ that controls its activity and action[180]. It has been previously shown, in tissue using immunohistochemistry that TGFβ1 and TGFβ3 are expressed at relatively high levels in normal and MMVD valves, with a relatively low expression of

TGFβ2, and in agreement with the results presented here, only TGFβ1 was detected in the extracellular space[174]. The significantly higher level of TGFβ1 detected in aVIC cultures compared to qVICs complements the data presented in previous chapters, and the wider literature, indicating its importance in MMVD [126, 133, 136, 174, 175].

When performing differential gene expression analysis no FDR correction could be applied to any of the datasets without the loss of all differentially expressed genes. This included when using a paired ANOVA, similar to Chapter 5, between treatment groups. This is likely due to the low number (n=3) of samples per group, as well as a degree of naturally occurring biological variability between samples inherent in using primary cell cultures[309]. Technical variability was minimised by performing all experiments at the same time, by the same person, using the same culture plastics and passage matching all cells. As discussed in Chapter 3 section 3.4, methods for improving future studies would be to try and minimise variability within sample groups by using the same breed and age of dog for cell extraction, which was performed for the qVIC phenotype, as well as increasing the number of samples. Nonetheless, valuable insights into the role of TGFβ1 signalling in VICs could still be identified and interpreted through gene enrichment analysis of the datasets without FDR correction.

Differential gene expression, PCA and sample-to-sample analysis (sections 6.3.4 and 6.3.5) all highlighted transcriptomic differences between each of the groups with qVICs treated with TGFβ1 showing more similarity with aVIC phenotype, and SB431542 treated aVICs showing more similarity with qVICs. Of the 102 shared differentially expressed genes between TGFβ1-treated qVICs and aVICs only one gene, encoding mastermind-like domain-containing protein 1 (MAMLD1), was found to show a different expression

pattern between the two groups. MAMLD1 is primarily involved in the gonadal development and its differential expression is likely inconsequential to MMVD[310]. As such this gene was excluded from downstream gene enrichment analysis.

In qVICs treated with TGFβ1 up-regulated DAVID GO terms (section 6.3.6) included extracellular matrix and extracellular space which relates to MMVD pathogenesis where expansion of the extracellular space is a hallmark of disease[2, 3, 61]. Down-regulated GO terms in this group's analysis included cardiac conduction system development and positive regulation of ERK1 and ERK2. The former of these can be related to the phenotypic switch that appears to be happening in the qVICs treated with TGFβ1 and has been suggested to change the cardiac potential in these cells[43]. The association of positive regulation of ERK1 and ERK2 cascade with the down-regulated genes in the TGFβ1 treated qVICs is difficult to explain. It is in contrast with the data reported in Chapters 3 and 4 where this GO term was associated with up-regulated genes in diseased valves, as well as reports of activation of ERK1 and ERK2 signalling in human MMVD[1, 133]. This may reflect the activation of a negative feedback loop in VICs in response to acute exposure to exogenous TGFβ1.

Examining the effects of SB431542 treatment on aVICs identified GO terms associated with down-regulated genes relevant to MMVD. Extracellular matrix, stress fiber, positive regulation of cell migration and focal adhesion can all be related to the aVIC phenotype[45, 113, 117]. Down-regulation of genes suggests that an attenuation of the aVIC phenotype is generated with SB431542 treatment. This implies that the signalling through TGFβRI is in part responsible for these disease phenotype traits. When comparing aVICs to qVICs amongst the GO terms associated with up-regulated genes there

appears to be a large number that are involved in cell division and DNA replication, (as seen in Chapter 3). This could be related to a more proliferative morphology seen in aVICs in culture as well as a moderate increase in the proliferation marker KI-67 in tissue [43, 45, 113]. When analysing the genes shared between TGFβ1-treated qVICs and aVICs GO terms associated with up-regulated genes can be more directly related to MMVD such as the previously mentioned extracellular space.

IPA analysis in this study (section 6.3.7), as with the previous chapters, gave insight into the underlying mechanisms responsible for the gene changes observed. Canonical pathway analysis showed that in TGFβ1-treated qVICs differentially expressed genes were most associated with the *Hepatic fibrosis/hepatic stellate cell activation*. This is in agreement with the results obtained in the tissue analysis (Chapters 3-5) and as discussed earlier, can be related to the activation of TGFβ1 signalling[184]. As such, this helps to add credence to the hypothesis that TGFβ1 signalling is being activated in MMVD. In support of the GO term analysis, canonical pathway analysis of the genes differentially expressed in aVICs compared to qVICs showed that the majority of the top associated pathways were involved in cell proliferation, again supporting the view that the aVICs have a more proliferative phenotype than qVICs[45, 113]. Both the differentially expressed genes in aVICs treated with SB431542 and the shared differentially expressed genes in aVICs compared to qVICs and qVICs treated with TGFβ1 were associated with cholesterol biosynthesis related pathways in canonical pathway analysis. Although these pathways have not previously been directly implicated in MMVD there is some evidence that TGFβ1 can play a role in cholesterol synthesis in keratinocytes[311]. However, what role this may play in MMVD development, if any, remains unclear.

Upstream regulator analysis, as expected, suggested the activation and inhibition of TGFβ1 signalling as being the most important pathway involved in the differentially expressed genes in the TGFβ1-treated qVICs and SB431542-treated aVICs respectively. This suggests that the other forms of gene enrichment analysis performed on these datasets are looking at the effects of changes in TGFβ1 signalling. This finding is particularly important in the SB431542-treated aVICs as this it inhibits TGFβRI kinase and so the gene changes related to this could be through signalling of TGFβ1-3 as well as potentially activin and nodal but not the BMP[307, 308]. These results suggest however that the gene changes caused by SB431542 treatment are due to inhibition TGFβ1 related canonical SMAD2/3 signalling specifically. Additionally, in the TGFβ1-treated qVICs analysis, TNF is the second upstream regulator associated with these genes, as was the case in Chapter 3. This further supports the view that TNF is identified as it shares many downstream targets with TGFβ1 and not because it is directly involved in disease pathogenesis.

Genes differentially expressed between aVICs and qVICs were associated primarily with pathways involved in the down-regulation of apoptotic pathways. This is an interesting finding as there is a narrative in the literature for the role of anti-apoptosis in MMVD, and specifically in aVICs[45, 126]. aVICs in normal circumstances, such as wound healing, would undergo apoptosis after injury had been resolved [177]. However, it has been suggested that in a chronic condition, such as MMVD, this apoptosis may not happen and aVICs are allowed to persist in the valve[45]. There is evidence for this in tissue with an increase in interstitial cells as the disease progresses, but only a moderate increase in KI-67, as well as evidence to show apoptosis is undertaken, but not completed in MMVD, and that this effect is under the control of TGFβ1[43, 126].

The data here seems to support these reports and further investigation of apoptosis in MMVD is warranted.

Upstream analysis showed that the genes sharing differential expression in aVICs and qVICs treated with TGFβ1 were associated with both TNF and TGFβ1. However, TGFβ1 showed activation as opposed to inhibition of TNF. This implies there is a positive role for TGFβ1 signalling not only in the qVICs treated with TGFβ1 but also in the aVICs isolated from naturally occurring diseased valves, further supporting TGFβ1 role in disease pathogenesis.

Network analysis of the top disease and functions associated with the genes differentially expressed in the qVICs treated with TGFβ1 and aVICs treated with SB431542 are pathways involved in cardiovascular disease. This indicates that gene changes induced by TGFβ1 signalling in these samples also play a role in cardiovascular disease. The genes differentially expressed in aVICs compared with qVICs were associated, similarly to previous analysis, with cell cycle-related disease and functions. The majority of the components were found to be upregulated, and as previously discussed this supports the role for a proliferative phenotype of aVICs in MMVD[45]. Analysis of the genes shared between aVICs compared to qVICs and qVICs treated with TGFβ1 showed a number of relevant disease and functions. The top disease and function biological terms included *cell morphology, cardiovascular disease* and *development disorder* these would appear relevant to MMVD where morphological changes in qVICs differentiating to aVICs, and reactivation of developmental pathways such as EndoMT are cardinal features of the disease [2, 43, 57]. Other interesting and potentially relevant disease and functions related shared group of genes found with *cell death and survival* and *cellular growth and proliferation*. These can both be linked to previous analyses implicating anti-apoptotic signalling and cell proliferation in MMVD pathogenesis. The fact

that these pathways can be associated with genes found in both spontaneously activated VICs and qVICs treated with TGFβ1 further implicates the role of TGFβ1 in MMVD.

The transcriptomic analysis showed that treatment of qVICs with TGFβ1, for only 72 hours, induces an aVIC-like transcriptomic phenotype. Conversely, inhibition of TGFβ signalling with SB431542 in aVICs, for 96 hours, reduces the expression of genes that are involved in the aVIC phenotype and disease-related processes. Comparison of aVICs to qVICs indicated a role for proliferative and anti-apoptotic pathways in disease, something which has been previously speculated in the literature[43, 45, 126]. However, when analysing the shared differentially expressed genes in aVICs and qVICs treated with TGFβ1, a role for TGFβ1 signalling in spontaneously occurring aVICs was found.

RT-qPCR validated 28 out of 30 the gene changes occurring in the microarray data, despite the lack of FDR correction (section 6.3.9). In addition, morphological analysis and proteoglycan deposition indicated that TGFβ1 treatment induced an aVIC phenotype in qVICs and SB431542 treatment attenuated the aVIC phenotype (section 6.3.10). This indicates that the gene changes analysed in this study relate to tangible changes in phenotype which are associated with MMVD, further establishing the role for TGFβ1 signalling in disease.

Comparison between aVICs and qVICs showed the increased gene expression of the hallmarks aVIC phenotype (*ACTA2*, *TAGLN* and *MYH10*) was detected both by microarray and RT-qPCR. *MYH10* expression was not significantly altered by treatment of either the qVICs or aVICs. This result is of interest given the sub-populations of aVIC (αSMA+, SMemb+ and αSMA/SMemb+)

described in canine MMVD valves (Chapter 1 section1.3.2)[2, 43, 110]. These results suggest either *MYH10* expression is induced by another factor, other than TGFβ1, involved in activation of VICs and disease progression, or *MYH10* expression is altered later in the phenotypic change of VICs. It has been postulated that the co-expression of *α*SMA and SMemb is indicative of a heightened differentiation state and so possibly the result of a later phenotypic change in these cells[2, 110]. Furthermore, aVICs which co-express *α*SMA and SMemb have been shown to express 5HT to a greater extent than the other aVIC sub-populations[43]. If this occurs in late-stage disease, it suggests the increased 5HT expression is primarily a result of heightened TGFβ signalling.

Interestingly, *HTR2B* expression was significantly altered, in both microarray and RT-qPCR analysis, in treatment groups, with increased expression in qVICs treated with TGFβ1 and down-regulation in aVICs treated with SB431542, as well as by RT-qPCR in aVICs. These novel findings indicate that the expression of *HTR2B* is under the control of TGFβ1 signalling. This is important as the up-regulation of *HTR2B* expression in canine disease has been used to support the hypothesis that 5HT signalling is responsible for MMVD pathogenesis[71, 133, 170-172]. However, in this study, when investigating the direct effect of 5HT signalling on qVICs, no significant changes in the expression of *ACTA2*, *TAGLN*, *MYH10* or *HTR2B* was detected at 4 or 7 days as well as no change in proteoglycan secretion after 7 days (section 6.3.11). Additionally, the use of the 5HTR2B antagonist LY272015 on aVICs did not induce a reduction of these genes, which would be indicative of a reversion in phenotype. Instead, an increase in *MYH10* was seen on day 7 and *HTR2B* on days 4 and 7. No significant change in proteoglycan deposition was detected at day 7 with the use of LY272015. These results contrast with the results obtained when investigating TGFβ1 signalling implying that at least in short-

term culture TGFβ1 has more relevance as the inducer of MMVD. Additionally, these results contrast with a report where LY272015 induced a trend for reduction in *HTR2B* and *ACTA2* expression in canine *ex vivo* valves in a dynamic culture, and partially block valve remodelling in mice[171]. No publications have looked at the effect of 5HT on canine qVIC phenotype *in vitro*. It has been suggested that 5HT could be signalling through 5HTR2B to induce greater expression of TGFβ1, causing autocrine signalling and activation of VICs[133]. 5HT has been shown to induce greater expression of TGFβ3 in avian embryonic hearts[169] but whether or not this happens in canine VICs is yet to be elucidated and warrants future research. Regardless of the potential role that 5HT may have in MMVD the results presented here, along with the data from previous chapters show a clear role for TGFβ1 signalling in MMVD. Additionally, inhibition of this pathway can result in some reversion of phenotype *in vitro* indicating that targeting TGFβ signalling may be of therapeutic value in future (see Chapter 7).

In conclusion, this study aimed to investigate the role of TGFβ1 signalling in VICs *in vitro*. Using optimised cell culture techniques the secretion of various factors implicated in disease was assessed, the effect of exogenous TGFβ1 on qVICs and TGFβ signalling inhibition was investigated through transcriptomic profiling, RT-qPCR, whole cell morphology and proteoglycan deposition, and the effect of 5HT signalling were also examined. The results support a role for TGFβ1 signalling in the development of the phenotypic changes and activation of VICs that are associated with MMVD.

Summary:

- TGFβ1 was secreted from both qVICs and aVICs in greater quantities than TGFβ2 and 3, with a significant increase of secretion found between qVICs and aVICs after 5 days
- TGFβ1 treatment of qVICs induced an aVIC phenotype after 3 days of treatment
- SB431542 treatment of aVICs helped attenuate the aVIC phenotype and reduce association with MMVD traits
- 5HT signalling, at least in short-term culture, does not appear to be able to induce an aVIC phenotype in qVICs

This study succeeded in its aim to investigate the role of TGFβ1 signalling in VICs *in vitro*. The data reported here support the results in previous chapters indicating a central role for TGFβ1 signalling in MMVD pathogenesis and that the partial attenuation of the spontaneously developed aVIC phenotype is therapeutically possible.

Chapter 7 Final conclusions and future prospective

7.1 Overview of the results

This project aimed to improve the understanding of the overall pathogenesis of canine MMVD. It was hypothesised that clear and discernible changes in gene expression will occur dependent on the Whitney grade of the disease and will be related to MMVD development. A primary focus was establishing what pathways were likely to be causal in disease progression, as this was lacking in previous studies. To achieve this aim and answer the hypothesis, transcriptomic analysis was performed on valves spanning the entire pathogenesis of disease (Whitney grade 0-4; Chapter 3 and 4), as well as early (Whitney grade 2) diseased valves that had been dissected into overtly diseased and normal regions (Chapter 5). Collectively these analyses, alongside various other findings, indicated a central role for TGFβ1 signalling in both early and late-stage disease. The TGFβ1 signalling pathway was then interrogated further *in vitro* (Chapter 6). TGFβ1 was shown to activate qVICs leading to the acquisition of a MMVD-like phenotype, and inhibition of canonical downstream SMAD2/3 signalling, using a TGFβRI kinase inhibitor in aVICs, was shown to attenuate this phenotype. This project has therefore succeeded in its goal in confirming the primary pathway that is important in the overall pathogenesis of the disease.

The consistent finding that TGFβ1 signalling was involved in MMVD development was not wholly unexpected, as previous studies (detailed in Chapter 1 section 1.5.1) have shown it to play a role in the activation of qVICs into aVICs. In addition, it has been shown that there is up-regulation of TGFβ1 protein and increased phosphorylation of downstream signalling components such as SMAD2/3, ERK1 and ERK2 suggestive of increased TGFβ1 signalling

in diseased valve tissue[43, 45, 60, 71, 124, 126, 133, 174-176]. In human transcriptomic analysis, TGFβ2 has been implicated in the changes in gene expression associated with disease valves as well as the TGFβ superfamily member BMP4[125, 131, 163]. Likewise, the two previous microarray studies performed in the dog found some gene expression changes that were indicative of upstream TGFβ signalling, for example BMP6 and endoglin[33, 150]. However, these studies had focused on comparing normal and late-stage disease so could not evaluate TGFβ signalling's role in MMVD initiation and progression.

Whole valve analysis of Whitney grade 1 and 2 valves (Chapter 3) did not show the anticipated early disease-related gene expression changes sufficient for meaningful downstream analysis and causal pathway identification when analysed on a by-grade basis. However, valuable insights were still gained when considering the level of expression of genes that showed significant differential expression in at least one grade of disease. This analysis showed that the small changes in expression detected in early disease, altered progressively throughout the disease process until ultimately this lead to the more significant changes detected in the latter grades of MMVD. This highlighted that several of the GO pathways (such as metalloendopeptidase activity, ERK1 and ERK2 cascade and heart development) that were seen in later disease, were also enriched over the entire progression of disease.

To further understand the role of differential gene expression, a study of MMVD in CKCS, a breed predisposed to the early onset disease, was undertaken (Chapter 4). Data presented in Chapter 4 indicates that enhanced or altered prothrombin, muscle contractility and calcium signalling (possibly the result of 5HT signalling through 5HTR2B) potentially might be involved in the predisposition to early MMVD development in CKCS. These results also suggest that dysfunctional platelets, which is a common disorder in CKCS,

may also be involved in early disease development in this breed through enhanced 5HT signalling [225-227].

Examining the molecular basis of early disease pathogenesis was revisited in Chapter 5 with the use of valvular dissection. This was shown to be a valuable approach as it allowed for the identification of genes that are associated with early disease-related pathways while using a high stringency statistical cut-off (FDR), and thereby improving on the Grade 1 and 2 data presented in Chapter 3. Additionally, evidence was found that the normal regions of the valve do not have disease-related gene changes and that the disease-related changes are localised to the overtly abnormal regions of these valves. The study found that the overtly diseased regions of Whitney grade 2 valves shared differential expression of genes and pathways that were also seen in the late grade whole valves, albeit showing lower fold changes than in late-stage disease. This fold difference is interesting as it suggests a linear relationship between gene expression and the severity of the disease.

A final experimental approach used in this study was to explore gene expression in cultured cells isolated from diseased and normal valves. The downstream analysis presented in Chapter 6 allows for further understanding of TGFβ1 signalling in MMVD. In agreement with previous accounts in other species TGFβ1 was able to induce the aVIC-like phenotype in qVICs and, supporting the role for this phenotype in disease, both the spontaneously derived aVICs and the TGFβ1-treated qVICs shared downstream signalling events which are important in the development of MMVD such as extracellular matrix deposition[45, 60, 85, 117]. Inhibition of the TGFβRI kinase, and subsequent canonical SMAD2/3 signalling indicated that this downstream signalling pathway and the ensuing gene expression changes are important for the MMVD-related biological functions seen in these cells. This

corroborates observations in human MMVD tissue[176]. However, in the timescale of these *in vitro* inhibitor experiments there was only a partial attenuation of the aVIC phenotype indicating that the role of other signalling pathways cannot be excluded. This includes the role of ERK1 and ERK2 cascade (a non-canonical signalling pathway downstream of TGFβ1 and other factors) that was consistently associated with up-regulated genes in tissue in this project (Chapter 3), a finding that has been reported in other canine and human valves studies[133, 168, 171, 173]. Interestingly, as discussed in Chapter 6 section 6.4, ERK1 and ERK2 cascade was associated with down-regulated genes in TGFβ1-treated qVICs from normal valves. However, this may be indicative of transient activation of this pathway and a resultant negative feedback loop in the normal repair process, rather than reflecting chronic signalling in disease. Other pathways such as 5HT signalling may also be activating the ERK1 and ERK2 cascade, which has been reported previously in MMVD. However, 5HT-treated qVICs and 5HTR2B antagonism in aVICs indicated, at least in the confines of the *in vitro* system utilised here, that this pathway on its own is not capable of inducing the MMVD phenotype. These findings do not eliminate 5HT signalling's potential involvement in late-disease progression, but further studies are required to elucidate its role.

7.2 Integration of transcriptomic analysis

To explore microarray datasets further, comparisons (as described in Chapter 2 section 2.6.4) of the differentially expressed genes in the diseased dissected regions to the Whitney grade 4 valves or the Whitney grade 2 valve set were performed. This analysis is summarised in **Figure 7-1** and **Figure 7-2**. Eleven and 75 genes were shared in the dissected diseased regions and the whole Whitney grade 2 and 4 valve analysis respectively. Seven of the 11 shared genes (**Appendix V: Table S1**) in the Whitney grade 2 dissected and whole

valves shared up- or down-regulation, whereas 42 and 23 genes shared up-or down-regulation with the grade 4 valves respectively. The 42 shared up-regulated genes could be attributed to 26 GO terms in DAVID analysis with the top ten shown in (**Appendix V: Table S2**). These include pathways which were implicated in late-stage disease (Chapter 3), such as neutrophil chemotaxis, extracellular space, integrin binding and positive regulation of ERK1 and ERK2 cascade. This analysis indicated that the gene expression changes occurring in diseased regions of early-stage disease were similar to those present in late-stage disease.

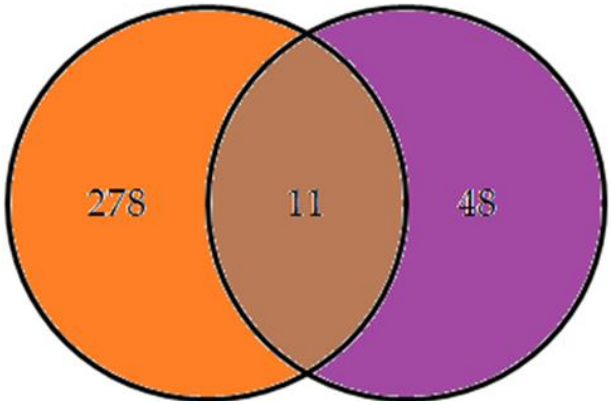

Figure 7-1. Venn diagram illustrating the number of shared differentially expressed genes in diseased dissected regions of Whitney grade 2 valves and whole Whitney grade 2 valves. In the left orange circle, the number of differentially expressed genes for diseased dissected regions not shared with whole Whitney grade 2 valves is shown. In the right purple circle, the number of differentially expressed genes for whole Whitney grade 2 valves not shared with dissected diseased regions of valves is shown. In the centre, the number of shared genes between the two datasets is shown.

Figure 7-2. Venn diagram illustrating the number of shared differentially expressed genes in diseased dissected regions of Whitney grade 2 valves and whole Whitney grade 4 valves. In the left orange circle, the number of differentially expressed genes for diseased dissected regions not shared with whole Whitney grade 4 valves is shown. In the right purple circle, the number of differentially expressed genes for whole Whitney grade 4 valves not shared with dissected diseased regions of valves is shown. In the centre, the number of shared genes between the two datasets is shown.

Further informative dataset comparisons were made by considering the microarray analysis performed on the TGFβ1-treated qVICs. Comparisons of these treated cells to the diseased regions of dissected Whitney grade 2 valves or to the whole Whitney grade 4 valves (**Figure 7-3** and **Figure 7-4** respectively) showed a relatively small number of gene cross-over between the valve and cell datasets. However, the majority of the shared genes showed similar up- or down-regulation trends and GO term analysis (**Appendix V: Tables S3-5)** of the genes up-regulated in grade 4 valves and TGFβ1-treated qVICs showed many terms related to MMVD. These GO terms included extracellular space/matrix as well as terms such as regulation of cell proliferation. This analysis directly associates *in vitro* TGFβ1 treatment with several characteristics involved in the development of disease in tissue. This also

substantiates the cell proliferation findings in the aVIC phenotype analysis in Chapter 6 in MMVD development of tissue as well.

Examining the genes that have differential expression, but do not show similar up- or down-regulation can also give some informative perspectives. For example, pre-microRNA 214 is up-regulated in TGFβ1-treated qVICs, but down-regulated in Whitney grade 4 valves. This is of interest as this microRNA plays a role in the development of fibrosis and its antagonism helps halt fibrosis developing in the kidney[312]. TGFβ signalling is a powerful inducer of fibrosis and up-regulation of pre- microRNA 214 suggest fibrotic pathways may be being induced in this *in vitro* system. In contrast, and although a fibrotic response is observed in human MMVD, this is absent in the canine disease[1, 2, 84]. This warrants future study as to the role of microRNA 214 in the tissue and cell culture response.

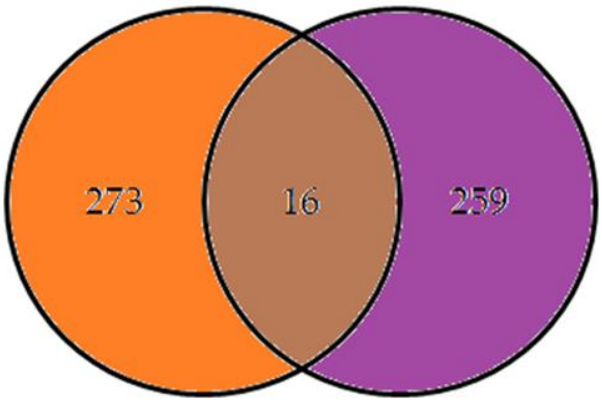

Figure 7-3. Venn diagram illustrating the number of shared differentially expressed genes in diseased dissected regions of Whitney grade 2 valves and TGFβ1-treated qVICs. In the left orange circle, the number of differentially expressed genes for diseased dissected regions not shared with TGFβ1-treated qVICs is shown. In the right purple, circle the number of differentially expressed genes in TGFβ1-treated qVICs not shared with dissected diseased regions of valves is shown. In the centre, the number of shared genes between the two datasets is shown.

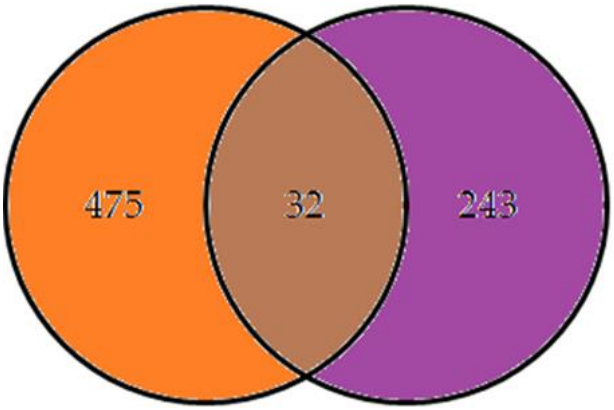

Figure 7-4. Venn diagram illustrating the number of shared differentially expressed genes in Whitney grade 4 valves and TGFβ1-treated qVICs. In the left orange circle, the number of differentially expressed genes for diseased dissected regions not shared with Whiney grade 4 valves is shown. In the right purple circle the number of differentially expressed genes TGFβ1-treated qVICs not shared with Whitney grade 4 valves is shown. In the centre, the number of shared genes between the two datasets is shown.

7.3 A model for the initiation and development of MMVD

The results presented in this project strongly suggest a central role for TGFβ1 signalling in all dogs with MMVD and that this signalling pathway controls various key aspects of the disease process. In culture, TGFβ1 was secreted into the extracellular matrix at a greater level than its sub-family members in the *in vitro* ELISA analysis in Chapter 6, consistent with results previously reported in the literature[174]. However, how the latently secreted form of TGFβ1 is activated in the valve to initiate disease progression remains uncertain. As discussed in Chapter 1 section 1.5.1, various conditions and factors can activate latent TGFβ1, with many of these occurring or present in the normal mitral valve. This includes stretch, tensile and shear stress, reactive oxygen species, thrombospondin, thrombin and 5HT signalling[169, 172, 179, 180, 205, 290]. Within the general population of the dog, it is likely that a combination of these

factors induces initial TGFβ1 signalling. Activation may then become sustained and pathological, due to higher or chronic secretion and accumulation of latent TGFβ1 from aVICs (Chapter 6), the increased proliferation and reduced apoptotic capability of aVICs (Chapters 3 and 6), alteration of the extracellular matrix composition by aVICs (Chapters 3-6) and/or persistent aberrant signalling during the natural ageing process. For predisposed breeds results presented in Chapter 4 support a role for the enhancement of one or more of the latent TGFβ1 activating agents (in the case of CKCS this could be through prothrombin and 5HT signalling) resulting in the early development of the disease. Platelet dysfunction and dysregulated calcium signalling could also be involved in the CKCS predisposition (Chapter 4). While the trigger for TGFβ1 signalling in MMVD remains speculative, identifying it as the major pathway in disease progression is of major benefit, especially in terms of identifying future therapeutic approaches to this disease.

It appears likely that many of the GO terms, canonical pathways and disease and functions suggested in the microarray gene analysis are consequent of TGFβ1 signalling being initiated. This includes pathways such as proteinaceous extracellular matrix, *hepatic fibrosis/hepatic stellate cell activation* and extracellular matrix/space. Not only are many of these pathways suggested after TGFβ1 treatment of qVICs (Chapter 6), but have also been shown in the literature to be a consequence of the aVIC phenotype and TGFβ1 signalling[46, 56, 142, 174, 179, 313]. In addition, developmental pathways (indicating EndoMT) seemed to be isolated to grade 3 and 4 valves (Chapter 3 section 3.3.7). This suggests that EndoMT is only present in later disease, and so is consequential to initial VIC activation and TGFβ1 signalling. However, as many of the genes involved in EndoMT (such as HAS2 and CD31) did not

show differential expression in any of these datasets further investigation into what grade of disease EndoMT occurs in is warranted.

Some pathways, as highlighted in section 7.1, could also be a result of other signalling mechanisms being activated in the valve such as the ERK1 and ERK 2 cascade (possibly triggered by 5HT signalling) or immune cell-mediated inflammatory/immune response. Nevertheless, the identification of these pathways throughout pathogenesis of the disease is of interest, both in understanding the disease process and identifying targets that may be useful for future therapeutic approaches.

Likewise, the finding that gene expression changes that occur in diseased regions of early and late stages of disease are ostensibly the same (section 7.2) is of interest. This suggests that the disease progresses through the spread of these changes in gene expression from the early nodules to the entire valve, rather than through changes in expression of different sets of genes over the disease course. This particular finding is of importance when considering the development of new therapeutics as it means that a drug that targets one of these important causal pathways could work at any stage of the disease. A proposed model for MMVD development derived from the results of this project and the relevant literature cited throughout the thesis is shown in **Figure 7-5**.

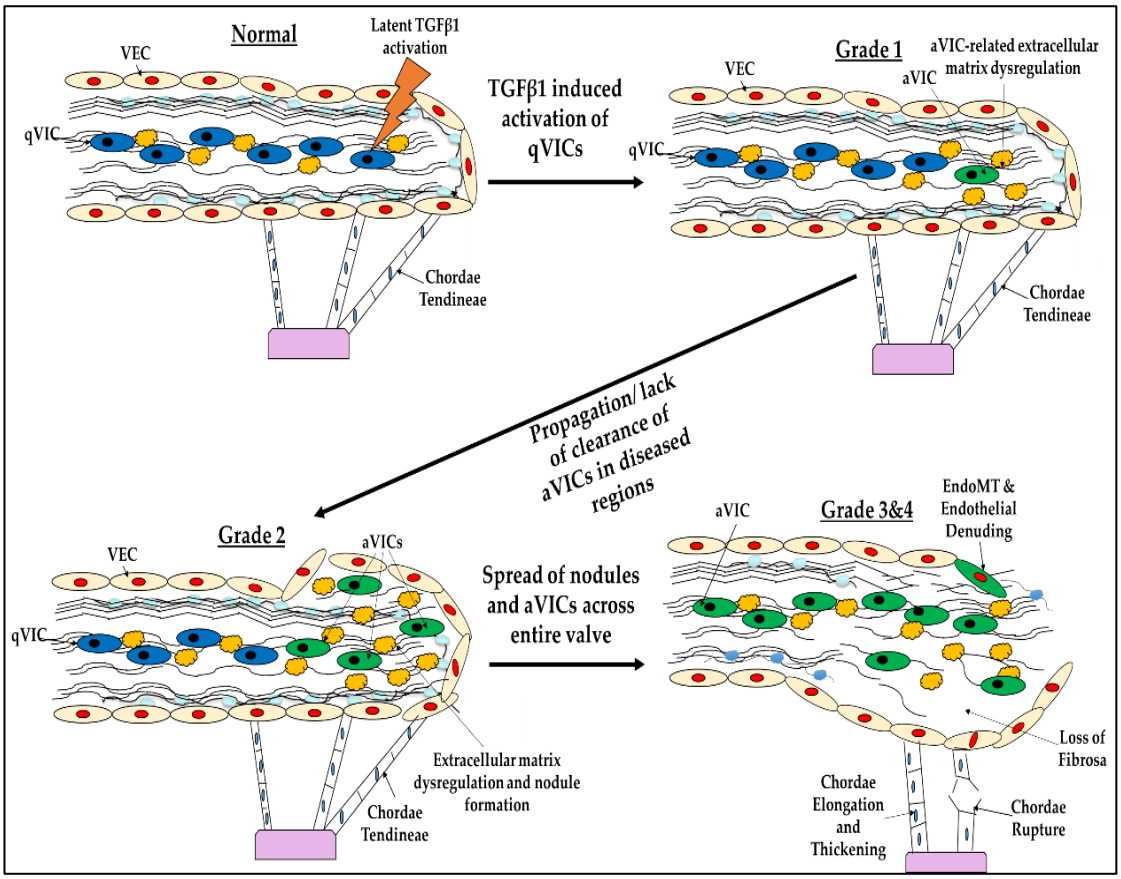

Figure 7-5. Proposed general model for MMVD progression. Initiation of MMVD is induced by latent TGFβ1 activation causing activation of a small number of aVICs, these then propagate as the disease progresses through Whitney grades resulting in deterioration of the valve and end-stage disease.

7.4 Proposals for future research

Although this project was able to give a range of insights into the pathogenesis of MMVD, both in tissue and *in vitro*, there are various aspects of the disease that remain unexplored, as well as new questions generated from the data presented here, in part because of the limitations of the approaches used. Suggestions for additional research that could overcome these issues and further elucidate the molecular pathogenesis of the disease in both humans and dogs are outlined below.

Transcriptomic analysis with microarrays has provided a very useful resource that allows for a broad base of knowledge to be generated and new hypotheses to be developed. However, as discussed in Chapter 2 section 2.1, the technology, although robust, more amenable to analyse and cheaper than similar alternatives, cannot give the depth of detail that using a technique such as RNA-seq could[264]. Using RNA-seq in this project would have led to similar conclusions to those presented here (since validation by qRT-PCR indicated that the expression microarray data were a robust quantification of gene expression), yet may have given greater insights into the underlying mechanisms occurring in disease development, especially when considering the breed specific changes in CKCS presented in Chapter 4. RNA-seq would have given information of any transcript variants (arising for example from alternative splicing or different promoter usage) specific to CKCS compared to other breeds that could have supported the propositions that altered calcium signalling, prothrombin or contractile related pathways are important in CKCS predisposition for MMVD. In this regard, as mentioned in Chapter 4 section 4.4, further research into the role these pathways play in early MMVD development in CKCS, especially into activation of latent TGFβ1, is needed, as well as more comprehensive histological comparison of normal CKCS valves to normal other breed valves, to establish if there are any differences between breeds.

Transcriptomic analysis by any method is limited as it only examines the level of RNA expression, which can be used to infer but not confirm active protein levels and the functional consequences of any changes. Limited proteomic studies have been performed in both the dog and human, with both ultimately indicating that the major proteomic changes occurring in MMVD, unsurprisingly, are related to the extracellular matrix and the increased

presence of proteoglycans and GAGs (supporting the findings in this thesis)[51, 140]. Having now established pathways of interest through the transcriptomic analysis, future research should have a focus on establishing the downstream signalling events in these pathways.

Downstream signalling events can be elucidated in tissue through the analysis of gene and protein expression and localisation by *in situ* hybridisation and immunohistochemistry respectively. However, interrogation of these pathways is perhaps best achieved *in vitro* primarily because of the reproducibility of results and the ability to interfere with specific pathways in question. This was shown in Chapter 6, with these results indicating that further interrogation of the downstream signalling events of TGFβ1 signalling in VICs, and the potential role of anti-apoptotic pathways and cellular proliferation, is warranted. However, there are a number of limitations to the *in vitro* system presented in Chapter 6. In a 2D static mono-culture system, the cell environment contrasts greatly with that *in vivo*. This will not only affect cell phenotype but also how these cells react to stimuli, such as TGFβ1 which, as discussed in Chapter 1 section 1.5.1, is known to produce highly context-specific signalling[178, 179]. Although the results presented in Chapter 6 did indicate the important role TGFβ1 signalling plays in VIC activation in a culture system, it was not able to completely recapitulate all events seen in the tissue analysis. This includes the failure to detect changes in the expression of microRNA 214, ADAMTS and MMPs (ADAMTS5, ADAMTS9 and MMP12), which are thought to play an important role in disease. These discrepancies may be due to the monoculture of VICs in the absence of VECs or the lack of a suitable 3D extracellular environment which may be simulated in culture with the use of fibrin or polyethylene based hydrogels[314-316]. A 3D extracellular environment alongside low serum culture conditions helps maintain the qVIC

phenotype [314-316]. Likewise, it has been shown that important reciprocal signalling occurs between VECs and VICs [42, 93]. With the adoption of a 3D co-culture, a better understanding of the signalling events downstream of TGFβ1 could be elucidated in comparison to 2D culture. Tensile strain or shear stress could also then be employed to these 3D valve models to investigate what role these may play in the initiation or sequestering of MMVD related pathways.

In addition to giving insights into the molecular mechanisms behind disease development, an *in vitro* model could be used in the testing and application of new therapeutics which are currently lacking in both human and canine MMVD treatment[244]. These could come in the form of drugs that specifically target downstream aspects of the TGFβ1 signalling pathway or the myofibroblastic aVIC cell population. Regardless of how TGFβ1 signalling is triggered initially in MMVD, its role throughout disease pathogenesis is clear and the partial attenuation of aVIC phenotype in Chapter 6 should not go understated. The use of drugs such as SB431542, however, is not suitable as TGFβ1 plays various important roles throughout the body and its global inhibition would cause serious side effects. If a system of delivery could be directed specifically to the mitral valves, this might prove very useful for the future therapeutic treatment of MMVD. Drug targeting of more unique receptors on myofibroblasts, such as platelet-derived growth factor receptors (PDGFR-β in the mitral valve), integrins, mannose-6-phosphate/insulin-like growth factor-II receptor, FAP (up-regulated in aVICS and TGFβ1-treated qVICS in Chapter 6) or retinol binding protein receptor might be feasible[317]. Receptor-recognizing peptides, for example PDGFR-β recognizing peptide, or antibodies may be coupled via linkers or carriers to a drug-like small molecule TGFβRI kinase inhibitor (such as SB431542) to improve drug pharmacological stability, specificity and delivery *in vivo*. Targeting and eliminating aVICs

specifically could be another way to treat MMVD. Biosurfactant di-rhamnolipid has been shown to target myofibroblasts preferentially to fibroblasts in skin *in vitro* and *in vivo*, with limited toxicity to surrounding cells, hence aiding the reduction of scar formation[318]. Future research goals could include investigations into pharmaceutical approaches such as these to provide a discrete effect on TGFβ1 signalling or aVICs.

Likewise, the *in vitro* platform could give insights into the mechanisms of action of the limited number of current therapeutics in the dog, such as pimobendan and spironolactone. It has recently been indicated that both these drugs can potentially slow the progress of canine MMVD[35, 260, 261]. This may be through their compensatory action on heart muscle contractility, which itself may implicate biomechanical stresses in MMVD development, but also could potentially be due to a direct effect of these drugs on the valve cells themselves. By treating cells *in vitro* with the active metabolites of these drugs it can be assessed if they have an effect on cell phenotype or extracellular matrix production. Additionally, as suggested in Chapter 4 section 4.4, the possible effects the drugs could have on different breeds (such as the CKCS) could be investigated. This could then help inform future treatment strategies including whether these drugs should be given earlier in MMVD development.

Beyond these proposals, further objectives could aim to examine in greater detail the differences and similarities between canine and human MMVD. This includes the predisposition for the development of fibrosis in human valvular disease but not in canine disease, which could lead to wider reaching understanding of fibrotic diseases as a whole[1]. A major issue in human MMVD research is the lack of both normal and early disease samples. As shown in Chapter 5, the dog offers a more readily available source of early diseased valves which can give insights into early disease pathogenesis. Also,

long-term longitudinal imaging and biomarker studies could be performed on a cohort of dogs to provide vital information into the changes that may occur during the induction of MMVD. In gaining a greater comparative understanding of the disease, therapeutics tested *in vitro* could then be further developed *in vivo* in the dog before testing in humans. This would serve as an efficient drug development model, as opposed to using a model species where the disease has to be induced experimentally, with both species benefitting from such an approach.

7.5 Conclusion

This study of MMVD using both tissue specimens and cells isolated from normal and diseased valves has highlighted the essential role of the TGFβ1 signalling pathway in the initiation and progression of the disease. Further work is required to elucidate the precise mechanisms by which TGFβ1 acts and the causes of the initial dysregulation of TGFβ1 levels. This study opens the way for the development of drugs targeted to the mitral valve for the amelioration or prevention of this devastating disease, both in dogs and potentially in humans.

References

1. Markby, G.R., K.M. Summers, V.E. MacRae, and B.M. Corcoran, Comparative transcriptomic profiling and gene expression for myxomatous mitral valve disease in the dog and human. *Vet Sci*, 2017. **4**(3): 34.

2. Markby, G., K.M. Summers, V.E. MacRae, J. Del-Pozo, and B.M. Corcoran, Myxomatous degeneration of the canine mitral valve: from gross changes to molecular events. *J Comp Pathol*, 2017. **156**(4): p. 371-383.

3. Buchanan, J.W., Chronic valvular disease (endocardiosis) in dogs. *Adv Vet Sci Comp Med*, 1977. **21**: p. 75-106.

4. Whitney, J.C., Observations on the effect of age on the severity of heart valve lesions in the dog. *J Small Anim Pract*, 1974. **15**(8): p. 511-22.

5. Davies, M.J., B.P. Moore, and M.V. Braimbridge, The floppy mitral valve. Study of incidence, pathology, and complications in surgical, necropsy, and forensic material. *Br Heart J*, 1978. **40**(5): p. 468-81.

6. Guthrie, R.B. and J.E. Edwards, Pathology of myxomatous mitral-valve - nature, secondary changes and complications. *Minnesota Medicine*, 1976. **59**(9): p. 637-647.

7. Read, R.C. and A.P. Thal, Surgical experience with symptomatic myxomatous valvular transformation (the floppy valve syndrome). *Surgery*, 1966. **59**(1): p. 173-182.

8. Read, R.C., A.P. Thal, and V.E. Wendt, Symptomatic valvular myxomatous transformation (the floppy valve syndrome). A possible forme fruste of the Marfan syndrome. *Circulation*, 1965. **32**(6): p. 897-910.

9. Whitney, J.C., Cardiovascular pathology. *J Small Anim Pract*, 1967. **8**(8): p. 459-465.

10. Pedersen, H.D. and J. Haggstrom, Mitral valve prolapse in the dog: a model of mitral valve prolapse in man. *Cardiovasc Res*, 2000. **47**(2): p. 234-243.

11. Pomerance, A. and J.C. Whitney, Heart valve changes common to man and dog . A comparative study. *Cardiovascular Research*, 1970. **4**(1): p. 61-67.

12. Lester, W.M., A.A. Damji, M. Tanaka, and I. Gedeon, Bovine mitral valve organ culture: role of interstitial cells in repair of valvular injury. *J Mol Cell Cardiol*, 1992. **24**(1): p. 43-53.

13. Rausch, M.K., W. Bothe, J.P. Kvitting, S. Goktepe, D.C. Miller, and E. Kuhl, In vivo dynamic strains of the ovine anterior mitral valve leaflet. *J Biomech*, 2011. **44**(6): p. 1149-1157.

14. Lester, W.M., A.A. Damji, I. Gedeon, and M. Tanaka, Interstitial cells from the atrial and ventricular sides of the bovine mitral valve respond differently to denuding endocardial injury. *In Vitro Cell Dev Biol*, 1993. **29A**(1): p. 41-50.

15. Sacks, M.S. and A.P. Yoganathan, Heart valve function: a biomechanical perspective. *Phil Trans of the Royal Soc B-Biol Sci*, 2007. **362**(1484): p. 1369-1391.

16. Cui, Y.C., K. Li, Y. Tian, W.M. Yuan, P. Peng, J.Z. Yang, B.J. Zhang, H.D. Zhang, A.L. Wu, and Y. Tang, A pig model of ischemic mitral regurgitation induced by mitral chordae tendinae rupture and implantation of an ameroid constrictor. *PLoS One*, 2014. **9**(12): e111689.

17. Dupuis, L.E., D.R. McCulloch, J.D. McGarity, A. Bahan, A. Wessels, D. Weber, A.M. Diminich, C.M. Nelson, S.S. Apte, and C.B. Kern, Altered versican cleavage in ADAMTS5 deficient mice; a novel etiology of myxomatous valve disease. *Dev Biol*, 2011. **357**(1): p. 152-164.

18. Kern, C.B., A. Wessels, J. McGarity, L.J. Dixon, E. Alston, W.S. Argraves, D. Geeting, C.M. Nelson, D.R. Menick, and S.S. Apte, Reduced versican cleavage due to Adamts9 haploinsufficiency is associated with cardiac and aortic anomalies. *Matrix Biology*, 2010. **29**(4): p. 304-316.

19. Pensinger, R.R., Comparative aspects of mitral valve disease in dogs. *Annals of the New York Academy of Sciences*, 1965. **118**(A10): p. 525-534.

20. Delling, F.N. and R.S. Vasan, Epidemiology and pathophysiology of mitral valve prolapse new insights into disease progression, genetics, and molecular basis. *Circulation*, 2014. **129**(21): p. 2158-2170.

21. Barlow, J.B. and W.A. Pocock, The significance of late systolic murmurs and mid-late systolic clicks. *Md State Med J*, 1963. **12**: p. 76-87.

22. Connell, P.S., R.I. Han, and K.J. Grande-Allen, Differentiating the aging of the mitral valve from human and canine myxomatous degeneration. *J Vet Cardiol*, 2012. **14**(1): p. 31-45.

23. Darke, P.G.G., Valvular Incompetence in Cavalier King Charles Spaniels. *Veterinary Record*, 1987. **120**(15): p. 365-366.

24. Beardow, A.W. and J.W. Buchanan, Chronic mitral valve disease in cavalier King Charles spaniels: 95 cases (1987-1991). *J Am Vet Med Assoc*, 1993. **203**(7): p. 1023-1039.

25. Haggstrom, J., H.D. Pedersen, and C. Kvart, New insights into degenerative mitral valve disease in dogs. *Vet Clin N Am-Sm Ani Prac*, 2004. **34**(5): p. 1209-1226.

26. Hamlin, R.L., A.M. Benitz, G.F. Ericsson, S. Cifelli, and C.P. Daurio, Effects of enalapril on exercise tolerance and longevity in dogs with heart failure produced by iatrogenic mitral regurgitation. *J of Vet Intern Med*, 1996. **10**(2): p. 85-87.

27. Greenhouse, D.G., A. Murphy, P. Mignatti, J. Zavadil, A.C. Galloway, and L.B. Balsam, Mitral valve prolapse is associated with altered extracellular matrix gene expression patterns. *Gene*, 2016. **586**(1): p. 56-61.

28. Freed, L.A., D. Levy, R.A. Levine, M.G. Larson, J.C. Evans, D.L. Fuller, B. Lehman, and E.J. Benjamin, Prevalence and clinical outcome of mitral-valve prolapse. *N Engl J Med*, 1999. **341**(1): p. 1-7.

29. d'Arcy, J.L., B.D. Prendergast, J.B. Chambers, S.G. Ray, and B. Bridgewater, Valvular heart disease: the next cardiac epidemic. *Heart*, 2011. **97**(2): p. 91-3.

30. Aupperle, H. and S. Disatian, Pathology, protein expression and signaling in myxomatous mitral valve degeneration: Comparison of dogs and humans. *J Vet Cardiol*, 2012. **14**(1): p. 59-71.

31. Ramanan, S.V., Cardiovascular disease in the Adventures of Sherlock Holmes. *Arch Intern Med*, 2001. **161**(5): p. 701-705.

32. Grau, J.B., L. Pirelli, P.J. Yu, A.C. Galloway, and H. Ostrer, The genetics of mitral valve prolapse. *Clin Genet*, 2007. **72**(4): p. 288-295.

33. Lu, C.C., M.M. Liu, G. Culshaw, M. Clinton, D.J. Argyle, and B.M. Corcoran, Gene network and canonical pathway analysis in canine myxomatous mitral valve disease: a microarray study. *Vet J*, 2015. **204**(1): p. 23-31.

34. Petric, A.D., Myxomatous mitral valve disease in dogs - an update and perspectives. *Mac Vet Rev*, 2015. **38**(1): p. 13-20.

35. Boswood, A., S.G. Gordon, J. Haggstrom, G. Wess, R.L. Stepien, M.A. Oyama, B.W. Keene, J. Bonagura, K.A. MacDonald, M. Patteson, S. Smith, P.R. Fox, K. Sanderson, R. Woolley, V. Szatmari, P. Menaut, W.M. Church, M.L. O'Sullivan, J.P. Jaudon, J.G. Kresken, J. Rush, K.A. Barrett, S.L. Rosenthal, A.B. Saunders, I. Ljungvall, M. Deinert, E. Bomassi, A.H. Estrada, M.J. Fernandez Del Palacio, N.S. Moise, J.A. Abbott, Y. Fujii, A. Spier, M.W. Luethy, R.A. Santilli, M. Uechi, A. Tidholm, C. Schummer, and P. Watson, Longitudinal analysis of quality of life, clinical, radiographic, echocardiographic, and laboratory variables in dogs with preclinical myxomatous mitral valve disease receiving pimobendan or placebo: The EPIC study. *J Vet Intern Med*, 2018. **32**(1): p. 72-85.

36. Fox, P.R., Pathology of myxomatous mitral valve disease in the dog. *J Vet Cardiol*, 2012. **14**(1): p. 103-126.

37. Fenoglio, J.J., Jr., P. Tuan Duc, A.L. Wit, A.L. Bassett, and B.M. Wagner, Canine mitral complex. Ultrastructure and electromechanical properties. *Circ Res*, 1972. **31**(3): p. 417-430.

38. Silbiger, J.J. and R. Bazaz, Contemporary insights into the functional anatomy of the mitral valve. *Am Heart J*, 2009. **158**(6): p. 887-895.

39. Rodriguez, F., F. Langer, K.B. Harrington, F.A. Tibayan, M.K. Zasio, A. Cheng, D. Liang, G.T. Daughters, J.W. Covell, J.C. Criscione, N.B. Ingels, and D.C. Miller, Importance of mitral valve second-order chordae for left ventricular geometry, wall thickening mechanics, and global systolic function. *Circulation*, 2004. **110**(11 Suppl 1): p. 115-122.

40. Corcoran, B.M., A. Black, H. Anderson, J.D. McEwan, A. French, P. Smith, and C. Devine, Identification of surface morphologic changes in

the mitral valve leaflets and chordae tendineae of dogs with myxomatous degeneration. *Am J Vet Res*, 2004. **65**(2): p. 198-206.

41. Hinton, R.B. and K.E. Yutzey, Heart valve structure and function in development and disease. *Annual Review of Physiology*, , 2011. **73**: p. 29-46.

42. Levine, R.A., A.A. Hagege, D.P. Judge, M. Padala, J.P. Dal-Bianco, E. Aikawa, J. Beaudoin, J. Bischoff, N. Bouatia-Naji, P. Bruneval, J.T. Butcher, A. Carpentier, M. Chaput, A.H. Chester, C. Clusel, F.N. Delling, H.C. Dietz, C. Dina, R. Durst, L. Fernandez-Friera, M.D. Handschumacher, M.O. Jensen, X.P. Jeunemaitre, H. Le Marec, T. Le Tourneau, R.R. Markwald, J. Merot, E. Messas, D.P. Milan, T. Neri, R.A. Norris, D. Peal, M. Perrocheau, V. Probst, M. Puceat, N. Rosenthal, J. Solis, J.J. Schott, E. Schwammenthal, S.A. Slaugenhaupt, J.K. Song, M.H. Yacoub, and N. Leducq Mitral Transatlantic, Mitral valve disease--morphology and mechanisms. *Nat Rev Cardiol*, 2015. **12**(12): p. 689-710.

43. Disatian, S., E.J. Ehrhart, 3rd, S. Zimmerman, and E.C. Orton, Interstitial cells from dogs with naturally occurring myxomatous mitral valve disease undergo phenotype transformation. *J Heart Valve Dis*, 2008. **17**(4): p. 402-411.

44. Han, R.I., A. Black, G.J. Culshaw, A.T. French, R.W. Else, and B.M. Corcoran, Distribution of myofibroblasts, smooth muscle-like cells, macrophages, and mast cells in mitral valve leaflets of dogs with myxomatous mitral valve disease. *Am J Vet Res*, 2008. **69**(6): p. 763-769.

45. Liu, A.C., V.R. Joag, and A.I. Gotlieb, The emerging role of valve interstitial cell phenotypes in regulating heart valve pathobiology. *Am J Pathol*, 2007. **171**(5): p. 1407-1418.

46. Aupperle, H., I. Marz, J. Thielebein, B. Kiefer, A. Kappe, and H.A. Schoon, Immunohistochemical characterization of the extracellular matrix in normal mitral valves and in chronic valve disease (endocardiosis) in dogs. *Res Vet Sci*, 2009. **87**(2): p. 277-283.

47. Culshaw, G.J., A.T. French, R.I. Han, A. Black, G.T. Pearson, and B.M. Corcoran, Evaluation of innervation of the mitral valves and the effects of myxomatous degeneration in dogs. *Am J Vet Res*, 2010. **71**(2): p. 194-202.

48. Han, R.I., C.H. Clark, A. Black, A. French, G.J. Culshaw, S.A. Kempson, and B.M. Corcoran, Morphological changes to endothelial and interstitial cells and to the extra-cellular matrix in canine myxomatous mitral valve disease (endocardiosis). *Vet J*, 2013. **197**(2): p. 388-394.

49. Han, R.I., A. Black, G. Culshaw, A.T. French, and B.M. Corcoran, Structural and cellular changes in canine myxomatous mitral valve disease: an image analysis study. *J Heart Valve Dis*, 2010. **19**(1): p. 60-70.

50. Borgarelli, M. and J.W. Buchanan, Historical review, epidemiology and natural history of degenerative mitral valve disease. *J Vet Cardiol*, 2012. **14**(1): p. 93-101.

51. Lacerda, C.M., S. Disatian, and E.C. Orton, Differential protein expression between normal, early-stage, and late-stage myxomatous mitral valves from dogs. *Proteomics Clin Appl*, 2009. **3**(12): p. 1422-1429.

52. Lester, W.M., Myxomatous mitral valve disease and related entities: The role of matrix in valvular heart disease. *Cardiovasc Pathol*, 1995. **4**(4): p. 257-264.

53. Hadian, M., B.M. Corcoran, and J.P. Bradshaw, Molecular changes in fibrillar collagen in myxomatous mitral valve disease. *Cardiovasc Pathol*, 2010. **19**(5): p. 141-148.

54. Grande-Allen, K.J., B.P. Griffin, N.B. Ratliff, D.M. Cosgrove, and I. Vesely, Glycosaminoglycan myxomatous mitral profiles of leaflets and chordae parallel the severity of mechanical alterations. *J Am Col Cardiol*, 2003. **42**(2): p. 271-277.

55. Gupta, V., J.E. Barzilla, J.S. Mendez, E.H. Stephens, E.L. Lee, C.D. Collard, R. Laucirica, P.H. Weigel, and K.J. Grande-Allen, Abundance and location of proteoglycans and hyaluronan within normal and myxomatous mitral valves. *Cardiovas Path*, 2009. **18**(4): p. 191-197.

56. Aupperle, H., J. Thielebein, B. Kiefer, I. Marz, G. Dinges, and H.A. Schoon, An immunohistochemical study of the role of matrix metalloproteinases and their tissue inhibitors in chronic mitral valvular disease (valvular endocardiosis) in dogs. *Vet J*, 2009. **180**(1): p. 88-94.

57. Lu, C.C., M.M. Liu, M. Clinton, G. Culshaw, D.J. Argyle, and B.M. Corcoran, Developmental pathways and endothelial to mesenchymal

transition in canine myxomatous mitral valve disease. *Vet J*, 2015. **206**(3): p. 377-384.

58. Bischoff, J. and E. Aikawa, Progenitor cells confer plasticity to cardiac valve endothelium. *J Cardiovasc Transl Res*, 2011. **4**(6): p. 710-719.

59. Kovacic, J.C., N. Mercader, M. Torres, M. Boehm, and V. Fuster, Epithelial-to-mesenchymal and endothelial-to-mesenchymal transition: from cardiovascular development to disease. *Circulation*, 2012. **125**(14): p. 1795-1808.

60. Rabkin, E., M. Aikawa, J.R. Stone, Y. Fukumoto, P. Libby, and F.J. Schoen, Activated interstitial myofibroblasts express catabolic enzymes and mediate matrix remodeling in myxomatous heart valves. *Circulation*, 2001. **104**(21): p. 2525-2532.

61. Black, A., A.T. French, J. Dukes-McEwan, and B.M. Corcoran, Ultrastructural morphologic evaluation of the phenotype of valvular interstitial cells in dogs with myxomatous degeneration of the mitral valve. *Am J Vet Res*, 2005. **66**(8): p. 1408-1414.

62. de Vlaming, A., K. Sauls, Z. Hajdu, R.P. Visconti, A.N. Mehesz, R.A. Levine, S.A. Slaugenhaupt, A. Hagege, A.H. Chester, R.R. Markwald, and R.A. Norris, Atrioventricular valve development: new perspectives on an old theme. *Differentiation*, 2012. **84**(1): p. 103-116.

63. Butcher, J.T., A.M. Penrod, A.J. Garcia, and R.M. Nerem, Unique morphology and focal adhesion development of valvular endothelial cells in static and fluid flow environments. *Arterioscler Thromb Vasc Biol*, 2004. **24**(8): p. 1429-1434.

64. Simmons, C.A., G.R. Grant, E. Manduchi, and P.F. Davies, Spatial heterogeneity of endothelial phenotypes correlates with side-specific vulnerability to calcification in normal porcine aortic valves. *Circ Res*, 2005. **96**(7): p. 792-799.

65. Davies, P.F., A.G. Passerini, and C.A. Simmons, Aortic valve: turning over a new leaf(let) in endothelial phenotypic heterogeneity. *Arterioscler Thromb Vasc Biol*, 2004. **24**(8): p. 1331-1333.

66. Miragoli, M., M.H. Yacoub, I. El-Hamamsy, J.L. Sanchez-Alonso, A. Moshkov, N. Mongkoldhumrongkul, M. Padala, S. Paramagurunathan, P. Sarathchandra, Y.E. Korchev, J. Gorelik, and A.H. Chester, Side-

specific mechanical properties of valve endothelial cells. *Am J Physiol Heart Circ Physiol*, 2014. **307**(1): p. 15-24.

67. Aikawa, E., P. Whittaker, M. Farber, K. Mendelson, R.F. Padera, M. Aikawa, and F.J. Schoen, Human semilunar cardiac valve remodeling by activated cells from fetus to adult - Implications for postnatal adaptation, pathology, and tissue engineering. *Circulation*, 2006. **113**(10): p. 1344-1352.

68. Dal-Bianco, J.P., E. Aikawa, J. Bischoff, J.L. Guerrero, M.D. Handschumacher, S. Sullivan, B. Johnson, J.S. Titus, Y. Iwamoto, J. Wylie-Sears, R.A. Levine, and A. Carpentier, Active adaptation of the tethered mitral valve insights into a compensatory mechanism for functional mitral regurgitation. *Circulation*, 2009. **120**(4): p. 334-342.

69. Gupta, V., J.A. Werdenberg, B.D. Lawrence, J.S. Mendez, E.H. Stephens, and K.J. Grande-Allen, Reversible secretion of glycosaminoglycans and proteoglycans by cyclically stretched valvular cells in 3D culture. *Ann Biomed Eng*, 2008. **36**(7): p. 1092-1103.

70. Lacerda, C.M.R., H.B. MacLea, J.D. Kisiday, and E.C. Orton, Static and cyclic tensile strain induce myxomatous effector proteins and serotonin in canine mitral valves. *J Vet Cardiol*, 2012. **14**(1): p. 223-230.

71. Orton, E.C., C.M. Lacerda, and H.B. MacLea, Signaling pathways in mitral valve degeneration. *J Vet Cardiol*, 2012. **14**(1): p. 7-17.

72. Summers, K.M., J.A. West, A. Hattam, D. Stark, J.J. McGill, and M.J. West, Recent developments in the diagnosis of Marfan syndrome and related disorders. *Med J Aust*, 2012. **197**(9): p. 494-497.

73. Loeys, B.L., U. Schwarze, T. Holm, B.L. Callewaert, G.H. Thomas, H. Pannu, J.F. De Backer, G.L. Oswald, S. Symoens, S. Manouvrier, A.E. Roberts, F. Faravelli, M.A. Greco, R.E. Pyeritz, D.M. Milewicz, P.J. Coucke, D.E. Cameron, A.C. Braverman, P.H. Byers, A.M. De Paepe, and H.C. Dietz, Aneurysm syndromes caused by mutations in the TGF-beta receptor. *N Engl J Med*, 2006. **355**(8): p. 788-798.

74. Rienhoff, H.Y., C.Y. Yeo, R. Morissette, I. Khrebtukova, J. Melnick, S.J. Luo, N. Leng, Y.J. Kim, G. Schroth, J. Westwick, H. Vogel, N. McDonnell, J.G. Hall, and M. Whitman, A mutation in TGFB3 associated with a syndrome of low muscle mass, growth retardation,

distal arthrogryposis and clinical features overlapping with marfan and loeys-dietz syndrome. *Am J of Med Gen Part A*, 2013. **161**(8): p. 2040-2046.

75. LeMaire, S.A., H. Pannu, V. Tran-Fadulu, S.A. Carter, J.S. Coselli, and D.M. Milewicz, Severe aortic and arterial aneurysms associated with a TGFBR2 mutation. *Nat Clin Pract Cardiovasc Med*, 2007. **4**(3): p. 167-171.

76. Loeys, B.L., J. Chen, E.R. Neptune, D.P. Judge, M. Podowski, T. Holm, J. Meyers, C.C. Leitch, N. Katsanis, N. Sharifi, F.L. Xu, L.A. Myers, P.J. Spevak, D.E. Cameron, J. De Backer, J. Hellemans, Y. Chen, E.C. Davis, C.L. Webb, W. Kress, P. Coucke, D.B. Rifkin, A.M. De Paepe, and H.C. Dietz, A syndrome of altered cardiovascular, craniofacial, neurocognitive and skeletal development caused by mutations in TGFBR1 or TGFBR2. *Nat Genet*, 2005. **37**(3): p. 275-281.

77. Melis, D., G. Cappuccio, V.M. Ginocchio, G. Minopoli, M. Valli, M. Corradi, and G. Andria, Cardiac valve disease: an unreported feature in Ehlers Danlos syndrome arthrocalasia type? *Ital J Pediatr*, 2012. **38**: p. 65.

78. Camerota, F., M. Castori, C. Celletti, M. Colotto, S. Amato, A. Colella, M. Curione, and C. Danese, Heart rate, conduction and ultrasound abnormalities in adults with joint hypermobility syndrome/Ehlers-Danlos syndrome, hypermobility type. *Clin Rheumatol*, 2014. **33**(7): p. 981-987.

79. Colige, A., L. Nuytinck, I. Hausser, A.J. van Essen, M. Thiry, C. Herens, L.C. Ades, F. Malfait, A.D. Paepe, P. Franck, G. Wolff, J.C. Oosterwijk, J.H. Smitt, C.M. Lapiere, and B.V. Nusgens, Novel types of mutation responsible for the dermatosparactic type of Ehlers-Danlos syndrome (Type VIIC) and common polymorphisms in the ADAMTS2 gene. *J Invest Dermatol*, 2004. **123**(4): p. 656-663.

80. Matsumaru, I., K. Eishi, K. Hashizume, H. Kawano, A. Tsuneto, and T. Hayashi, Clinical and pathological features of degenerative mitral valve disease: billowing mitral leaflet versus fibroelastic deficiency. *Ann Thorac Cardiovasc Surg*, 2014. **20**(6): p. 987-994.

81. Anyanwu, A.C. and D.H. Adams, Etiologic classification of degenerative mitral valve disease: Barlow's disease and fibroelastic deficiency. *Semin Thorac Cardiovasc Surg*, 2007. **19**(2): p. 90-96.

82. Hjortnaes, J., J. Keegan, P. Bruneval, E. Schwartz, F.J. Schoen, A. Carpentier, R.A. Levine, A. Hagege, and E. Aikawa, Comparative Histopathological Analysis of Mitral Valves in Barlow Disease and Fibroelastic Deficiency. *Semin Thorac Cardiovasc Surg*, 2016. **28**(4): p. 757-767.

83. Chen, Y.T., J. Wang, A.S. Wee, Q.W. Yong, E.L. Tay, C.C. Woo, V. Sorokin, A.M. Richards, and L.H. Ling, Differential MicroRNA Expression Profile in Myxomatous Mitral Valve Prolapse and Fibroelastic Deficiency Valves. *Int J Mol Sci*, 2016. **17**(5).

84. Roberts, W.C., T.J. Vowels, J.M. Ko, and R.F. Hebeler, Gross and histological features of excised portions of posterior mitral leaflet in patients having operative repair of mitral valve prolapse and comments on the concept of missing (= ruptured) chordae tendineae. *J Am Col Cardiol*, 2014. **63**(16): p. 1667-1674.

85. Paranya, G., S. Vineberg, E. Dvorin, S. Kaushal, S.J. Roth, E. Rabkin, F.J. Schoen, and J. Bischoff, Aortic valve endothelial cells undergo transforming growth factor-beta-mediated and non-transforming growth factor-beta-mediated transdifferentiation in vitro. *Am J Path*, 2001. **159**(4): p. 1335-1343.

86. Leask, R.L., N. Jain, and J. Butany, Endothelium and valvular diseases of the heart. *Microsc Res Tech*, 2003. **60**(2): p. 129-37.

87. Chalajour, F., H. Treede, A. Ebrahimnejad, H. Lauke, H. Reichenspurner, and S. Ergun, Angiogenic activation of valvular endothelial cells in aortic valve stenosis. *Exp Cell Res*, 2004. **298**(2): p. 455-64.

88. Balachandran, K., P.W. Alford, J. Wylie-Sears, J.A. Goss, A. Grosberg, J. Bischoff, E. Aikawa, R.A. Levine, and K.K. Parker, Cyclic strain induces dual-mode endothelial-mesenchymal transformation of the cardiac valve. *Proc Natl Acad Sci U S A*, 2011. **108**(50): p. 19943-19948.

89. Richards, J., I. El-Hamamsy, S. Chen, Z. Sarang, P. Sarathchandra, M.H. Yacoub, A.H. Chester, and J.T. Butcher, Side-specific endothelial-dependent regulation of aortic valve calcification: interplay of hemodynamics and nitric oxide signaling. *Am J Pathol*, 2013. **182**(5): p. 1922-1931.

90. Farrar, E.J. and J.T. Butcher, Heterogeneous susceptibility of valve endothelial cells to mesenchymal transformation in response to TNF alpha. *An of Biomed Eng*, 2014. **42**(1): p. 149-161.

91. Mahler, G.J., E.J. Farrar, and J.T. Butcher, Inflammatory cytokines promote mesenchymal transformation in embryonic and adult valve endothelial cells. *Arterioscler Thromb Vasc Biol*, 2013. **33**(1): p. 121-30.

92. Pagnozzi, L.A. and J.T. Butcher, Mechanotransduction mechanisms in mitral valve physiology and disease pathogenesis. *Front Cardiovasc Med*, 2017. **4**:83.

93. Butcher, J.T. and R.M. Nerem, Valvular endothelial cells regulate the phenotype of interstitial cells in co-culture: effects of steady shear stress. *Tissue Eng*, 2006. **12**(4): p. 905-915.

94. Shapero, K., J. Wylie-Sears, R.A. Levine, J.E. Mayer, and J. Bischoff, Reciprocal interactions between mitral valve endothelial and interstitial cells reduce endothelial-to-mesenchymal transition and myofibroblastic activation. *J Mol Cell Cardiol*, 2015. **80**: p. 175-185.

95. Armstrong, E.J. and J. Bischoff, Heart valve development: endothelial cell signaling and differentiation. *Circ Res*, 2004. **95**(5): p. 459-470.

96. Chakraborty, S., M.D. Combs, and K.E. Yutzey, Transcriptional regulation of heart valve progenitor cells. *Pediatr Cardiol*, 2010. **31**(3): p. 414-421.

97. Combs, M.D. and K.E. Yutzey, Heart valve development: regulatory networks in development and disease. *Circ Res*, 2009. **105**(5): p. 408-421.

98. Butcher, J.T. and R.R. Markwald, Valvulogenesis: the moving target. *Philos Trans R Soc Lond B Biol Sci*, 2007. **362**(1484): p. 1489-1503.

99. Puceat, M., Embryological origin of the endocardium and derived valve progenitor cells: from developmental biology to stem cell-based valve repair. *Biochim Biophys Acta*, 2013. **1833**(4): p. 917-922.

100. Song, W.M., K. Jackson, and P.G. McGuire, Degradation of type IV collagen by matrix metalloproteinases is an important step in the epithelial-mesenchymal transformation of the endocardial cushions. *Dev Bio*, 2000. **227**(2): p. 606-617.

101. Camenisch, T.D., A.P. Spicer, T. Brehm-Gibson, J. Biesterfeldt, M.L. Augustine, A. Calabro, Jr., S. Kubalak, S.E. Klewer, and J.A. McDonald, Disruption of hyaluronan synthase-2 abrogates normal cardiac morphogenesis and hyaluronan-mediated transformation of epithelium to mesenchyme. *J Clin Invest*, 2000. **106**(3): p. 349-360.

102. Timmerman, L.A., J. Grego-Bessa, A. Raya, E. Bertran, J.M. Perez-Pomares, J. Diez, S. Aranda, S. Palomo, F. McCormick, J.C. Izpisua-Belmonte, and J.L. de la Pompa, Notch promotes epithelial-mesenchymal transition during cardiac development and oncogenic transformation. *Genes Dev*, 2004. **18**(1): p. 99-115.

103. Brown, C.B., A.S. Boyer, R.B. Runyan, and J.V. Barnett, Requirement of type III TGF-beta receptor for endocardial cell transformation in the heart. *Science*, 1999. **283**(5410): p. 2080-2082.

104. Boyer, A.S., I.I. Ayerinskas, E.B. Vincent, L.A. McKinney, D.L. Weeks, and R.B. Runyan, TGF beta 2 and TGF beta 3 have separate and sequential activities during epithelial-mesenchymal cell transformation in the embryonic heart. *Dev Bio*, 1999. **208**(2): p. 530-545.

105. Ma, L.J., M.F. Lu, R.J. Schwartz, and J.F. Martin, Bmp2 is essential for cardiac cushion epithelial-mesenchymal transition and myocardial patterning. *Development*, 2005. **132**(24): p. 5601-5611.

106. Sugi, Y., H. Yamamura, H. Okagawa, and R.R. Markwald, Bone morphogenetic protein-2 can mediate myocardial regulation of atrioventricular cushion mesenchymal cell formation in mice. *Dev Bio*, 2004. **269**(2): p. 505-518.

107. Armstrong, E.J. and J. Bischoff, Heart valve development - Endothelial cell signaling and differentiation. *Circul Res*, 2004. **95**(5): p. 459-470.

108. Ernst, E., P. Schneider, and G. Trautwein, [Electron microscopic studies on amyloidosis of the atrioventricular valves of the dog (author's transl)]. *Beitr Pathol*, 1974. **152**(4): p. 361-382.

109. Ernst, E., P. Schneider, and G. Trautwein, [Etiology and pathogenesis of the endocardiosis and endocarditis in dogs. II. Anatomicopathological findings]. *Dtsch Tierarztl Wochenschr*, 1973. **80**(14): p. 322-328.

110. Lu, C.C., M.M. Liu, G. Culshaw, A. French, and B. Corcoran, Comparison of cellular changes in Cavalier King Charles spaniel and mixed breed dogs with myxomatous mitral valve disease. *J Vet Cardiol*, 2016. **18**(2): p. 100-109.

111. Mow, T. and H.D. Pedersen, Increased endothelin-receptor density in myxomatous canine mitral valve leaflets. *J Cardiovasc Pharmacol*, 1999. **34**(2): p. 254-260.

112. Olsen, L.H., K. Mortensen, T. Martinussen, L.I. Larsson, U. Baandrup, and H.D. Pedersen, Increased NADPH-diaphorase activity in canine myxomatous mitral valve leaflets. *J Comp Pathol*, 2003. **129**(2-3): p. 120-230.

113. Liu, A.C. and A.I. Gotlieb, Characterization of cell motility in single heart valve interstitial cells in vitro. *Histol Histopathol*, 2007. **22**(8): p. 873-882.

114. Rabkin-Aikawa, E., M. Farber, M. Aikawa, and F.J. Schoen, Dynamic and reversible changes of interstitial cell phenotype during remodeling of cardiac valves. *J Heart Valve Dis*, 2004. **13**(5): p. 841-847.

115. Della Rocca, F., S. Sartore, D. Guidolin, B. Bertiplaglia, G. Gerosa, D. Casarotto, and P. Pauletto, Cell composition of the human pulmonary valve: a comparative study with the aortic valve--the VESALIO Project. Vitalitate Exornatum Succedaneum Aorticum labore Ingegnoso Obtinebitur. *Ann Thorac Surg*, 2000. **70**(5): p. 1594-1600.

116. Wiester, L.M. and C.M. Giachelli, Expression and function of the integrin alpha9beta1 in bovine aortic valve interstitial cells. *J Heart Valve Dis*, 2003. **12**(5): p. 605-616.

117. Rutkovskiy, A., A. Malashicheva, G. Sullivan, M. Bogdanova, A. Kostareva, K.O. Stenslokken, A. Fiane, and J. Vaage, Valve interstitial cells: the key to understanding the pathophysiology of heart valve calcification. *J Am Heart Assoc*, 2017. **6**(9): e006339.

118. Hinz, B. and G. Gabbiani, Mechanisms of force generation and transmission by myofibroblasts. *Cur Op Biotech*, 2003. **14**(5): p. 538-546.

119. Sousa, A.M., T.G. Liu, O. Guevara, J. Stevens, B.L. Fanburg, M. Gaestel, D. Toksoz, and U.S. Kayyali, Smooth muscle alpha-actin expression and

myofibroblast differentiation by TGF beta are dependent upon MK2. *J Cell Biochem*, 2007. **100**(6): p. 1581-1592.

120. Assinder, S.J., J.A. Stanton, and P.D. Prasad, Transgelin: an actin-binding protein and tumour suppressor. *Int J Biochem Cell Biol*, 2009. **41**(3): p. 482-486.

121. Liu, M.M., T.C. Flanagan, C.C. Lu, A.T. French, D.J. Argyle, and B.M. Corcoran, Culture and characterisation of canine mitral valve interstitial and endothelial cells. *Vet J*, 2015. **204**(1): p. 32-39.

122. Obayashi, K., S. Miyagawa-Tomita, H. Matsumoto, H. Koyama, T. Nakanishi, and H. Hirose, Effects of transforming growth factor-beta 3 and matrix metalloproteinase-3 on the pathogenesis of chronic mitral valvular disease in dogs. *Am J Vet Res*, 2011. **72**(2): p. 194-202.

123. Balachandran, K., P. Sucosky, H. Jo, and A.P. Yoganathan, Elevated cyclic stretch alters matrix remodeling in aortic valve cusps: implications for degenerative aortic valve disease. *Am J Physiol Heart Circ Physiol*, 2009. **296**(3): p. 756-764.

124. Moesgaard, S.G., H. Aupperle, M.M. Rajamaki, T. Falk, C.E. Rasmussen, N.E. Zois, and L.H. Olsen, Matrix metalloproteinases (MMPs), tissue inhibitors of metalloproteinases (TIMPs) and transforming growth factor-beta (TGF-beta) in advanced canine myxomatous mitral valve disease. *Res Vet Sci*, 2014. **97**(3): p. 560-567.

125. Hulin, A., C.F. Deroanne, C.A. Lambert, B. Dumont, V. Castronovo, J.O. Defraigne, B.V. Nusgens, M.A. Radermecker, and A.C. Colige, Metallothionein-dependent up-regulation of TGF-beta2 participates in the remodelling of the myxomatous mitral valve. *Cardiovasc Res*, 2012. **93**(3): p. 480-489.

126. Surachetpong, S., T. Jiranantasak, A. Rungsipipat, and E.C. Orton, Apoptosis and abundance of Bcl-2 family and transforming growth factor beta1 signaling proteins in canine myxomatous mitral valves. *J Vet Cardiol*, 2013. **15**(3): p. 171-180.

127. Ernst, E., P. Schneider, and G. Trautwein, [Endocardiosis of canine atrioventricular valves. IV. Electron microscopy studies]. *Zentralbl Veterinarmed A*, 1974. **21**(5): p. 400-416.

128. Barth, P.J., H. Koster, and R. Moosdorf, CD34+ fibrocytes in normal mitral valves and myxomatous mitral valve degeneration. *Pathol Res Pract*, 2005. **201**(4): p. 301-304.

129. Barth, P.J., T.S.Z. Schweinsberg, A. Ramaswamy, and R. Moll, CD34(+) fibrocytes, alpha-smooth muscle antigen-positive myofibroblasts, and CD117 expression in the stroma of invasive squamous cell carcinomas of the oral cavity, pharynx, and larynx. *Virchows Archiv*, 2004. **444**(3): p. 231-234.

130. Geirsson, A., M. Singh, R. Ali, H. Abbas, W. Li, J.A. Sanchez, S. Hashim, and G. Tellides, Modulation of transforming growth factor-beta signaling and extracellular matrix production in myxomatous mitral valves by angiotensin II receptor blockers. *Circulation*, 2012. **126**(11): p. 189-197.

131. Thalji, N.M., M.A. Hagler, H. Zhang, G. Casaclang-Verzosa, A.A. Nair, R.M. Suri, and J.D. Miller, Nonbiased molecular screening identifies novel molecular regulators of fibrogenic and proliferative signaling in myxomatous mitral valve disease. *Circ Cardiovasc Genet*, 2015. **8**(3): p. 516-528.

132. Hulin, A., L.J. Anstine, A.J. Kim, S.J. Potter, T. DeFalco, J. Lincoln, and K.E. Yutzey, Macrophage transitions in heart valve development and myxomatous valve disease. *Arterioscler Thromb Vasc Biol*, 2018. **38**(3): p. 636-644.

133. Disatian, S. and E.C. Orton, Autocrine serotonin and transforming growth factor beta 1 signaling mediates spontaneous myxomatous mitral valve disease. *J Heart Valve Dis*, 2009. **18**(1): p. 44-51.

134. Lin, C., D. Zhu, G. Markby, B.M. Corcoran, C. Farquharson, and V.E. Macrae, Isolation and characterization of primary rat valve interstitial cells: a new model to study aortic valve calcification. *J Vis Exp*, 2017 **129**(56126) : doi10.3791/56126.

135. Porras, A.M., N.C. van Engeland, E. Marchbanks, A. McCormack, C.V. Bouten, M.H. Yacoub, N. Latif, and K.S. Masters, Robust generation of quiescent porcine valvular interstitial cell cultures. *J Am Heart Assoc*, 2017. **6**(3): e005041.

136. Waxman, A.S., B.G. Kornreich, R.A. Gould, N.S. Moise, and J.T. Butcher, Interactions between TGF beta 1 and cyclic strain in

modulation of myofibroblastic differentiation of canine mitral valve interstitial cells in 3D culture. *J Vet Cardiol,*, 2012. **14**(1): p. 211-221.

137. Rohr, S., Cardiac fibroblasts in cell culture systems: myofibroblasts all along? *J Cardiovasc Pharm*, 2011. **57**(4): p. 389-399.

138. Latif, N., A. Quillon, P. Sarathchandra, A. McCormack, A. Lozanoski, M.H. Yacoub, and A.H. Chester, Modulation of human valve interstitial cell phenotype and function using a fibroblast growth factor 2 formulation. *PLoS One*, 2015. **10**(6): e0127844.

139. Durbin, A.D. and A.I. Gotlieb, Advances towards understanding heart valve response to injury. *Cardiovasc Pathol*, 2002. **11**(2): p. 69-77.

140. Tan, H.T., T.K. Lim, A.M. Richards, T. Kofidis, K.L. Teoh, L.H. Ling, and M.C. Chung, Unravelling the proteome of degenerative human mitral valves. *Proteomics*, 2015. **15**(17): p. 2934-2944.

141. Soini, Y., J. Satta, M. Maatta, and H. Autio-Harmainen, Expression of MMP2, MMP9, MT1-MMP, TIMP1, and TIMP2 mRNA in valvular lesions of the heart. *J Pathol*, 2001. **194**(2): p. 225-231.

142. Aupperle, H., I. Marz, J. Thielebein, G. Dinges, and H.A. Schoon, Histomorphological findings and expression of matrix metalloproteinases and their tissue specific inhibitors (TIMPs) in normal tricuspid valves and in chronic tricuspid valvular disease in dogs. *Vet J*, 2010. **183**(2): p. 176-183.

143. Li, Q., L.M. Freeman, J.E. Rush, G.S. Huggins, A.D. Kennedy, J.A. Labuda, D.P. Laflamme, and S.S. Hannah, Veterinary medicine and multi-omics research for future nutrition targets: metabolomics and transcriptomics of the common degenerative mitral valve disease in dogs. *OMICS*, 2015. **19**(8): p. 461-470.

144. Klein, T. and R. Bischoff, Physiology and pathophysiology of matrix metalloproteases. *Amino Acids*, 2011. **41**(2): p. 271-290.

145. Togashi, M., K. Tamura, T. Nitta, M. Ishizaki, Y. Sugisaki, and Y. Fukuda, Role of matrix metalloproteinases and their tissue inhibitor of metalloproteinases in myxomatous change of cardiac floppy valves. *Path Intern*, 2007. **57**(5): p. 251-259.

146. Mahimkar, R., A. Nguyen, M. Mann, C.C. Yeh, B.Q. Zhu, J.S. Karliner, and D.H. Lovett, Cardiac transgenic matrix metalloproteinase-2

expression induces myxomatous valve degeneration: a potential model of mitral valve prolapse disease. *Cardiovasc Pathol*, 2009. **18**(5): p. 253-261.

147. Matrisian, L.M., Metalloproteinases and their inhibitors in matrix remodeling. *T in Gen*, 1990. **6**(4): p. 121-125.

148. Li, Y.Y., C.F. McTiernan, and A.M. Feldman, Interplay of matrix metalloproteinases, tissue inhibitors of metalloproteinases and their regulators in cardiac matrix remodeling. *Cardiovas Res*, 2000. **46**(2): p. 214-224.

149. Raffetto, J.D. and R.A. Khalil, Matrix metalloproteinases and their inhibitors in vascular remodeling and vascular disease. *Biochem Pharm*, 2008. **75**(2): p. 346-359.

150. Oyama, M.A. and S.V. Chittur, Genomic expression patterns of mitral valve tissues from dogs with degenerative mitral valve disease. *Am J Vet Res*, 2006. **67**(8): p. 1307-1318.

151. Kelwick, R., I. Desanlis, G.N. Wheeler, and D.R. Edwards, The ADAMTS (A Disintegrin and Metalloproteinase with Thrombospondin motifs) family. *Genome Biol*, 2015. **16**(113): doi: 10.1186/s13059-015-0676-3.

152. Gabriel, L.A., L.W. Wang, H. Bader, J.C. Ho, A.K. Majors, J.G. Hollyfield, E.I. Traboulsi, and S.S. Apte, ADAMTSL4, a secreted glycoprotein widely distributed in the eye, binds fibrillin-1 microfibrils and accelerates microfibril biogenesis. *Invest Ophthalmol Vis Sci*, 2012. **53**(1): p. 461-469.

153. Han, R.I., G. Impoco, G. Culshaw, A.T. French, A. Black, and B.M. Corcoran, Cell maceration scanning electron microscopy and computer-derived porosity measurements in assessment of connective tissue microstructure changes in the canine myxomatous mitral valve. *Vet J*, 2013. **197**(2): p. 502-505.

154. Cole, W.G., D. Chan, A.J. Hickey, and D.E. Wilcken, Collagen composition of normal and myxomatous human mitral heart valves. *Biochem J*, 1984. **219**(2): p. 451-460.

155. Lis, Y., M.C. Burleigh, D.J. Parker, A.H. Child, J. Hogg, and M.J. Davies, Biochemical characterization of individual normal, floppy and rheumatic human mitral valves. *Biochem J*, 1987. **244**(3): p. 597-603.

156. Whittaker, P., D.R. Boughner, D.G. Perkins, and P.B. Canham, Quantitative structural analysis of collagen in chordae tendineae and its relation to floppy mitral valves and proteoglycan infiltration. *Br Heart J*, 1987. **57**(3): p. 264-269.

157. Tamura, K., Y. Fukuda, M. Ishizaki, Y. Masuda, N. Yamanaka, and V.J. Ferrans, Abnormalities in elastic fibers and other connective-tissue components of floppy mitral valve. *Am Heart J*, 1995. **129**(6): p. 1149-1158.

158. Murata, K., Acidic glycosaminoglycans in human heart valves. *J Mol Cell Cardiol*, 1981. **13**(3): p. 281-292.

159. McDonald, P.C., J.E. Wilson, S. McNeill, M. Gao, J.J. Spinelli, F. Rosenberg, H. Wiebe, and B.M. McManus, The challenge of defining normality for human mitral and aortic valves: geometrical and compositional analysis. *Cardiovasc Pathol*, 2002. **11**(4): p. 193-209.

160. Fornieri, C., M. Baccarani-Contri, D. Quaglino, Jr., and I. Pasquali-Ronchetti, Lysyl oxidase activity and elastin/glycosaminoglycan interactions in growing chick and rat aortas. *J Cell Biol*, 1987. **105**(3): p. 1463-1469.

161. Radermecker, M.A., R. Limet, C.M. Lapiere, and B. Nusgens, Increased mRNA expression of decorin in the prolapsing posterior leaflet of the mitral valve. *Interact Cardiovasc Thorac Surg*, 2003. **2**(3): p. 389-394.

162. Reinboth, B., E. Hanssen, E.G. Cleary, and M.A. Gibson, Molecular interactions of biglycan and decorin with elastic fiber components: biglycan forms a ternary complex with tropoelastin and microfibril-associated glycoprotein 1. *J Biol Chem*, 2002. **277**(6): p. 3950-3957.

163. Sainger, R., J.B. Grau, E. Branchetti, P. Poggio, W.F. Seefried, B.C. Field, M.A. Acker, R.C. Gorman, J.H. Gorman, 3rd, C.W. Hargrove, 3rd, J.E. Bavaria, and G. Ferrari, Human myxomatous mitral valve prolapse: role of bone morphogenetic protein 4 in valvular interstitial cell activation. *J Cell Physiol*, 2012. **227**(6): p. 2595-2604.

164. Del Galdo, F., M.P. Lisanti, and S.A. Jimenez, Caveolin-1, transforming growth factor-beta receptor internalization, and the pathogenesis of systemic sclerosis. *Curr Opin Rheumatol*, 2008. **20**(6): p. 713-719.

165. Sowa, G., Caveolae, caveolins, cavins, and endothelial cell function: new insights. *Front Physiol*, 2012. **2**(120): doi: 10.3389/fphys.2011.00120.

166. Olsen, L.H., M. Fredholm, and H.D. Pedersen, Epidemiology and inheritance of mitral valve prolapse in Dachshunds. *J Vet Intern Med*, 1999. **13**(5): p. 448-456.

167. Chiu, J.J., B.S. Wung, J.Y.J. Shyy, H.J. Hsieh, and D.L. Wang, Reactive oxygen species are involved in shear stress-induced intercellular adhesion molecule-1 expression in endothelial cells. *Arteriosclerosis Thrombosis and Vascular Biology*, 1997. **17**(12): p. 3570-3577.

168. Hulin, A., C. Deroanne, C. Lambert, J.O. Defraigne, B. Nusgens, M. Radermecker, and A. Colige, Emerging pathogenic mechanisms in human myxomatous mitral valve: lessons from past and novel data. *Cardiovascular Pathology*, 2013. **22**(4): p. 245-250.

169. Buskohl, P.R., M.J. Sun, R.P. Thompson, and J.T. Butcher, Serotonin potentiates transforming growth factor-beta3 induced biomechanical remodeling in avian embryonic atrioventricular valves. *PLoS One*, 2012. **7**(8): e42527.

170. Cremer, S.E., S.G. Moesgaard, C.E. Rasmussen, N.E. Zois, T. Falk, M.J. Reimann, S. Cirera, H. Aupperle, M.A. Oyama, and L.H. Olsen, Alpha-smooth muscle actin and serotonin receptors 2A and 2B in dogs with myxomatous mitral valve disease. *Res Vet Sci*, 2015. **100**: p. 197-206.

171. Driesbaugh, K.H., E. Branchetti, J.B. Grau, S.J. Keeney, K. Glass, M.A. Oyama, N. Rioux, S. Ayoub, M.S. Sacks, J. Quackenbush, R.J. Levy, and G. Ferrari, Serotonin receptor 2B signaling with interstitial cell activation and leaflet remodeling in degenerative mitral regurgitation. *J Mol Cell Cardiol*, 2018. **115**: p. 94-103.

172. Goldberg, E., J.B. Grau, J.H. Fortier, E. Salvati, R.J. Levy, and G. Ferrari, Serotonin and catecholamines in the development and progression of heart valve diseases. *Cardiovasc Res*, 2017. **113**(8): p. 849-857.

173. Oyama, M.A. and R.J. Levy, Insights into serotonin signaling mechanisms associated with canine degenerative mitral valve disease. *J of Vet In Med*, 2010. **24**(1): p. 27-36.

174. Aupperle, H., I. Marz, J. Thielebein, and H.A. Schoon, Expression of transforming growth factor-beta1, -beta2 and -beta3 in normal and diseased canine mitral valves. *J Comp Pathol*, 2008. **139**(2-3): p. 97-107.

175. Cushing, M.C., J.T. Liao, and K.S. Anseth, Activation of valvular interstitial cells is mediated by transforming growth factor-beta 1 interactions with matrix molecules. *Mat Bio*, 2005. **24**(6): p. 428-437.

176. Hagler, M.A., T.M. Hadley, H. Zhang, K. Mehra, C.M. Roos, H.V. Schaff, R.M. Suri, and J.D. Miller, TGF-beta signalling and reactive oxygen species drive fibrosis and matrix remodelling in myxomatous mitral valves. *Cardiovasc Res*, 2013. **99**(1): p. 175-184.

177. Walker, G.A., K.S. Masters, D.N. Shah, K.S. Anseth, and L.A. Leinwand, Valvular myofibroblast activation by transforming growth factor-beta: implications for pathological extracellular matrix remodeling in heart valve disease. *Circ Res*, 2004. **95**(3): p. 253-260.

178. Zhang, Y.E., Non-Smad pathways in TGF-beta signaling. *Cell Res*, 2009. **19**(1): p. 128-139.

179. Zhang, Y.E., Mechanistic insight into contextual TGF-beta signaling. *Curr Opin Cell Bio*, 2018. **51**: p. 1-7.

180. Annes, J.P., J.S. Munger, and D.B. Rifkin, Making sense of latent TGF beta activation. *J Cell Sci*, 2003. **116**(2): p. 217-224.

181. Shi, Y.G. and J. Massague, Mechanisms of TGF-beta signaling from cell membrane to the nucleus. *Cell*, 2003. **113**(6): p. 685-700.

182. Poniatowski, L.A., P. Wojdasiewicz, R. Gasik, and D. Szukiewicz, Transforming growth factor beta family: insight into the role of growth factors in regulation of fracture healing biology and potential clinical applications. *Media of Inflam*, 2015.

183. Chen, Y.G. and J. Massague, Smad1 recognition and activation by the ALK1 group of transforming growth factor-beta family receptors. *J Biol Chem*, 1999. **274**(6): p. 3672-3677.

184. Bataller, R. and D.A. Brenner, Liver fibrosis. *J Clin Invest*, 2005. **115**(2): p. 209-218.

185. Meng, X.M., D.J. Nikolic-Paterson, and H.Y. Lan, TGF-beta: the master regulator of fibrosis. *Nat Revs Nephrol*, 2016. **12**(6): p. 325-338.

186. Antoni, D., H. Burckel, E. Josset, and G. Noel, Three-dimensional cell culture: a breakthrough in vivo. *Int J Mol Sci*, 2015. **16**(3): p. 5517-5527.

187. Berger, M., J.A. Gray, and B.L. Roth, The expanded biology of serotonin. *Annu Rev Med*, 2009. **60**: p. 355-366.

188. Nebigil, C.G., P. Hickel, N. Messaddeq, J.L. Vonesch, M.P. Douchet, L. Monassier, K. Gyorgy, R. Matz, R. Andriantsitohaina, P. Manivet, J.M. Launay, and L. Maroteaux, Ablation of serotonin 5-HT(2B) receptors in mice leads to abnormal cardiac structure and function. *Circulation*, 2001. **103**(24): p. 2973-2979.

189. Ni, W. and S.W. Watts, 5-hydroxytryptamine in the cardiovascular system: focus on the serotonin transporter (SERT). *Clin Exp Pharmacol Physiol*, 2006. **33**(7): p. 575-583.

190. Walther, D.J. and M. Bader, A unique central tryptophan hydroxylase isoform. *Biochem Pharmacol*, 2003. **66**(9): p. 1673-1680.

191. Walther, D.J., J.U. Peter, S. Bashammakh, H. Hortnagl, M. Voits, H. Fink, and M. Bader, Synthesis of serotonin by a second tryptophan hydroxylase isoform. *Science*, 2003. **299**(5603): p. 76.

192. Gershon, M.D. and J. Tack, The serotonin signaling system: from basic understanding to drug development for functional GI disorders. *Gastroenterology*, 2007. **132**(1): p. 397-414.

193. Hoyer, D., D.E. Clarke, J.R. Fozard, P.R. Hartig, G.R. Martin, E.J. Mylecharane, P.R. Saxena, and P.P.A. Humphrey, International Union of Pharmacology Classification of Receptors for 5-Hydroxytryptamine (Serotonin). *Pharmacol Revs*, 1994. **46**(2): p. 157-203.

194. Connolly, H.M., J.L. Crary, M.D. McGoon, D.D. Hensrud, B.S. Edwards, W.D. Edwards, and H.V. Schaff, Valvular heart disease associated with fenfluramine-phentermine. *N Engl J Med*, 1997. **337**(9): p. 581-588.

195. Graham, D.J. and L. Green, Further cases of valvular heart disease associated with fenfluramine-phentermine. *N Engl J Med*, 1997. **337**(9): p. 635.

196. Fitzgerald, L.W., T.C. Burn, B.S. Brown, J.P. Patterson, M.H. Corjay, P.A. Valentine, J.H. Sun, J.R. Link, I. Abbaszade, J.M. Hollis, B.L. Largent, P.R. Hartig, G.F. Hollis, P.C. Meunier, A.J. Robichaud, and D.W. Robertson, Possible role of valvular serotonin 5-HT2B receptors in the cardiopathy associated with fenfluramine. *Mol Pharm*, 2000. **57**(1): p. 75-81.

197. Gustafsson, B.I., K. Tommeras, I. Nordrum, J.P. Loennechen, A. Brunsvik, E. Solligard, R. Fossmark, I. Bakke, U. Syversen, and H. Waldum, Long-term serotonin administration induces heart valve disease in rats. *Circulation*, 2005. **111**(12): p. 1517-1522.

198. Fox, D.J. and R.S. Khattar, Carcinoid heart disease: presentation, diagnosis, and management. *Heart*, 2004. **90**(10): p. 1224-1228.

199. Edwards, N.C., M. Yuan, O. Nolan, T.A. Pawade, T. Oelofse, H. Singh, H. Mehrzad, Z. Zia, J.I. Geh, D.H. Palmer, C.J.H. May, J. Ayuk, T. Shah, S.J. Rooney, and R.P. Steeds, Effect of valvular surgery in carcinoid heart disease: an observational cohort study. *J of Clin Endocrin & Met*, 2016. **101**(1): p. 182-189.

200. Cremer, S.E., G.E. Singletary, L.H. Olsen, K. Wallace, J. Haggstrom, I. Ljungvall, K. Hoglund, C.A. Reynolds, N. Pizzinat, and M.A. Oyama, Serotonin concentrations in platelets, plasma, mitral valve leaflet, and left ventricular myocardial tissue in dogs with myxomatous mitral valve disease. *J Vet Intern Med*, 2014. **28**(5): p. 1534-1540.

201. Lee, C.M., J.I. Han, M.H. Kang, S.G. Kim, and H.M. Park, Polymorphism in the serotonin transporter protein gene in Maltese dogs with degenerative mitral valve disease. *J Vet Sci*, 2018. **19**(1): p. 129-135.

202. Elangbam, C.S., J.G. Wehe, J.C. Barton, D.L. Krull, A. Nyska, T. Crabbs, and G.E. Kissling, Evaluation of glycosaminoglycans content and 5-hydroxytryptamine 2B receptor in the heart valves of Sprague-Dawley rats with spontaneous mitral valvulopathy--a possible exacerbation by dl-amphetamine sulfate in Fischer 344 rats? *Exp Toxicol Pathol*, 2006. **58**(2-3): p. 89-99.

203. Connolly, J.M., M.A. Bakay, J.T. Fulmer, R.C. Gorman, J.H. Gorman, 3rd, M.A. Oyama, and R.J. Levy, Fenfluramine disrupts the mitral valve interstitial cell response to serotonin. *Am J Pathol*, 2009. **175**(3): p. 988-997.

204. Perez, J., N. Diaz, I. Tandon, R. Plate, C. Martindale, and K. Balachandran, Elevated serotonin interacts with angiotensin-II to result in altered valve interstitial cell contractility and remodeling. *Cardiovasc Eng Technol*, 2018. **9**(2): p. 168-180.

205. Jian, B., J. Xu, J. Connolly, R.C. Savani, N. Narula, B. Liang, and R.J. Levy, Serotonin mechanisms in heart valve disease I: serotonin-induced up-regulation of transforming growth factor-beta1 via G-protein signal transduction in aortic valve interstitial cells. *Am J Pathol*, 2002. **161**(6): p. 2111-2121.

206. Hutcheson, J.D., L.M. Ryzhova, V. Setola, and W.D. Merryman, 5-HT2B antagonism arrests non-canonical TGF-beta 1-induced valvular myofibroblast differentiation. *J Mol Cell Cardiol*, 2012. **53**(5): p. 707-714.

207. Jaffre, F., P. Bonnin, J. Callebert, H. Debbabi, V. Setola, S. Doly, L. Monassier, B. Mettauer, B.C. Blaxall, J.M. Launay, and L. Maroteaux, Serotonin and angiotensin receptors in cardiac fibroblasts coregulate adrenergic-dependent cardiac hypertrophy. *Circ Res*, 2009. **104**(1): p. 113-123.

208. Borgarelli, M. and J. Haggstrom, Canine degenerative myxomatous mitral valve disease: natural history, clinical presentation and therapy. *Vet Clin North Am Small Anim Pract*, 2010. **40**(4): p. 651-663.

209. Chetboul, V., F. Serres, R. Tissier, H.P. Lefebvre, C.C. Sampedrano, V. Gouni, L. Poujol, G. Hawa, and J.L. Pouchelon, Association of Plasma N-Terminal Pro-B-Type Natriuretic Peptide concentration with mitral regurgitation severity and outcome in dogs with asymptomatic degenerative mitral valve disease. *J of Vet Intern Med*, 2009. **23**(5): p. 984-994.

210. Borgarelli, M., P. Savarino, S. Crosara, R.A. Santilli, D. Chiavegato, M. Poggi, C. Bellino, G. La Rosa, R. Zanatta, J. Haggstrom, and A. Tarducci, Survival characteristics and prognostic variables of dogs with mitral regurgitation attributable to myxomatous valve disease. *J Vet Intern Med*, 2008. **22**(1): p. 120-128.

211. Thrusfield, M.V., C.G.G. Aitken, and P.G.G. Darke, Observations on breed and sex in relation to canine heart-valve incompetence. *J Small Anim Pract*, 1985. **26**(12): p. 709-717.

212. Parker, H.G. and P. Kilroy-Glynn, Myxomatous mitral valve disease in dogs: Does size matter? *J Vet Cardiol*, 2012. **14**(1): p. 19-29.

213. Schutte, J.E., F.A. Gaffney, L. Blend, and C.G. Blomqvist, Distinctive anthropometric characteristics of women with mitral-valve prolapse. *Am J of Med*, 1981. **71**(4): p. 533-538.

214. Raggi, P., T.Q. Callister, N.J. Lippolis, and D.J. Russo, Is mitral valve prolapse due to cardiac entrapment in the chest cavity? A CT view. *Chest*, 2000. **117**(3): p. 636-642.

215. Paajanen, T.A., N.K.J. Oksala, P. Kuukasjarvi, and P.J. Karhunen, Short stature is associated with coronary heart disease: a systematic review of the literature and a meta-analysis. *Euro Heart J*, 2010. **31**(14): p. 1802-1809.

216. Boyko, A.R., P. Quignon, L. Li, J.J. Schoenebeck, J.D. Degenhardt, K.E. Lohmueller, K. Zhao, A. Brisbin, H.G. Parker, B.M. vonHoldt, M. Cargill, A. Auton, A. Reynolds, A.G. Elkahloun, M. Castelhano, D.S. Mosher, N.B. Sutter, G.S. Johnson, J. Novembre, M.J. Hubisz, A. Siepel, R.K. Wayne, C.D. Bustamante, and E.A. Ostrander, A simple genetic architecture underlies morphological variation in dogs. *PLoS Biol*, 2010. **8**(8): e1000451.

217. Jones, P., K. Chase, A. Martin, P. Davern, E.A. Ostrander, and K.G. Lark, Single-nucleotide-polymorphism-based association mapping of dog stereotypes. *Genetics*, 2008. **179**(2): p. 1033-1044.

218. Chase, K., D.R. Carrier, F.R. Adler, T. Jarvik, E.A. Ostrander, T.D. Lorentzen, and K.G. Lark, Genetic basis for systems of skeletal quantitative traits: principal component analysis of the canid skeleton. *Proc Natl Acad Sci U S A*, 2002. **99**(15): p. 9930-9935.

219. French, A.T., R. Ogden, C. Eland, G. Hemani, R. Pong-Wong, B. Corcoran, and K.M. Summers, Genome-wide analysis of mitral valve disease in Cavalier King Charles Spaniels. *Vet J*, 2012. **193**(1): p. 283-286.

220. Madsen, M.B., L.H. Olsen, J. Haggstrom, K. Hoglund, I. Ljungvall, T. Falk, G. Wess, H. Stephenson, J. Dukes-McEwan, V. Chetboul, V.

Gouni, H.F. Proschowsky, S. Cirera, P. Karlskov-Mortensen, and M. Fredholm, Identification of 2 loci associated with development of myxomatous mitral valve disease in Cavalier King Charles Spaniels. *J Hered*, 2011. **102 Suppl 1**: p. 62-67.

221. Stern, J.A., W.H. Hsue, K.H. Song, E.S. Ontiveros, V.L. Fuentes, and R.L. Stepien, Severity of mitral valve degeneration is associated with chromosome 15 loci in whippet dogs. *Plos One*, 2015. **10**(10): e0141234.

222. Lewis, T., S. Swift, J.A. Woolliams, and S. Blott, Heritability of premature mitral valve disease in Cavalier King Charles spaniels. *Vet J*, 2011. **188**(1): p. 73-76.

223. Swift, S., The problem of inherited diseases. 5: Valvular disease in Cavalier King Charles spaniels. *J Small Anim Pract*, 1996. **37**(10): p. 505-506.

224. Asher, L., G. Diesel, J.F. Summers, P.D. McGreevy, and L.M. Collins, Inherited defects in pedigree dogs. Part 1: disorders related to breed standards. *Vet J*, 2009. **182**(3): p. 402-411.

225. Cowan, S.M., J.W. Bartges, R.E. Gompf, J.R. Hayes, T.D. Moyers, C.C. Snider, D.A. Gerard, R.M. Craft, R.A. Muenchen, and R.C. Carroll, Giant platelet disorder in the Cavalier King Charles Spaniel. *Exp Hematol*, 2004. **32**(4): p. 344-350.

226. Olsen, L.H., A.T. Kristensen, J. Haggstrom, A.L. Jensen, B. Klitgaard, H. Hansson, and H.D. Pedersen, Increased platelet aggregation response in Cavalier King Charles Spaniels with mitral valve prolapse. *J Vet Intern Med*, 2001. **15**(3): p. 209-216.

227. Tarnow, I., A.T. Kristensen, H. Texel, L.H. Olsen, and H.D. Pedersen, Decreased platelet function in Cavalier King Charles Spaniels with mitral valve regurgitation. *J Vet Intern Med*, 2003. **17**(5): p. 680-686.

228. Becker, P.S., L.A. Clavell, and D.S. Beardsley, Giant platelets with abnormal surface glycoproteins: A new familial disorder associated with mitral valve insufficiency. *J Pediat Hematol Onco*, 1998. **20**(1): p. 69-73.

229. Hoglund, K., J. Haggstrom, S. Hanas, A.C. Merveille, V. Gouni, M. Wiberg, J. Lundgren Willesen, K.M. Entee, L. Mejer Sorensen, L. Tiret, E.H. Seppala, H. Lohi, V. Chetboul, M. Fredholm, A.S. Lequarre, and I.

Ljungvall, Interbreed variation in serum serotonin (5-hydroxytryptamine) concentration in healthy dogs. *J Vet Cardiol*, 2018. **20**(4): p. 244-253.

230. Atkins, C., J. Bonagura, S. Ettinger, P. Fox, S. Gordon, J. Haggstrom, R. Hamlin, B. Keene, V. Luis-Fuentes, and R. Stepien, Guidelines for the diagnosis and treatment of canine chronic valvular heart disease. *J Vet Intern Med*, 2009. **23**(6): p. 1142-1150.

231. Hezzell, M., Pathology and prognosis of canine myxomatous mitral valve disease. *In Practice*, 2018. **40**: p. 3-6.

232. Hezzell, M.J., A. Boswood, W. Moonarmart, and J. Elliott, Selected echocardiographic variables change more rapidly in dogs that die from myxomatous mitral valve disease. *J Vet Cardiol*, 2012. **14**(1): p. 269-279.

233. Nishimura, R.A., C.M. Otto, R.O. Bonow, B.A. Carabello, J.P. Erwin, L.A. Fleisher, H. Jneid, M.J. Mack, P.T.O. Gara, V.H. Rigolin, and T.M. Sundt, 2017 AHA/ACC focused update of the 2014 AHA/ACC guideline for the management of patients with valvular heart disease A report of the american college of cardiology/american heart association task force on clinical practice guidelines. *Circulation*, 2017. **135**(25): p. 1159-1195

234. Winter, R.L., A.B. Saunders, S.G. Gordon, J.S. Buch, and M.W. Miller, Biologic variability of N-terminal pro-brain natriuretic peptide in healthy dogs and dogs with myxomatous mitral valve disease. *J Vet Cardiol*, 2017. **19**(2): p. 124-131.

235. Hezzell, M.J., A. Boswood, Y.M. Chang, W. Moonarmart, K. Souttar, and J. Elliott, The combined prognostic potential of serum high-sensitivity cardiac troponin I and N-terminal pro-B-type natriuretic peptide concentrations in dogs with degenerative mitral valve disease. *J Vet Intern Med*, 2012. **26**(2): p. 302-311.

236. Ljungvall, I., K. Hoglund, A. Tidholm, L.H. Olsen, M. Borgarelli, P. Venge, and J. Haggstrom, Cardiac Troponin I is associated with severity of myxomatous mitral valve disease, age, and C-reactive protein in dogs. *J Vet Intern Med*, 2010. **24**(1): p. 153-159.

237. Moonarmart, W., A. Boswood, V. Luis Fuentes, D. Brodbelt, K. Souttar, and J. Elliott, N-terminal pro B-type natriuretic peptide and left

ventricular diameter independently predict mortality in dogs with mitral valve disease. *J Small Anim Pract*, 2010. **51**(2): p. 84-96.

238. Winter, R.L., A.B. Saunders, S.G. Gordon, M.W. Miller, G.T. Fosgate, J.S. Suchodolski, and J.M. Steiner, Biologic variability of cardiac troponin I in healthy dogs and dogs with different stages of myxomatous mitral valve disease using standard and high-sensitivity immunoassays. *Vet Clin Pathol*, 2017. **46**(2): p. 299-307.

239. Li, Q., L.M. Freeman, J.E. Rush, and D.P. Laflamme, Expression profiling of circulating microRNAs in canine myxomatous mitral valve disease. *Int J Mol Sci*, 2015. **16**(6): p. 14098-14108.

240. Yang, V.K., K.A. Loughran, D.M. Meola, C.M. Juhr, K.E. Thane, A.M. Davis, and A.M. Hoffman, Circulating exosome microRNA associated with heart failure secondary to myxomatous mitral valve disease in a naturally occurring canine model. *J Extracell Vesicles*, 2017. **6**(1).

241. Jung, S. and A. Bohan, Genome-wide sequencing and quantification of circulating microRNAs for dogs with congestive heart failure secondary to myxomatous mitral valve degeneration. *Am J Vet Res*, 2018. **79**(2): p. 163-169.

242. Hulanicka, M., M. Garncarz, M. Parzeniecka-Jaworska, and M. Jank, Plasma miRNAs as potential biomarkers of chronic degenerative valvular disease in Dachshunds. *BMC Vet Res*, 2014. **10**(205): p1-8.

243. Markham, R., S. Kyranis, N. Aroney, K. Lau, K. Poon, G. Scalia, and D. Walters, Transcatheter mitral valve intervention: an emerging treatment for mitral regurgitation. *Intern Med J*, 2018. **48**(4): p. 382-390.

244. Menciotti, G. and M. Borgarelli, Review of diagnostic and therapeutic approach to canine myxomatous mitral valve disease. *Vet Sci*, 2017. **4**(4): e47.

245. Klement, P., C.M. Feindel, H.E. Scully, E. Mesher, G. Klement, P. Del Nido, and G.J. Wilson, Mitral valve replacement in dogs. Surgical technique and postoperative management. *Vet Surg*, 1987. **16**(3): p. 231-237.

246. Orton, E.C., T.B. Hackett, K. Mama, and J.A. Boon, Technique and outcome of mitral valve replacement in dogs. *J Am Vet Med Assoc*, 2005. **226**(9): p. 1508-1511.

247. Takashima, K., A. Soda, R. Tanaka, and Y. Yamane, Long-term clinical evaluation of mitral valve replacement with porcine bioprosthetic valves in dogs. *J Vet Med Sci*, 2008. **70**(3): p. 279-83.

248. White, R.N., R.L. Stepien, R.A. Hammond, D.J. Holden, A.M. Torrington, H.R. Milner, M.A. Cobb, and S.H. Hellens, Mitral valve replacement for the treatment of congenital mitral dysplasia in a bull terrier. *J Small Anim Pract*, 1995. **36**(9): p. 407-410.

249. Borgarelli, M., O. Lanz, N. Pavlisko, J.A. Abbott, G. Menciotti, M. Aherne, S.M. Lahmers, K.K. Lahmers, and J.S. Gammie, Mitral valve repair in dogs using an ePTFE chordal implantation device: a pilot study. *J Vet Cardiol*, 2017. **19**(3): p. 256-267.

250. Mizuno, T., T. Mizukoshi, and M. Uechi, Long-term outcome in dogs undergoing mitral valve repair with suture annuloplasty and chordae tendinae replacement. *J Small Anim Pract*, 2013. **54**(2): p. 104-107.

251. Nishida, M., Y. Kagawa, T. Mizukoshi, M. Mizuno, T. Mizuno, K. Harada, and M. Uechi, Post-mortem evaluation of expanded polytetrafluoroethylene (ePTFE) used in mitral valve repair in dogs. *J Vet Cardiol*, 2012. **14**(1): p. 307-312.

252. Uechi, M., Mitral valve repair in dogs. *J Vet Cardiol*, 2012. **14**(1): p. 185-192.

253. Uechi, M., T. Mizukoshi, T. Mizuno, M. Mizuno, K. Harada, T. Ebisawa, J. Takeuchi, T. Sawada, S. Uchida, A. Shinoda, A. Kasuya, M. Endo, M. Nishida, S. Kono, M. Fujiwara, and T. Nakamura, Mitral valve repair under cardiopulmonary bypass in small-breed dogs: 48 cases (2006-2009). *J Am Vet Med Assoc*, 2012. **240**(10): p. 1194-1201.

254. Atkins, C.E., B.W. Keene, W.A. Brown, J.R. Coats, M.A. Crawford, T.C. DeFrancesco, N.J. Edwards, P.R. Fox, L.B. Lehmkuhl, M.W. Luethy, K.M. Meurs, J.P. Petrie, F.S. Pipers, S.L. Rosenthal, J.A. Sidley, and J.H. Straus, Results of the veterinary enalapril trial to prove reduction in onset of heart failure in dogs chronically treated with enalapril alone for compensated, naturally occurring mitral valve insufficiency. *Javma-J Amer Vet Med Assoc*, 2007. **231**(7): p. 1061-1069.

255. Bernay, F., J.M. Bland, J. Haggstrom, L. Baduel, B. Combes, A. Lopez, and V. Kaltsatos, Efficacy of spironolactone on survival in dogs with

naturally occurring mitral regurgitation caused by myxomatous mitral valve disease. *J Vet Intern Med*, 2010. **24**(2): p. 331-341.

256. Pouchelon, J.L., N. Jamet, V. Gouni, R. Tissier, F. Serres, C.C. Sampedrano, M. Castaignet, H.P. Lefebvre, and V. Chetboul, Effect of benazepril on survival and cardiac events in dogs with asymptomatic mitral valve disease: A retrospective study of 141 cases. *J Vet Intern Med*, 2008. **22**(4): p. 905-914.

257. Haggstrom, J., A. Boswood, M. O'Grady, O. Jons, S. Smith, S. Swift, M. Borgarelli, B. Gavaghan, J.G. Kresken, M. Patteson, B. Ablad, C.M. Bussadori, T. Glaus, A. Kovacevic, M. Rapp, R.A. Santilli, A. Tidholm, A. Eriksson, M.C. Belanger, M. Deinert, C.J.L. Little, C. Kvart, A. French, M. Ronn-Landbo, G. Wess, A. Eggertsdottir, M.L. O'Sullivan, M. Schneider, C.W. Lombard, J. Dukes-McEwan, R. Willis, A. Louvet, and R. DiFruscia, Longitudinal analysis of quality of life, clinical, radiographic, echocardiographic, and laboratory variables in dogs with myxomatous mitral valve disease receiving pimobendan or benazepril: The QUEST study. *J Vet Intern Med*, 2013. **27**(6): p. 1441-1451.

258. Lombard, C.W., O. Jons, and C.M. Bussadori, Clinical efficacy of pimobendan versus benazepril for the treatment of acquired atrioventricular valvular disease in dogs *J Amer Vet Med Assoc*, 2006. **42**(4): p. 249-261.

259. Verdouw, P.D., J.M. Hartog, D.J. Duncker, W. Roth, and P.R. Saxena, Cardiovascular profile of pimobendan, a benzimidazole-pyridazinone derivative with vasodilating and inotropic properties. *Eur J Pharmacol*, 1986. **126**(1-2): p. 21-30.

260. Boswood, A., J. Haggstrom, S.G. Gordon, G. Wess, R.L. Stepien, M.A. Oyama, B.W. Keene, J. Bonagura, K.A. MacDonald, M. Patteson, S. Smith, P.R. Fox, K. Sanderson, R. Woolley, V. Szatmari, P. Menaut, W.M. Church, M.L. O'Sullivan, J.P. Jaudon, J.G. Kresken, J. Rush, K.A. Barrett, S.L. Rosenthal, A.B. Saunders, I. Ljungvall, M. Deinert, E. Bomassi, A.H. Estrada, M.J. Fernandez Del Palacio, N.S. Moise, J.A. Abbott, Y. Fujii, A. Spier, M.W. Luethy, R.A. Santilli, M. Uechi, A. Tidholm, and P. Watson, Effect of pimobendan in dogs with preclinical myxomatous mitral valve disease and cardiomegaly: The EPIC study-A randomized clinical trial. *J Vet Intern Med*, 2016. **30**(6): p. 1765-1779.

261. Hezzell, M.J., A. Boswood, J. Lopez-Alvarez, N. Lotter, and J. Elliott, Treatment of dogs with compensated myxomatous mitral valve disease with spironolactone-a pilot study. *J Vet Cardiol*, 2017. **19**(4): p. 325-338.

262. Kalia, A. and R.P. Gupta, Proteomics: a paradigm shift. *Crit Rev Biotechnol*, 2005. **25**(4): p. 173-198.

263. Bilitewski, U., DNA microarrays: an introduction to the technology. *Methods Mol Biol*, 2009. **509**: p. 1-14.

264. Wang, Z., M. Gerstein, and M. Snyder, RNA-Seq: a revolutionary tool for transcriptomics. *Nat Rev Genet*, 2009. **10**(1): p. 57-63.

265. Korbel, J.O., A.E. Urban, J.P. Affourtit, B. Godwin, F. Grubert, J.F. Simons, P.M. Kim, D. Palejev, N.J. Carriero, L. Du, B.E. Taillon, Z. Chen, A. Tanzer, A.C. Saunders, J. Chi, F. Yang, N.P. Carter, M.E. Hurles, S.M. Weissman, T.T. Harkins, M.B. Gerstein, M. Egholm, and M. Snyder, Paired-end mapping reveals extensive structural variation in the human genome. *Science*, 2007. **318**(5849): p. 420-426.

266. Kawaji, H., J. Severin, M. Lizio, A. Waterhouse, S. Katayama, K.M. Irvine, D.A. Hume, A.R. Forrest, H. Suzuki, P. Carninci, Y. Hayashizaki, and C.O. Daub, The FANTOM web resource: from mammalian transcriptional landscape to its dynamic regulation. *Genome Biol*, 2009. **10**(4).

267. Vera, J.C., C.W. Wheat, H.W. Fescemyer, M.J. Frilander, D.L. Crawford, I. Hanski, and J.H. Marden, Rapid transcriptome characterization for a nonmodel organism using 454 pyrosequencing. *Mol Ecol*, 2008. **17**(7): p. 1636-1647.

268. Schroeder, A., O. Mueller, S. Stocker, R. Salowsky, M. Leiber, M. Gassmann, S. Lightfoot, W. Menzel, M. Granzow, and T. Ragg, The RIN: an RNA integrity number for assigning integrity values to RNA measurements. *BMC Mol Biol*, 2006. **7**(3): doi:10.1186/1471-2199-7-3.

269. Bolstad, B.M., R.A. Irizarry, M. Astrand, and T.P. Speed, A comparison of normalization methods for high density oligonucleotide array data based on variance and bias. *Bioinformatics*, 2003. **19**(2): p. 185-193.

270. Freeman, T.C., L. Goldovsky, M. Brosch, S. Van Dongen, P. Maziere, R.J. Grocock, S. Freilich, J. Thornton, and A.J. Enright, Construction,

visualisation, and clustering of transcription networks from Microarray expression data. *Plos Computational Biology*, 2007. **3**(10): p. 2032-2042.

271. Theocharidis, A., S. van Dongen, A.J. Enright, and T.C. Freeman, Network visualization and analysis of gene expression data using BioLayout Express(3D). *Nat Protoc*, 2009. **4**(10): p. 1535-1550.

272. Kennedy, J.A., X. Hua, K. Mishra, G.A. Murphy, A.C. Rosenkranz, and J.D. Horowitz, Inhibition of calcifying nodule formation in cultured porcine aortic valve cells by nitric oxide donors. *European Journal of Pharmacology*, 2009. **602**(1): p. 28-35.

273. Naito, K., C. Tanaka, M. Mitsuhashi, H. Moteki, M. Kimura, H. Natsume, and M. Ogihara, Signal Transduction Mechanism for Serotonin 5-HT2B Receptor-Mediated DNA Synthesis and Proliferation in Primary Cultures of Adult Rat Hepatocytes. *Biol Pharm Bull*, 2016. **39**(1): p. 121-129.

274. Shearin, A.L. and E.A. Ostrander, Leading the way: canine models of genomics and disease. *Dis Model Mech*, 2010. **3**(1-2): p. 27-34.

275. Busca, R., J. Pouyssegur, and P. Lenormand, ERK1 and ERK2 Map Kinases: Specific Roles or Functional Redundancy? *Front Cell Dev Biol*, 2016. **4**:(53): doi10.3389/fcell.2016.00053.

276. Hutcheson, J.D., J. Chen, M.K. Sewell-Loftin, L.M. Ryzhova, C.I. Fisher, Y.R. Su, and W.D. Merryman, Cadherin-11 regulates cell-cell tension necessary for calcific nodule formation by valvular myofibroblasts. *Arterioscl Thromb and Vasc Bio*, 2013. **33**(1): p. 114-120.

277. Nenan, S., E. Boichot, V. Lagente, and C.P. Bertrand, Macrophage elastase (MMP-12): a pro-inflammatory mediator? *Mem Inst Oswaldo Cruz*, 2005. **100 Suppl 1**: p. 167-172.

278. Liu, S.L., Y.H. Bae, C. Yu, J. Monslow, E.A. Hawthorne, P. Castagnino, E. Branchetti, G. Ferrari, S.M. Damrauer, E. Pure, and R.K. Assoian, Matrix metalloproteinase-12 is an essential mediator of acute and chronic arterial stiffening. *Scient Reports*, 2015. **5(**17189): doi 10.1038/srep17189.

279. Yang, L., R.M. Froio, T.E. Sciuto, A.M. Dvorak, R. Alon, and F.W. Luscinskas, ICAM-1 regulates neutrophil adhesion and transcellular

migration of TNF-alpha-activated vascular endothelium under flow. *Blood*, 2005. **106**(2): p. 584-592.

280. Lammermann, T. and R.N. Germain, The multiple faces of leukocyte interstitial migration. *Semin Immunopathol*, 2014. **36**(2): p. 227-251.

281. Chuaqui, R.F., R.F. Bonner, C.J. Best, J.W. Gillespie, M.J. Flaig, S.M. Hewitt, J.L. Phillips, D.B. Krizman, M.A. Tangrea, M. Ahram, W.M. Linehan, V. Knezevic, and M.R. Emmert-Buck, Post-analysis follow-up and validation of microarray experiments. *Nat Genet*, 2002. **32 Suppl**: p. 509-514.

282. Beckman, K.B., K.Y. Lee, T. Golden, and S. Melov, Gene expression profiling in mitochondrial disease: assessment of microarray accuracy by high-throughput Q-PCR. *Mitochondrion*, 2004. **4**(5-6): p. 453-470.

283. Swift, S., A. Baldin, and P. Cripps, Degenerative valvular disease in the cavalier king charles spaniel: results of the UK breed scheme 1991-2010. *J Vet Intern Med*, 2017. **31**(1): p. 9-14.

284. Birkegard, A.C., M.J. Reimann, T. Martinussen, J. Haggstrom, H.D. Pedersen, and L.H. Olsen, Breeding restrictions decrease the prevalence of myxomatous mitral valve disease in Cavalier King Charles Spaniels over an 8- to 10-year period. *J Vet Intern Med*, 2016. **30**(1): p. 63-68.

285. Beardow, A.W. and J.W. Buchanan, Chronic mitral-valve disease in Cavalier King Charles Spaniels - 95 cases (1987-1991). *J Amer Vet Med Asso*, 1993. **203**(7): p. 1023-1029.

286. Batchelor, D.J., P.J. Noble, P.J. Cripps, R.H. Taylor, L. McLean, M.A. Leibl, and A.J. German, Breed associations for canine exocrine pancreatic insufficiency. *J Vet Intern Med*, 2007. **21**(2): p. 207-214.

287. Summers, J.F., D.G. O'Neill, D.B. Church, P.C. Thomson, P.D. McGreevy, and D.C. Brodbelt, Prevalence of disorders recorded in Cavalier King Charles Spaniels attending primary-care veterinary practices in England. *Canine Genet Epidemiol*, 2015. **2**:(4): doi 10.1186/s40575-015-0016-7.

288. Borissoff, J.I., H.M.H. Spronk, and H. ten Cate, Mechanisms of disease the hemostatic system as a modulator of atherosclerosis. *N Engl J Med*, 2011. **364**(18): p. 1746-1760.

289. Bae, J.S., I.S. Kim, and A.R. Rezaie, Thrombin down-regulates the TGF-beta-mediated synthesis of collagen and fibronectin by human proximal tubule epithelial cells through the EPCR-dependent activation of PAR-1. *J of Cell Phys*, 2010. **225**(1): p. 233-239.

290. Chang, J.Z.C., Y.P. Hsieh, W.H. Lin, H.M. Chen, and M.Y.P. Kuo, Activation of transforming growth factor-1 by thrombin via integrins v1, v3, and v5 in buccal fibroblasts: Suppression by epigallocatechin-3-gallate. *Head Neck- J Sci Spec*, 2017. **39**(7): p. 1436-1445.

291. Wang, Z.G., D.Z. Wang, G.C.T. Pipes, and E.N. Olson, Myocardin is a master regulator of smooth muscle gene expression. *PNAS*, 2003. **100**(12): p. 7129-7134.

292. Herrmann, C., J. Wray, F. Travers, and T. Barman, Effect of 2,3-butanedione monoxime on myosin and myofibrillar ATPases. An example of an uncompetitive inhibitor. *Biochemistry*, 1992. **31**(48): p. 12227-12232.

293. McDermott, J.C., M.C. Cardoso, Y.T. Yu, V. Andres, D. Leifer, D. Krainc, S.A. Lipton, and B. Nadal-Ginard, hMEF2C gene encodes skeletal muscle- and brain-specific transcription factors. *Mol Cell Biol*, 1993. **13**(4): p. 2564-2577.

294. Hata, K., Y. Goto, S. Futaki, Y. Ohgoshi, H. Yaku, O. Kawaguchi, T. Takasago, A. Saeki, T.W. Taylor, T. Nishioka, and H. Suga., Mechanoenergetic effects of pimobendan in canine left ventricles. Comparison with dobutamine. *Circulation*, 1992. **86**(4): p. 1291-1301.

295. Nagy, E., D.C. Andersson, K. Caidahl, M.J. Eriksson, P. Eriksson, A. Franco-Cereceda, G.K. Hansson, and M. Back, Upregulation of the 5-lipoxygenase pathway in human aortic valves correlates with severity of stenosis and leads to leukotriene-induced effects on valvular myofibroblasts. *Circulation*, 2011. **123**(12): p. 1316-1325.

296. Benjamini, Y. and Y. Hochberg, Controlling the false discovery rate - a practical and powerful approach to multiple testing. *J Roy Stat Soc Series B-Metho*, 1995. **57**(1): p. 289-300.

297. Lander, E.S., Array of hope. *Nat Gene*, 1999. **21**: p. 3-4.

298. Fare, T.L., E.M. Coffey, H.Y. Dai, Y.D.D. He, D.A. Kessler, K.A. Kilian, J.E. Koch, E. LeProust, M.J. Marton, M.R. Meyer, R.B. Stoughton, G.Y.

Tokiwa, and Y.Q. Wang, Effects of atmospheric ozone on microarray data quality. *Analyt Chem*, 2003. **75**(17): p. 4672-4675.

299. Johnson, W.E., C. Li, and A. Rabinovic, Adjusting batch effects in microarray expression data using empirical Bayes methods. *Biostatistics*, 2007. **8**(1): p. 118-127.

300. Chen, C., K. Grennan, J. Badner, D.D. Zhang, E. Gershon, L. Jin, and C.Y. Liu, Removing batch effects in analysis of expression microarray data: an evaluation of six batch adjustment methods. *Plos One*, 2011. **6**(2) e17238.

301. Mavropoulou, A., S. Guazzetti, P. Borghetti, E. De Angelis, and C. Quintavalla, Cytokine expression in peripheral blood mononuclear cells of dogs with mitral valve disease. *Vet J*, 2016. **211**: p. 45-51.

302. Fonfara, S., S.R. Tew, P. Cripps, J. Dukes-McEwan, and P.D. Clegg, Increased blood mRNA expression of inflammatory and anti-fibrotic markers in dogs with congestive heart failure. *Res Vet Sci*, 2012. **93**(2): p. 879-885.

303. Hoppe, A., I. Ilkavets, S. Dooley, and H.G. Holzhutter, Metabolic consequences of TGFb stimulation in cultured primary mouse hepatocytes screened from transcript data with ModeScore. *Metabolites*, 2012. **2**(4): p. 983-1003.

304. Mulholland, D.L. and A.I. Gotlieb, Cell biology of valvular interstitial cells. *Can J Cardiol*, 1996. **12**(3): p. 231-236.

305. Taylor, P.M., P. Batten, N.J. Brand, P.S. Thomas, and M.H. Yacoub, The cardiac valve interstitial cell. *Int J Biochem Cell Biol*, 2003. **35**(2): p. 113-118.

306. Taylor, P.M., S.P. Allen, and M.H. Yacoub, Phenotypic and functional characterization of interstitial cells from human heart valves, pericardium and skin. *J Heart Valve Dis*, 2000. **9**(1): p. 150-158.

307. Inman, G.J., F.J. Nicolas, J.F. Callahan, J.D. Harling, L.M. Gaster, A.D. Reith, N.J. Laping, and C.S. Hill, SB-431542 is a potent and specific inhibitor of transforming growth factor-beta superfamily type I activin receptor-like kinase (ALK) receptors ALK4, ALK5, and ALK7. *Molecular Pharmacology*, 2002. **62**(1): p. 65-74.

308. Laping, N.J., E. Grygielko, A. Mathur, S. Butter, J. Bomberger, C. Tweed, W. Martin, J. Fornwald, R. Lehr, J. Harling, L. Gaster, J.F. Callahan, and B.A. Olson, Inhibition of transforming growth factor (TGF)-beta 1-induced extracellular matrix with a novel inhibitor of the TGF-beta type I receptor kinase activity: SB-431542. *Mol Pharmacol*, 2002. **62**(1): p. 58-64.

309. Bryant, P.A., G.K. Smyth, R. Robins-Browne, and N. Curtis, Technical variability is greater than biological variability in a microarray experiment but both are outweighed by changes induced by stimulation. *Plos One*, 2011. **6**(5): e19556.

310. Laporte, J., P. Kioschis, L.J. Hu, C. Kretz, B. Carlsson, A. Poustka, J.L. Mandel, and N. Dahl, Cloning and characterization of an alternatively spliced gene in proximal Xq28 deleted in two patients with intersexual genitalia and myotubular myopathy. *Genomics*, 1997. **41**(3): p. 458-462.

311. Yamane, T., A. Muramatsu, M. Shimura, K. Kobayashi-Hattori, and Y. Oishi, Transforming growth factor-1 induces cholesterol synthesis by increasing HMG-CoA reductase mRNA expression in keratinocytes. *Biosci Biotech and Biochem*, 2016. **80**(7): p. 1379-1381.

312. Denby, L., V. Ramdas, R. Lu, B.R. Conway, J.S. Grant, B. Dickinson, A.B. Aurora, J.D. McClure, D. Kipgen, C. Delles, E. van Rooij, and A.H. Baker, MicroRNA-214 antagonism protects against renal fibrosis. *J Am Soc Nephrol*, 2014. **25**(1): p. 65-80.

313. Dobaczewski, M., W. Chen, and N.G. Frangogiannis, Transforming growth factor (TGF)-beta signaling in cardiac remodeling. *J Mol Cell Cardiol*, 2011. **51**(4): p. 600-606.

314. Mabry, K.M., R.L. Lawrence, and K.S. Anseth, Dynamic stiffening of poly(ethylene glycol)-based hydrogels to direct valvular interstitial cell phenotype in a three-dimensional environment. *Biomaterials*, 2015. **49**: p. 47-56.

315. Liu, M.M., T.C. Flanagan, S. Jockenhovel, A. Black, C.C. Lu, A.T. French, D.J. Argyle, and B.M. Corcoran, Development and evaluation of a tissue-engineered fibrin-based canine mitral valve three-dimensional cell culture system. *J Comp Pathol*, 2018. **160**: p. 23-33.

316. Ma, H., A.R. Killaars, F.W. DelRio, C. Yang, and K.S. Anseth, Myofibroblastic activation of valvular interstitial cells is modulated by

spatial variations in matrix elasticity and its organization. *Biomaterials*, 2017. **131**: p. 131-144.

317. Yazdani, S., R. Bansal, and J. Prakash, Drug targeting to myofibroblasts: Implications for fibrosis and cancer. *Adv Drug Deliv Rev*, 2017. **121**: p. 101-116.

318. Shen, C., L. Jiang, H. Shao, C. You, G. Zhang, S. Ding, T. Bian, C. Han, and Q. Meng, Targeted killing of myofibroblasts by biosurfactant di-rhamnolipid suggests a therapy against scar formation. *Sci Rep*, 2016. **6**: (37553).

Appendices

All Excel files contained in a USB stick enclosed with the following titles.

Appendix I: Gene lists from Chapter 3

Chapter 3 Table S1 - Normal compared to Grade 1 gene list

Chapter 3 Table S2 - Normal compared to Grade 2 gene list

Chapter 3 Table S3 - Normal compared to Grade 3 gene list

Chapter 3 Table S4 - Normal compared to Grade 4 gene list

Appendix II: Gene lists from Chapter 4

Chapter 4 Table S1 - CKCS grade 3 and 4 valves compared to other breed grade 3 and 4 valves

Chapter 4 Table S2 - Normal valves compared to CKCS grade 3 and 4 valves

Chapter 4 Table S3 - Normal valves compared to other breed grade 3 and 4 valves

Appendix III: Gene lists from Chapter 5

Chapter 5 Table S1 - Normal region of diseased valves compared to diseased region of diseased valves

Chapter 5 Table S2 - Normal whole valves compared to dissected normal regions of diseased valves

Appendix IV: Gene lists from Chapter 6

Chapter 6 Table S1 - Vehicle-treated aVICs compared to SB431542-treated aVICs

Chapter 6 Table S2 - Vehicle-treated qVICs compared to TGFB1-treated qVICs

Chapter 6 Table S3 - Vehicle-treated qVICs compared to vehicle-treated aVICs

Appendix V: List of shared genes and associated GO terms from Chapter 7

Gene Symbol	Full Gene Name	Grade 2 Fold Change	Dissected Fold Change
LOC476900	Uncharacterised	-4	-3
CDKN2A	Cyclin-dependent kinase inhibitor 2A	1.62	2.49
MARCH1	Mitochondrial amidoxime reducing component 1	1.64	-2.23
CRLF1	Cytokine receptor-like factor 1	1.67	2.61
CLEC5A	C-type lectin domain family 5, member A	1.69	1.68
NRXN1	Neurexin 1	-3.4	1.74
GPD1	Glycerol-3-phosphate dehydrogenase 1	2.14	-7.81
SLC22A1	Solute carrier family 22 member 1	2.16	-8.91
CSTA	Cystatin A	2.27	2.38
LOC608320	Uncharacterised	3.29	4.23
LOC612122	Uncharacterised	3.31	4.22

Table S1. Genes shared between dissected diseased regions of grade 2 valves and whole Whitney grade 2 valves. Genes in yellow share up- or down-regulation in both datasets

Category	Term	Gene count	P-value	FDR
GOTERM_BP_DIRECT	Neutrophil chemotaxis	4	1.52E-04	0.19483
GOTERM_BP_DIRECT	Positive regulation of cytokine secretion	3	4.14E-04	0.52992
GOTERM_BP_DIRECT	Positive regulation of ERK1 and ERK2 cascade	4	0.00261	3.2984
GOTERM_CC_DIRECT	Extracellular space	7	0.0112	9.89786
GOTERM_BP_DIRECT	Positive regulation of angiogenesis	3	0.01284	15.282
GOTERM_BP_DIRECT	Eosinophil chemotaxis	2	0.0174	20.1661
GOTERM_CC_DIRECT	Extracellular matrix	3	0.02248	18.9797
GOTERM_BP_DIRECT	Innate immune response	3	0.03594	37.4701
GOTERM_MF_DIRECT	Integrin binding	2	0.03806	30.8271
GOTERM_MF_DIRECT	CCR chemokine receptor binding	2	0.04427	34.9519

Table S2. Functional analysis chart summary of the top ten GO terms associated with up-regulated shared genes in dissected diseased regions and whole Whitney grade 4 valves.

Gene Symbol	Full Gene Name	TGFβ-treated qVICs Fold Change	Dissected Fold Change
NDP	Norrie disease	-4.41	1.74
EBF2	Early B-cell factor 2	-2.2	-1.57
F2RL2	Coagulation factor II recptor-like 2	-2.13	-2.17
SELL	Selectin L	-2.07	1.95
SLC10A6	Solute carrier family 10 member 6	-1.96	-1.67
LIFR	Leukemia inhibitory factor receptor	-1.76	-1.76
HBEGF	Heparin binding EGF like growth factor	-1.73	1.9
ADH4	Alcohol dehydrogenase 4	-1.62	-1.73
LYVE1	Lympahtic vessel endotehlial hyluronan receptor 1	-1.52	-1.61
CTHRC1	Collagen triple helix repeat containing 1	1.55	1.72
PLAUR	Plasminogen activator urokinase receptor	1.74	1.6
ENSCAFG00000002086	Uncharacterised	1.79	1.58
ACTA2	Actin alpha 2 smooth muscle	1.95	1.79
TUBB3	Tubulin beta III	2.29	2.07
CH25H	Cholesterol 25-hydroxylase	2.68	1.7
HTR2B	5HT receptor 2B	3.71	1.57

Table S3. Genes shared between dissected diseased regions and TGFβ1-treated qVICs. Genes in yellow share up- or down-regulation in both datasets.

Gene Symbol	Full Gene Name	TGFβ-treated qVICs Fold Change	Grade 4 Fold Change
SCARA5	Scavenger receptor class A member 5	-2.41	-1.59
F2RL2	Coagulation factor II receptor like 2	-2.13	-1.62
TNFRSF19	TNF receptor member 19	-2.01	-1.8
SLC10A6	Solute carrier family 10 member 6	-1.96	-1.67
EPHA3	EPH receptor A3	-1.95	3.19
VCAM1	Vascular cell adhesion molecule	-1.83	1.73
AHNAK2	AHNAK nucleoprotein 2	-1.78	1.68
SLC2A12	Solute carrier family 2 member 12	-1.75	-1.72
SLC22A23	Solute carrier family member 23	-1.67	-1.7
PLCB1	Phospholipase C Beta 1	-1.67	1.52
SYNDIG1	Synapse differentiation inducing 1	-1.6	1.55
TPX2	TPX2 microtubule associated	-1.58	1.52
ANLN	Anillin actin binding protein	-1.57	1.67
BMP6	Bone morphogenetic protein 6	1.52	2.19
BTK	Bruton agammaglobulinemia tyrosine kinase	1.64	1.81
TPM2	Tropomyosin 2	1.66	2.83
ENSCAFG00000002086	Uncharacterised	1.79	3.2
SERPINE1	Serpin peptidase inhibitor clade E 1	1.88	4.34
ACTA2	Actin alpha 2 smooth muscle	1.95	3.24
LIF	Leukemia inhibitory factor	1.96	1.53
WFDC5	WAP four disulfide core 5	2.01	-3.68
ENSCAFG00000010877	Uncharacterised	2.01	-1.57
MFSD2A	Major facilitator superfamily 2A	2.13	1.9
LTBP2	Latent TGF beta binding protein 2	2.3	1.84
ENSCAFG00000027039	Uncharacterised	2.48	-1.58
PAPPA	Pregnancy associated plasma protein A	2.5	2.05
ST5	Suppression of tumorigenecity 5	2.53	1.55
MIR214	MicroRNA 214	2.61	-2.73
LOC486400	Uncharacterised	3.19	2.35
HTR2B	5HT receptor 2B	3.71	3.11
TNC	Tenascin C	3.75	1.64
RGS1	Regulator of G-protein signalling 1	5.81	2.41

Table S4. Genes shared between Whitney grade 4 valves and TGFβ1-treated qVICs. Genes in yellow share up- or down-regulation in both datasets.

Category	Term	Gene count	P-value	FDR
GOTERM_CC_DIRECT	Extracellular matrix	3	0.00309	2.48202
GOTERM_CC_DIRECT	Extracellular space	5	0.00394	3.14982
GOTERM_BP_DIRECT	Positive regulation of cell proliferation	3	0.013	14.3349
GOTERM_CC_DIRECT	Extracellular region	3	0.0265	19.578
GOTERM_BP_DIRECT	Positive regulation of endothelial cell proliferation	2	0.03751	36.3796
GOTERM_CC_DIRECT	Extrinsic component of plasma membrane	2	0.04559	31.5178
GOTERM_BP_DIRECT	Osteoblast differentiation	2	0.06538	55.0582
GOTERM_BP_DIRECT	Positive regulation of gene expression	2	0.09994	71.2176
GOTERM_BP_DIRECT	Regulation of cell proliferation	2	0.09994	71.2176

Table S5. Functional analysis chart summary of the nine GO terms associated with up-regulated shared genes in Whitney grade 4 valves and TGFβ1-treated qVICs.

Appendix VI: Publications and abstracts

Publications

Markby, G.R., K.M. Summers, V.E. MacRae, and B.M. Corcoran, Comparative transcriptomic profiling and gene expression for myxomatous mitral valve disease in the dog and human. *Vet Sci*, 2017. **4**(3).

Markby, G., K.M. Summers, V.E. MacRae, J. Del-Pozo, and B.M. Corcoran, Myxomatous degeneration of the canine mitral valve: from gross changes to molecular events. *J Comp Pathol*, 2017. **156**(4): p. 371-383.

Lin, C., D. Zhu, **G.R. Markby**, B.M. Corcoran, C. Farquharson, and V.E. Macrae, isolation and characterization of primary rat valve interstitial cells: A new model to study aortic valve calcification. *J Vis Exp*, 2017 **129**(56126): doi10.3791/56126

Tan, K. **G. R. Markby**, R. Muirhead, R. Blake, M. Liu, L. Bergeron, G. Fici, B.M. Corcoran. Canine cell cultures as models of myxomatous valve degeneration; the role of TGFβ. *J. Mol. Cell. Cardiol.* Under review

Further to the above publications, it is expected that up to four primary author research papers will be possible. This includes;

Markby, G.R., K.M. Summers, V.E. MacRae, and B.M. Corcoran, Ontogenic changes in gene expression in canine MMVD, molecular events over a lifetime. In preparation.

Markby, G.R., K.M. Summers, V.E. MacRae, and B.M. Corcoran, Cavalier King Charles Spaniel specific gene changes in MMVD, a transcriptomic study. In preparation.

Markby, G.R., K.M. Summers, V.E. MacRae, and B.M. Corcoran, Region dependent transcriptomic differences in early MMVD. In preparation.

Markby, G.R., K.M. Summers, V.E. MacRae, K. Tan, and B.M. Corcoran. Transcriptomic assessment of VICs in MMVD. In preparation.

Finally, middle authorship will also be on two further papers ;

Tsang, H-G, M.E.B. McCulloch, **G.R. Markby**, E. Clark, B.M. Corcoran, V.E. MacRae, K.M. Summers. An atlas of the cardiovascular transcriptome in the domestic sheep, *Ovis aries* In preparation.

Bode, E. **G.R. Markby**, B.M. Corcoran, Culshaw, G. 11β-Hydroxysteroid dehydrogenases involvement in kidney disease in dogs affected with congestive heart failure. In preparation.

Abstracts

Gene Changes In Early Stage (Canine) Myxomatous Mitral Valve Disease. **Greg R. Markby**, Kim M. Summers, Vicky MacRae and Brendan M. Corcoran. Poster and 4-minute presentation, Heart Valve Society Scientific Meeting, Monaco 2-4th March 2017.

Role of TGFβ1 in the Pathogenesis of Canine Myxomatous Mitral Valve Disease (MMVD). **Greg R. Markby**, Kim M. Summers, Vicky MacRae and Brendan M. Corcoran. Poster, Heart Valve Society Scientific Meeting, New York 12-14th April 2018.

Ontogenic Transcriptomic Profiling Identifies Signalling Pathways Driving Pathogenesis in Canine Myxomatous Mitral Valve Disease. **Greg R. Markby**, Kim M. Summers, Vicky MacRae and Brendan M. Corcoran. 20-minute presentation, Companion Animal Genetic Health meeting, Edinburgh 14-15th May 2018.

A Role for TGFβ1 in the Pathogenesis of Canine Myxomatous Mitral Valve Disease (MMVD. **Greg R. Markby**, Kim M. Summers, Vicky MacRae and Brendan M. Corcoran. Poster presentation, Cardiovascular science symposium 2018, Edinburgh 14th June 2018.